Modeling the origins of melanoma using zebrafish and human embryonic stem cells

by

Scott James Callahan

A Dissertation

Presented to the Faculty of the Louis V. Gerstner, Jr.

Graduate School of Biomedical Sciences,

Memorial Sloan-Kettering Cancer Center

in Partial Fulfillment of the Requirements for the Degree of

Doctor of Philosophy

New York, NY

December 2018

Lorenz Studer, MD PhD Dissertation Mentor	Date
Richard White, MD PhD Dissertation Mentor	Date

DEDICATION

To my dad, for always inspiring me to be better

To my mom, for unconditional support

To my wife, Carol, my best friend and sweetheart

To my son, Jack, the highlight of every day

ABSTRACT

The ability of cancer to self-propagate is shared with adult stem cells. This shared trait led to the hypothesis that adult stem cells may be more apt to transformation. To address the impact of the differentiation status of the cell of origin on melanoma this study utilized two complementary systems: transgenic zebrafish and melanocytes differentiated from hESCs. Transformation was initiated in precursor neural crest (NC), precursor melanoblast (MB), or late stage melanocyte (MEL).

To model the importance of cell of origin in fish, we have engineered transgenic fish that drive $BRAF^{V600E}$ expression in $p53^{-/-}$ fish under the control of NC, MB, and MEL promoters. To model melanoma in human cells we have engineered a hES line to express mutant $BRAF^{V600E}$ under the control of a DOX inducible promoter with genetic knockouts for p53, Rb1, and/or p16. We then differentiated the hES cells to NC, MB, or MEL and induced mutant BRAF expression at the defined stages and looked for comparative tumorigenesis.

In both models, BRAF expression initiated in MEL is insufficient to drive tumors. BRAF expression initiated at the precursor MB stage drives aggressive melanomas. BRAF expression initiated at the precursor NC stage produces undifferentiated tumors. These findings suggest that the differentiation state of the cell of origin is limited for initiating melanoma. The impact of $BRAF^{V600E}$ appears to be context dependent with a distinct transcriptional impact at each stage. Importantly, hES derived tumors appear to be representative of patients when clustered on a TCGA plot.

Second Project: Cancer modeling by Transgene Electroporation in Adult Zebrafish

Transgenic animals are invaluable for modeling cancer, but often require complex of multiple germline alleles to obtain the desired combinations. Oncogenic transgenes can be rapidly tested by mosaic expression in zebrafish that typically lack spatial and temporal control of tumor onset, which limits their utility for the study of tumor progression and metastasis. To overcome these limitations, we have developed a method called Transgene Electroporation in Adult Zebrafish (TEAZ). TEAZ can deliver DNA constructs with promoter elements of interest to drive fluorophores, oncogenes, or CRISPR-Cas9- based mutagenic cassettes in specific cell types. Using TEAZ, we created a highly aggressive melanoma model in fully immunocompetent animals. TEAZ speeds up tumor onset when compared to typical embryo injections. The resulting tumors initiated at highly defined locations, enable tracking their progression and deep invasion into tissues and metastatic deposits. TEAZ can be deployed to other tissues and cell types such as the heart, muscle or brain with the use of suitable transgenic promoters. The versatility of TEAZ makes it widely accessible for rapid modeling of somatic gene alterations and cancer progression at a scale not achievable in other *in vivo* systems.

BIOGRAPHICAL SKETCH

Scott Callahan was born in Princeton, NJ to Robert and Kristen Callahan. One of five boys, he attended the local elementary, middle, and high public school which was also where he met his future wife, Carol. He stayed local for college and attended Princeton University, where he majored in Chemical Engineering and minoring in Engineering Biology, and also played on both the varsity soccer and squash teams. During that time, he was also able to experience a variety of exciting research opportunities. He worked in industry at Onconova Therapeutics in Philadelphia, and Wuxi Pharmaceuticals in Shanghai, China. Scott also worked in the academic labs of Dr. Celeste Nelson and Dr. Robert Prud'homme at Princeton and Dr. Peter Scales at the University of Melbourne.

Upon graduating, Scott moved to New York City and worked as a technician at Mount Sinai Medical Center under the mentorship of Dr. Aneel Aggarwal. At Mount Sinai, he used X-ray crystallography to study the mechanisms of DNA specificity for a family of restriction enzymes. The family is of interest because of their highly homologous amino acid sequences yet divergent DNA binding specificities. The goal of the research was to identify the binding amino acids and rationally engineer user-specified DNA specificity. The work culminated in two first author publications. In July 2012, Scott began his Ph.D. program at the Louis V. Gerstner Jr. Graduate School of Biomedical Sciences at Memorial Sloan Kettering Cancer Center. During his graduate studies, Scott has investigated the

origin of melanoma phenotypes using both human embryonic stem cells and zebrafish, under the mentorship of Dr. Lorenz Studer and Dr. Richard White.

ACKNOWLEDGEMENTS

During my time at Memorial Sloan Kettering I have had the distinct privilege of being mentored by two incredibly talented and kind professors in Dr. Lorenz Studer and Dr. Richard White. The two investigators have built incredibly different but equally great and supportive lab environments that have challenged me to grow and learn. They have both been irreplaceable for my education and project.

Having worked in two great labs I have been fortunate to be surrounded by great scientists and role models. Lab meetings were always a source of ideas and inspiration. Too many to name, I would like to thank all of my lab mates (past and present). I would like to offer a special thank you to a few particularly influential members. Dr. Yvonne Mica initiated the hES cell of origin project. Dr. Arianna Baggiolini has been irreplaceable to the hES work. Nathaniel R. Campbell processed the RNA-seq data. Dr. Yan Zhang taught me everything I know about zebrafish. Stephanie Tepan helped get TEAZ up and running.

I would like to thank my thesis committee members for the exceptional guidance provided by the members of my thesis committee, Dr. Jedd Wolchok and Dr. Jenn Zallen. Both investigators have been with me from the beginning of the project and have both offered very refreshing viewpoints and suggestions

throughout. Also, I would like to thank Dr. Kathryn Anderson for agreeing to chair my Dissertation Defense Committee and Dr. Youriv Houvras for acting as my external examiner.

The help of several collaborations has propelled this thesis. Bio-informaticians (Dr. Tuan Trieu, Dr. Ekta Khurana, Dr. Christian Mosimann, Dr. Helen Lindsay, Dr. Alexa Burger), Pathologists (Dr. Travis Hollmann and Dr. Satish Tickoo), and the Antitumor Assessment Core (Besnik Qeriki and Dr. Elisa De Stanchina)

I would like to thank my funding sources: The Ruth L. Kirschstein National Research Service Award form the National Institute of Health, The 2014 Research Scholar Award from the Joanna M. Nicolay Melanoma Foundation and The Robert B. Catell Fellowship from Memorial Sloan Kettering Cancer Center.

I would like to thank the graduate school for the unbelievable support through my career. Particular thanks to Dr. Ken Marians and Maria Torres.

Finally and most importantly, I would like to thank my family and friends for their unending support and necessary, fun distractions. They have buoyed me during my times of struggle and celebrated me during my triumphs and have always inspired me to be my best. No one more than my wife Carol who has been there for me at every twist and turn.

Table of Contents

LIST OF TABLES

LIST OF FIGURES

LIST OF ABBREVIATIONS

α-MSH: α-melanocyte-stimulating hormone

ACT: Adoptive Cell Therapy

ACTH: Adrenocorticotropic hormone

C-terminus: carboxyl-terminus

cAMP: cyclic adenosine monophosphate

Cas9: CRISPR associated protein 9

cDNA: complementary DNA

CREB: cAMP responsive-element-binding protein

CRISPR: clustered regularly interspaced short palindromic repeats

DCT: Dopachrome Tautomerase (TRP2 or TYRP2)

Double fish: zebrafish with germline mutations Tg(mitfa:BRAF(V600E));$p53^{-/-}$

DNA: deoxyribonucleic acid

dNTP: deoxyribonucleoside triphosphate

DOX: doxycycline

DP: dermal papilla

DSCs: Dermal Stem Cells

DSi: Dual SMAD inhibition

E. coli: Escherichia coli

EDN: Endothelin

EDNRB: Endothelin receptor B

EdU: 5-ethynyl-2'-deosyuridine

EMT: Epithelial-to-mesenchymal transition

ERK: Extracellular signal-regulated kinases, also known as MAPK

EPI-NCSC: epidermal-Neural Crest Stem Cells

ESCs: Embryonic stem cells

FACS: fluorescence-activated cell sorting

FBS: fetal bovine serum

FGF: Fibroblast growth factor

hpf: hours post fertilization

GFP: Green fluorescent protein

(fluorescent protein excites: 395nm emits: 509nm)

GSEA: Gene Set Enrichment Analysis

GSK3β: glycogen synthase kinase 3β

H&E: hematoxylin and eosin

hESCs: Human embryonic stem cells

HF: Hair Follicle

ICI: Immune checkpoint inhibitor

IF: Interfollicular

iBRAF: Dox-inducible $BRAF^{V600E}$ that has been engineered into the AAVS1 locus

kDa: kilodalton

MAPK: mitogen-activated protein kinase

mESCs: Mouse embryonic stem cells

MB: Melanoblast

MC1R: Melanocortin-1 receptor

MEL: Melanocyte

miniCoopR: Tol2 flanked plasmid encoding (*mitfa*:GFP; *mitfa*:mitfa cds)

MITF: Microphthalmia-associated transcription factor

MSCs: Melanocyte Stem Cells

α-MSH: α-Melanocyte Stimulating Hormone

N-terminal: amino-terminal

NCC: Neural crest cell

ncRNA: non-coding RNA

NCSC: Neural crest stem cell

NF-κB: nuclear factor kappa-light-chain-enhancer of activated B cells

NF1: neurofibromin 1

NOD-SCID: Non-obese diabetic-severe combined immune-deficiency mice

OIS: Oncogene Induced Senescence

PCA: Principal component analysis

PCR: polymerase chain reaction

PKA: protein kinase A

PI3K: phosphatidylinositol-4,5-bisphosphate 3-kinase

POMC: Proopiomelanocortin

PNST: Peripheral Nerve Sheath Tumors

PSCs: Pluripotent stem cells

PTEN: phosphatase and tensin homolog

qPCR: quantitative reverse transcription PCR

RNA: ribonucleic acid

ROS: reactive oxygen species

RT: Room Temperature

RTKs: Receptor Tyrosine Kinases

SCF: Steel factor or stem cell factor

SCPs: Schwann cell precursors

SKP: skin-derived precursors cells (coined by Freda Miller) with NC-like features

SMGs: significantly mutated genes

SOS: Son of sevenless

SOX10: SRY (sex determining region Y)-box 10

SV40ER: simian vacuolating virus 40 (SV40) Early Region

TdTomato: tandem dimer tomato

(fluorescent protein excites: 554nm emits: 581nm)

TEAZ: Transgene Electroporation in Adult Zebrafish

TERT: telomerase reverse transcriptase

Tg: transgene

TKO: triple knockout cells (genetic knock out for p53, p16, Rb1)

Triple fish: zebrafish with germline mutant Tg(mitfa:BRAF(V600E));$p53^{-/-}$;$mitfa^{-/-}$

TYR: Tyrosinase

TYRP1: Tyrosinase-related protein 1

TYRP2: Dopachrome Tautomerase (TRP2 or TYRP2)

UVR: Ultraviolet radiation

WT: wild type genetic background

CHAPTER ONE: INTRODUCTION

1.1. Melanocytes

Melanin Biogenesis and Transfer

Melanin Biogenesis

Melanocytes are the specialized cells that produce the protective skin-darkening pigment melanin. Melanin is a complex heteropolymer that absorbs light across the entire visible and UV spectrum and serves as the body's natural sunscreen. Melanocytes constitutively produce a basal level of melanin but excessive UV exposure stimulates melanocytes to increase melanin production in an effort to further protect against UV damage. This protective darkening of the skin has the popularly recognized impact of tanning.

Melanin exists in two forms, either a yellow-red pheomelanin or the black-brown eumelanin. And while all humans produce both forms, variations in their relative abundance contribute to the wide-range of natural skin tones. While serving a similar function, pheomelanin and eumelanin differ in color, size, shape, and packing of their granules, which impacts their properties and function *in vivo* [1]. Pheomelanin is reactive to UVR exposure and has inferior photoprotective properties [1]. Red-haired individuals have comparatively high-levels of pheomelanin resulting in diminished sun protection, increased photoaging and higher rates of skin cancer [2].

Both melanin structures are initiated by the rate-limiting biochemical break down of tyrosine into 3,4-dihydroxyphenylalanine (dopa) that is governed by the enzyme tyrosinase (TYR) (Figure 1.1). The Dopa intermediate can then be pushed towards production of either of the melanin structures. Eumelanin production requires the processing of Dopa via successive hydroxylation, oxidation, and carboxylation reaction governed by tyrosinase-related protein 1 (Tyrp1) and tyrosinase-related protein 2 (TYRP2 or DCT). If cellular levels of TYRP1 and TYRP2 are low, dopa is broken down in a single cysteine-dependent reduction step to pheomelanin [1].

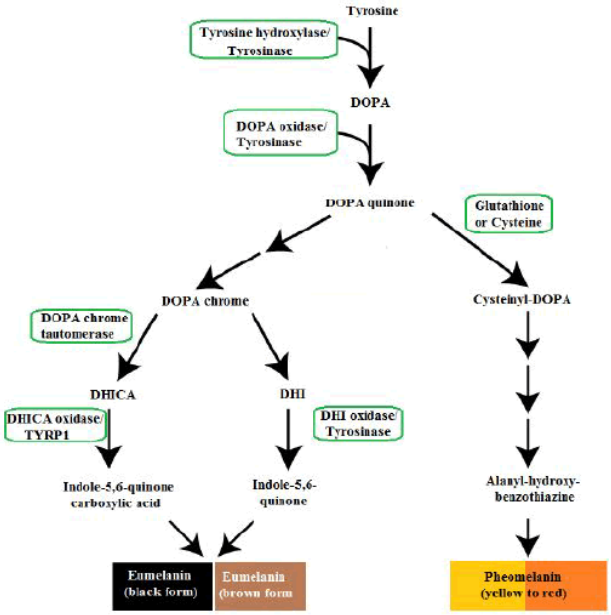

Figure 1.1 Simplified scheme of melanin synthesis in melanocytes.
Tyrosine is broken down into either eumelanin or pheomelanin with enzymatic help from the TYR, TYRP1, and TYRP2 enzymes (adapted from Shah et al. 2018) [3]

Melanin synthesis is spatially contained within melanosomes, which are membrane bound intracellular organelles unique to pigment cells. The sequestration of melanin production within the melanosomes allows for the

chemical reactions to proceed under careful local control of protein levels and acidity [4]. Furthermore, melanosomes allow for the sequestration of cytotoxic intermediates (including 5,6-dihydroxyindole and 5,6-dihydroxyindole-2-carboxylic acid) produced during melanin synthesis. Beyond sequestering intermediates, melanosomes have been shown to scavenge cytotoxic metabolites and chemotherapies [5, 6]. Several genetic pigmentation disorders have mutations in proteins governing melanosome structure, leading to leakage and endogenous melanogenic cytotoxicity [7, 8].

Melanosome structures can be divided into four distinct stages (I, II, III, IV) along their biogenesis pathway [9, 10] (Figure 1.2). The first two stages are unpigmented and collectively known as early melanosomes or premelanosomes as melanin synthesis has not initiated yet. Stage I melanosomes are lysosome-like spherical organelle that are developing an intraluminal proteinaceous fibril matrix [11, 12]. In stage II the fibril matrix in the melanosome is completed and the organelle morphologically transitions to an ellipsoid shape. In stage III melanin synthesis begins. The melanin is deposited onto the fibril scaffold yielding progressively thicker and blacker fibrils that are eventually completely concealed by stage IV [13]. Stage IV melanosomes are fully opaque and mature with virtually indistinguishable internal structures.

	Stage I	Stage II	Stage III	Stage IV
Shape	Spherical	Elongated	Elliptical	Elliptical
Structure		Fibril striations	Melanin deposits on fibrils	Melanin accumulates to conceal fibrils
TYR/TYRP1/TYRP2		YES	YES	YES
Melaninization			initiation	finishes
Color			Brown	Dark brown/black

Figure 1.2 Melanosome features.
Melanosomes are segregated by their differentiation state from Stage I pre-melanosomes to Stage IV fully differentiated, mature melanosomes [14]

The genes regulating pigmentation are highly specific and tightly regulated to the fully mature, pigmented melanocyte. As the remainder of the project will reference the pigmentation/differentiation genes, several key genes are listed here with brief descriptions.

Tyrosinase protein 1 (TYRP1/ gp75) – TYRP1 is a melanocyte-specific transmembrane glycoprotein that is localized to the melanosome and cell surface of melanocytes [15]. TYRP1 expression is tightly restricted to fully differentiated melanocytes and is only present in stage III and IV melanosomes. TYRP1 plays an enzymatic role in melanin synthesis and a role in stabilizing tyrosinase protein and modulating its catalytic activity. TYRP1 is also implicated in maintenance of melanosome structure. In mice, mutations in TYRP1 (Oculocutaneous albinism type 3) result in a pigmentation defect with the appearance of a brown coat rather than a black coat [16]. TYRP1 expression is regulated by MITF (Microphthalmia-associated transcription factor) and is activated from Stage III onwards [17].

Tyrosinase (TYR) – Tyrosinase is a catalytic oxidase and acts as an enzyme for the rate-limiting step controlling the production of melanin [9, 12]. TYR expression is regulated by MITF. TYR protein is sorted into melanosomes and is only present in stage III and IV melanosomes limiting expression to fully differentiated melanocytes.

Melanocytes Protein PMEL (PMEL/gp100/silver) is the main component of stage I and II melanosomes and gives the melanosome its defined shape. In the absence of PMEL, melanosomes do not form fibrillar structure and maintain enlarged, rounded appearance [9, 18]. PMEL expression is regulated by MITF and is activated from Stage I onwards.

Melanocyte microenvironment

Melanocytes are found in the epidermis, iris, heart, ear, nasal cavity, brain and adipose tissue [19-27]. For the purpose of this study we will focus solely on epidermal melanocytes and epidermal-derived melanoma. There are two distinct types of epidermal melanocytes: Hair Follicle (HF) Melanocytes and Interfollicular (IF) melanocytes.

The primary purpose of melanin is to serve as a protective barrier against harmful UV rays. As melanocytes only make up a small portion of the epidermis, this protection would be virtually useless if the melanocytes did not share the melanin with adjacent cells. The confined melanosome allows for efficient

downstream transfer of intact, pigmented melanosomes to neighboring keratinocytes. The distribution of melanosomes to keratinocytes affords an even color distribution and protection across the epidermis.

Sun exposure activates p53 in keratinocytes, increasing their production of Proopiomelanocortin (POMC) (Figure 1.3). Differential processing of POMC results in the production of ACTH, α-melanocyte-stimulating hormone (α-MSH), β-MSH, γ-MSH, and other hormones including β-endorphin (β-END) and β-lipotropic hormone (β-LPH) [28]. Binding of α-MSH to MC1R on neighboring melanocytes activates MITF and results in increased melanin production [29]. In return, keratinocytes actively engulf the melanosome-containing dendritic processes of the melanocytes yielding an even distribution of pigmentation [30].

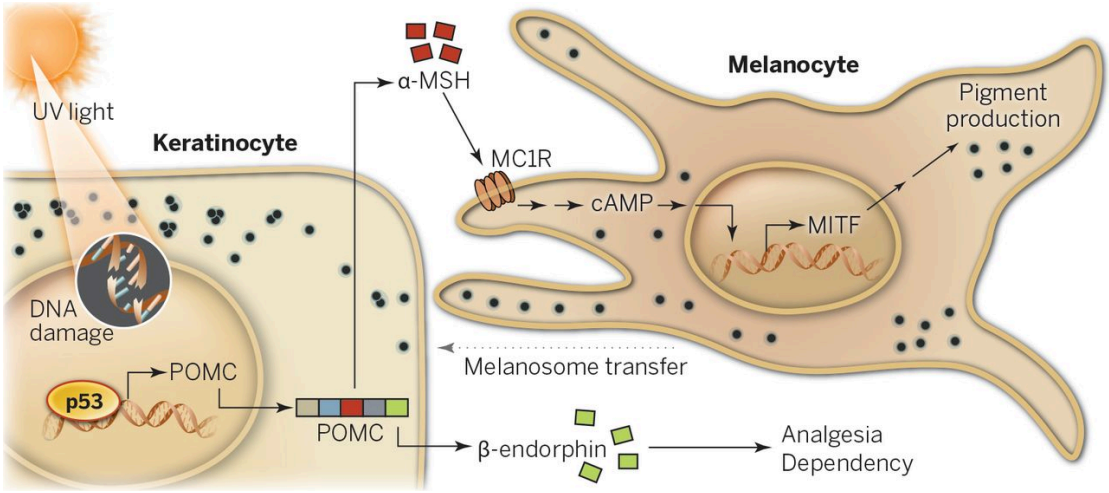

Figure 1.3 Cutaneous response to UV radiation.
The UV rays of tanning drive p53-mediated upregulation of proopiomelanocortin (POMC) in keratinocytes. Post-translational cleavage of POMC leads to secretion of α-MSH and stimulation of MC1R on adjacent melanocytes. MC1R stimulation results in melanin synthesis and eventual transfer of melanin-containing vesicles (melanosomes) to keratinocytes. *[31] (adapted from Lo et al. 2014)*

The decision between pheomelanin and eumelanin is regulated at multiple levels with multiple inputs. A key regulatory input is the melanocortin-1 receptor (MC1R) on melanocytes [32]. The importance of MC1R was first discovered with the realization that mice with a mutated extension locus display a reddish blond coat rather than the black coat typically found in the C57BL/6 background [33]. When wild-type (WT) MC1R is activated by its agonists α-melanocyte-stimulating hormone (α-MSH) and adrenocorticotropic hormone (ACTH) it leads to the downstream conversion of adenylyl cyclase into cyclic adenosine monophosphate (cAMP). cAMP accumulation promotes the activation of protein kinase A (PKA) which in turn phosphorylates cAMP responsive binding element (CREB). Phosphorylated CREB is a transcription factor that directly upregulates microphthalmia transcription factor (MITF). MITF is the “master transcription factor of melanocyte development” and actively upregulates a pigmentation transcriptional program including TYR, TYRP1, and TYRP2 [34].

Hair follicle (HF) melanocytes are responsible for pigmenting hair. In the adult hair follicle, the pigmentation unit resides in the hair bulb immediately on top of the dermal papilla (DP) fibroblasts and consists of approximately five keratinocytes for every melanocyte. Pigmentation results from a complex signaling network between the three cell types [35]. The DP fibroblasts secrete TGF-beta signaling to regulate the rate of melanocyte division [36]. Keratinocytes secrete a series of factors (including bFGF, ET-1, IL-1α/1β, ACTH, α-MSH, PGE_2/$PGF_{2\alpha}$, GM-CSF, NO, TNF-α, NGF, BMP-4) to regulate melanogenesis,

melanocyte dendricity and melanocyte proliferation [14, 36]. The melanocytes secrete melanin encapsulated in melanosomes to protect the fibroblasts and keratinocytes.

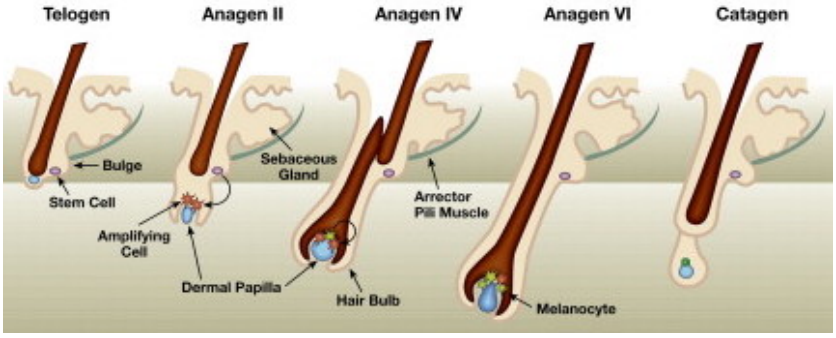

Figure 1.4 Hair follicle pigmentation is regulated by the hair cycle.
Melanocytes sit at the base of the hair bulb and release pigmented melanosomes into the shaft to pigment the hair follicle. HF melanocyte turnover is carefully regulated by the natural hair follicle cycle [37]. (adapted from Steingrimsson et al. 2005)

Hair follicle pigmentation is largely controlled by the natural hair cycle. The hair coat of mammals constantly turns over throughout the adult life of the animal (Figure 1.4). To generate each new hairs, existing follicles undergo cycles of growth (anagen), regression (catagen) and rest (telogen) [38]. Follicular melanogenesis is stringently coupled to the anagen (growth) stage of the hair cycle during which time HF melanocytes transfer melanin granules into keratinocytes to form pigmented hair shafts. During each anagen phase, hair follicles generate an entirely new hair shaft from tip to root, including new hair follicle melanocytes. For human scalp hair, the typical anagen growth phase lasts 3 years but can last up to 25 years in extreme cases [39, 40]. During catagen proliferation and differentiation cease and there is extensive apoptosis. During

telogen the hair follicle largely rests, as there is no significant proliferation, apoptosis or differentiation. Follicular melanogenesis is off for both catagen and telogen [35]. Telogen can be followed by exogen wherein the club hair is lost. Exogen does not happen in every hair cycle.

The interfollicular (IF) melanocytes are typically distributed at infrequent but regular intervals along the basal layer of the epidermis (Figure 1.5). The IF melanocytes are surrounded by keratinocytes with their respective density ranging from about 1:4 to about 1:10 depending on the location within the skin [27]. IF melanocytes bind to the basal lamina via integrin receptors, and attach to surrounding keratinocytes by E-cadherin–mediated attachments [30]. Interestingly, the number of melanocytes is not correlated with race or gender [41]. Rather, darker skin is simply the readout of more active melanocytes, as all individuals have approximately 1500 melanocytes per square millimeter of skin surface. Contrary to the cyclical nature of HF melanocytes, epidermal melanocytes pigment continuously. Pigmentation levels are modulated in response to global hormonal signals and local UV exposure.

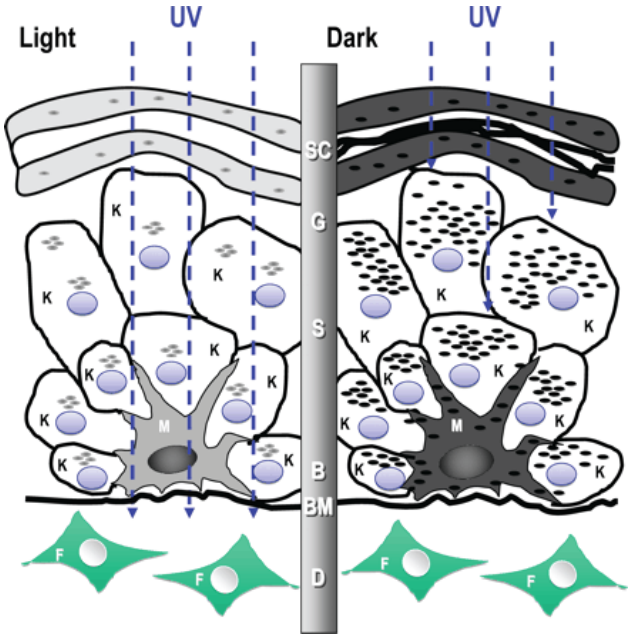

Figure 1.5 Interfollicular melanocytes.

Interfollicular or epidermal melanocytes sit at the interface of the basement membrane and the keratinocyte layer. IF melanocytes are very dendritic and contact a large number of keratinocytes [14]. Light skinned and dark skinned individuals have the same number of melanocytes but the melanocytes from dark skinned individuals produce more melanin. From top to bottom: SC, stratum corneum; G, stratum granulosum; S, stratum spinosum; B, stratum basale; BM, basement membrane; D, dermis. Cell types: K, keratinocyte; M, melanocyte; F, fibroblast; shaded oval, melanin granule (adapted from Yamaguchi 2007) [42]

Hair follicle and interfollicular melanocytes are morphologically distinct despite sharing a common cell of origin in the early epidermis. The stage IV HF melanocytes are bigger, more dendritic, and more mature than their IF counterparts [43]. The HF melanosomes are similarly larger with more expanded Golgi Apparatus and rough endoplasmic reticulum [44, 45]. The diversity in melanosome structure results in divergent fates for the melanin product. Eumelanin produced by the epidermal melanocytes degrades in the differentiating layers of the epidermis. Conversely, eumelanin granules transferred into hair cortical keratinocytes remain minimally digested leading to similarly pigmented proximal and distal ends of a typical scalp hair shaft [44].

Melanocyte developmental biology

Neural Crest biology

Melanocytes are derived from the transient, migratory population of cells unique to vertebrates known as the Neural Crest Cells (NCC). The neural crest is defined during gastrulation and is at the edge of the neural plate on the border between the neural and non-neural ectoderm (Figure 1.6). The neural plate forms out of the embryonic disc opposite the primitive streak and its location is dictated by the notochord. The neural plate is visible around 4 weeks of development in humans and it differentiates into neuroectoderm [14]. During neurulation, the NCCs or neural fold (bordering the neural plate) fold up at the dorsal midline and form the neural tube [46, 47]. The NCCs that form the roof of the neural tube (opposite the notochord) undergo an epithelial-to-mesenchymal transition (EMT) before migrating away to give rise to a diverse population of differentiated cells. NCC derivatives include both mesoderm (smooth muscle cells, osteoblasts, adipocytes, chondrocytes) and ectoderm cells (melanocytes, schwann cells, neurons) [46]. Neural crest stem cells express the transcription factor Sox10 and can be isolated by an antibody to p75 [48]. Sox10 expression is required for maintaining pluripotency of the Neural Crest population and this population is co-labeled with crestin early in development of the zebrafish embryo [49-53]. The fates of the crest cells are defined in part by the anatomic location within the roof plate; with NCC traditionally grouped as either cranial, vagal, trunk or sacral [54]. Facial melanocytes are mainly derived from the cranial NCC while the remainder of the body is primarily seeded with melanocytes derived from the trunk NCC.

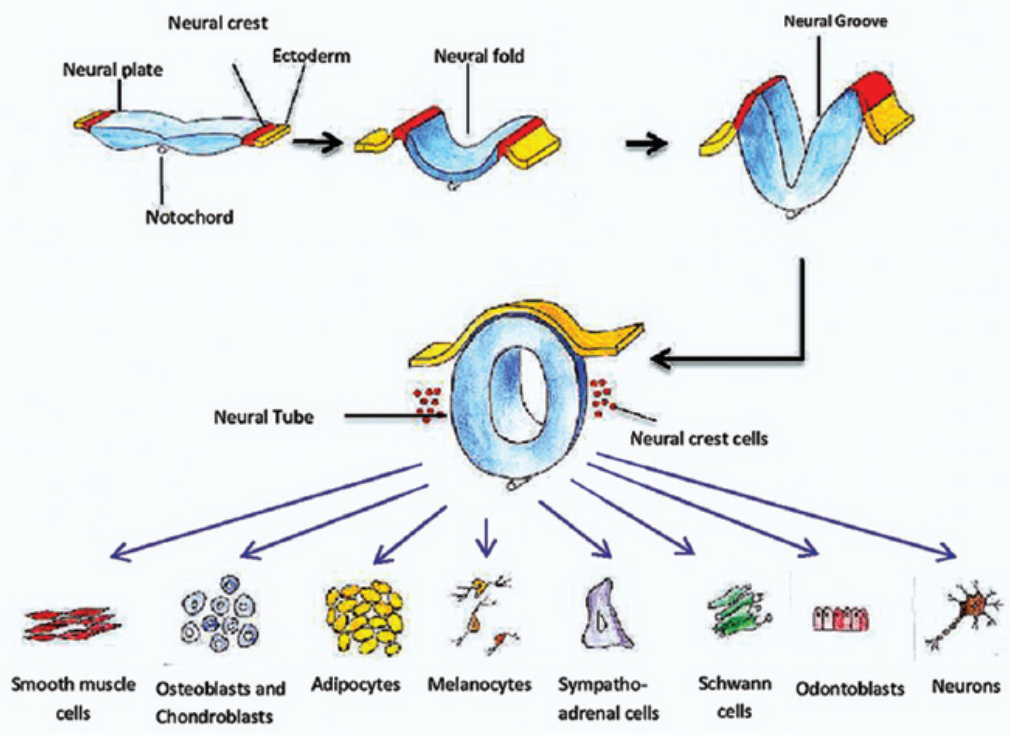

Figure 1.6 Neural crest pluripotency and migration.
NC cells migrate from the tip of the neural tube to diverse locations during embryogenesis and give rise to a variety of cell types in the adult. (adapted from Shyamla 2015) [55]

The genes regulating neural crest differentiation and specification are tightly regulated and often essential to NC survival. As the rest of the project will reference several neural crest genes they are listed here with brief descriptions.

SRY-box 10 (SOX10) – SOX10 expression is first detected right before NCCs delaminate from the neural tube and expression persists in some NCC derivatives including Schwann cells and melanocytes. SOX10 expression is essential for NCC survival, as mutations in SOX10 in both mice and zebrafish lead to cell death within the neural crest lineage and a wide-range of neural crest derived defects into adulthood, including melanocyte loss [52, 56]. SOX10 has been demonstrated to maintain multipotency and inhibit neuronal differentiation

of NCC *in vivo* [57]. There are species-specific differences in the regulation of SOX10 as SOX10 is maintained throughout melanocyte differentiation in humans but is down regulated in melanoblasts in zebrafish and mice [58].

Crestin (*ctn*) – Crestin is a functionally uncharacterized zebrafish gene that is a member of a family of retroelements [59]. Crestin expression marks the neural crest during embryonic development, but becomes undetectable by ~72 hpf. Interestingly, crestin is specifically upregulated in melanoma tumors in adult zebrafish [53]. Given the essentially zero background in adulthood, *crestin* reactivation is a selective marker for tumor initiation [60].

Endothelin receptor type B (EDNRB) – EDRNB is not specific to NCC, but its expression in NCC is turned on by SOX10. EDNRB is a G-protein-coupled receptor that activates a phosphatidylinositol-calcium second messenger system in response to ligand (endothelin) binding. Hirschsprung disease type 2, is due to homozygous loss of EDNRB, which leads to defects in NCC and enteric neuron migration [61]. Furthermore endothelin signaling can induce phenotype switching in melanoma cells *in vivo* [62]

SRY-box 9 (SOX9) – Sox9 is another member of the Sox family of transcription factors. SOX9 differentiates cells derived from all three germ layers and its expression is not limited to the NCC population. Furthermore, a subset of both ectoderm- and endoderm-derived tissues continue to express *Sox9* in adult

mature organs [63]. Interestingly, SOX9 is expressed in melanocytes in both neonatal and adult human skin and is upregulated by UVB exposure [64].

Melanoblast biology

In melanocyte (MB) development, neural crest stem cells are first restricted to a bipotent glial-melanocyte lineage progenitor that is common to Schwann cells before further differentiating into unpigmented, but melanin producing, committed melanoblast [65]. During human development, melanoblast migration takes place around six to eight weeks of development and the majority of MB are localized within the epidermis by 12-13 weeks [14]. While migrating to their final location, MB will multiply [66]. Human melanoblasts migrate to the basal layer of the epidermis where they reside either in the hair bulge or surrounded by keratinocytes (forming pigmentation units) to serve as precursors to the mature, pigmented melanocytes. The neural crest cells that will become melanocytes are known to up regulate MITF (microphthalmia-associated transcription factor). However, there remains some uncertainty over whether melanocyte fate is determined prior to or during migration [67]. MITF is a master regulator of melanocyte development and acts a transcription factor responsible for controlling much of melanocyte development including activation of dct (dopachrome tautomerase) [34, 68, 69]. The differentiation and maturation of melanoblasts into pigmented melanoblasts occurs concomitant with colonization of the hair bulb and expression of tyrosinase, oca2 and pmel.

The genes regulating melanoblast differentiation and specification are tightly regulated. They are essential in cementing the fate of melanocyte precursors during the period prior to pigmentation. As the rest of the project will reference several melanoblast genes they are listed here with brief descriptions.

Microphthalmia-associated transcription factor (MITF) – MITF is the "melanocyte master regulator" and is the earliest known marker of commitment to the melanocyte lineage. MITF is first expressed in melanoblasts shortly after neural crest emigration and its expression is used to label melanoblasts *in vivo*. MITF is an important transcription factor for driving melanocyte pathways regulating pigmentation (Dct, tyrosinase, Trp1) and later melanocyte survival (Bcl2) [70]. Moreover, ectopic expression of MITF in fibroblasts is sufficient to drive pigmentation [71, 72]. Intriguingly, once melanoblasts express *mitf* mRNA, their survival becomes dependent on functional MITF protein [70]. The SCF/cKIT, Wnt, and αMSH/MC1R pathways regulate the transcription of MITF (Figure 1.7). The following proteins also have a demonstrated impact on MITF expression: Pax3, CREB, Sox10, and Lef1 [73, 74]. There are several different splicing isoforms of MITF with varying 5' exons that have differing documented roles. A specific isoform (MITF-M) is uniquely expressed in melanocytes [75]. MITF is upstream and regulates the expression levels of DCT, TYR, TYRP1, and MITF itself [17]. Distinct from the human genome, the zebrafish genome has two copies of the MITF (*mitfa* and *mitfb*) that appear homologous to distinct isoforms generated by alternative mRNA splicing of the single mammalian human MITF

gene [76]. The zebrafish mitfb is sufficient to rescue pigmentation of the retinal pigment epithelial cells but not neural crest melanoblasts in the absence of mitfa. The mitfa promoter has been used to effectively drive expression in the body melanoblasts and melanocytes of the embryonic and adult zebrafish with only limited expression in the eye [74, 77].

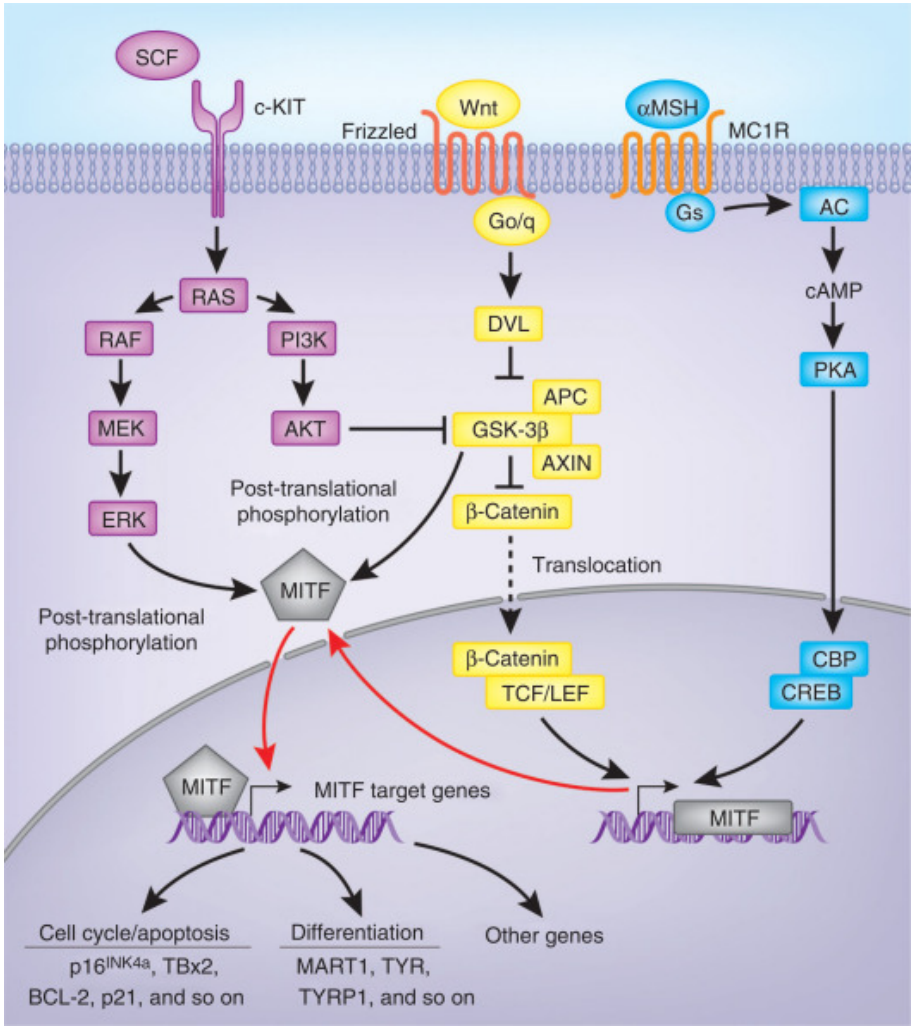

Figure 1.7 Regulation of Microphthalmia-associated transcription factor (MITF).

MITF dictates the pigment cell phenotype by regulating melanocyte-specific genes involved in melanoblast survival, lineage commitment, and melanocyte proliferation and survival. MITF expression, post-translational modifications, and down-stream pathway are strongly influenced by multiple upstream pathways, including c-Kit (purple), Wnt/β-Catenin (yellow), and α-MSH (blue) [78]. (adapted from Hocker 2008)

Dopachrome tautomerase (DCT/TYRP2/tyrosine-related protein 2) – DCT is downstream of MITF and is frequently used as a marker of melanoblasts during development or melanocyte stem cells within the adult skin. Mice with a homozygous deletion for DCT are viable and do not show any abnormalities in DCT-expressing sites (skin, retinal pigment epithelium, substantia nigra) [79]. However, the mice are do have reduced melanin content in their hair resulting in a dilute coat color. Interestingly, primary melanocytes cultured from the $DCT^{-/-}$ mouse are viable and show a normal distribution of TYR and TYRP1. While DCT is not essential for the melanocyte lineage it is an important genetic marker of the melanoblast. DCT is also frequently referred to as TYRP2.

Mast/stem cell growth factor receptor (cKIT/ SCFR /CD117) – cKIT is a receptor tyrosine kinase whose primary ligand is stem cell factor (SCF) [80]. Ligand binding leads to the prototypical receptor tyrosine kinase (RTK) dimerization and cross-phosphorylation with downstream cascade signaling typically via the MAPK or PI3K pathways. KIT expression is not restricted to the melanocyte lineage. KIT plays a critical role in the development of a variety of mammalian cell types including hematopoietic progenitor cells, mast cells, primordial germ cells, and intestinal cells of Cajal [81]. Emphasizing its role in development, homozygous deletions for either cKIT or SCF are embryonic lethal. In melanocyte differentiation, Transcription Factor Activator Protein 2 alpha (TFAP2α) activates expression of cKit, which in turn stimulates a pathway activating transcription factor Microphthalmia (Mitf). Furthermore, KIT is an

oncogene with activating mutations found in melanoma, gastrointestinal stromal tumors, testicular seminoma, mast cell disease, and acute myeloid leukemia [82]. The role of cKIT in the various stages of melanocytes development has been dissected using a cKIT-blocking antibody [83]. cKIT is required for NCC migration into the dermis and for melanocyte proliferation in the epidermal layer. However, cKIT is dispensable for the periods while melanocytes establish themselves within the epidermis or while melanocytes integrate into the developing hair follicle.

Adult Stem Cells

Tissue resident stem cells in adulthood

While some tissues within the body are perpetually renewing (i.e. blood, testis, gut), the majority of the cells and tissues within the adult body exhibit a very low and occasionally undetectable level of turnover. Amongst the organs with low turnover, some tissues rapidly regenerate in response to injury (i.e. liver and muscle) while still others are less resilient (i.e. brain, heart). The inability to regenerate following injury was interpreted as an absence of tissue-resident stem cells. However, the paradigm has shifted with the appreciation that even non-renewing, post-mitotic tissue like the brain has a low level of cell turnover [84-88]. Over the past several decades, tissue-resident adult stem/progenitor cells have been identified and characterized in almost every organ of the body [84, 89-99]. This new appreciation for tissue-resident adult stem cells brought an explosion of

proposals and research on how best to exploit this population for regeneration and anti-aging therapeutic interventions [100, 101].

Aging is linked to a loss of stem cell activity and the resultant diminished ability for tissue regeneration. The mechanism of diminished stem cell capacity with age appears to be cell-type specific [102-109]. Some tissues have been demonstrated to have a decrease in quantity of tissue-resident stem cells with age, while still other tissues paradoxically see an increase in quantity. Independent of the mechanism, all tissues to date have shown a decreased capability of tissue resident stem cells in aging.

Melanocyte stem cells in adulthood

Adult epidermal melanocytes are long-living cells with an unknown lifespan, which is presumed to be in the decades. By contrast, adult human hair follicle melanocytes proliferate, differentiate and subsequently die by apoptosis each hair cycle. This means that HF melanocytes die every 3-8 years at the end of each hair cycle [44]. Given that subsequent hair follicles are also pigmented, researchers have long hypothesized the presence of tissue resident stem cells within the epidermis [110, 111]. Extensive research has established the presence of precursor cells in the epidermis that are not irreversibly fated to become melanocytes [112-117]. Independent research groups have identified precursor cells within the epidermis and coined them melanocyte stem cells (MSCs), Skin-Derived Precursor (SKP) cells, dermal stem cells (DSCs), epidermal-neural crest

stem cells (EPI-NCSC), or Schwann cell precursors (SCPs). The relationship between some of these precursor cells in the skin is unclear as each cell type has been identified and studied independently. However, it is clear that there are stem cells within the epidermis that remain pluripotent into adulthood and are transcriptionally comparable to NCCs.

A melanocyte stem-cell (MSC) compartment for mice was first identified in the hair follicle bulge (Figure 1.8) [36]. Beginning each hair cycle, the MSC asymmetrically divides yielding a melanocytes precursor that migrates down to the hair bulb while maintaining an undifferentiated melanocyte stem cell in the hair bulge. Single cell transcriptional profiling from mouse hair follicle melanocyte stem cells revealed high expression of Pax3 and DCT with notable absence of pigmentation genes tyrosinase, pmel, Mc1r. Interestingly, Melanocytes stem cells lacked expression of melanoblast markers Ednrb, Kit, sox10 and mitf [118]. The presence of Melanocyte Stem Cells (MSC) is conserved in the hair bulge in humans [36, 119].

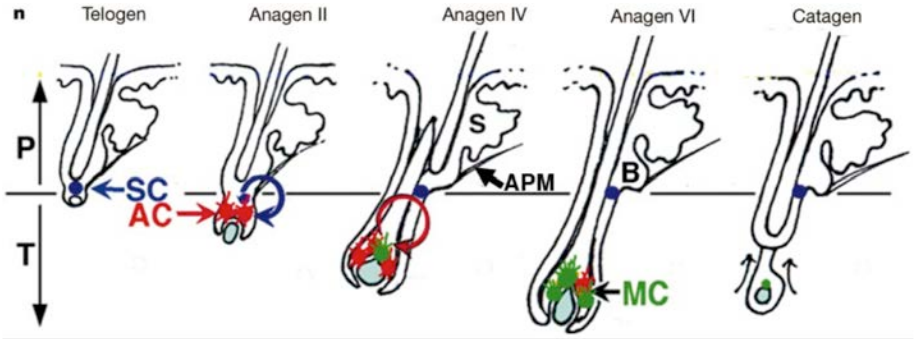

Figure 1.8 Schematic of melanocyte behavior during hair cycling.
Melanocyte stem cells (SC, blue) are maintained in the hair bulge throughout the hair cycle, and are reactivated at early anagen to supply amplifying progeny (AC, red) to the hair matrix, where most of them mature into differentiated melanocytes (MC, green). B,

bulge region; S, sebaceous gland; APM, arrector pili muscle; P, permanent portion; T, transient portion [36]. (adapted from Nishimura 2002)

Skin-derived precursor (SKP) cells were discovered by the Freda Miller lab and are localized adjacent to the follicle dermal papillae (Figure 1.9). SKP cells express high levels of the neural crest markers Slug, Snail, Twist, PAX3, SOX9, p75, and Nestin [120]**.** SKP cells are exclusively stimulated in anagen and shut down during telogen in a hair cycle dependent manner. Importantly, akin to NC cells, the SKP cells migrate to the sympathetic ganglia, skin, spinal nerve and DRG when transplanted into a stage-30 chick embryo *in ovo* [120]. Finally, these studies have gone on to show that explants of these adult NCCs can be expanded clonally and differentiated into mesodermal and peripheral neural progeny including adipocytes, skeletogenic cell types, and Schwann cells [120-124]. The ability to differentiate into both germ layers argues that these cells are truly undifferentiated progenitors that are not yet programmed towards any particular cell fate but rather retain a pluripotency akin to neural crest cells. While the majority of the characterization work was done on mouse derived SKP cells, a human equivalent has been isolated and characterized from adult foreskin [125]. Interestingly, foreskin does not contain hair follicles so the human equivalent isolated to date is likely not associated with the DP but rather deeper in the dermis [126].

Dermal Stem Cells (DSCs) are neural crest-like progenitor cells that reside deeper in the dermis and have been studied by the Meenhard Herlyn lab. Akin to SKPs, DSCs are isolated from human glabrous foreskin (Figure 1.9). To focus on

precursors from outside the hair follicles, the epidermis and basement membrane of foreskins were dissected away from the dermis prior to isolating DSCs [127]. Therefore, DSCs are multipotent cells that reside deep in the dermis. DSCs grow as three-dimensional spheres, display a capacity for self-renewal and express NGFRp75, nestin and OCT4, but not melanocyte markers. In addition, cells derived from single-cell clones were able to differentiate into multiple lineages including melanocytes. Finally, Li et al. demonstrated using a three-dimensional (3D) skin reconstruct model that DSCs home to the epidermis to differentiate into melanocytes.

EPI-NCSCs are neural crest-derived multipotent stem cells that persist into adulthood and have been studied almost exclusively by the Sieber-Blum lab [116, 128]. EPI-NCSCs reside in the bulge of hair follicles rather than the Dermal Papillae like the SKPs. EPI-NCSCs also express neural crest markers. Further microarray analysis demonstrated that SKP cells are transcriptionally comparable to neural crest cells rather than melanoblasts [129]. Importantly, these studies have gone on to show that explants of these adult NCCs can be expanded clonally and differentiated into mesoderm (osteocytes) and ectoderm (melanocytes) [130]. While the majority of this work was done on mouse derived SKP cells a human equivalent has been isolated and characterized from the hair bulge of adult skin [130]. As these cells are easily accessible and expandable, they have been extensively studied as a potential therapeutic source for cell replacement therapy.

Fate mapping studies have show that melanocytes can also arise from Schwann cell progenitors associated with nerve fibers following injury [131, 132]. Furthermore, the SCPs have been demonstrated to serve as a stem cell niche for neuroendocrine cells of the adrenal medulla [133]. While it is unclear if in the absence of injury melanocytes in the adult repopulate through this mechanism, SCPs have been proposed as another cell source with NCC-like capabilities.

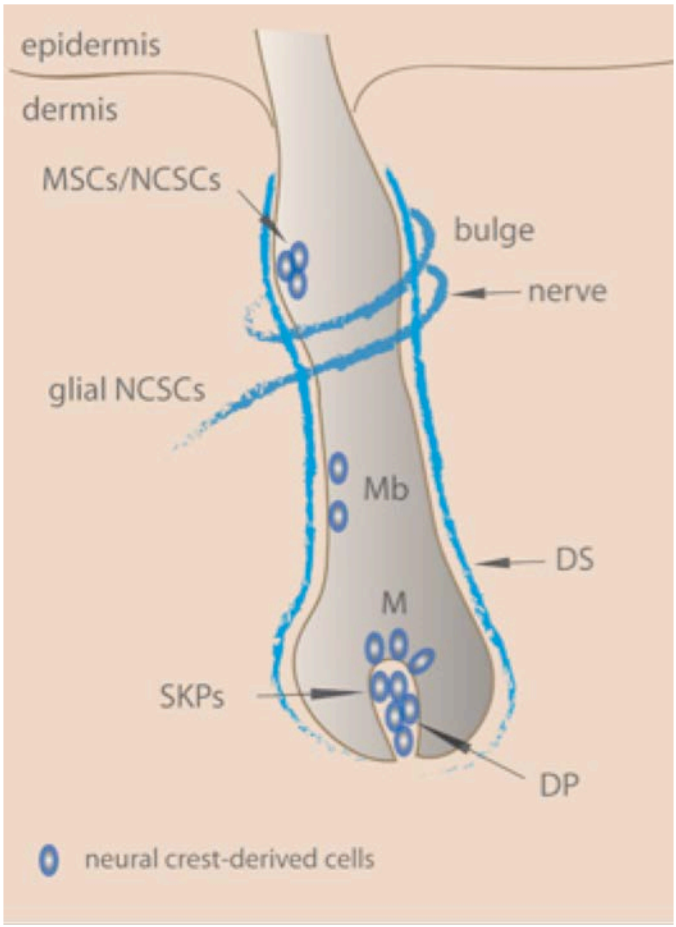

Figure 1.9 Summary of neural crest stem cell precursors in the hair follicle.
The adult skin harbors NCSC-like precursors into adulthood in the bulge (MSCs), dermal papilla (SKPs), dermis (dermal stem cells, not shown) or adjacent to glial cells (glial precursors) [134]. (adapted from Shakhova 2010)

1.2. Melanoma

Disease

Epidemiology

Melanoma is derived of the melanocyte lineage and is the deadliest form of skin cancer, despite accounting for less than 2% of skin cancer cases [135]. If diagnosed early, melanoma can often be cured by surgical resection. However, upon metastasis, melanoma is extremely deadly. Unfortunately, rates of melanoma have been steadily rising over the past 30 years. The American Cancer Society estimates that 91,270 new melanomas will be diagnosed (about 55,150 in men and 36,120 in women) and about 9,320 people will die of melanoma this year [135]. Melanoma is predominantly diagnosed in the elderly with the average age of melanoma diagnosis being 63 years old [135]. However, epidemiological studies have demonstrated a positive association between early age sunburn and subsequent risk of melanoma [136].

Diagnosis

Melanomas typically present as an asymmetrical, irregularly bordered, multicolored or tan/brown spot or growth that continues to increase in size over time. They can often be mistaken for normal moles, which are common small, round brown spots on the skin resulting from melanocytic overgrowth that appear early in life and are similarly caused by sun exposure. Melanoma can be distinguished from moles by changes to the shape or color of existing moles or

appearance of new moles. Early signs of melanoma are summarized by the mnemonic “ABCDE” (Figure 1.10) [137].

- **A**symmetry
- **B**orders (irregular with edges and corners)
- **C**olor (variegated)
- **D**iameter (greater than 6 mm (0.24 in), about the size of a pencil eraser)
- **E**volving over time

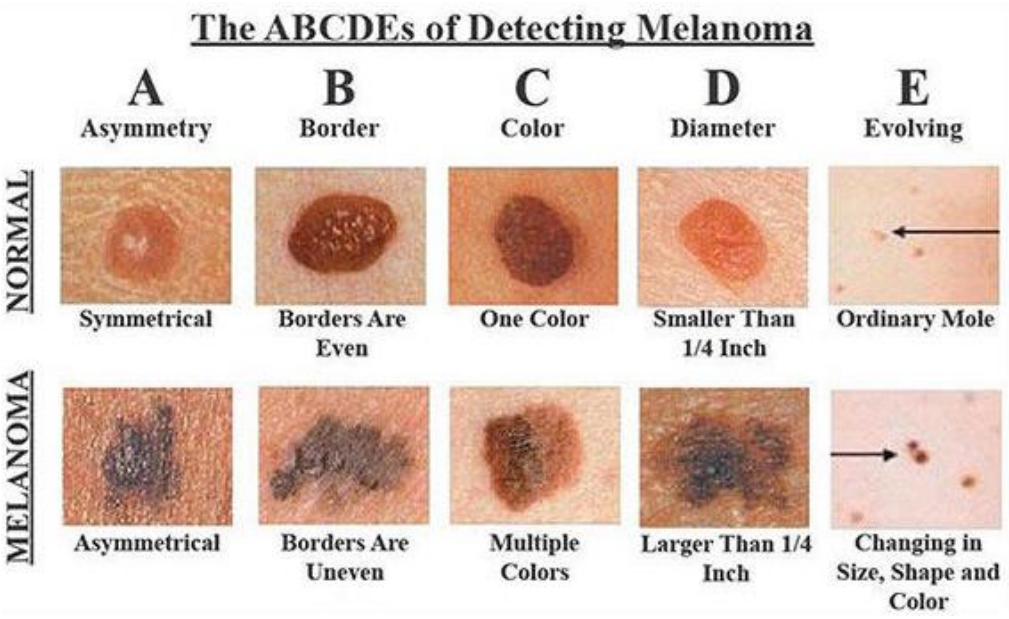

Figure 1.10 The ABCDEs of Melanoma.
Malignant melanoma can be differentiated from non-malignant, normal, melanocytic overgrowth by the ABCDEs [138]. (adapted from www.skincancer.org)

Prognosis

Melanoma progression is divided into either radial or vertical growth. Radial growth is defined by horizontal progression within the epidermis parallel to the surface. The prognosis for melanoma still in the radial growth phase is excellent

as metastases are very uncommon. Vertical growth is characterized by progression perpendicular to the surface, penetrating the deeper tissue. Penetration into the subcutaneous layer is accompanied by access to blood and lymph vessels with the potential to metastasize portending poor prognosis [139].

The depth of cancer progression is a strong predictor of patient outcome. The depth of melanoma progression has historically been described using “Clark level” and “Breslow’s depth” scales. Clinically, melanoma is classified into five different stages (ranging from 0-4) depending on the cancer progression. The first stage (stage 0) is melanoma in situ. Stage 1 is characterized by tumors that are up to 1 millimeter thick. Stage 2 melanoma means a tumor that has grown more than 2 millimeters thick. Stage 3 melanoma is no longer decreed by size but by the spread of cancer to the lymph system or regional skin sites. Finally, stage 4 is characterized by the spread of cancer to distant skin or other organs of the body.

The five stages are used to categorized patients and prognosticate drug treatments and survival statistics. Early stage melanomas that have not spread are easily treated surgically. However, once melanoma has metastasized beyond the lymph nodes surgery is no longer curative and patients must be treated with more systemic therapies including chemotherapy, radiation therapy, targeted therapy and immunotherapy. Despite the clean segregation along staging lines,

melanoma is extremely heterogeneous between patients and staging is not sufficient to prognosticate every tumor.

Risk Factors

Cancers arise as a result of genetic mutations that lead to uncontrolled proliferation unhinged from normal environmental cues. The primary source of DNA damage in melanoma is mutagenic ultraviolet light from the sun [140]. However, other non-UV sources of DNA mutations (as in the BRAFV600E gene) occur through as yet undefined mechanisms. On average, melanoma patients have the highest DNA mutation rate among all cancer patients (except those patients with inherited deficiencies in mismatch repair or DNA polymerase mutations) [141]. The sites of mutations within the genome appear to be chance, but ≥60% of mutations follow a confirmed UV mutation signature of converting a cytosine to thymine at a dipyrimidine site [142, 143]. The majority of somatic DNA mutations will be extraneous to cell survival or function and will not impact cell fate. Yet other DNA mutations will be deleterious to cell survival, resulting in cell death. Still, a small percentage of random mutations can cause cancer by activating oncogenes or inactivating tumor suppressors and driving a heritable growth advantage.

Avoiding direct sun exposure by taking shade or utilizing sunscreen is the best protection against harmful UV exposure. However, humans do need sunlight for Vitamin D and to maintain a healthy lifestyle [144]. Fortunately, melanin serves

as the body's natural sunscreen for when we don't avoid the sunlight. The protective nature of melanin can be easily read out through the epidemiology data proving darker skinned individuals are naturally more refractory against melanoma. Statistically, the lifetime risk for melanoma is only 0.1% for black skinned individuals, while rising to 0.58% for Hispanics, and 2.6% for white skinned individuals [135]. White skinned people are 20 times more likely than black skinned people to get melanoma.

Genetics

In a large-scale DNA sequencing project of melanoma, Hodis et al. found 86,813 coding mutations across 121 tumors for a median mutation rate of 14.4 coding mutations per megabase (Figure 1.11) [145]. This is the highest median mutation burden amongst all cancer types [146]. Given the heterogeneity and volume of mutations between patients, distinguishing driver mutations from passenger mutations has been difficult. As a result, computational methods (MutSig and InVEx) have been utilized to identify statistically significantly mutated genes (SMGs) based on patient-specific mutation frequencies and spectra, mRNA expression levels, and gene-specific DNA replication times. The 13 SMGs were identified as oncogenes BRAF (52%), NRAS (28%), IDH1 (5.7%), DDX3X (6.3%), RAC1 (6.3%), and MAP2K1 (5.1%) and tumor suppressors CDKN2A (13%), TP53 (15%), PTEN (8.5%), NF1 (14%), RB1 (3.8%), PPP6C (7%), and ARID2 (14%). In addition to mutations, copy number variations are commonly found in KIT, PDGFRA, VEGFR2, CDK4, CCND1, MDM2, TERT, PD-

L1, and MITF. Using the available experimental data and mutual exclusivity of certain oncogenes, The Cancer Genome Atlas (TCGA) established a framework for genomic classification of melanoma into four subtypes: mutant BRAF, mutant RAS, mutant NF1, and Triple-WT (wild-type). The mutant BRAF subgroup accounts for nearly half of the patients and is by far the largest subgroup.

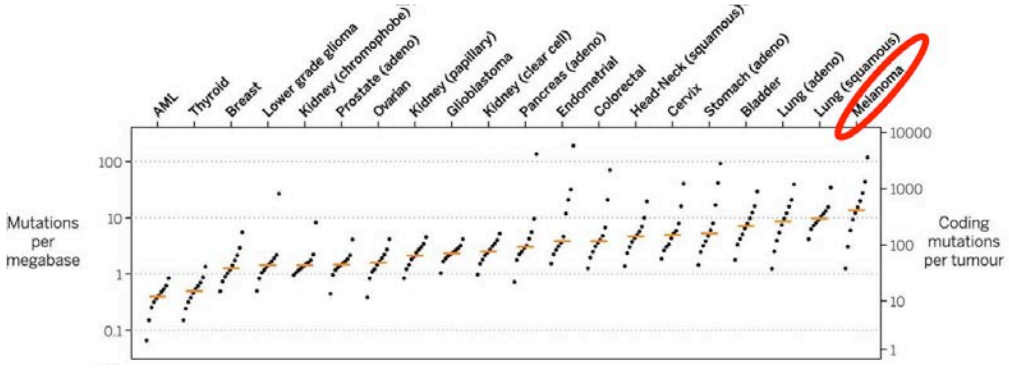

Figure 1.11 Melanoma has the highest mutation rate amongst cancers.
Melanoma (red circle) has the highest mutation burden amongst 20 tumor types with an orange bar denoting the median burden of all samples [146]. (adapted form Martincorena, 2015)

While functional testing is necessary to verify all the driver mutations, the large sequencing projects have clearly elucidated that melanoma is the result of a series of mutations and no single mutation is sufficient to drive tumorigenesis. This finding collaborates the popularly held paradigm that most cancers result from an accumulation of mutations over time with each successive driver mutation causing a wave of progressively faster growth [147-149]. Each mutation alone is unlikely to yield a proliferative advantage, and may actually hinder growth. But the clones that amass the greatest pro-growth combination will inevitably outcompete neighboring cells to form a tumor. Remarkably, many of

the mutations verified to support tumor growth can already be found in normal healthy skin [147]. The most common mutation in melanoma ($BRAF^{V600E}$) is positive in roughly 80% of pre-malignant nevi [150-152], further supporting the notion that melanoma arises from an accumulation of mutations.

Non-Coding Mutations in Melanoma

Beyond the widespread manipulations in DNA, melanoma is also regulated by noncoding changes in both epigenetics and non-coding RNA. Epigenetics refers to reversible modifications of the genome that activate or inhibit transcription. Several epigenetic regulators (including IDH2, TET1/2, EZH2 and SETDB1) are frequently mutated in melanoma leading to widespread epigenetic changes with downstream roles in tumor growth [153-155]. In addition to mutations in the open reading frame of epigenetic regulators, oncogenes (including TERT) can be transcriptionally induced by mutations in the promoter region [156, 157]. As well as genetic mutations provoking epigenetic changes, melanoma is frequently characterized by aberrant promoter methylation in the absence of mutations, leading to transcriptional silencing of important tumor suppressors (including CDKN2A, PTEN, and MGMT) [158-162].

To model the epigenetic changes during melanoma initiation, Fiziev compared two isogenic cells human foreskin melanocyte lines where one line has been transformed by viral induction (via $BRAF^{V600E}$ overexpression and knockdown of PTEN). The group carefully profiled the cells both transcriptionally and for over

35 epigenetic modifications [163]. This study found that conversion into tumorigenic melanocytes is coupled with loss of histone acetylation and H3K4me2/3 specifically on regulatory regions proximal to specific cancer regulatory genes but not at a global level.

Only 2% of the human genome sequence is translated into proteins [164]. Initially the remaining 98% of the genome was thought to be “junk DNA”, but recent advances in sequencing technology has illustrated that up to 70% of the junk DNA is actually transcribed into non-coding RNA (ncRNA) transcripts [165]. While ncRNA is not translated into proteins, ncRNA play a vital role in protein coding gene expression with essential roles in development and cancer. ncRNA have been shown to directly impact regulation of differentiation, apoptosis, cell proliferation, and metastasis [166-168]. Some studies have found that melanoma becomes addicted to the ncRNA signature for growth. Appreciation for the impact of ncRNA in melanoma has led to their use as prognostic markers of melanoma. Epigenetics and ncRNA are likely important mediators of therapeutic response that are underappreciated.

MAPK pathway

Receptor tyrosine kinases (RTKs) are a class of transmembrane proteins (including EGFR, IGFR, FGFR, TrKA/B, PDGFR) on the outer cell surface that respond to mitogen from the microenvironment [169]. Mitogen binding will typically stabilize RTK dimerization driving subsequent trans-phosphorylation by

its partner receptor that leads to the initiation of an intracellular signal pathway. This phosphorylation enables docking proteins such as GRB2 to bind the RTK, which in turn binds the guanine nucleotide exchange factor Son of Sevenless (SOS). Binding activates SOS to remove the GDP from an inactivated member of the RAS family (notably H-RAS and K-RAS). RAS activates by binding GTP. Activated RAS activates the protein kinase activity of the RAF family (notably BRAF). BRAF is a serine/threonine protein kinase that activates the MAPK/ERK signaling pathway with an oversized role in melanoma. Activated RAF kinase dimerizes and phosphorylates MEK (MEK1 and MEK2). Following activation, MEK phosphorylates and activates mitogen-activated protein kinase (MAPK or ERK). ERK regulates translations by phosphorylating ribosomal protein S6 kinase along with a whole range of survival, proliferation and transcription signals via binding to transcription factors C-myc, ETS, JUN, FOX, MNK, CREB [170].

To avoid aberrant MAPK signaling, the pathway is kept under tight control with a whole series of feedback mechanisms to prevent over activation (Figure 1.12). The extensive negative feedback loops can act either via direct posttranslational modification of pathway components by downstream protein kinases or by the induction of *de novo* gene synthesis of specific pathway inhibitors. Nearly all components of the MAPK cascade are regulated by phosphorylation by downstream kinases on specific amino acid sites leading to reduced activity. ERK1/2 has been shown to directly phosphorylate RTKs, SOS, RAF, and MEK [171-175]. Furthermore, ERK mediated translations activates negative feedback

loops through the expression of phosphatases (including DUSP6) or adaptor proteins (including SPROUTY) [176, 177]. The mitogen specific activation coupled with the numerous feedback mechanisms combine for precise control of the magnitude, duration, and location of MAPK signaling under normal conditions.

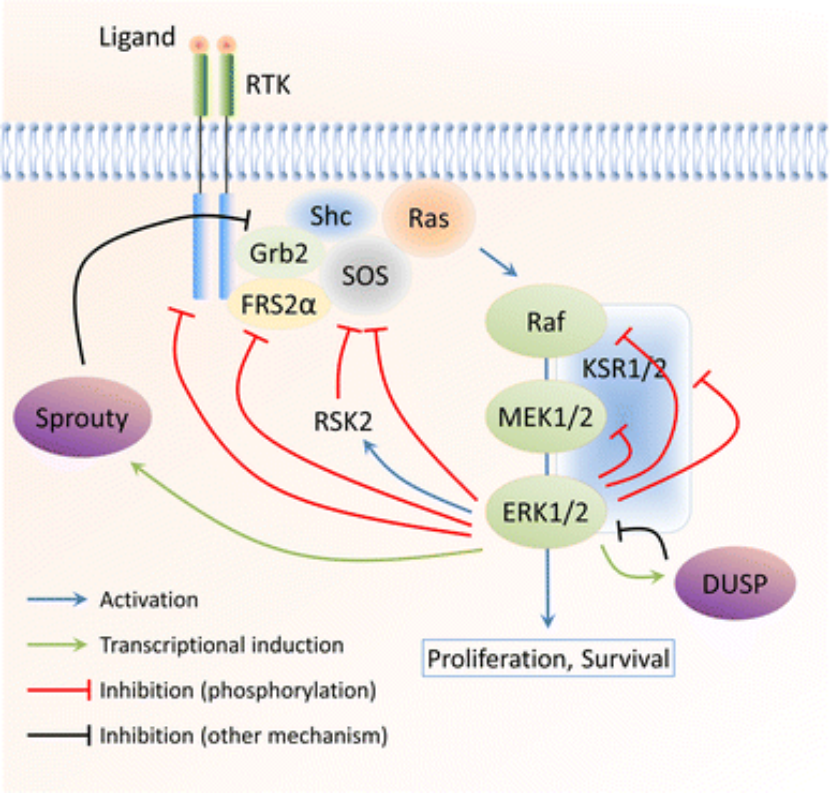

Figure 1.12 Negative feedback within the MAPK pathway.
The MAPK pathway is subject to a large number of negative feedback loops including direct phosphorylation of inhibitory sites by ERK1/2, as well as transcriptionally induced feedback regulators (DUSPs and Sprouty) [178]. (adapted form Lake, 2016)

The mitogen-activated protein kinase (MAPK) pathway is persistently activated in the majority of melanomas. About 40-50% of all melanomas have mutations in the BRAF gene with over 90% of those mutations encoding for a single

nucleotide substitution converting glutamic acid for valine ($BRAF^{V600E}$: nucleotide 1799 T > A; codon GTG > GAG). The second most common mutation is $BRAF^{V600K}$ substituting lysine for valine (GTG > AAG), which accounts for 5-6%. Both mutations constitutively activate BRAF independent of upstream ligand-dependent receptor tyrosine kinase (RTK) [179]. $BRAF^{V600E}$ activates downstream signaling at a rate of 138-fold increase over wildtype BRAF [180]. Furthermore, both mutations are resistant to feedback mechanisms, as $BRAF^{V600E}$ and $BRAF^{V600K}$ no longer require upstream signaling or dimerization to induce downstream signaling.

Targeted inhibitors

Traditional cancer treatment relied on physically targeting the tumor with surgery or radiation. In the early 20^{th} century, chemotherapy brought about a revolutionary way of treating cancer based on its characteristic rapid growth. Chemotherapy encompasses a broad category of drugs that generically inhibits fast dividing cells by targeting cellular division or DNA replication. While both methods are very effective at treating cancer both have significant drawbacks. Surgery is limited to physically contained tumors that are surgically accessible without damaging the healthy tissue. Therefore, surgery is ineffective in treating metastatic melanoma. The improvements in radiation therapy have broadened the scope of treatable tumors but the treatment is troubled by the DNA damage of radiation occasionally leading to future tumor growth. Chemotherapy is

generally effective at inhibiting tumor growth but has a very small therapeutic window as healthy fast growing cells (including hair, the gut) are also impacted.

Defining driver mutations unique to the tumor enables researchers to design targeted therapies that specifically inhibit tumor growth. Leading the charge in melanoma treatment are Mitogen Activated Protein Kinase (MAPK) pathway inhibitors (mainly targeting MEK and mutant BRAF) [181, 182]. Vemurafenib treatment was the first targeted therapy to be approved in melanoma and targets mutant $Braf^{V600E}$ [179, 183]. Despite improved progression-free and overall survival, initial responders inevitably mutate to acquire resistance and reactivation of the mitogen-activated protein kinase (MAPK) pathway [184, 185]. The sustained importance of MAPK signaling was demonstrated by the treatment of BRAF resistant patients with MEK inhibitors [186]. Currently, the standard of care is combined treatment with BRAF and MEK inhibitors which delays progression-free survival and resistance [187, 188]. Even with the dual therapy treatment, patients will relapse with further mutations activating the MAPK pathway [189]. The reliance and perseverance of melanoma to drive the MAPK pathway with each relapse really emphasizes the importance of MAPK signaling in melanoma.

Immunotherapy

Targeted therapy has been plagued by inevitable tumor relapse, encouraging physicians to seek alternative methods of cancer treatment. Immunotherapy

treats cancer by stimulating the immune system to combat the tumor. Immunotherapy falls into two buckets: immune checkpoint therapy and adoptive cell therapy (ACT). Immune checkpoint therapies stimulate the quiescent immune T-cells that are frequently present within melanoma tumors by blocking CTLA-4 or PD-1 signals [190]. Immune checkpoint inhibitor (ICI) trials have been encouraging in a subset of melanoma patients showing durable responses that are still ongoing [191-194]. In analyzing the collection of ICI trials to date, initial antitumor response appears to be a binary event, with most non-responders progressing at a rate consistent with an innate resistance. Innate resistance is attributed to insufficient tumor reactive T-cell generation, inadequate anti-tumor T-cell effector function or impaired T-cell memory [195, 196]. In addition to the innately resistant patients, late relapses are now emerging with longer follow-up of clinical trial populations, suggesting the emergence of acquired resistance likely due to the same three rationales.

Adoptive T-cell Therapy (ACT) is an umbrella term that accounts for various methods to generate a robust immune-mediated antitumor response through the ex-vivo manipulation of T cells. ACT can be accomplished through the ex-vivo selection and expansion of tumor-infiltrating lymphocytes (TILs), or through ex-vivo gene transfer of a synthetic TCR (sTCR) or genetic engineering of chimeric antigen receptor (CAR) into T cells [197, 198]. ACT therapies are much more challenging logistically as each patient requires a tailored cell therapy, making progress slow and expensive. CAR T-Cell therapy has largely been pioneered in

B-Cell ALL with limited efforts to date in melanoma. While demonstrating initial success, patients that do relapse on ACT generally decline due to tumor-antigen escape, lack of ACT-cell persistence, and lack of ACT-cell function. Moreover, as these trials are all very current the enduring impact of these treatments on patient safety and survival will take time to fully evaluate [190, 199]. The next line of therapy appears to be combining immunotherapy with targeted therapy to enhance response rates [200]. Although these novel therapies have drastically improved patient prognosis, better understanding of melanoma initiation and progression may help uncover the mechanism behind the diverse responses amongst patients [201].

Melanoma Transcriptional Heterogeneity

The shift in melanoma progression from radial to vertical growth is coupled with an increased probability for metastasis. This shift to vertical growth is also connected with a presence of heterogeneity within the tumor [202]. The conversion in melanoma has been explained with a variety of different descriptors that is worth exploring further.

Epithelial-to-Mesenchymal Transition (EMT) in Melanoma

Adult melanocytes sit within the basement membrane where they are tightly attached to neighboring keratinocytes enabling crosstalk controlling their morphology, growth, adhesion, and migration [203]. During melanoma initiation

melanocytes must detach these strong bonds with keratinocytes, resulting in unrestrained proliferation and subsequent invasion.

Epithelial-to-Mesenchymal Transition (EMT) is the biological conversion that allows a polarized epithelial cell to break its interactions with the surrounding basement membrane and assume a mesenchymal phenotype. Elizabeth Hay first described EMT when modeling the primitive streak formation in Chick [204]. Since then EMT has been used to describe several processes during development including the migration of neural crest cells. An increased migratory capacity, invasiveness, and production of ECM components characterize EMT. During development, cells undergoing EMT undertake a complete conversion into mesenchymal cells. Upon completion, the cell can migrate away from the epithelial layer from which it had previously been constrained. EMT cells are often molecularly characterized by changes in expression to a series of transcription factors (including ↑SNAIL, ↑SLUG, ↑TWIST), cytoskeletal proteins (including ↓cytokeratin, ↓E-cadherin, ↑N-cadherin, ↑VIMENTIN), and cell-surface proteins (↓ZO-1, ↑Fibronectin) that must be altered to enable migration.

Delamination of cells from the primary tumor to initiate metastases is analogous to the epithelial-to-mesenchymal transition found during development [205]. However, co-labeling of epithelial and mesenchymal programs within the same cancer cell led to the paradigm of a partial or incomplete EMT [206-208].

Experimentally, EMT transcription factors (including SNAIL1, SNAIL2, TWIST1, and ZEB1) are sufficient to induce a partial EMT program [209-212]. EMT transcription factors were shown to increase migration and metastases along with chemoresistance [213-215].

Whether EMT is required for epithelial cancer cells to break ties with the cellular environment and migrate has been an open debate for decades. Several key experiments in GEMM have argued that partial-EMT is dispensable for successful metastasis. Genetic deletion of SNAIL1 and TWIST1 in pancreatic cancer found that partial EMT cells did acquire chemoresistance but that the EMT transcription factors do not directly facilitate metastasis [215]. A study found that ZEB1 deletion impaired but did not entirely prevent metastasis [216]. By contrast SNAIL1 deletion was essential for breast cancer metastasis [217]. Interestingly, a study that looked at breast cancer metastases was able to find cancer cells at the metastatic site without evidence of previous mesenchymal expression [214]. Taken together these studies suggest a complete EMT is not required for metastasis but the necessity and extent of a partial EMT is still open for debate. The confusion may be simply dependent upon the molecular markers analyzed.

Phenotype Switching

The “cancer stem cell” model proposed that a subset of tumor cells possess stem cell-like properties including the ability to self-renew, seed/maintain tumors and

provide a reservoir of therapeutically resistance cells [218-220]. According to the model, cancer stem cells are the source of metastases and relapse following treatment. Cancer therapy inevitably relapses because cancer stem cells are therapeutically resistant and eventually repopulate the entire tumor. While not central to the model, the cancer stem cell model does presume that the tumor initiating subpopulation is rare. As all tumor cells can self-renew, the early 2000s were populated with a rush of studies performing limiting dilution studies to identify and isolate the tumor-initiating cells [221-226]. Landmark work from Quintana et al. found that the melanoma cancer stem cell isn't rare at all, but rather extremely prevalent in all cell lines and patients [227, 228]. These studies characterized the capacity of individual tumor cells to form tumors when transplanted into immunocompromised mice. However, tumor formation in a transplant assay does not necessarily infer the ability of primary tumor cells to invade surrounding tissue to form heterogeneous metastases clinically.

The cellular phenotypes that promote melanoma proliferation and metastatic spreading are not synonymous. Melanoma initiation requires increased cellular proliferation and suppressed cellular senescence. Metastasis requires a more mesenchymal signature with enhanced migration and invasion. Tumor cells transcriptionally chose a "Go or Grow" signature as the cost of a migratory signature is decreased proliferation and vice versa [229].

It was originally hypothesized that metastatic properties arose from a stepwise accumulation of promoting mutations [230]. While some genetic mutations can increase metastatic potential, genetics alone cannot explain the difference between metastatic and primary cancer cells. The alternative explanation is that changing microenvironments drive phenotypic switches in cancer cells enabling metastasis. Phenotype switching implies that any cancer cell has the potential to be a “cancer stem cell” and that the microenvironment is the arbiter rather than supplemental genetic mutations within the cancer cells (Figure 1.13). However, phenotype switching is not mutually exclusive to the genetic paradigm, as certain genetic lesions may permit cells to respond differentially to the microenvironment. Furthermore, there may be a hierarchy of phenotype switching, with a subset of cells bearing stem cell characteristics for prolonged periods.

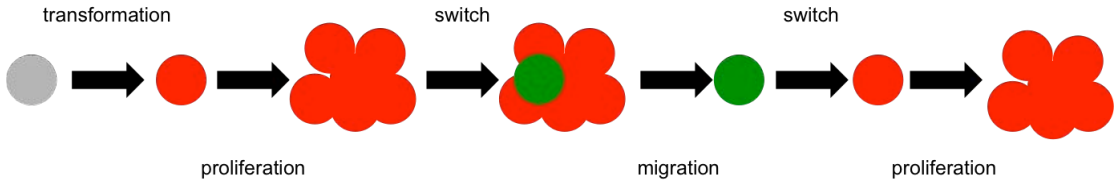

Figure 1.13 Phenotype switching in melanoma.
This is a schematic of transformation and phenotype switching within melanoma. Melanoma cells transfigure back and forth between a proliferative and invasive phenotype [138].

The phenotype switching leading to metastasis is dynamically regulated at the transcriptional level by the tumor microenvironment (TME). The specific factors impacting cell fate decisions are an active area of research. Wnt5a and EDN3b

are two examples of TME derived ligands that directly affect cell motility and invasion of metastatic melanoma [62, 231-234].

Phenotype switching is regulated downstream of MITF in what has been coined the “MITF-rheostat model”. The role of MITF in melanoma is complicated. In melanocytes, MITF induces a G1 cell cycle exit through up-regulation of the $p12^{Cip1}$ and $p16^{INK4a}$ [235, 236]. Additionally, a low level of MITF increases invasiveness (via Dia1) and enhances anti-senescence signaling [237]. Moreover, MITF is known to be down-regulated upon BRAF expression [238]. Paradoxically, MITF is required in melanomas with activated BRAF and is one of the more amplified genes in melanoma [239-242]. Carreira et al. proposed the “MITF rheostat” model to describe the pro and anti-proliferative impact of MITF [237]. The MITF rheostat model proposes that melanoma cells can be clustered into three distinct phenotypes: MITF positive/TYR positive; MITF positive/TYR negative; and MITF negative. The biological readout of MITF expression in healthy melanocytes ranges from apoptosis in the absence of MITF, invasive properties with low MITF, excessive proliferation at intermediate levels and terminal differentiation with very high levels of MITF. The MITF low population has also been characterized as AXL or BRN2 high and therapy resistant [243, 244]. In melanoma, the loss of tumor suppressors likely avoids the irreversible fates of apoptosis or terminal differentiation.

In melanoma, transcriptional profiling of 86 cell lines identified the presence of two distinct phenotypic signatures (Figure 1.14) [245]. One set of cells were weakly invasive, but rapidly proliferating cells that are inhibited by TGF-β. The second set of cells divided slowly but was highly migratory/invasive and was resistant to TGF-β-mediated growth inhibition. The presence of two distinct transcription signatures was independently validated [246]. At first glance the two distinct signatures *in vitro* implied two fixed melanoma states. However, when transplanted *in vivo* both classes of tumors generated heterogeneous tumors with cells of both expression profiles, highlighting the potential of melanoma cells to phenotype switch *in vivo* [247, 248]. Phenotype switching has since been attributed to a host of different environmental cues that drive a more or less differentiated phenotype [62, 249-251]. This relative plasticity within melanoma contributes to (and in some cases is caused by) therapeutic resistance [252].

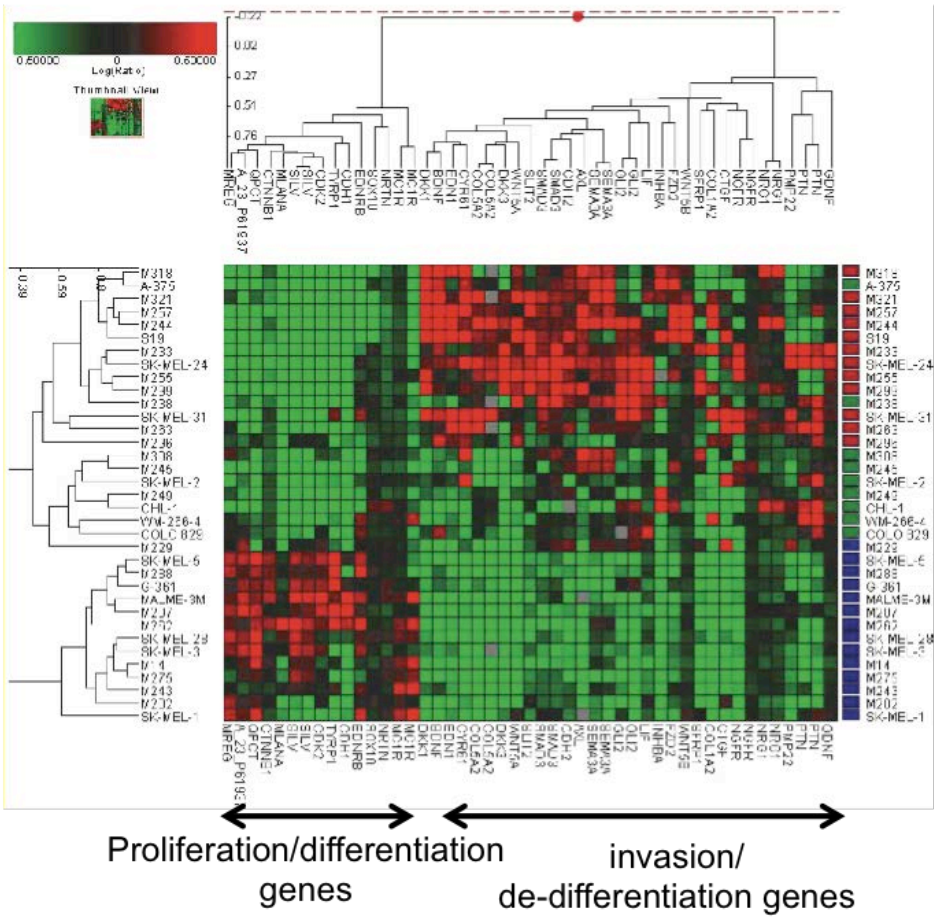

Figure 1.14 Invasive or proliferative states in melanoma.
Supervised clustering of 35 melanoma cell lines based on the expression pattern of selective genes associated with MITF and its downstream signaling pathway, melanocyte function, melanin synthesis, noncanonical Wnt and Tgfβ pathways, and neuronal mediators of NCC development. Two-dimensional clustering of based on the expression generated by an ANOVA [246]. (adapted form Tap et al. 2010)

Re-activation of Neural Crest Paradigm

Animal model of melanoma typically rely on genetic mutations under melanocyte specific control creating a “cancerized field” [253]. However, the majority of melanocytes do not transform, inferring that genetic mutations are not sufficient to initiate a tumor. White et al. found that melanoma initiation is ascribed to a re-activation of a neural crest expression profile in a subset of genetically modified

melanocytes (Figure 1.15) [53, 60]. The tumor initiating cells can be visualized *in vivo* with a reporter for *crestin* expression. *Crestin* is a zebrafish gene that is normally specific to neural crest but is re-expressed in melanoma tumors. The re-activation of crestin is tightly correlated with a re-activation of a general neural crest profile including *sox10*. The re-activation of neural crest is an epigenetic mechanism for cancer initiation. This additional hurdle in transformation helps explain why oncogenic mutations can be so prevalent in adult tissue without a higher incidence of tumorigenesis [146, 147, 152]. Interestingly, de-differentiation in cancer initiation is not unique to melanoma [254-256].

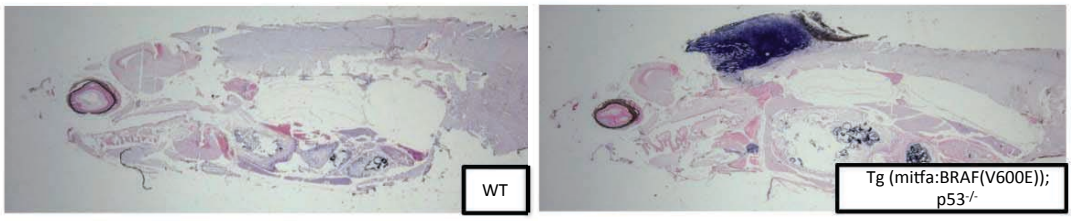

Figure 1.15 Re-activation of a neural crest program in melanoma.
In situ hybridization of sagittal sections of WT and Tg(mitfa:BRAF^{V600E}); p53$^{-/-}$ adults reveal homogeneous crestin expression (blue) only within the dorsal melanoma; it is absent from normal adult tissues [53]. (adapted form White, 2011)

1.3. Modeling Cancer

Cell Culture Models of Melanoma

Melanoma has been historically modeled *in vitro* by surgically capturing melanoma samples from patients and maintaining the cells in culture. If placed under appropriate culture conditions, tumor cells will aggressively propagate and recapitulate many of the cancer phenotypes including tumor growth when

injected subcutaneously into immunocompromised mice. Cellular diversity can be generated by propagating the cells under varying bottleneck conditions or by introducing additional genetic mutations. Alternatively, cancer lines can be generated from patients with different melanoma mutations or features.

Cancer cell lines grown on plastic culture dishes are known to drift genetically and phenotypically from their source. Patient-derived xenografts (PDX) were first described in 1969 as an alternative cell culturing of tumor tissue that more closely resembles the clinic [257, 258]. Melanoma PDX accurately model clinical responses and identify second line combination therapies based on genomic and proteomic profiling [259, 260]. Furthermore, extensive efforts have been undertaken to assemble a comprehensive collection of PDX tumors that represent the heterogeneity of melanoma [261, 262].

Cell line and PDX models have been useful models initiated from established tumors, but neither model offers a platform for studying melanoma initiation. To study melanoma initiation, researchers isolated and transformed primary human melanocytes *in vitro* using a specific set of oncogenes (SV40ER, hTERT, RAS or MET) [263]. The melanoma model was then subsequently improved to include more physiologically common mutations (N-Ras^{G12V}, CDK4^{R24C}, p53^{DN}, hTERT), but at the expense of less transformed phenotypes [264]. Interestingly, expression of the most common melanoma mutation BRAF^{V600E} induces an oncogene-induced-senescence (OIS) in a telomere independent mechanism

[265]. The OIS senescence is commonly found in human nevi suggesting the need for tumor suppressor loss for melanoma initiation as opposed to nevi formation. More recently, human melanocytes have been weakly transformed *in vitro* using genes frequently mutated in melanoma ($BRAF^{V600E}$, sh_p53, $Rb1^{-/-}$) [266]. These models combine to suggest that the over expression of mutant BRAF coupled with loss of tumor suppressors should be sufficient to transform human melanocytes *in vitro*.

Animal Models of Melanoma

Cell culture models are excellent for studying cell-intrinsic mechanisms of melanoma in a controlled environment. However, cancer does not develop in isolation, as tumors are constantly interacting with and responding to external signals. Animal models recapitulate cancer initiation and progression in an intact environment.

Xenograft animal models

A xenograft model involves injecting cancer cell lines into animal models to monitor tumor progression. The xenograft animal is a simple and rapid tumor assay that recapitulates parts of the *in vivo* model. Xenograft tumors generally enable speedy tumor formation and metastasis assays. The gold standard host for xenograft studies remains the immunocompromised mouse but recent research has illustrated the benefit of using a zebrafish host for improved *in vivo* imaging and affordable studies at larger scale [62, 267, 268]. The independent

culturing of cell lines and animal hosts allow the researcher to assay the tumor host and source independently. However, xenograft tumors do not recapitulate the appropriate microenvironment or tumor initiation. Additionally, the majority of xenograft tumors require the use of immunocompromised host for tumor formation. Syngeneic models are the exception to the rule and do not require immunocompromised hosts.

UV-induced animal models

Spontaneous animal models of malignant melanoma using UV radiation alone are restricted to a South American opossum (*Monodelphis domestica*), a hybrid fish (*Xiphophorus*), and Angora goats [269]. However, due to concerns with husbandry and experimental manipulations, the majority of melanoma research has been done in mice and zebrafish. UV radiation to generate melanoma in zebrafish is still in the nascent stage [270]. UV radiation in mice is insufficient to induce melanoma when combined with additional transgenic (*tyr*-SV40E, *tyr*-Ras, *tyr*-HGF/SF) or chemical (DMBA) insults [271-274]. UV radiation to generate melanoma is very physiologically relevant to the disease but inherently yields inconsistent sites of mutation, resulting in undefined molecular biology and difficulties in replicating assays.

Transgenic animal models

Transgenic animal models enable researchers to define the molecular genetics and tumor latency when compared to the more physiologically relevant UV-

radiation models. Akin to cellular models of melanoma, overexpression of $BRAF^{V600E}$ in melanocytes leads to OIS and nevi [275]. Transgenic melanoma models have been built in mice when melanocyte driven $BRAF^{V600E}$ or RAS is coupled with tumor suppressor loss of PTEN, CKDN2A, or p53 [276-278]. The established transgenic zebrafish model of melanoma couples melanocyte specific $BRAF^{V600E}$ with p53 mutations [279]. Transgenic models are typically hampered by the inability to distinguish secondary tumors from metastatic spreading. More elegant mouse models of transgenic melanoma have been advanced using inducible cre/lox or tet-inducible expression systems to more cleanly define primary tumor initiation and progression. Finally, some animal models have enabled local induction of transgenesis using lentiviruses for local application of cre recombinase enabling for localized and temporal control of expression [280]. However, these models still require cre/lox genetic backgrounds be established first.

Electroporation

Despite the documented power of transgenic tumor models for mechanism discovery and drug testing, their application poses several significant drawbacks: i) the majority of established models do not exhibit spatio-temporal control, such that the timing and anatomical location of tumor onset remains variable [53, 60, 279], ii) they generally do not enable the introduction of serial somatic oncogenic events for modeling second and third hit mutations after onset [281, 282]; and iii) discerning multifocal primary tumors versus true metastatic spread of a single

tumor is challenging [60]. These issues pose significant limitations for investigating tumor progression and metastasis.

Transplantation-based methods address some of these issues: tumors can be dissected from a transgenic tumor-bearing animal or from patient-derived xenografts (PDXs), and then serially transplanted into recipient animals such as the *casper* recipient strain to allow detailed *in vivo* imaging [267, 268, 283-286]. Alternatively, stable cell lines can be generated from a transgenic animal, such as the ZMEL1 melanoma line, which can be similarly used for transplantation studies [268]. While these transplantation approaches allow for precise spatiotemporal control and are amenable to imaging of metastasis, these experiments often require immunosuppression of the recipients either through irradiation or genetic manipulation of immune cells [285], in addition to the initial generation of the suitable cell line. Recent work from the Langenau lab has shown that syngeneic fish can be used as transplant recipients, but these require that the tumors be developed in that particular genetic background, limiting their broad use across cancer [287]. Furthermore, transplantation cancer models implant foreign tumors into inherently artificial microenvironments. An approach that would enable introduction of oncogenic effects into adult somatic tissue in a spatio-temporally controlled way is therefore highly desirable.

Electroporation applies electrical pulses to generate pores within the cell membrane, enabling extracellular biomolecules (including DNA) to enter the cell

[288, 289]. Electroporation is widely used for stable introduction of DNA elements into cells in tissue culture and into chick and mouse embryos. Electroporation has occasionally been utilized in adult zebrafish but these studies have been limited to cell tracking and transient morpholino knockdowns and has never been applied to cancer modeling [290-293]. Several studies in mice have harnessed electroporation to introduce transgenes into select adult tissues, including retina, muscle, brain, and prostate [294-297] and has been used to model tumors such as pancreatic cancer [294, 298, 299]. However, these approaches require surgery of the mice and can only be limited to a small number of animals at a time, limiting the number of subjects that can be reasonably studied in each experiment. As discussed in Chapter 5 below we have optimized electroporation as a method in zebrafish melanoma modeling.

Human Embryonic Stem Cells

Embryonic stem cells (ESCs) are the population of cells derived from the inner mass of the blastocyst. Phenotypically ESCs are specialized in their ability to self-renew and for their pluripotency. Self-renewal refers to their capability to propagated in their undifferentiated state indefinitely. Pluripotency denotes the ability of ESCs to give rise to any cell within the adult body through a series of fate decisions at the epigenetic level known as differentiation.

Developmental biology research in model organisms has strengthened our appreciation of the intricate balances in signaling required for human development. However, species-specific differences in the signaling

requirements for human development have necessitated the need for direct studying of human cells. Given the ethical and practical concerns of developmental assays in humans, human embryonic stem cells (hESCs) are the best experimental tool available for studying development in a human system. Fortunately, the strong background of developmental research in model organisms can guide the hESC studies for generating testable hypotheses and assays.

The collections of experimental platforms through which ESCs are guided towards specific cellular fates are coined directed differentiations. Directed differentiations are designed to mimic the combinations and temporal regulation of exogenous signaling molecules and their agonists that precursor cells would experience during normal development *in vivo* [300]. The changing cellular fates can then be characterized through gene expression studies to confirm the step-wise activation of genes that recapitulate the progression of cells through developmentally relevant progenitor cells before producing mature differentiated states [301, 302]. A demonstrative example of the faithful representation of progenitor cells produced *in vitro* is the sequential fate potential of hESC-derived neural progenitors to give rise to neurons before becoming gliogenic [303]. Importantly the purpose of this study, hES-derived melanocytes are made via the production of neural crest and melanoblast precursors [8, 304].

The ability to derive virtually any cell in the body provides a platform for disease modeling and eventual cell replacement therapies. Given their replicative potential, hESCs are a source of virtually limitless cells for disease modeling of cells that are difficult to work with due to limited numbers, accessibility or developmental timing. hESC-derived mature cells can generate limitless supplies for modeling fate decisions or performing chemical and genetic screens. For example, the directed differentiations to derive dopamine neurons (the rare population of neurons lost in Parkinson's patients) has enabled researchers to study an otherwise difficult to obtain tissue [305, 306]. Furthermore, the large quantity of dopamine neurons has enabled researchers to envision a cell replacement therapy for treating Parkinson's disease [307, 308].

Embryonic stem cell research has been plagued by ethical concerns surrounding the derivation of embryonic stem cells from aborted fetus tissue. Accompanying funding restraints on federal funding has compounded these ethical issues. In a landmark discovery, Yamanka and colleagues found that four transcription factors (Oct4, Klf4, Sox2, c-Myc) were sufficient to revert fibroblasts back to an induced pluripotent state that exhibited ES-like morphology and pluripotency [309, 310]. The discovery of induced Pluripotent Stem Cells (iPSCs) has alleviated the ethical and practical concerns over the generation of novel lines while enabling researchers to generate isogenic lines from patients of interest. Directed differentiation using iPSCS enables researchers to assay patient specific diseases in genetically matched backgrounds.

Disease specific hESCs have been derived to study a number of diseases and developmental disorders. However, hESCs are a relatively untapped resource in the study of cancer. ESC-derived cancer studies have been limited to the study of familial genetics in cancer prone syndromes (Li-Fraumeni syndrome, Noonan syndrome, Myelodysplasia syndrome) and brain tumors (Diffuse Intrinsic Pontine Gliomas and Glioblastoma Multiforme) [311-320]. Improved techniques in generating iPSCs, directed differentiation, genetic engineering and genetic sequencing analysis strongly suggest the need for more hESC-derived cancer research.

1.4. Hypothesis

Melanoma phenotypes can be traced to the cell of origin

The diversity in pigmentation, cell morphology, genetic expression profile, drug response and growth rate amongst melanoma cells has been a long-established yet poorly understood phenomenon [321-323]. Alan Houghton of MSKCC proposed this diversity may be explained by the differentiation status of the initial cell(s) transformed and sought to compare the surface markers present on melanomas to distinct stages of normal melanocyte development [324, 325]. Recent advances in genetic profiling and immunohistochemistry have supported the notion of two distinct melanoma populations, with one type representative of a more neuronal/invasive gene signature and the second group exhibiting a melanocytic/proliferative gene signature (fig. 1) [246, 247, 326, 327]. These

finding have produced a model that the differentiation status of the tumor is deterministic of the growth rate, pigmentation, transcriptome, and drug resistance profile.

Cancer is characterized by unrestricted, self-renewing cells, eventually forming tumors that deprive healthy tissues of resources. Albeit in a controlled fashion, the ability to self-renew is shared by pluripotent stem cells and naturally present progenitors in the adult. This shared ability to self-propagate led to the hypothesis that progenitor cells may be either more apt to transformation into cancer or more apt to transform with distinct tumor phenotypes. Work in several solid tumor types (rhabdomyosacroma, clear cell sarcoma, etc.) has confirmed the hypothesis, while results in brain cancer contradict this idea [328-331]. Recent work by other labs has established the presence of multipotent melanocyte progenitors within the epidermis of adult humans, opening up the possibility for melanoma genesis from a more pluripotent and less differentiated cell [332, 333]. Uncovering the importance of cell of origin will test the hypothesis that the cell in which melanoma arises dictates its subsequent clinical behavior; providing insights on treating malignant melanomas based on their cell of origin and not just the bulk population.

To address the impact of the differentiation status of the cell of origin on melanoma this study utilizes two complementary systems: human melanocytes derived from iPS cells and a transgenic zebrafish model of melanoma. We have

generated a robust and repeatable protocol for the production of pigmented melanocytes via melanocyte progenitors from human pluripotent cells. We have introduced oncogenic mutations (including $BRAF^{V600E}$) at defined stages of differentiation and characterized the tumorigenic phenotypes both *in vitro* and *in vivo*. To complement the human cell culture work, we have utilized the well-established *in vivo* zebrafish melanoma model to drive tumorigenesis in cells at each progenitor stage. By expressing $BRAF^{V600E}$ under promoters for lineage specific genes we have queried the importance of differentiation status of the cell of origin on melanoma phenotypes *in vivo*.

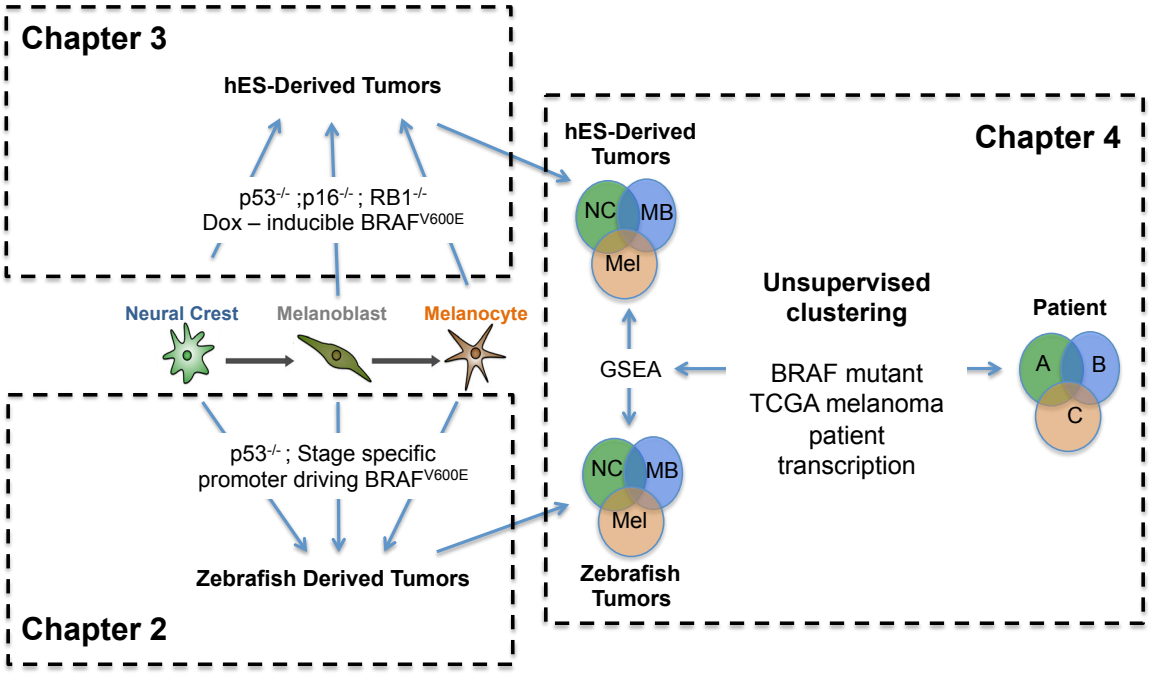

Figure 1.16 Hypothesis: does cell of origin define melanoma?
Chapter 2 will assay the derivation of transgenic zebrafish with melanoma initiated at the neural crest, melanoblast or melanocyte stage by over-expression of $BRAF^{V600E}$ in a p53 deficient background. Chapter 3 will assay the induction of $BRAF^{V600E}$ in an isogenic hES line (WT or TKO background) after directed differentiation to the same three distinct stages. Chapter 4 is the comparison of transcriptional data between the two models and between the models and patient data to instruct novel clustering of patients.

We hypothesize that cell of origin will impact the molecular identify of the resultant tumor. To address this question at the transcriptional level we have first established gene expression data (RNA-sequencing) for tumors derived from each stage of differentiation in both model systems (Figure 1.16). For the hPSC-derived tumor models we have analyzed RNA-sequencing data from *in vitro* transformed cells (n=3 biological replicates for each of the three stages). For the zebrafish tumors, we have dissected whole tumors for RNA-seq analysis (n=6 biological replicates for each of the three stages). We then first assessed whether hPSC-derived and zebrafish tumors independently segregate according to cell of origin using unsupervised clustering and principal component analysis. We have also assessed whether stage-specific differences show comparable subgrouping in the two independent model systems; forming a transcriptional signature for each subtype. Next we utilized the mRNA profiles of all patients from the TCGA dataset (>400 currently) and correlated our signatures with the reported transcriptional subclasses (i.e. “Mitf low”, “Keratin”, “Immune”).

Melanoma modeling in adult somatic tissue

To model how tumors natively form in somatic tissues, we developed a system with precise spatiotemporal control of tumor initiation in a fully immunocompetent adult zebrafish. Here, we report oncogenesis via Transgene Electroporation into Adult Zebrafish (TEAZ). We find that TEAZ allows for the development of complex, aggressive melanomas driven by expression of oncogenic $BRAF^{V600E}$ in concert with loss of the tumor suppressors *p53* and *rb1*. These tumors are highly

invasive and eventually metastasize to distant locations, unlike previous transgenic zebrafish melanoma models, which do not spontaneously metastasize [279]. Because electrodes and DNA solutions can be placed at defined locations, TEAZ allows for delivery of transgenes specifically to the anatomical locations of interest to in less than a few minutes to produce easily scalable models. Given the wealth of functionally uncharted genetic lesions discovered from sequencing human tumors, TEAZ allows for testing of candidate mutations in a rapid, scalable *in vivo* system.

CHAPTER TWO: CELL OF ORIGIN STUDIES IN ZEBRAFISH

2.1 Zebrafish

Zebrafish are a powerful *in vivo* animal model for studying cancer. Zebrafish are small with easy and affordable husbandry enabling very large sample sizes (n=100s). Furthermore, zebrafish rapidly reach sexual maturity and females typically lay up to several hundred eggs per mating. Upon fertilization, the transparent zebrafish embryo develops outside the mother, making the observation and manipulation of the embryos quite simple. The large clutch size, small animal size, and external development allows for easy accessibility to drug and chemical screens [53]. Finally, even adult fish are relatively thin and transparent enabling superior *in vivo* visualization capabilities deep into the animal for monitoring *in vivo* primary tumor growth, metastases and survival rates [62, 268].

Zebrafish melanoma model using transgenesis

Zebrafish are a particularly useful model for genetic studies in vertebrate animals due to the ease of creating transgenic animals. Upon fertilization, the transparent zebrafish embryo develops outside the mother, making the manipulation of the embryos from the single cell stage logistically simple. To insert transgenes into the genome of the fish, DNA is typically injected directly into the single-cell stage with a needle. Originally, transgenes were introduced into the zebrafish germline by injecting naked DNA [334]. However, advances in Tol2 transposable elements

have been coupled with a series of modular vectors that allow for easy plasmid modification and efficient downstream insertions in the zebrafish genome (Figure 2.1) [335, 336].

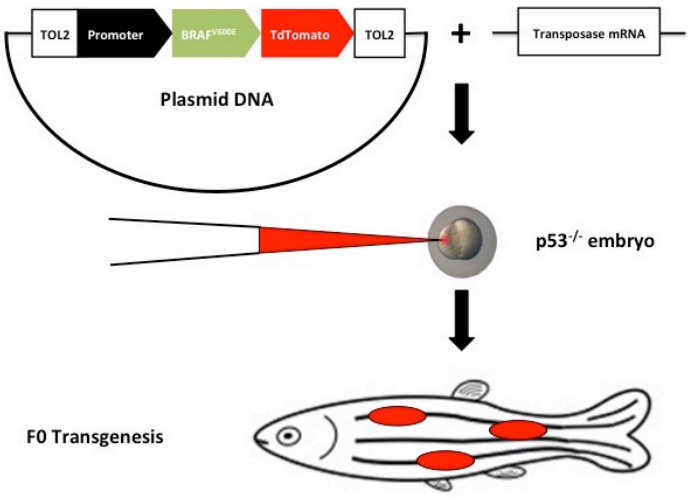

Figure 2.1 Schematic of zebrafish F0 transgenesis.
F0 zebrafish transgenic melanoma fish are engineered by injecting transposase mRNA with TOL2 flanked plasmids encoding a promoter driving BRAF(V600E) fused to TdTomato into p53 deficient single-cell embryos.

The zebrafish offers a powerful *in vivo* system to study the importance of the cell of origin in melanoma due to the well-characterized and highly penetrant melanoma model. The Zon lab established that expression of $BRAF^{V600E}$ under the expression of the melanoblast mitfa promoter in a $p53^{-/-}$ background yielded melanomas within approximately 4-12 months post fertilization (Figure 2.2) [53, 279]. The fish generally develop 1-2 tumors per fish and the tumors closely resemble human melanoma patients at a histological and transcription level.

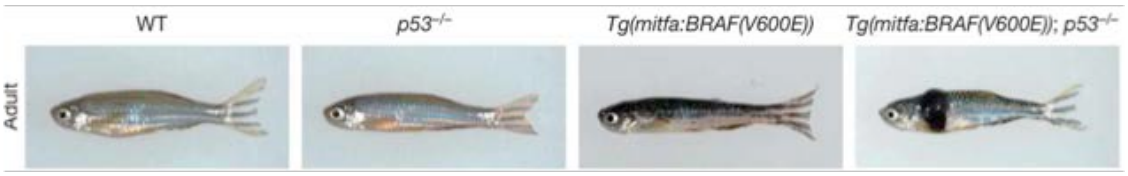

Figure 2.2. Illustration of the 100% penetrant model of zebrafish melanoma.
Zebrafish deficient for p53 develop normally and are indistinguishable from wild-type siblings in terms of viability and fertility [337]. Transgenic zebrafish expressing $BRAF^{V600E}$ under the control of the melanoblast specific promoter mitfa, Tg(mitfa:$BRAF^{V600E}$) develop pigmentation abnormalities but not cancer. Tg(mitfa:$BRAF^{V600E}$) develop melanoma when crossed with p53 deficient fish. (adapted from White, et al. 2011) [53]

The zebrafish melanoma model is 100% penetrant when expressing mutant BRAF in melanocytes of a fish that is p53 deficient. However, neither mutation alone is sufficient to drive tumorigenesis. Fish that are homozygous deficient in *p53* but wildtype for *braf* develop with normal stripe patterns and without melanoma at any penetrance. The p53 deficient fish develop easily distinguishable malignant peripheral nerve sheath tumors (PNST) late in life with a low penetrance [337]. Fish that are wildtype for *p53* but over express mutant BRAF under the *mitfa* promoter develop abnormal stripe patterns with melanocytic patches that resemble human nevi [279]. However, without p53 loss, the mutant BRAF fish do not progress to melanoma. The necessity of two-hits to drive melanoma formation can be reliably exploited to initiate melanoma in distinct cells of origin.

2.2 Results

Tumor penetrance in transgenic zebrafish initiating melanoma at the neural crest, melanoblast, or melanocyte stage

Utilizing the ease of high-throughput transgenesis in zebrafish, we have driven $BRAF^{V600E}$ expression at various stages of melanocyte development using lineage and stage specific promoters that correspond to the neural crest (*sox10*, *ednrb1a*), melanoblast (*mitfa*, *dct*) and melanocyte (*tyrp1*, *pmela*) stages of melanocyte differentiation [60, 279, 338, 339]. Creating stable transgenic tumor lines proved challenging as the oncogenic BRAF was consistently silenced in second generations. Therefore, we moved to a F0 screen using a limited pool of promoters for quantitative studies (*sox10, mitfa, tyrp1*). For each transgenic animal we tracked overall survival and tumor free survival. The mutant BRAF was fused to tdTomato in the transgenic fish so tumors could be easily tracked and excised for histology and expression profiling downstream. The fluorescence also allowed us to censure BRAF independent Peripheral Nerve Sheath Tumors (PNSTs) from our tumor curves.

When mutant $BRAF^{V600E}$ expression was driven by the melanoblast promoter *mitfa* in p53 null fish (n=94 biological replicates), melanomas form with a median survival of 53 weeks (Figure 2.3), reaching 100% penetrance after approximately 71 weeks (data not shown). When mutant $BRAF^{V600E}$ expression is driven by neural crest promoter *sox10* in p53 null fish (n=92 biological replicates), melanomas form with median survival of 21 weeks (Fig. 2.3), reaching 100%

penetrance after approximately 60 weeks (data not shown). Interestingly, when mutant BRAF^{V600E} expression is driven by melanocyte *tyrp1* in p53 null fish (n=49 biological replicates), tumors do not form within the 70 weeks of tracking (Fig. 2.3). The uninjected negative control fish (n= 86 biological replicates) did not develop tumors (excluding BRAF independent PNST) during the tracking.

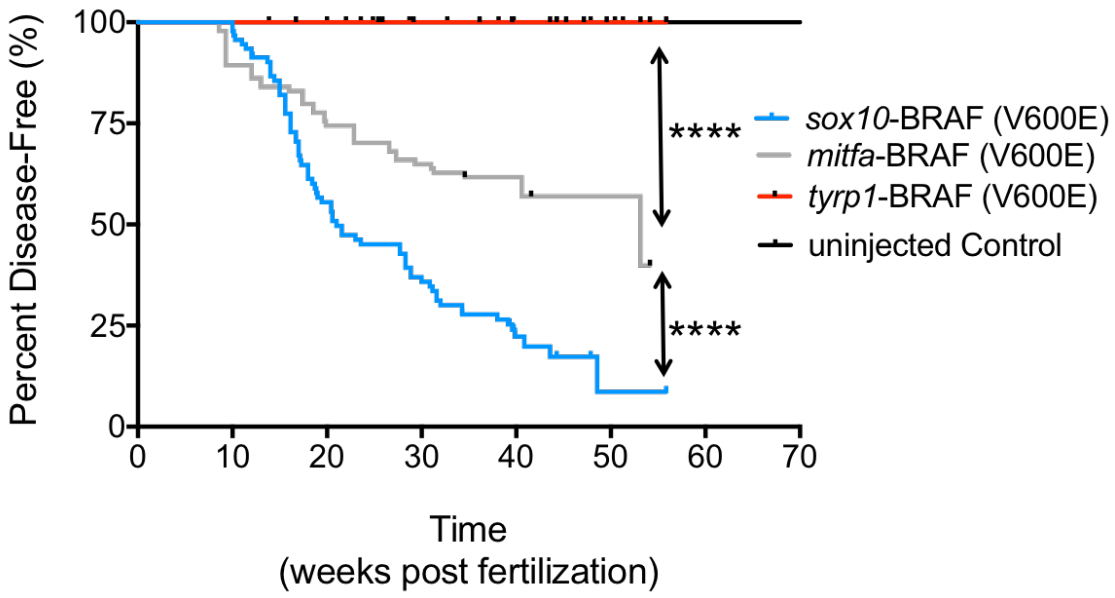

Figure 2.3 Kaplan-Meier curves for F0 transgenic zebrafish survival.
Kaplan-Meier curve of F0 p53$^{-/-}$ transgenic zebrafish injected with plasmids driving BRAF^{V600E} fused to TdTomato under either a neural crest promoter (sox10, n=92 biological replicates), melanoblast promoter (mitfa, n=94 biological replicates), or melanocyte promoter (tyrp1, n=49 biological replicates) or uninfected control (n=86 biological replicates). p < 0.0001 comparing sox10 and tyrp1 curves, p < 0.0001 comparing sox10 and mitfa curves, p < 0.0001 comparing mitfa and tyrp1 curves, log-rank (Mantel-Cox) test.

Characterize zebrafish melanomas generated at melanoblast stages of differentiation:

When the MB mitfa promoter drives mutant BRAF^{V600E} expression in p53 null fish, melanomas develop with 100% penetrance. The transgenic tumors primarily

initiated on the surface of the fish within the dorsal melanocytic stripe near the head or near the tail. Additionally, these fish had very disrupted melanocytic stripe patterns along the body of the fish. Importantly, the tumors consistently appeared of melanocytic origin by location and pigmentation (Figure 2.4). This nicely recapitulated what had been seen in previously published studies [53, 60, 279, 340].

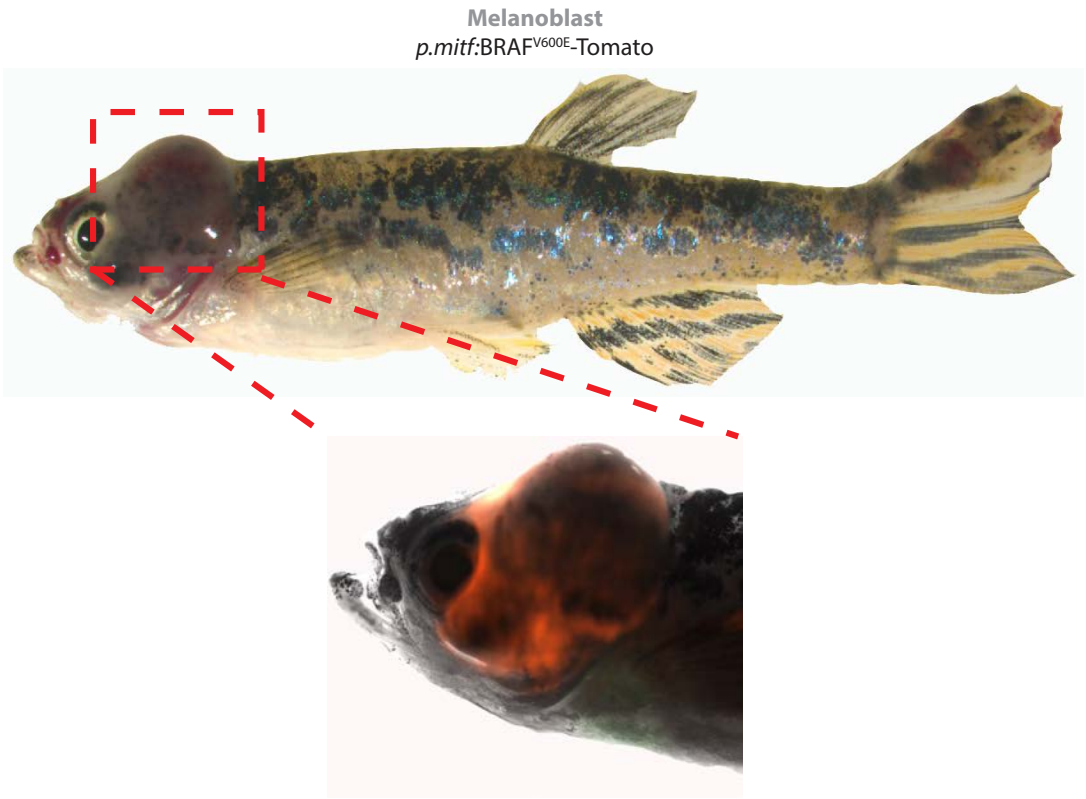

Figure 2.4 Melanoblast tumor
*Representative tumor developed from the mitfa:*BRAF^{V600E}*;p53*$^{-/-}$ *transgenic fish.*

Anecdotally, this finding was re-capitulated when BRAF^{V600E} was expressed using the melanoblast *dct* promoter in the p53$^{-/-}$ background. Survival statistics and transcriptional profiles for the dct promoter were not collected. However, *dct*-

driven tumors strongly suggested a melanoma diagnosis both in both morphology and histology.

Transgenic zebrafish initiating $BRAF^{V600E}$ in a p53 deficient background at the neural crest stage using the previously published *sox10* promoter (n=92) developed tumors faster than the tumors driven at the melanoblast stage [338]. Transgenic zebrafish *sox10* driven tumors developed either in the head or in the body of the fish but deep within the skin; which is not typical for melanoma (Figure 2.5). Additionally, the *sox10* tumors never developed pigmentation suggesting that these tumors were very undifferentiated and perhaps not even melanoma. Finally, the *sox10:*$BRAF^{V600E}$ fish surprisingly did not develop any pigment defects. These finding were supported by identical observations in transgenic fish where the transgene was expressed with the previously published *crestin* promoter or a cloned fragment capturing the *ednrb1a* promoter [60]. Again, survival statistics and transcriptional profiles were not collected for *crestin* or *ednrb1a*.

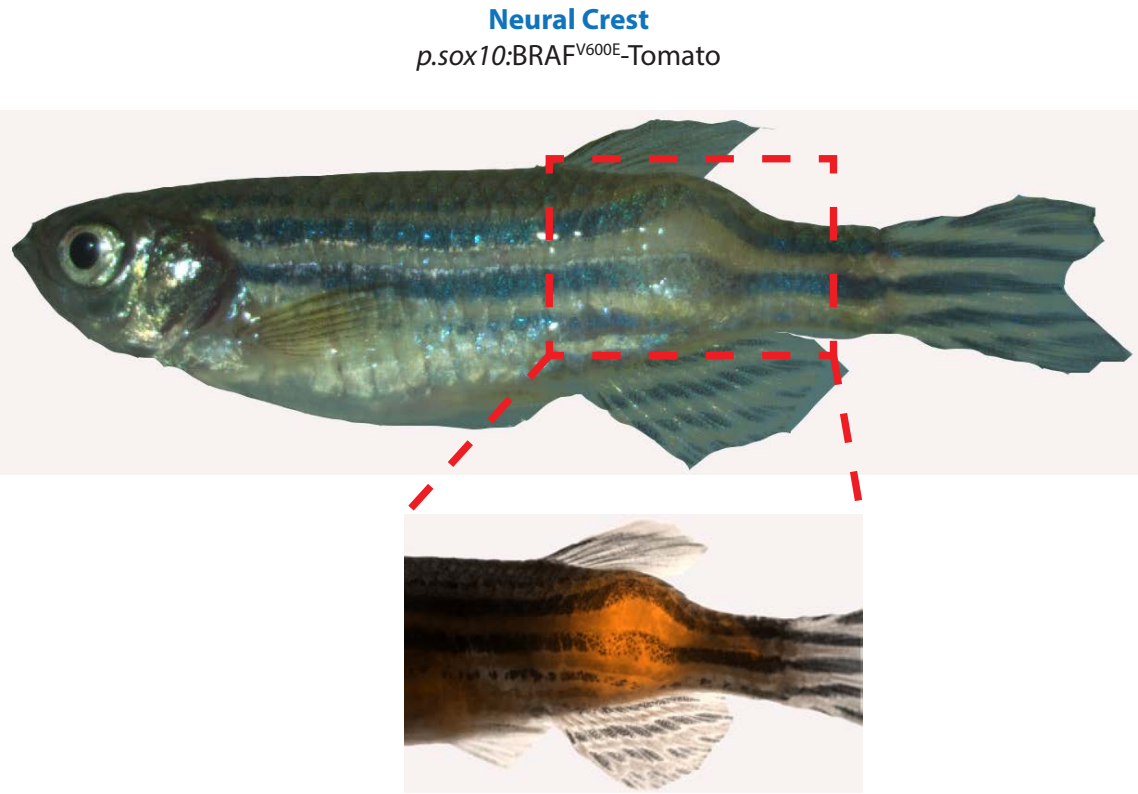

Figure 2.5 Neural Crest tumor.
*Representative tumor developed from the sox10:*BRAF^{V600E}*;p53*$^{-/-}$ *transgenic fish.*

Finally, transgenic fish expressing BRAF^{V600E} at the fully differentiated melanocytic stage using the previously published *tyrp1* promoter (n=49) in a p53 deficient background did not develop tumors [339]. The transgenic fish did occasionally develop pigmentation defects that resemble nevi (Figure 2.6) but the fish generally did not develop any pigmentation defects. While not quantified, expression of *tyrp1*:gfp in embryos demonstrated that the promoter was sufficiently strong and specific to drive expression in melanocytes (Figure 2.7). This was a surprising finding and was phenocopied using a cloned fragment containing the *pmela* promoter in (p53$^{-/-}$; *pmela*:BRAF^{V600E}) transgenic fish. The lack of tumorigenesis with the *tyrp1* promoter suggests that melanoma

tumorigenesis would require additional mutations to originate in a fully differentiated melanocyte.

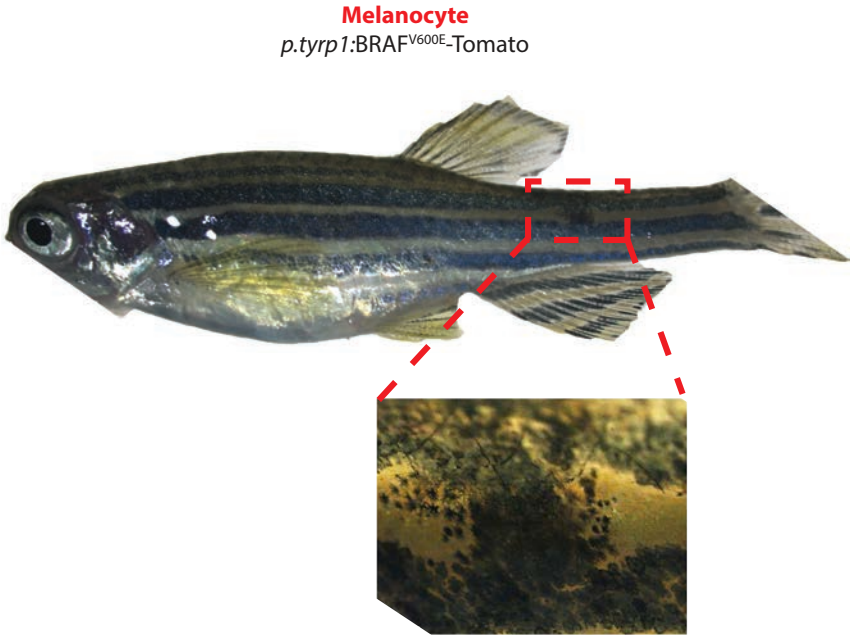

Figure 2.6 Melanocyte nevi
*Representative fish with a nevi from the tyrp1:*BRAF^{V600E} *;p53*$^{-/-}$ *transgenic fish.*

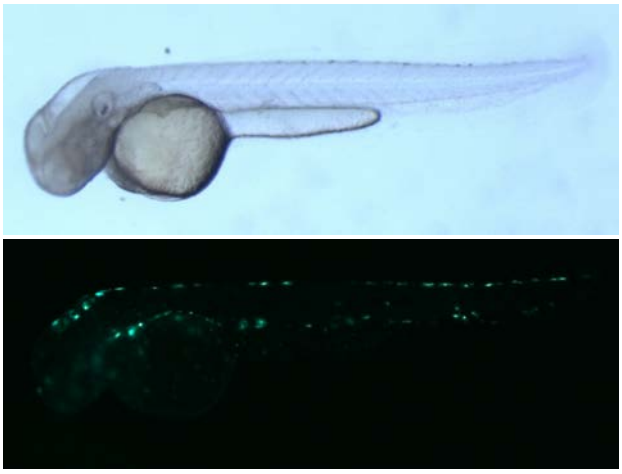

Figure 2.7 Specific *tyrp1*:GFP expression in melanocytes
Representative fish at 48 hpf expressing tyrp1:GFP and treated with phenylthiocarbamide (PTU) to block melanin synthesis. Image is adapted from Dr. Chuck Kaufman (unpublished).

Immunohistochemistry of transgenic zebrafish tumors

To establish the differentiation status of the tumor cells and morphological characteristics, we performed histology post-mortem on several tumor samples from each genotype. The histology slides were graded by pathologists in a blinded manner and compared to human melanomas of diverse origins. Immunohistochemistry was performed for melanoma related antigens to confirm the diagnosis. Immunohistochemistry studies were complicated by the limited availability of specific antibodies for zebrafish antigens.

Histology sections from *mitfa*:BRAF^{V600E} ;p53$^{-/-}$ transgenic tumors stained diffusely positively for BRAF^{V600E} and phospho-ERK confirming the expression of the transgene and subsequent activation of the MAPK pathway in the tumors (Figure 2.8) (n = 2 biological replicates). Pigmentation was visible (albeit sparse) within the sections suggesting a melanoma diagnosis. The tumors also stained diffusely positive for SOX10 expression, which confirms the strong re-activation of the neural crest lineage in melanoma genesis in the zebrafish melanoma model [53, 60]. The *mitfa*-driven tumors did not stain for any of the neuroblastoma antigens used (NCAM, HuC/HuD), confirming the melanoma diagnosis. Finally, the Hematoxylin and eosin (H&E) stain of the *mitfa*-driven tumors closely resembled human melanoma patients, validating the *mitfa*:BRAF^{V600E} ;p53$^{-/-}$ transgenic zebrafish as a relevant model for studying human melanoma.

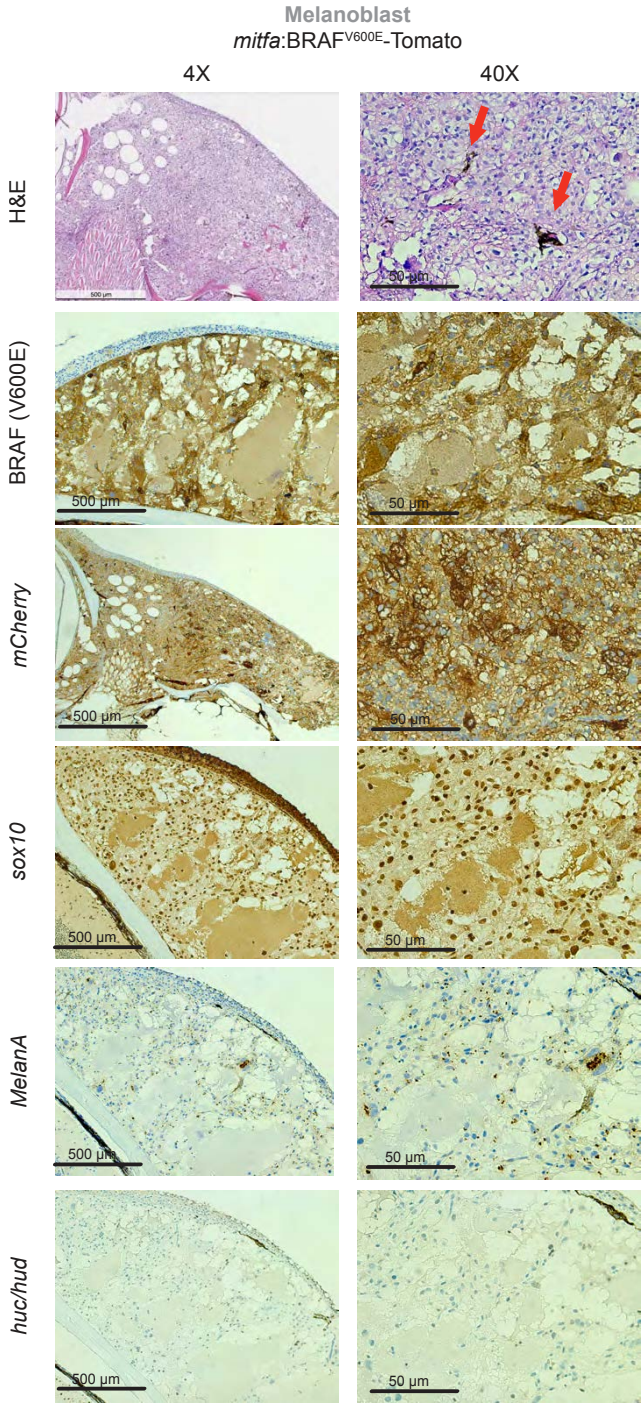

Figure 2.8 Immunohistochemistry of melanoblast-driven tumor from *mitfa*:BRAF^{V600E};p53$^{-/-}$ transgenic zebrafish

Representative tumor was stained for H&E, BRAFV600E, mCherry, sox10, melanA, or huc/hud. Melanin within the tumor is highlighted with the red arrows. Imaged at 4x or 40x with scale bars of 500 µm or 50 µm respectively. n=2 biological replicates. (Pathology visualized in collaboration with Dr. Travis Hollmann and Dr, Satish Tickoo of the MSKCC Pathology Core)

Histology sections from *sox10*:BRAF^{V600E} ;p53$^{-/-}$ transgenic tumors stained diffusely positively for BRAF^{V600E} and *phospho-erk* confirming the expression of the transgene and subsequent activation of the MAPK pathway in the tumors (Figure 2.9) (n = 5 biological replicates). The tumors stained diffusely positive for *sox10* expression, which validates the strong expression of the *sox10* promoter and the appropriate expression of the transgene. The *sox10*-driven tumors did stain sparsely positive for the neuroblastoma antigens used (NCAM, HuC/HuD), suggesting that the tumor was less differentiated than the melanoblast driven tumors. Interestingly, pigmentation was visible (albeit very sparse) within the sections suggesting that the tumors are at least partially of the melanocyte/neural crest lineage. The Hematoxylin and eosin (H&E) stain of the *sox10*-driven tumor suggested a very undifferentiated tumor type with bi-directional hints of melanoma (including some pigment) as well as hints of neuroblastoma.

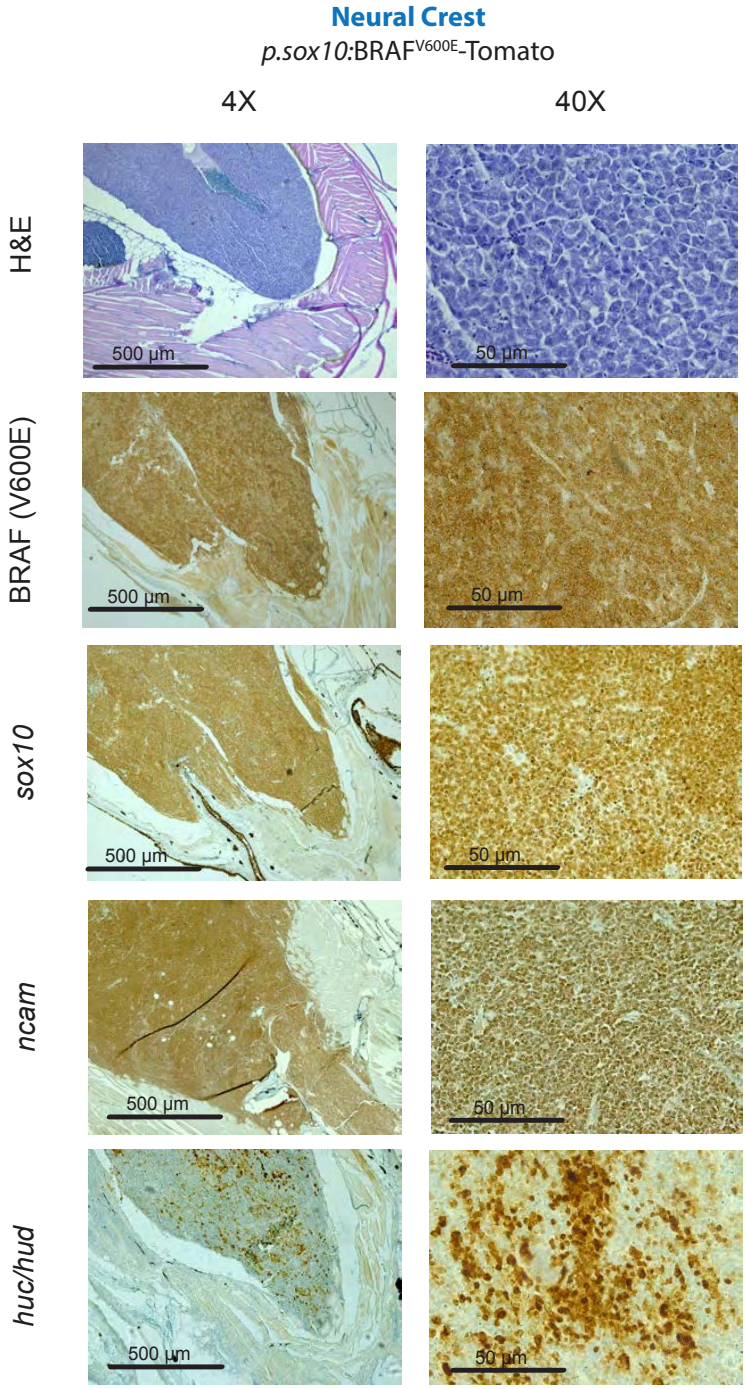

Figure 2.9 Immunohistochemistry of neural crest-driven tumors from *sox10*:BRAF^{V600E};p53$^{-/-}$ transgenic zebrafish

Representative tumor was stained for H&E, BRAFV600E, sox10, ncam, or huc/hud. Imaged at 4x or 40x with scale bars of 500 µm or 50 µm respectively. n=5 biological replicates. (Pathology visualized in collaboration with Dr. Travis Hollmann and Dr, Satish Tickoo of the MSKCC Pathology Core)

Transgenic fish from the genetic background *typr1*:BRAF^{V600E} ;p53$^{-/-}$ did not develop tumors, Several representative fish were sacrificed and fixed for immunohistochemistry (n = 2 biological replicates). The melanocytes within the skin of the fish stained positively for BRAF^{V600E} and *phospho-erk* confirming the expression of the transgene and subsequent activation of the MAPK pathway in the skin (Figure 2.10). The skin contained a high proportion of *sox10* positive cells. The lack of large tumor sections made it difficult for further characterization studies.

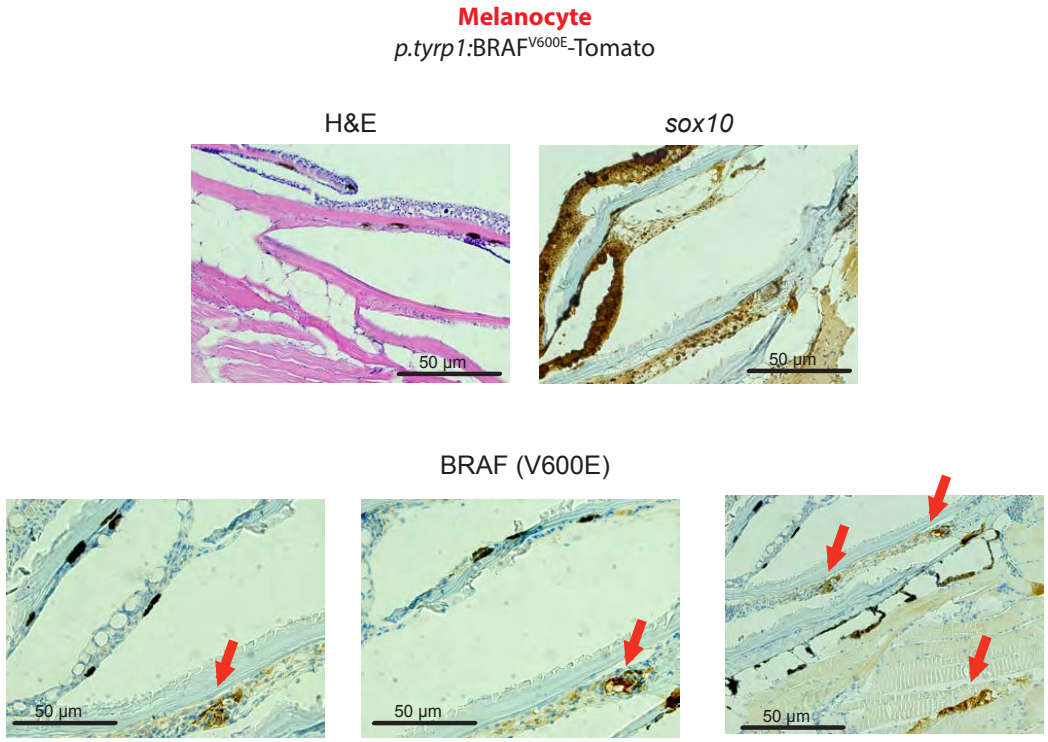

Figure 2.10 Immunohistochemistry of epidermal layer from *tyrp1*:BRAF^{V600E};p53$^{-/-}$ transgenic zebrafish

Representative epidermal layer was stained for H&E, sox10 and BRAF^{V600E}. Mutant BRAF staining within the skin is highlighted with the red arrows. Imaged at 40x with scale bars of 50 µm. n=2 biological replicates. (Pathology visualized in collaboration with Dr. Travis Hollmann and Dr, Satish Tickoo of the MSKCC Pathology Core)

Transcriptional Data

To transcriptionally profile the transgenic tumors we dissected out the tumors and submitted for RNA-sequencing with polyA selection using an Illumina HiSeq 2x150bp configuration. The fish were easily dissected with scalpels using the immunoflourescent scopes to identify the fused transgene. We collected, isolated and submitted RNA from 19 fish tumors (7 *sox10* driven body tumors, 5 *sox10* driven head tumors, 6 *mitfa* driven tumors) for RNA-sequencing. RNA-seq analysis performed in collaboration with Nathaniel R. Campbell from the White Lab at Memorial Sloan Kettering. The *sox10*-driven tumors are transcriptionally distinct from the *mitfa*-driven tumors and cluster independently when using unbiased methods for whole genome clustering (Figure 2.11). The two subgroups starkly separated in PCA space along PC1, which accounts for 54% of the variance. Interestingly, the clustering does not segregate based on anatomical location.

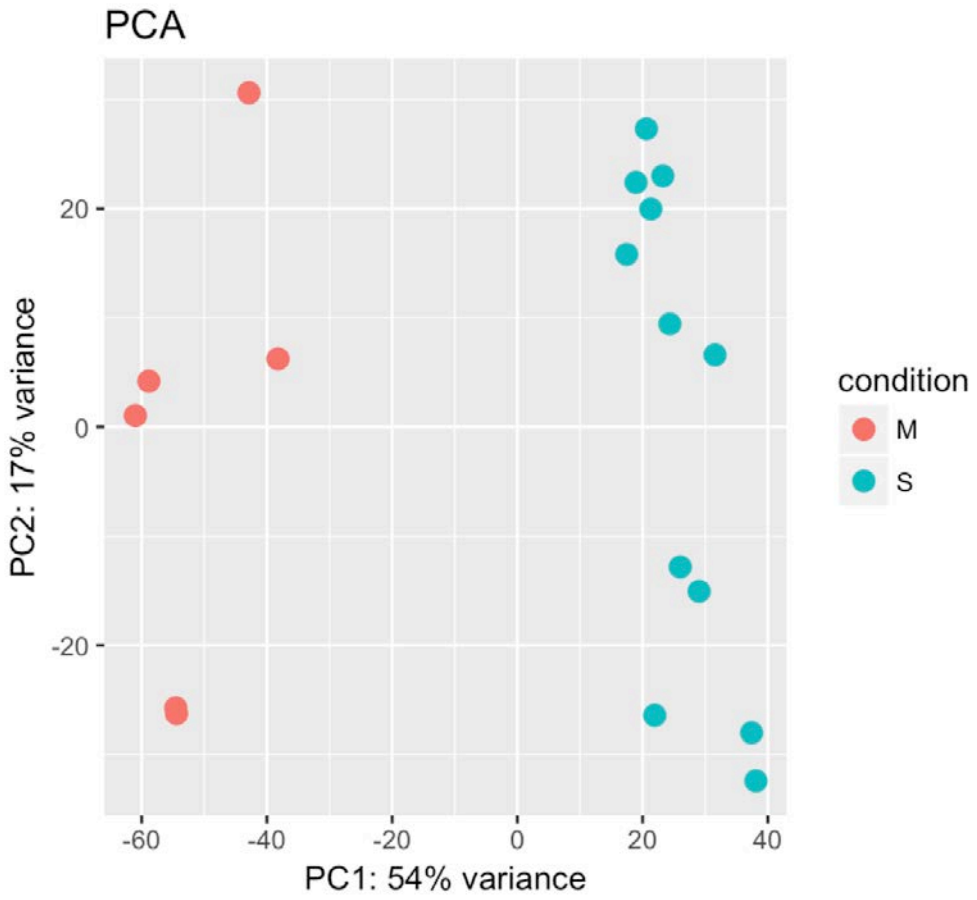

Figure 2.11 Principal component analysis (PCA) of transgenic zebrafish tumors

PCA of 5 mitfa tumors (m, red) and 12 sox10 tumors (S, teal) for whole genome RNA-seq yields a clear separation. (RNA-seq analysis performed in collaboration with Nathaniel R. Campbell from the White Lab at Memorial Sloan Kettering)

To uncover the differentially regulated processes between the *mitfa*-derived and the *sox10*-derived tumors we compared the top differentially expressed genes between the two sets of tumors. Interestingly, the top 10 genes over expressed in *mitfa*-derived tumors when compared to expression in *sox10*-derived tumors were all related to the differentiation and pigmentation of melanocytes (Figure 2.12). This corroborates the histology finding that *mitfa*-derived tumors are more differentiated. Conversely, the top 10 over-expressed genes in the *sox10*-derived

tumors are neuronal genes. Interestingly, the lineage specific genes that are responsible for neural crest, melanoblast and melanocyte specification fall in a row with late differentiation-linked genes being slightly (but not exclusively) over represented in the *mitfa*-derived tumors (DCT, MITF, KIT) and precursor-linked genes being slightly (but not exclusively) over expressed in the *sox10*-derived tumors (SOX9, SOX10, PAX3).

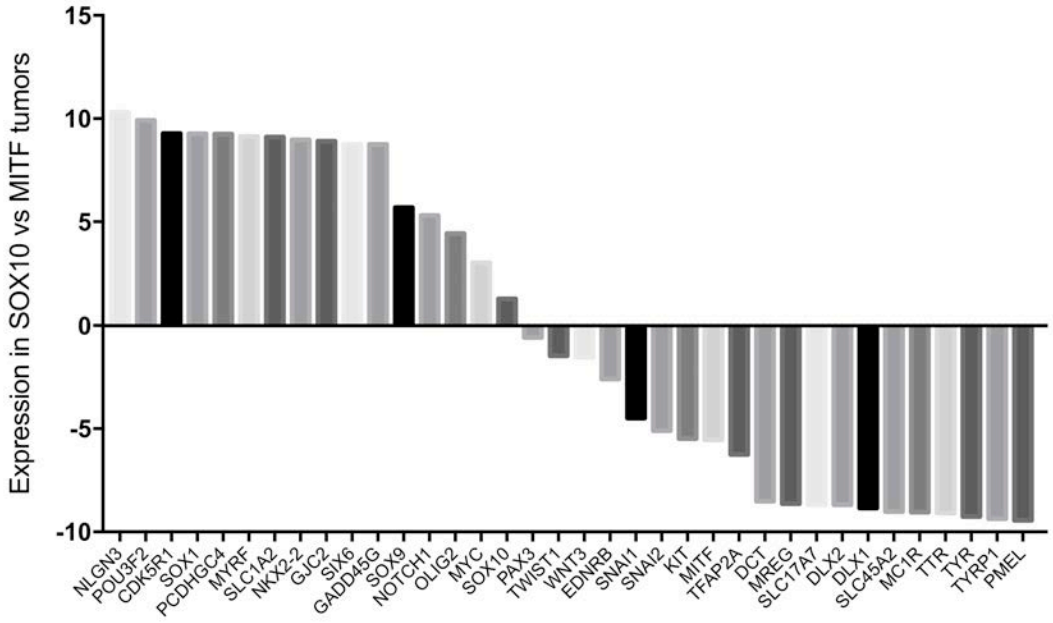

Figure 2.12 Differentially expressed genes between melanoblast and neural crest derived tumors

Differentially expressed genes between the melanoblast and neural crest derived tumors as identified by RNA-sequencing. The top 10 most differentially expressed genes in either direction are presented along with important neural crest/melanoblast specification genes. Figure represents the ratio of the mean expression between the sox10-derived (n = 12 biological replciates) and mitfa-derived (n = 6 biological replciates) tumors (RNA-seq analysis performed in collaboration with Nathaniel R. Campbell from the White Lab at Memorial Sloan Kettering)

Ideally we would compare the expression levels between the tumors and the non-tumor generating tyrp1:BRAF melanocytes, but we do not have RNA-seq

expression data for the non-transformed melanocytes. To interpret the downstream pathways that are differentially regulated between the *mitfa*-driven and the *sox10*-driven tumors we performed Gene Set Association Analysis (GSEA) and pathway analyses. One of the top gene sets up regulated in the *sox10*-driven tumors over the *mitfa*-driven tumors is a gene set associated with poor survival statistics in neuroblastoma (Figure 2.13) [341]. The gene set was enriched with an association score of 0.517741 and a normalized association score of 1.7042046. The normalized enrichment score evaluates how well ordered expression gene set resembles the provided dataset when compared to all the possible permutations of the same gene set.

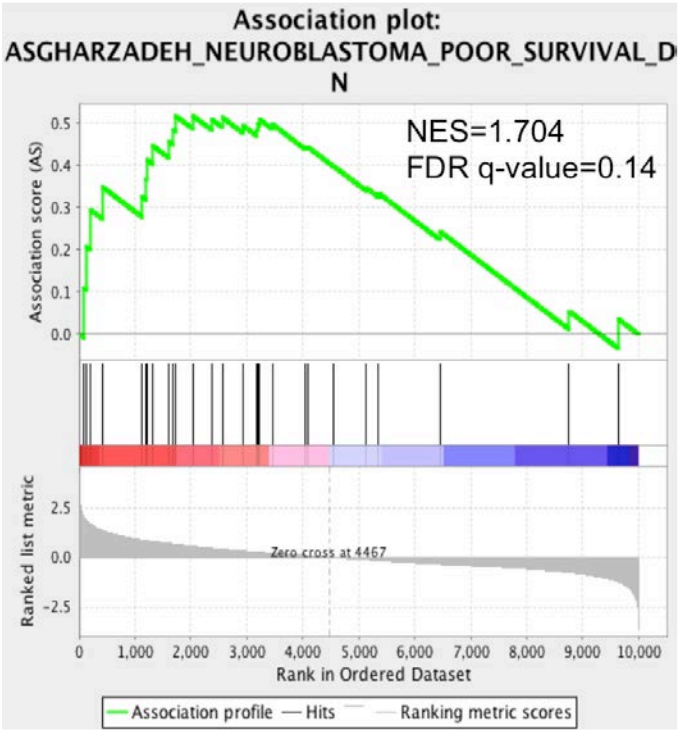

Figure 2.13 sox10-derived fish neuroblastoma

Gene set association analysis (GSAA) shows that sox10-derived zebrafish tumors closely resemble poor prognosis neuroblastoma. (RNA-seq analysis performed in collaboration with Nathaniel R. Campbell from the White Lab at Memorial Sloan Kettering)

2.3 Discussion

There is a very clear delineation of phenotypes depending on the promoter driving $BRAF^{V600E}$ when coupled with *p53* deficiency. The *mitfa*:$BRAF^{V600E}$ transgenic fish recapitulated the previously published findings and developed melanoma at a very high penetrance. Interestingly, *sox10*:$BRAF^{V600E}$ transgenic fish developed tumors with a shorter latency, but the tumors did not represent typical melanoma at the morphological, histological or transcription level. The *tyrp1*:$BRAF^{V600E}$ transgenic fish are surprisingly resistant to cancer inferring that the activation of mutant BRAF in a fully differentiated, $p53^{-/-}$ melanocyte is not sufficiently oncogenic.

Previously published work clearly argues for the necessity of *sox10* up regulation in melanocytes for melanoma expressed with the *mitfa* promoter [53, 60]. This corroborates with the paradigm that both SOX10 and MITF are highly expressed in melanoma and both are required for melanoma growth. However, driving the oncogene off the sox10 promoter does not produce stereotypical melanoma. These two data points are not contradictory, but rather argue for a very narrow developmental window for melanoma formation in the fish. For melanoma to progress melanocytes must re-activate *sox10* and a neural crest program but only after *mitfa* and a melanoblast commitment program have been activated in the cell first. If the oncogenic program is turned on prior to melanoblast formation the resulting tumors contain some aspects of melanoma (i.e. pigmentation) but will mostly resemble a very undifferentiated neuroblastoma. Furthermore, the

same oncogenic program is no longer sufficient to yield a tumor if the cell has already activated a differentiated melanocyte program (*tyrp1* promoter). These findings do not dictate that melanoma can never originate in the more differentiated cell type, but rather that these cells are more resistant given the same oncogenic exposure and may require additional mutations or epigenetic changes. Together these fish tell a very nuanced story, arguing that the MITF+ melanoblast is the most susceptible cell type capable of giving rise to melanoma in the fish using this oncogenic combination.

CHAPTER THREE: CELL OF ORIGIN STUDIES IN HUMAN EMBRYONIC STEM CELLS

3.1 hES-derived melanocytes

The Studer lab recently established a protocol for the rapid and highly efficient derivation of mature and functional melanocytes from human pluripotent stem cells (hPSCs) of both human ESC and iPSC origin in a feeder-free, *in vitro* system (Fig. 3.1) [8, 304]. The protocol mimics normal melanocyte development by first proceeding through a neural crest progenitor (*sox10*$^{+}$, *p75*$^{+}$) and melanoblast (*sox10*$^{+}$*, c-kit*$^{+}$*, mitf*$^{+}$*, dct*$^{+}$) stage before reaching a mature pigment-producing melanocyte (*tyr*$^{+}$*, oca2*$^{+}$*, pmel*$^{+}$). Importantly, our differentiation conditions enable us to isolate and maintain highly scalable populations of pure melanocytes as well as defined human neural crest intermediates, and melanocyte progenitor populations (bipotent glial-melanocyte stem cell and melanoblasts) in culture. The resulting hPSC-derived melanocytes appear indistinguishable from primary melanocytes with comparable transcriptional profiles and functional hallmarks as demonstrated by electron microscopy, skin reconstruction and *in vivo* transplantation assays [24]. Using this unique platform we studied the importance of cell of origin on melanoma development. The protocol allowed us to induce oncogenesis in defined populations of cells representative of each state along the melanocytic lineages in a manner that could not be done previously (Figure 3.1). Past studies aimed at transforming primary human cells were limited to the use of differentiated melanocytes and

lacked a scalable source of stage-specific human neural crest or melanocyte progenitors.

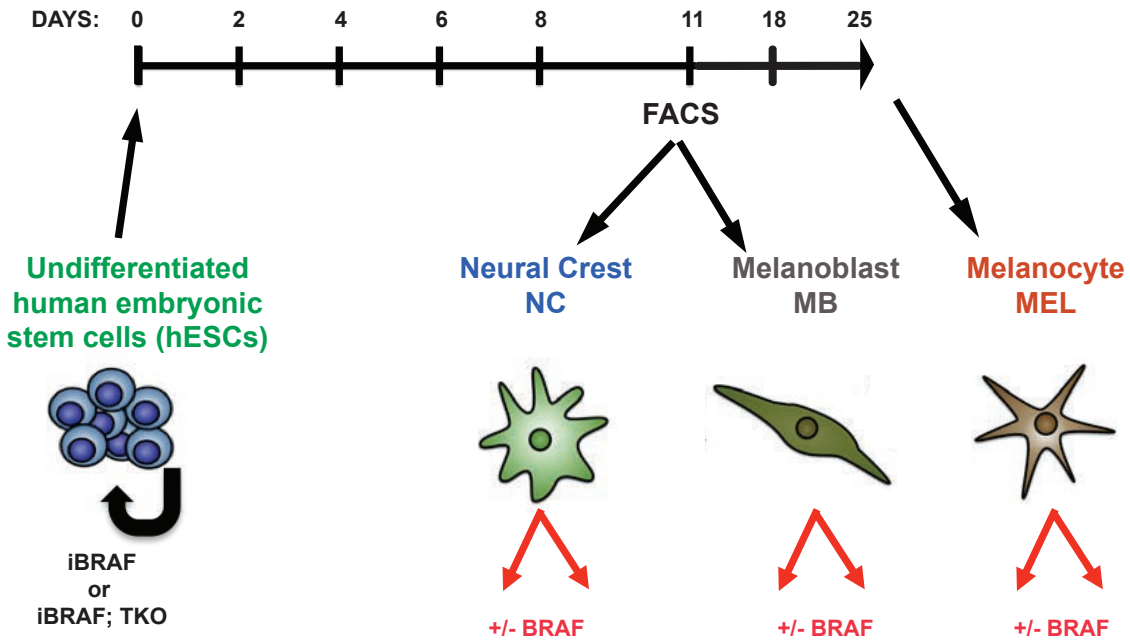

Figure 3.1 Schematic of hES-based melanoma cell of origin modeling
Human embryonic stem cells are differentiated into neural crest, melanoblast or melanocyte cells before inducing oncogenic BRAF^{V600E}. The protocol will be done in WT hES and TKO hES (p53$^{-/-}$; p16$^{-/-}$; rb1$^{-/-}$) [8]. (figure adapted from Mica et al, 2013)

3.2 Results

Generation of transgenic hES lines

Engineering of inducible BRAF^{V600E} hESCs

In order to reliably induce expression of the mutant BRAF^{V600E} at the distinct stages of differentiation we engineered the hES parent line for inducible expression. The Huangfu lab at MSKCC recently introduced an inducible CRISPR-cas9 into the “safe harbor” AAVS1 (also known as PPP1R12C) locus

[342, 343]. The locus had been previously shown to support robust and sustained transgene expression in a manner similar to that of the Rosa26 locus in mice [344]. To introduce the inducible system, hESCs were electroporated with two TALENS directed at the locus and two donor vectors for homologous recombination. One donor plasmid contained a doxycycline-inducible Cas9 expression cassette (Puro-Cas9 donor), and the other carried a constitutive reverse tetracycline transactivator (M2rtTA) expression cassette (Neo-M2rtTA donor). For our studies, we sub-cloned mutant BRAF^{V600E} to replace the Cas9 expression cassette (see Figure 3.2).

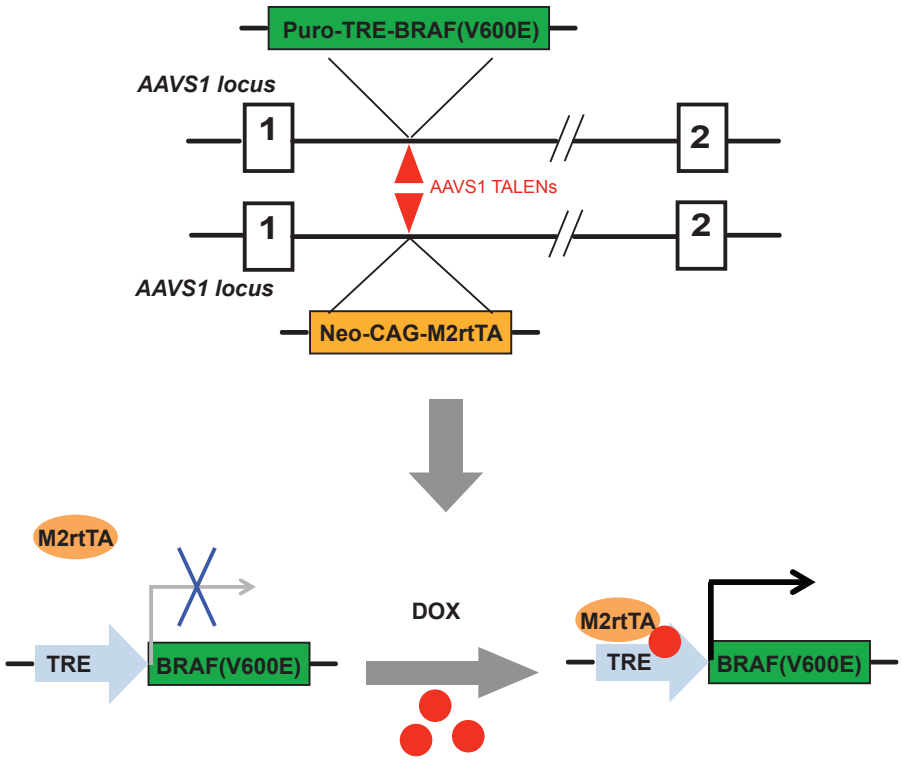

Figure 3.2 Schematic of AAVS1 targeting of inducible mutant BRAF
Double strand breaks are introduced by a pair of TALENs enabling simultaneous homology-directed repair (HDR) of both Puro-BRAF^{V600E} and Neo-M2rtTA cassettes into the AAVS1 alleles in trans. BRAF^{V600E} expression is then induced through doxycycline treatment in clonal iBRAF lines. (adapted from Zhu et al. 2013) [343]

Adapting the Huangfu iCRISPR technology for iBRAF enabled us to efficiently induce $BRAF^{V600E}$ expression in hESC or any hES-derived cells. To test expression levels we introduced doxycycline (DOX) into the hESC media and analyzed transcript expression by qPCR and protein levels by western blot (see Figure 3.3). Importantly, the mutant BRAF expression is very tightly regulated by DOX exposure and does not leak any expression in the absence of DOX. The mutant BRAF expression is tunable depending on DOX levels. Interestingly, the phospho-ERK levels do not increase following mutant BRAF expression, which suggests that the MAPK pathway is already over saturated in hESC.

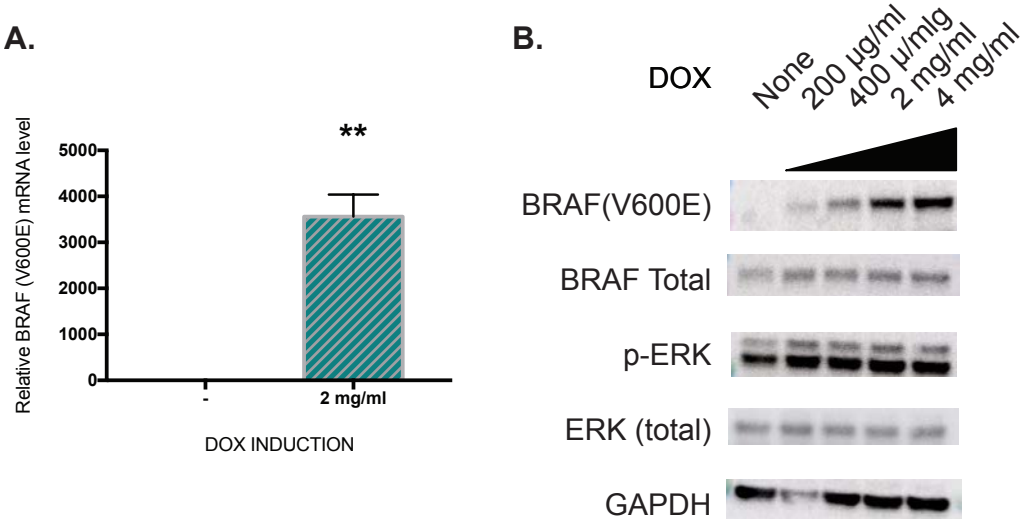

Figure 3.3 iBRAF expression in hESCs

Inducible mutant BRAF is reliably expressed following DOX exposure at both the mRNA transcript level (A) and the protein level (B) in hESC of iBRAF. Samples were collected following 48 hours of exposure to DOX in hESC media. qPCR is represents 2 biological replicates with 2 technical replicates (p-value = 0.009). WB is representative example of 2 biological replicates of 1 technical replicate each.

Engineering loss of tumor suppressors

The animal models and human cell line transformation studies suggest that melanoma transformation will require loss of tumor suppressors in addition to the expression of oncogenic BRAF [263, 264, 266, 275-277, 279]. To choose the combinations of second hit mutations to transform the cells we looked to human cell lines studies, animal studies, and next generation sequencing of patient data. The most physiologically relevant *in vitro* transformation implicated RB1 and TP53 [266]. The animal studies require loss of TP53, CDKN2A, or PTEN [276, 277, 279]. A meta-analysis of somatic mutations in melanomas revealed that the top two most frequently mutated genes in mutant BRAF tumors are TTN and TP53 [345]. The authors reasoned that the TTN mutations are likely passenger mutations due to gene length bias, given that TTN is the longest gene in the human genome [346]. The second most frequently mutated gene was TP53, found in 21.5% of BRAF-mutated tumors (p-value = 0.011). We hypothesized that oncogenic BRAF will transform when combined with loss of TP53, CDKN2A, RB1 and/or PTEN.

To generate knock out hESCs we employed the CRISPR cas9 system to introduce double strands breaks in gRNA target sites of interest [347, 348]. The gRNA were synthesized in gBLOCKS and were co-electroporated into hESC with constitutively active Cas9-fused to GFP [349, 350]. Clones were then sorted for GFP (which implied Cas9 expression) and then grown up as single cell clones. Clones were then screened via sequencing for knockouts in the tumor

suppressor genes of interest. We selected for clones with knockouts all the permutations of TP53, CDKN2A, RB1 and/or PTEN. For downstream studies we focused primarily on the iBRAF; TKO line which has a DOX-inducible $BRAF^{V600E}$ in the AAVS1 locus and homozygous inactivating mutations in TP53, P16, and RB1 (Figure 3.4).

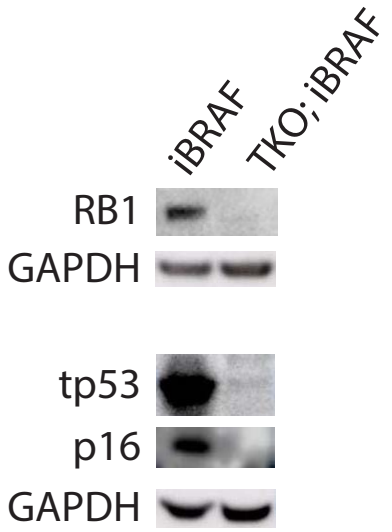

Figure 3.4 Genetic knockout of tumor suppressors.
Western blot analysis shows the genetic knockout of TP53, P16, and RB1 in TKO line. RB1 is blotted in iBRAF;TKO hESC-derived MEL while tp53 and p16 are blotted in iBRAF;TKO hESC-derived MB. The stages of differentiation are selected for increased expression of the tumor suppressor for simplicity of visualization. Representative of 4 biological replicates.

hESC directed differentiation into neural crest, melanoblast, and melanocytes

We next wanted to use these models to assess how the oncogenic mutations act in the Neural Crest, Melanoblast and Melanocyte, analogous to what we did in the fish. The Studer lab recently published a protocol for directed differentiation of pluripotent stem cells into the various ectoderm lineages (including neural

crest cells) using the chemically defined E8/E6 culture platform [300, 351]. In unpublished data, we have converted the Mica et al. hES-derived melanocyte protocol for a KSR based system into a chemically simplified and defined E8/E6 protocol [8, 304]. The new E8-based melanocyte directed differentiation protocol combines the first 6 days of the Tchieu et al. NC protocol with the addition of EDN3 and BMP4 for the remaining 4 days of specification to drive a melanoblast fate (Figure 3.5) [300]. The day-11 cells are then re-plated in droplets onto PO/LAM/FN plates into a melanocytic differentiation media and differentiated identically to the Mica et al day-11 melanocyte protocol [8, 304]. As the melanocyte media selectively kills off contaminants and the melanocytes continually expand it is difficult to quantify an efficiency or yield but the protocol is very robust and repeatable for melanocyte production.

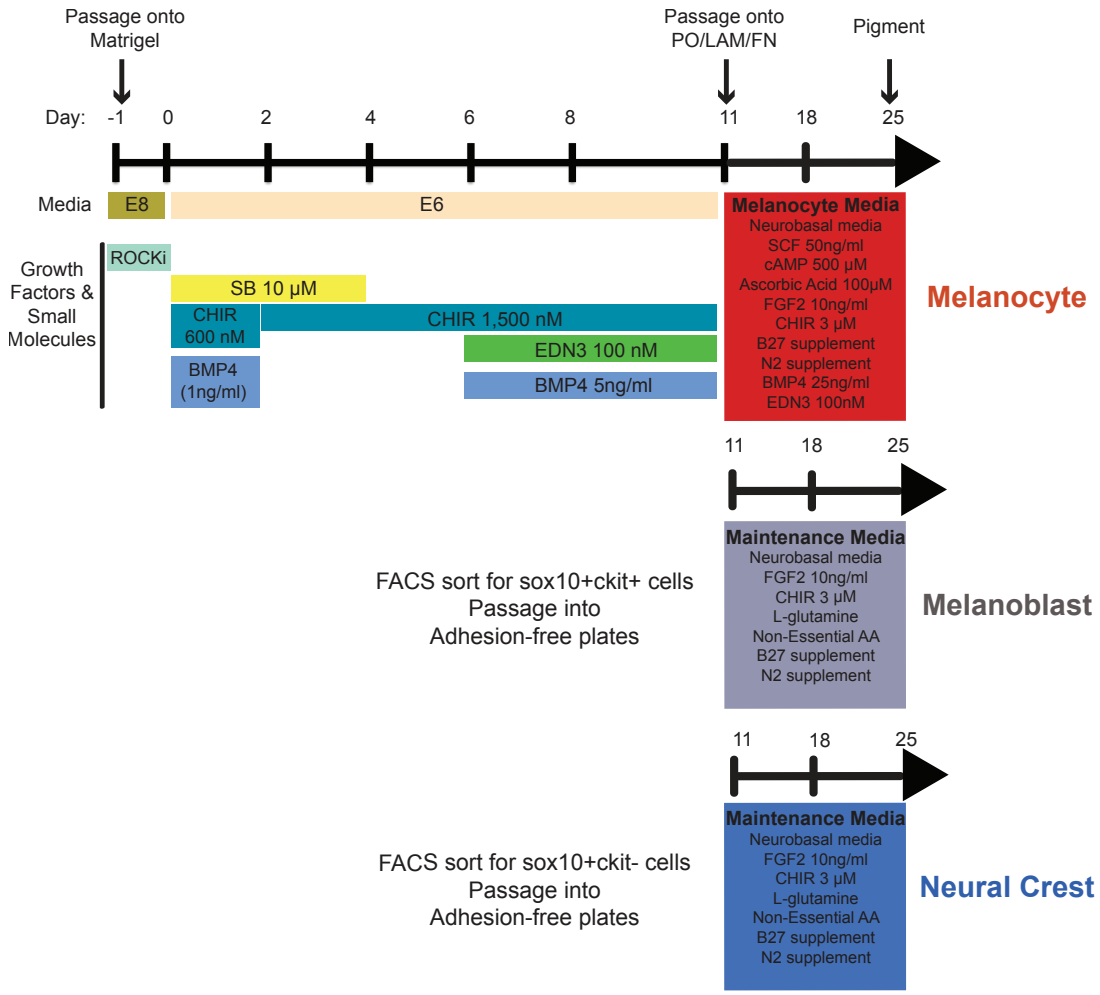

Figure 3.5 Differentiation scheme to generate NC, MB, or MEL from hESC. *Schematic for the directed differentiation of hESCs into NC, MB, or MEL using the chemically-defined E8/E6 media system. At day 11 of the differentiation cells can be FACS sorted for SOX10 and cKIT expression to isolate NC or MB. Alternative day 11 cell can be re-plated in droplets with or without sorting and differentiated into MEL. (adapted from Mica et al. 2012)* [8]

The differentiation can be halted at day-11 to sort out and maintain isogenic neural crest cells or melanoblasts. These subpopulations are sorted out using fluorescence-activated cell sorting (FACS) for the germline SOX10:GFP transgene coupled with the presence or absence of cKIT expression. Neural crest cells will sort out as SOX10+cKIT- whereas melanoblast cells are SOX10+cKIT+ (Figure 3.6). The SOX10- cKIT- cells are differentiations

contaminants that did not differentiate. It is unclear what SOX10- cKIT+ cells represent, but it is possible that SOX10- cKIT+ cells have already passed through a NC stage have turned down SOX10 and are now representative of a MSC fate. Both NC and MB cells can be maintained as clusters in low-adhesion plates.

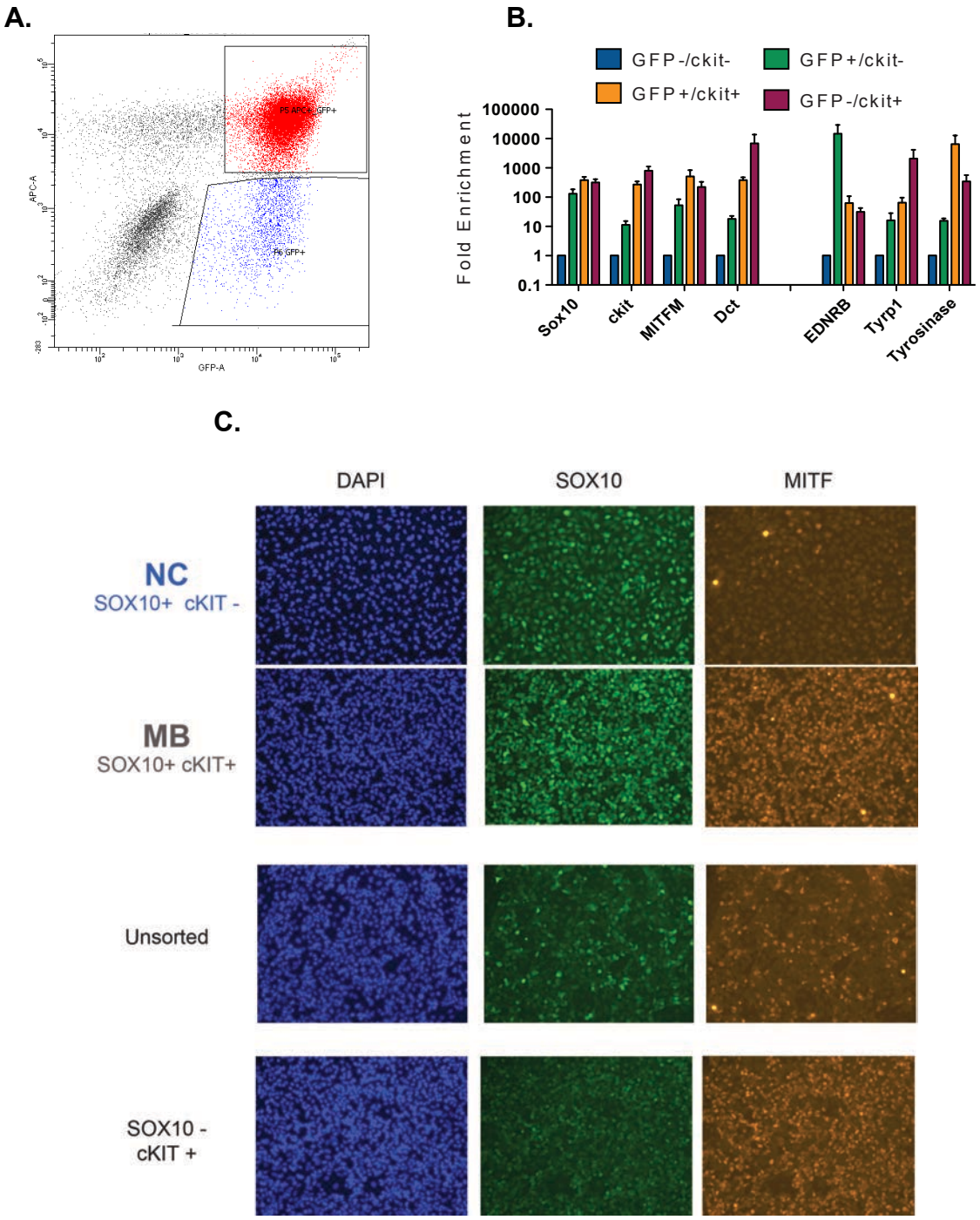

Figure 3.6 FACS Sorting neural crest and melanoblasts.

(A) *FACS sorting the SOX10+cKIT- or SOX10+cKIT+ fractions respectively at day 11 of the differentiation can isolate NC and MB cells. Representative plot from n=10 biological replicates.* ***(B)*** *The transcript expression levels for neural crest and melanoblast cells are analyzed by qPCR following sorting [8]. n = 3 biological replicates. (qPCR results performed by Dr. Yvonne Mica and published in Mica et al. 2013)*

(C) *Immunofluorescence for expression of sox10:GFP and MITF confirms the NC and MB identity. Representative images from n = 3 biological replicates.*

Alternatively, the directed differentiation can be continued past day-11 towards the melanocytic fate. The directed differentiation utilizes a selective melanocytic media that was designed by Mica et al, which negates the need for sorting and still yields a 100% pure melanocytic population. The culture will begin to pigment around day-25 with completely black medias around day-40 (Figure 3.7). hES-derived mature melanocytes express the typical differentiation genes including TYRP1 and HMB45. The melanocytes continue to proliferate, making quantification difficult. If the culture is maintained at a high density the culture will thicken to the point of blocking all light and preventing the cells from being visualized under bright-field.

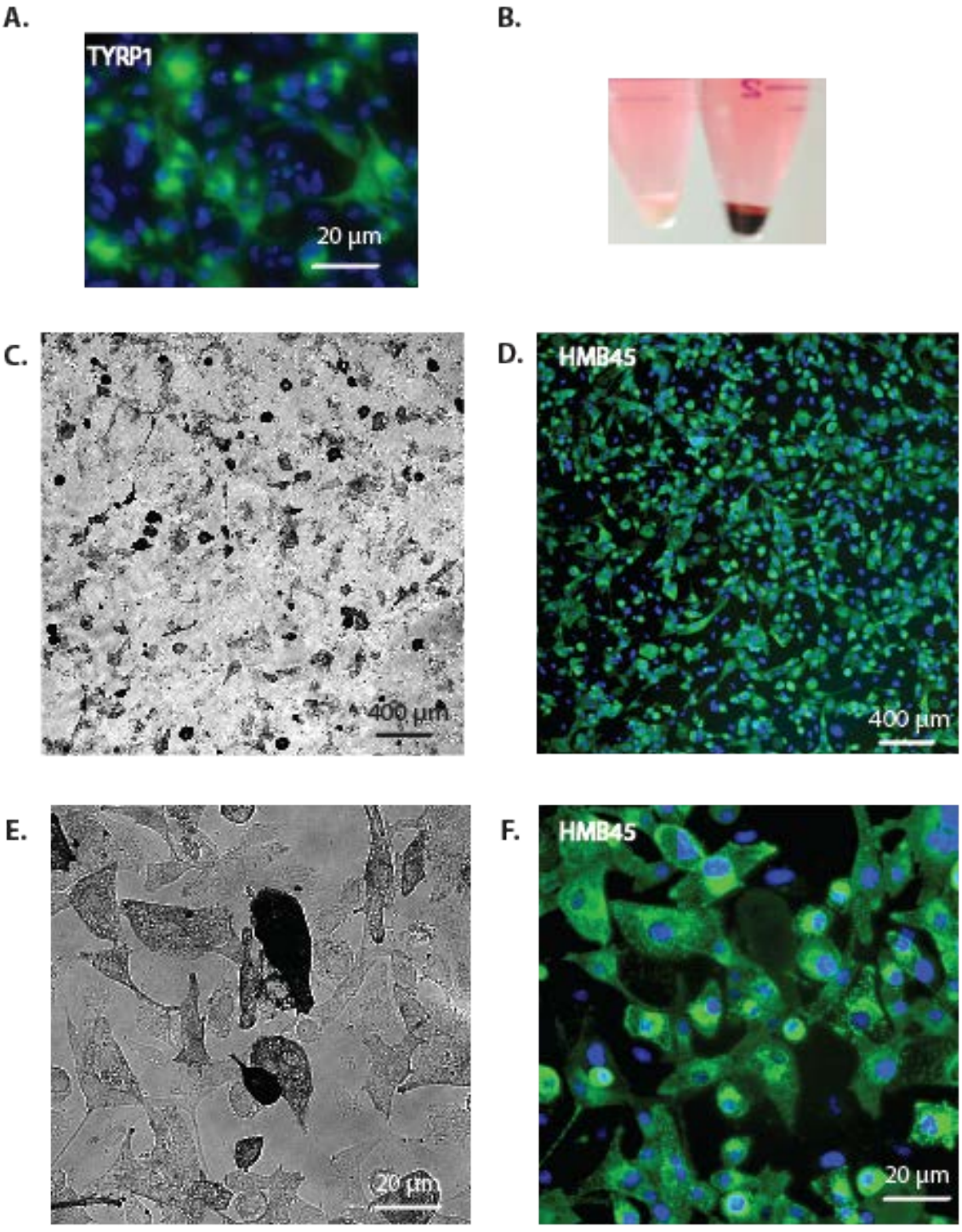

Figure 3.7 hES-derived melanocyte characterization.
(A) *The pigmented cells stain for the melanocyte markers TYRP1.* ***(B)*** *The pigmented Day 25 cells (right) can be easily visualized and distinguished from Day 11 cells (left) when pelleted. (**C-F**) Only melanocytes will persist in the Melanocyte Differentiation media. By day 40 every cell stains positively for the melanocyte marker HMB45. Representative images from n = 3 biological replicates.*

Validating iBRAF following directed differentiation

Next we tested that the inducible mutant BRAF is still active and tunable after differentiating to the melanocyte stage (see Figure 3.8a). Importantly, we confirmed that iBRAF induces to equivalent levels independent of tumor suppressor loss (see Figure 3.8b).

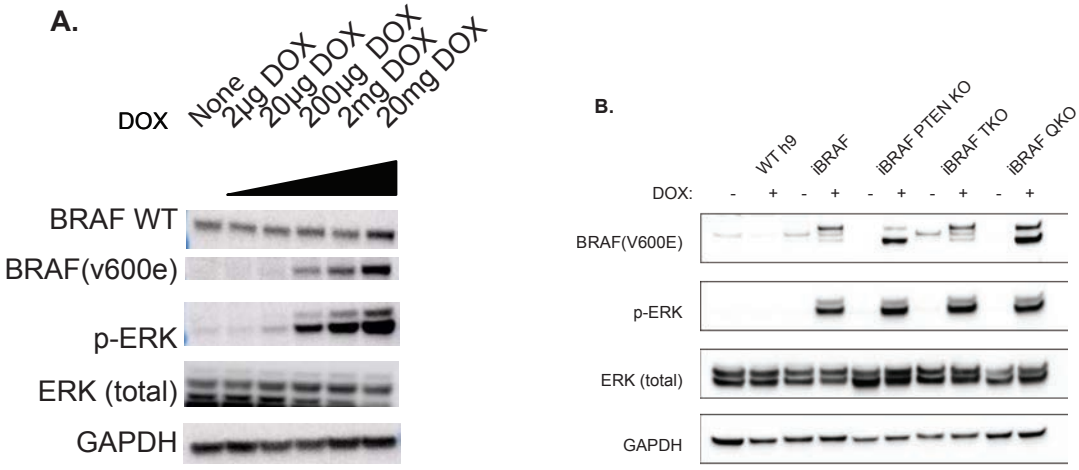

Figure 3.8 iBRAF in melanocytes.
(left) *iBRAF remains inducible and tunable in hES-derived WT iBRAF melanocytes.* ***(right)*** *iBRAF induce the MAPK pathway to comparable levels independent of genetic background. TKO = TP53$^{-/-}$;CDKN2A$^{-/-}$;RB1$^{-/-}$. QKO = TP53$^{-/-}$;CDKN2A$^{-/-}$;RB1$^{-/-}$ PTEN$^{-/-}$. (Figure 3.8B produced in collaboration with Dr. Arianna Baggiolini from the Studer Lab at Memorial Sloan Kettering)*

For inter-stage comparison it is important to insure that MAPK pathway is inducible to comparable levels following DOX induction of iBRAF independent of differentiation state. To compare levels isogenic cells were differentiated to NC, MB, MEL levels and MAPK levels were assayed in the presence or absence of iBRAF induction. Interestingly, the BRAF^{V600E} protein levels are not comparable across the differentiation states with melanocytes exhibiting significantly diminished levels (see Figure 3.9). This is despite the strong induction levels

exhibited in melanocytes in Figure 3.8. However, the downstream MAPK marker pERK is activated all conditions following doxycycline treatment independent of differentiation state, which is important for downstream comparisons of transformation and transcription changes.

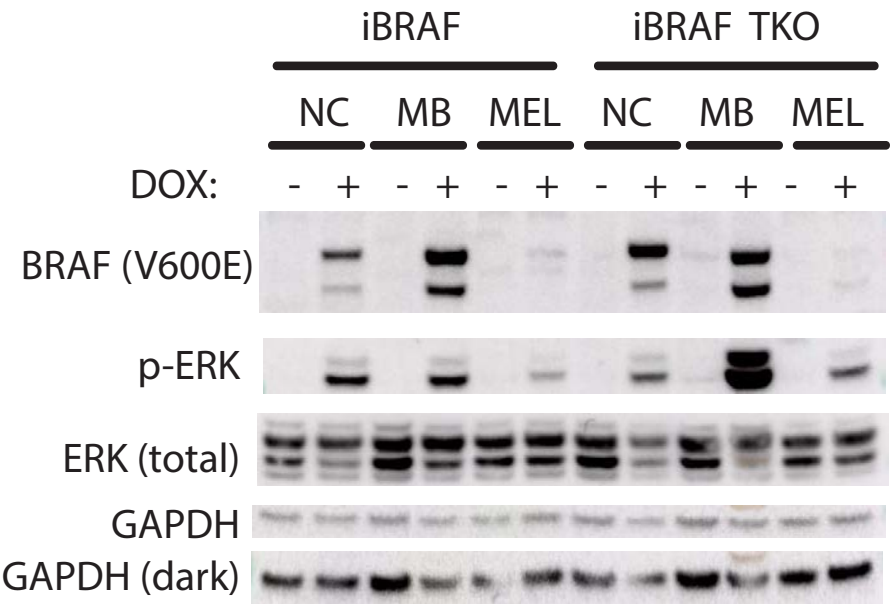

Figure 3.9 iBRAF across differentiation states.
Mutant BRAF is inducible in iBRAF at the NC, MB, and MEL stage in both the WT and TKO genetic background. The mutant BRAF levels are disparate between the developmental stages but the MAPK pathway activation (visualized through pERK levels) is independent of stage of differentiation. Representative blot from n = 3 biological replicates.

Tumor modeling

Tumor modeling in vitro

To assess if differentiation state (NC, MB, or MEL) of the cell of origin is deterministic of the tumorigenic state *in vitro* we quantified the number of cells in S-phase with or without iBRAF using EdU (5-ethynyl-2'-deosyuridine) labeling. EdU is a nucleoside-analog of thymidine and is incorporated into the DNA during

active DNA synthesis. The NC and MB stages were maintained in adhesion-free plates with maintenance media while the MEL stage was maintained on adhesion plates with melanocyte differentiation media so comparisons cannot be directly made between the melanocyte stage and early stages.

Mutant BRAF did not impact the proliferation rate of WT cells at any of the three-differentiation states (NC, MB, or MEL) in a statistically significant manner (Figure 3.10). The WT melanocytes slow their proliferation rate when exposed to mutant BRAF, but again not in a statistically significant manner. This contradicts the previously published result that $BRAF^{V600E}$ induces melanocyte senesce. The lack of senescence is likely a result of the pro-growth differentiation media in which we grow the cells.

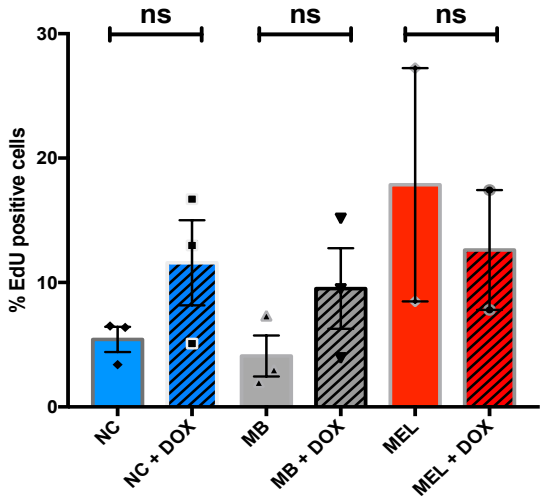

Figure 3.10 EdU labeling in WT iBRAF hES-derived cells.
The numbers of WT iBRAF hES-derived cells in S-phase were quantified in the presence or absence of mutant BRAF at the NC, MB, and MEL stages. The cells were exposed to DOX for 48 hours prior to quantification. While there are small changes in numbers of dividing cells the differences were not statistically significant. n = 3 independent experiments. (EdU experiments performed in collaboration with Dr. Arianna Baggiolini from the Studer Lab at Memorial Sloan Kettering)

Mutant BRAF increases the proliferation of TKO melanoblasts in a statistically significant way (Figure 3.11). Interestingly, mutant BRAF does not impact the proliferation rate of NC or MEL TKO cells. This stage specific impact of mutant BRAF on proliferation rate has not been previously reported and strongly suggests that the differentiation stage of the cell of origin in melanoma is important, with melanoblasts being the most sensitive.

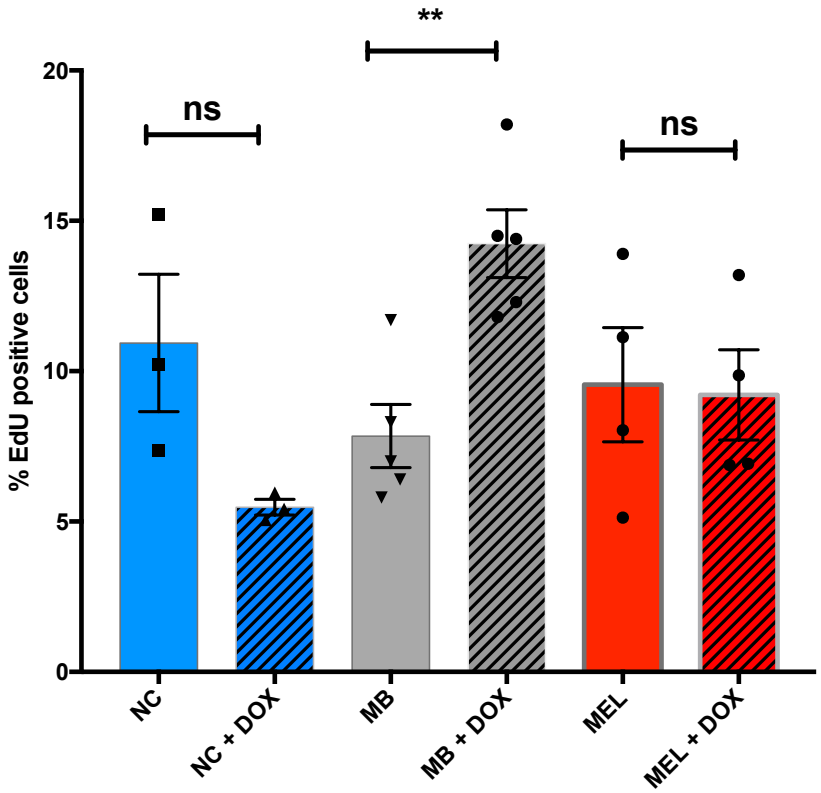

Figure 3.11 EdU labeling in TKO;iBRAF hES-derived cells.
The numbers of TKO;iBRAF hES-derived cells in S-phase were quantified in the presence or absence of mutant BRAF at the NC, MB, and MEL stages. The cells were exposed to DOX for 48 hours prior to quantification. Mutant BRAF leads to increased proliferation in TKO cells at the MB stage in a statistically significant way. Mutant BRAF does not alter proliferation at the NC or MEL stage in TKO cells in a statistically significant way. n = 3 independent experiments. (EdU experiments performed in collaboration with Dr. Arianna Baggiolini from the Studer Lab at Memorial Sloan Kettering)

Tumor modeling in vivo

The gold standard assay for cellular transformation is tumor growth when xenografted into immunocompromised mice. To assess if differentiation state (NC, MB, or MEL) of the cell of origin is deterministic of the tumorigenic state or tumor phenotype *in vivo* we injected cells into the flanks of non-obese diabetic-severe combined immune-deficiency (NOD-SCID) mice (3 mice or 6 injections per a group). For controls we injected cells in the presence or absence of iBRAF as well as in WT and TKO cells. For a positive control we injected A375 melanoma cells, which grew rapidly. For each injection we started with 500,000 cells embedded in matrigel and charted the growth as a single tumor curve. Tumor volume was monitored closely for 1 year, at which time the animals were sacrificed, tumors were excised, and tissue was preserved for analysis.

Neural Crest cells are slightly transformed when genetic loss of TP53, RB1, and CDKN2A is coupled with $BRAF^{V600E}$ over-expression (Figure 3.12). Tumors grew with a very long latency with only four of the six tumors hitting a true exponential phase by the close of the study at 307 days. By contrast, the TKO NC cells without mutant BRAF expression did not grow tumors. The TKO NC cells with DOX are statistically larger than the TKO NC cells without DOX (p-value = 0.033). Similarly to the TKO NC cells without DOX, the WT neural crest cells did not exhibit exponential tumor growth with only slight expansion in a few animals after extreme latency. These results indicate that TKO NC cells with $BRAF^{V600E}$

over-expression are tumorigenic *in vivo*, but the tumorigenecity is weak and there is no suggestion that these cells are capable of metastasis.

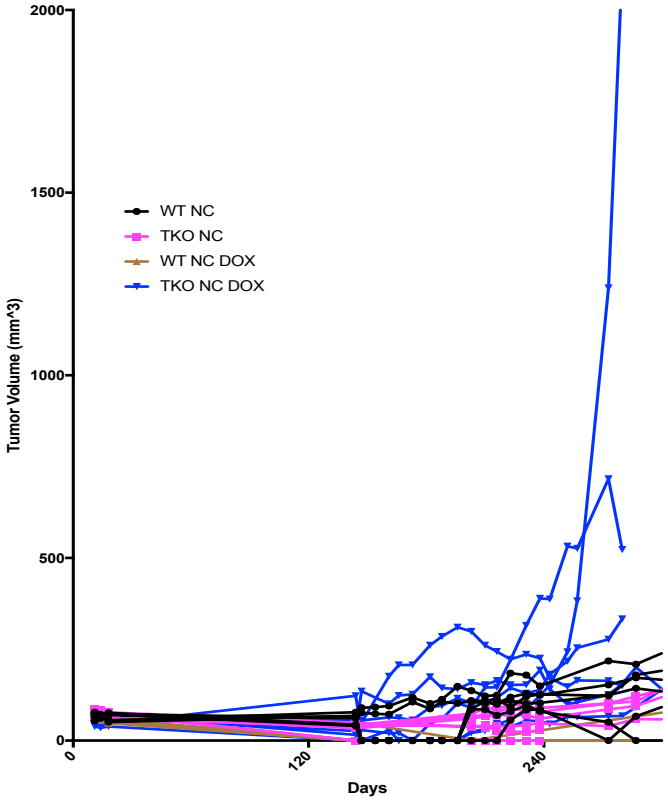

Figure 3.12 Mouse xenograft of hES-derived neural crest cells.
TKO;iBRAF neural crest cells are weakly transformed when mutant BRAF^{V600E} is induced by DOX. By comparisons, TKO NC cells do not grow without BRAF^{V600E} induction and WT NC cells do not grow with or without BRAF^{V600E}. TKO.NC+DOX vs. TKO.NC is statistically different with a p-value=0.033. Each line represents an independent cell injection. n = 6 independent tumors per group. (xenograft experiments performed in collaboration with the Antitumor Assessment Core at MSKCC)

In contrast, melanoblast cells are readily transformed when genetic loss of TP53, RB1, and CDKN2A is coupled with BRAF^{V600E} over-expression (Figure 3.13). Tumors grew with a long latency with four of the six tumors exhibiting exponential by 307 days. By contrast, the TKO MB cells without mutant BRAF expression grow tumors (6 of 6 tumors) that persistently expand but never exhibit

exponential growth. The WT melanoblast do not expand at all *in vivo* and do not present palpable tumors for measurement at the close of the study. The TKO MB cells with DOX are statistically larger than the WT MB cells without DOX (p-value = 0.011). These results indicate that TKO MB cells with $BRAF^{V600E}$ over-expression are strongly tumorigenic *in vivo*, but there is no suggestion that these cells are metastatic in this model.

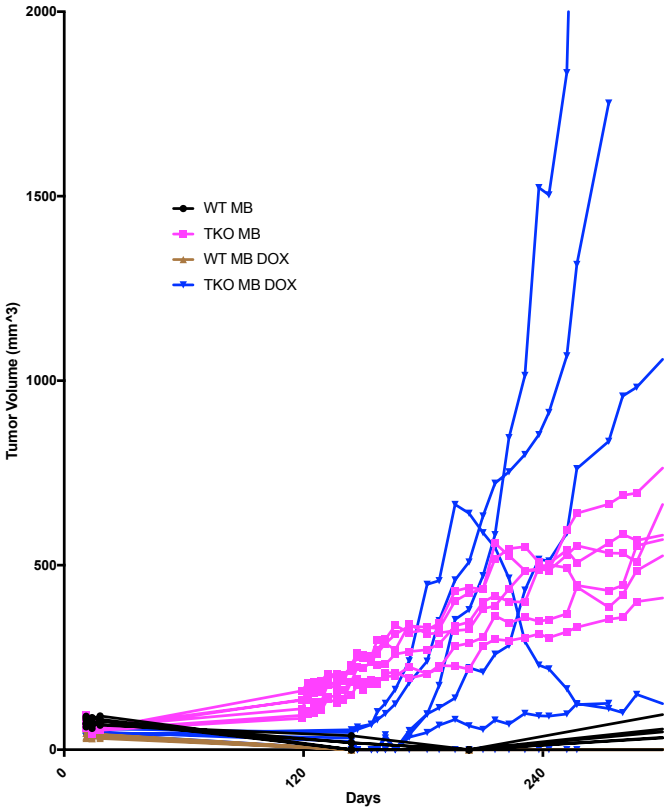

Figure 3.13 Mouse xenograft of hES-derived melanoblasts.
TKO melanoblasts are transformed when mutant $BRAF^{V600E}$ is induced by DOX. By comparisons, TKO MB cells without $BRAF^{V600E}$ induction grow slowly throughout the protocol. WT MB cells do not grow with or without $BRAF^{V600E}$. TKO.MB+DOX vs. WT.MB is statistically different with a p-value of 0.011. Each line represents an independent cell injection. n = 6 independent tumors per group. (xenograft experiments performed in collaboration with the Antitumor Assessment Core at MSKCC).

In contrast to the hES-derived NC and MB, hES-derived Melanocytes are not transformed when genetic loss of TP53, RB1, and CDKN2A is coupled with $BRAF^{V600E}$ over-expression (Figure 3.14). There is one outlier tumor that grew in the TKO.MEL+DOX condition. However, no other hES-derived melanocyte (WT or TKO with or without DOX) had palpable tumor growth. The TKO MEL cells with DOX are not statistically larger than the WT MEL cells without DOX (p-value = 0.996). The mice euthanized at the close of the study do not have any palpable tumor growth, but upon dissection, pigmented melanocytes were present at the site of injection. The injected MEL are not killed or cleared during the study, suggesting that the cells may be senescent, akin to human nevi. Future studies are underway to query if the cells are senescent. These results indicate that TKO MEL cells with $BRAF^{V600E}$ over-expression are not tumorigenic *in vivo*.

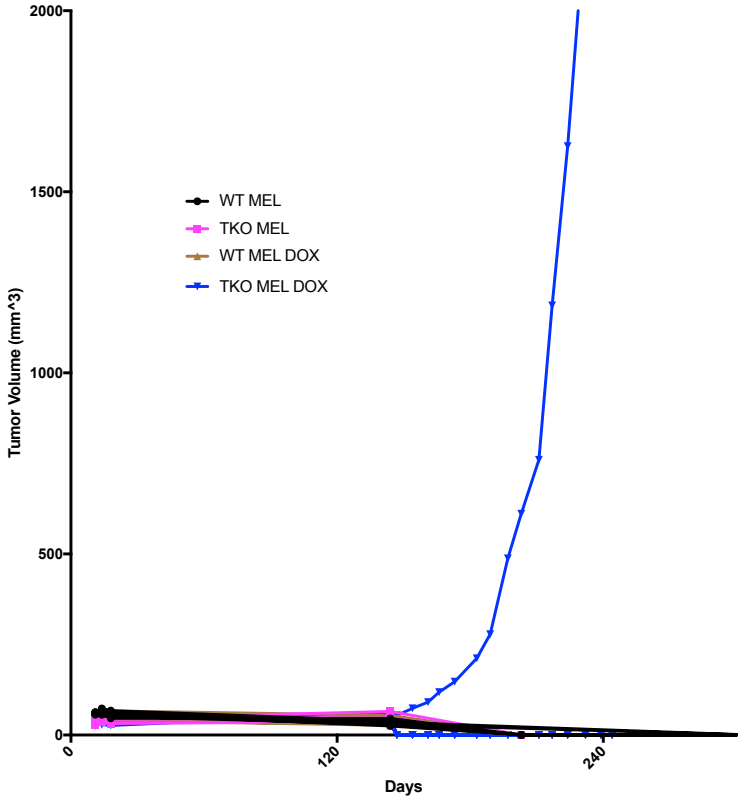

Figure 3.14 Mouse xenograft of hES-derived melanocytes
hES-derived melanocytes (WT or TKO) are not tumorigenic in vivo with or without mutant BRAF. One outlier tumor from the TKO.MEL+DOX did grow. TKO.MEL+DOX vs. WT.MEL is not statistically different with a p-value of 0.996. Each line represents an independent cell injection. n = 6 independent tumors per group. (xenograft experiments performed in collaboration with the Antitumor Assessment Core at MSKCC).

Histopathology of hES-derived tumors

To establish the differentiation status and morphological characteristics of the tumors, we performed histology post-mortem on several representative hES-derived tumor samples. The histology slides were graded by pathologists in a blinded manner and compared to human melanomas of diverse origins. The single melanocyte-derived tumor was characterized as a spindle cell tumor (possibly melanoma) with very little differentiation with some focal coarse pigment but lacks the typical prominent nucleoli of melanoma (see Fig. 3.15a,d).

The melanoblast-derived tumors were generally similar with overwhelmingly spindle cell morphology but less elongated and less cytoplasmic leading to a more epithelioid quality with nesting (see Fig. 3.15b,e). Finally, the neural crest-derived tumor had a very high mitotic index with striated atypical mitosis and some large pleomorphic nuclei (see Fig. 3.15c,f). Taken together the tumors were described as very proliferative, spindle cell tumors with relatively little differentiation making diagnosis difficult without further staining.

Immunohistochemistry was performed to determine the oncogenic phenotypes of the tumors (Figure 3.15). First, all the tumors were stained with a mutant $BRAF^{V600E}$ specific antibody to insure DOX induced transgene expression (see Fig. 3.15g-l). Importantly, both mutant BRAF and the downstream MAPK pathway (pERK) are diffusely positive in all the tumors (see Fig. 3.15g-r). Furthermore, the tumors have a high fraction of Ki67-positive nuclei corroborating the exponential growth visualized in the tumor curves (see Fig. 3.15s-x).

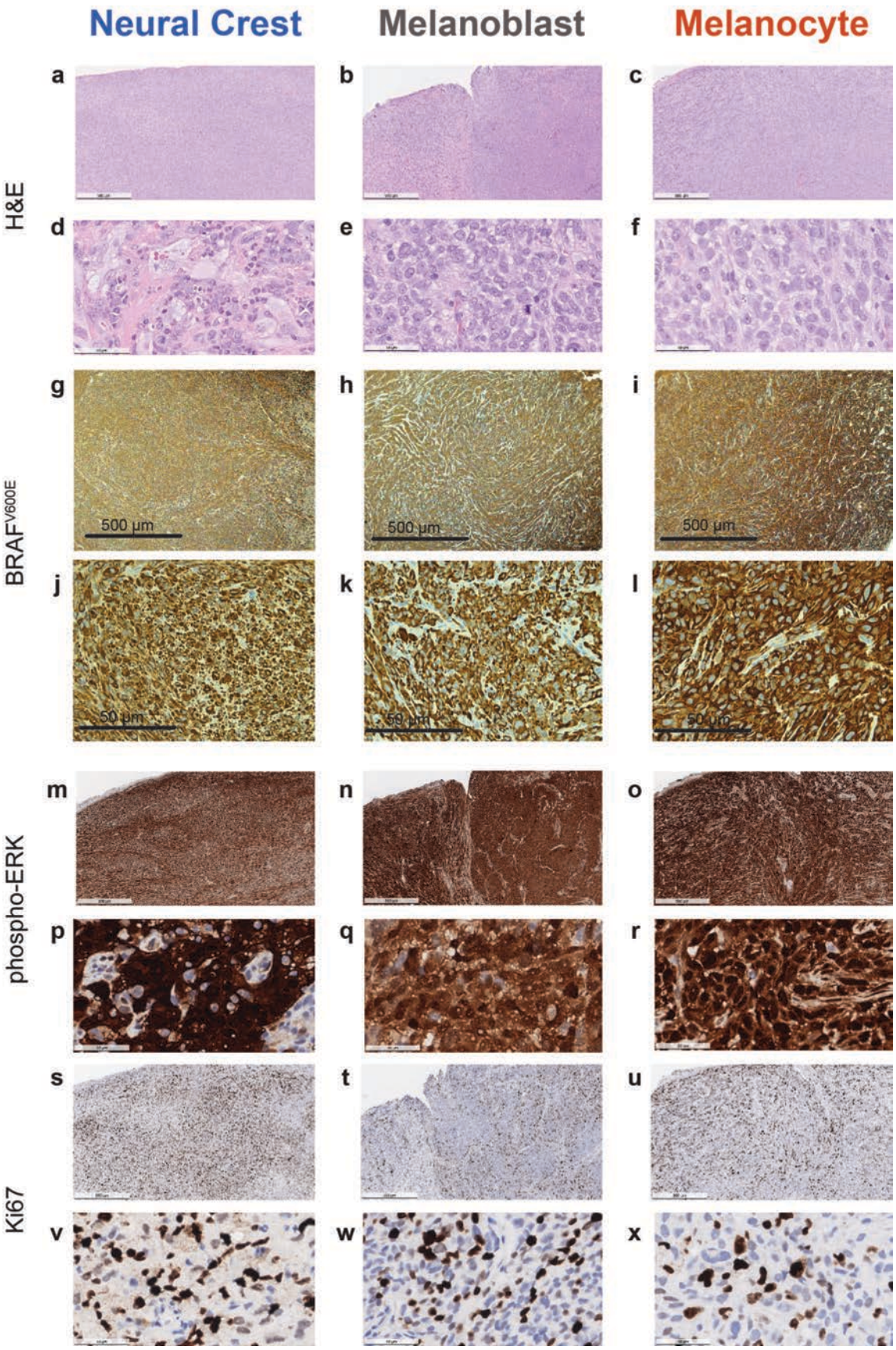
Neural Crest
Melanoblast
Melanocyte
H&E
BRAF^{V600E}
phospho-ERK
Ki67
a
b
c
d
e
f
g
h
i
j
k
l
m
n
o
p
q
r
s
t
u
v
w
x
500 µm
500 µm
500 µm
50 µm
50 µm
50 µm

Figure 3.15 Pathology of hES-derived tumors.
The hES-derived tumors that grew in vivo are poorly differentiated, spindled cell tumors. The tumors are all diffusely positive for mutant BRAF and pERK indicating proper expression and activation of the transgene. The tumors are very proliferative and all have a very high fraction of Ki67 positive nuclei. All images are taken at 4X (a-c, g-i, m-o, s-u) or 40X (d-f, j-l, p-r, v-x) scale bars 50μm and 500μm respectively. NC, n=2. MB, n=2. MEL, n = 1. (Pathology done in collaboration with Dr. Satish Tickoo and Dr. Travis Hollmann from the MSKCC Pathology Department)

Immunohistochemistry was then performed to determine the developmental lineage and differentiation phenotypes (Figure 3.16). In diagnosing malignant melanoma, S-100 protein is the most sensitive but least specific marker [352, 353]. Similarly, SOX10 is typically positive in malignant melanoma with few exceptions [354]. MITF is more specific to melanoma, but is absent in some melanomas [355]. Notably desmoplastic melanoma typically do not express SOX10 or MITF. cKIT expression is less frequently used to distinguish tumor types but is highly expressed in our system [356]. The MEL and MB derived tumors stain diffusely positive for S-100, SOX10, and cKIT suggesting a malignant melanoma (see Fig. 3.16i-n, q-v). The MITF is cytoplasmic and not nuclear and therefore interpreted as negative (see Fig. 3.16o-p, w-x). By contrast, the NC-derived tumor is only patchy positive for S-100 and negative for SOX10 suggesting a genuinely heterogeneous and undifferentiated tumor of less clear origin/diagnosis. The NC-derived tumor is similarly negative for MITF and only dimly positive for cKIT. Together these stains suggest that MB and MEL tumors are definitively melanomas (perhaps desmoplastic melanoma) while the NC tumors are very poorly differentiated tumors with some characteristics of desmoplastic melanoma.

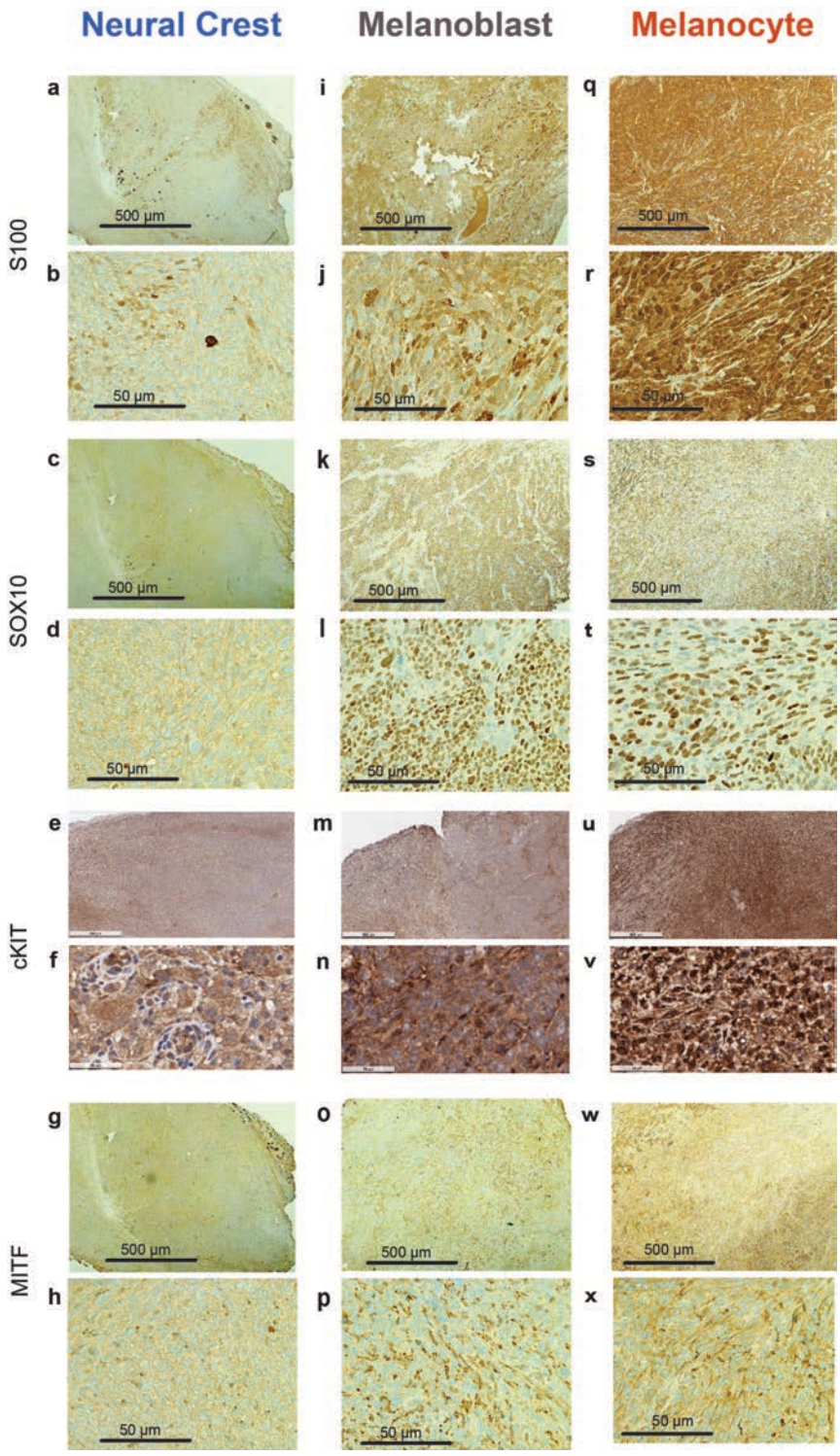

Figure 3.16 Differentiation markers of hES-derived tumors.

The hES-derived tumors that grew in vivo were stained for S100, SOX10, cKIT, and MITF. All images are taken at 4X (a,c,e,g,I,k,m,o,q,s,u,w) or 40X (b,d,f,h,j,l,n,p,r,t,v,x) with scale bars at 50µm and 500µm respectively. NC, n=2. MB, n=2. MEL, n = 1. (Pathology done in collaboration with Dr. Satish Tickoo and Dr. Travis Hollmann from the MSKCC Pathology Department)

The neural crest-derived tumors are poorly differentiated as they do not express melanocytic markers. We next tested for the presence of neuroblastoma and more general neural crest markers, akin to the *sox10*-transgenic fish tumors (Figure 3.17). MelanA is a routine marker for melanocyte differentiation but is frequently down-regulated in melanoma, particularly in spindle-cell melanoma [357]. Close examination of the MelanA staining suggested that all the tumor cells in the three conditions are negative. The positive MelanA staining is exclusively restricted to the small-nuclei, infiltrating neutrophils confirming that the hES-derived tumors are not highly differentiated melanomas. NCAM expression is frequently used to distinguish differentiation states within neuroblastoma, but can also be used to identify more metastatic melanoma or less differentiated desmoplastic melanoma [358-360]. The MB and MEL tumors stain positively for NCAM but the NC tumor is predominantly negative. Finally, HuC/D expression is strongly tied to neuroblastoma; HuD vaccinations have been used to treat animal models of neuroblastoma [361]. The neural crest/neuronal HuC/D marker stained diffusely positively in the *sox10*-fish neuroblastoma-like tumors [362]. All three tumors stain weakly positive for HuC implicating intra-tumor pockets of poorly differentiated or potentially metastatic prone cells. The HuC staining is more diffuse in the NC-derived tumors unveiling a less-differentiated tumor. The IHC staining further confirms a desmoplastic melanoma diagnosis for the MB and MEL derived tumors and a very poorly differentiated tumor (with some melanoma characteristics) in the NC derived tumors.

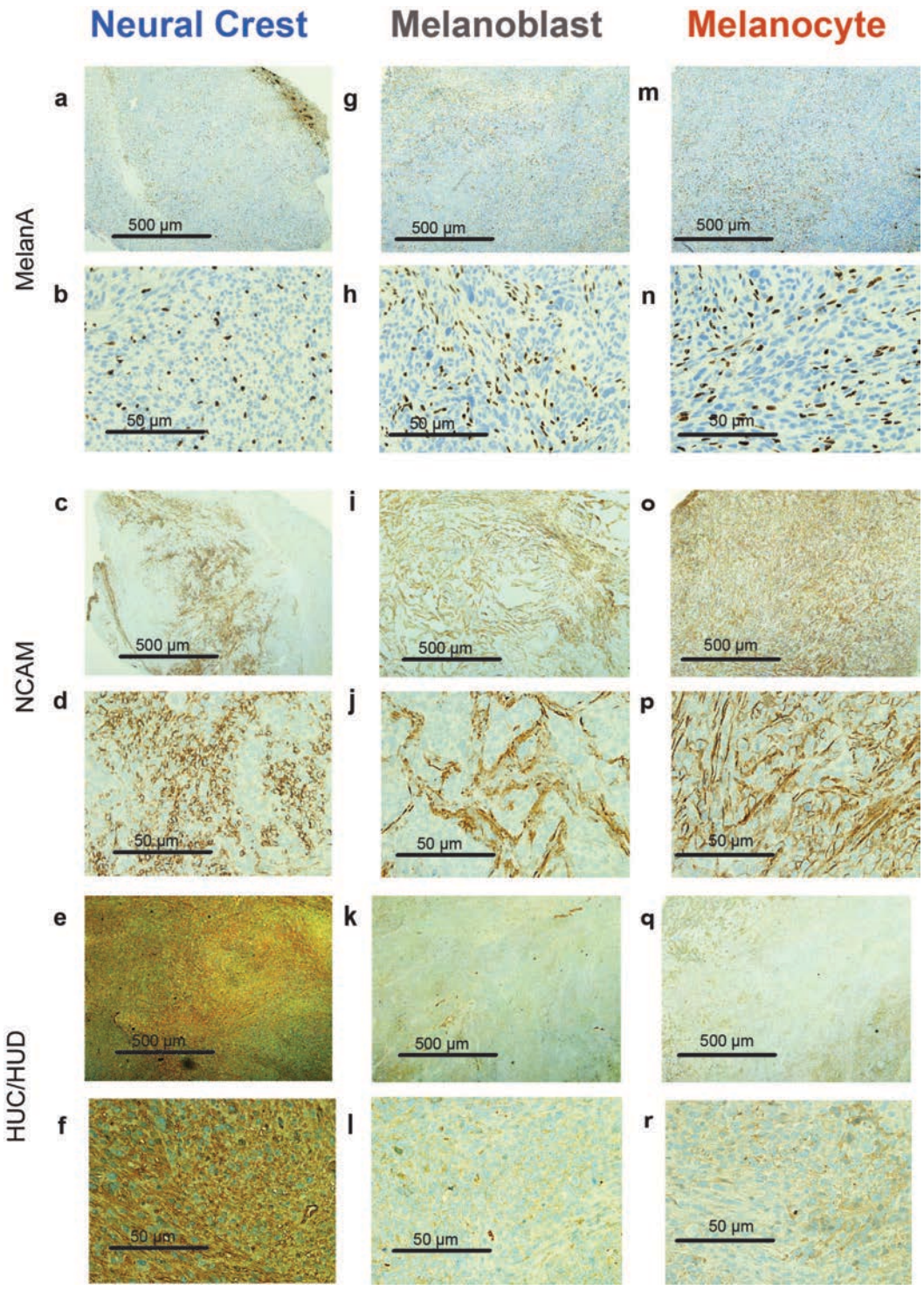

Figure 3.17 Immunohistochemistry of hES-derived tumors.
The hES-derived tumors that grew in vivo were stained for MelanA, NCAM, and HuC/HuD. All images are taken at 4X (a,c,e,g,l,k,m,o,q,s,u,w) or 40X (b,d,f,h,j,l,n,p,r,t,v,x) with scale bars at 50µm and 500µm respectively. NC, n=2. MB, n=2. MEL, n = 1. (Pathology done in collaboration with Dr. Satish Tickoo and Dr. Travis Hollmann from the MSKCC Pathology Department)

Transcriptional Data

To characterize the hES-derived cells *in vitro* we performed transcriptional profiling via RNA-sequencing with polyA selection using an Illumina HiSeq 2x150bp configuration. Transcriptional profiling was performed in triplicate on either WT or TKO hESC that have been differentiated into NC, MB and MEL. The differentiated cells were then maintained in the presence or absence of DOX (inducing $BRAF^{V600E}$) for two weeks before collecting total RNA. The transcriptional data allows us to first validate the three differentiation states. The sampling also allows us to compare the impact of mutant $BRAF^{V600E}$ at each stage of differentiation in the presence or absence of tumor suppressors.

To validate the differentiation states of NC, MB and MEL at each stage we compared the normalized RNA-seq counts for several important lineage genes during melanocyte differentiation (Figure 3.18). The melanocyte lineage genes are known to upregulate during differentiation from NC to MB and finally MEL. The upregulation of cKIT from NC to MB confirms that our FACS was successful. Furthermore, the correlated upregulation of MITF, DCT, PMEL, TYR, and TYRP1 validates our differentiation and isolation protocols. Finally, the lineage genes validate that our protocols work in both WT and TKO hESCs.

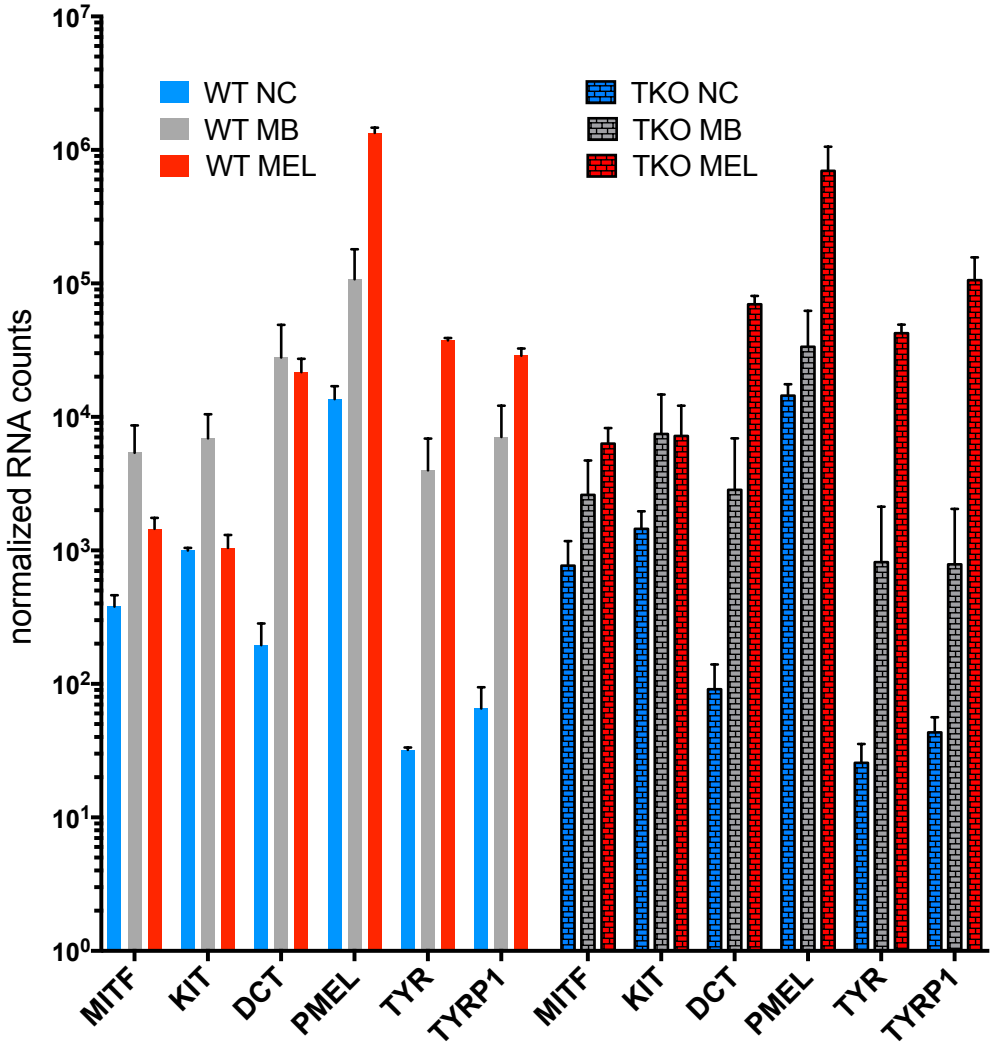

Figure 3.18 Validation of hES-derived neural crest and melanoblast by RNA-seq

The normalized RNA counts (means with standard deviation error bars) for lineage specific genes in hES-derived NC, MB and MEL from either the WT or TKO cell lines. (RNA-seq analysis was performed in collaboration with the Dr. Tuan Trieu from the Khurana lab at Weill Cornell)

Upon validating the differentiation status of the samples we queried the impact of the transgene $BRAF^{V600E}$ within each context. To analyze the number of genes impacted on a global level we performed differential expression analysis between the matched +/-DOX samples for each stage and for each genetic background. The resulting differentially expressed genes were then plotted with the mean

normalized count on the x-axis for each gene and the log fold change upon DOX for that same gene on the y-axis. Interestingly, the number of transcriptional changes upon mutant BRAF expression is very dependent upon the stage of differentiation, with $BRAF^{V600E}$ having a large effect on Neural Crest and Melanoblast cells, and minimal effect on Melanocyte cells. This stage specificity is true whether the tumor suppressors are knocked out or not (Figure 3.19). Mutant BRAF expression statistically changes (p-value < 0.05) a significant number of genes (WT: 760↑, 778↓; TKO 789↑, 1051↓) when activated at the neural crest stage (see Figure 3.18a,b). Similarly, mutant BRAF expression statistically changes (p-value < 0.05) a significant number of genes (WT: 737↑, 1022↓; TKO 737↑, 624↓) when activated at the melanoblast stage (see Figure 3.18c,d). In contrast, mutant BRAF expression does changes very few genes in the melanocyte stage (WT: 24↑, 384↓; TKO 23↑, 114↓) when activated in melanocytes (see Figure 3.18e,f). Therefore, mutant BRAF has a large impact on transcription at the NC and MB stage but a relatively minimal impact on transcription at the melanocyte stage. The context dependent impact of mutant BRAF despite the comparable pERK levels, indicates that melanocytes are either missing necessary co-factors or the epigenetic state is refractory to MAPK-pathway transcription changes.

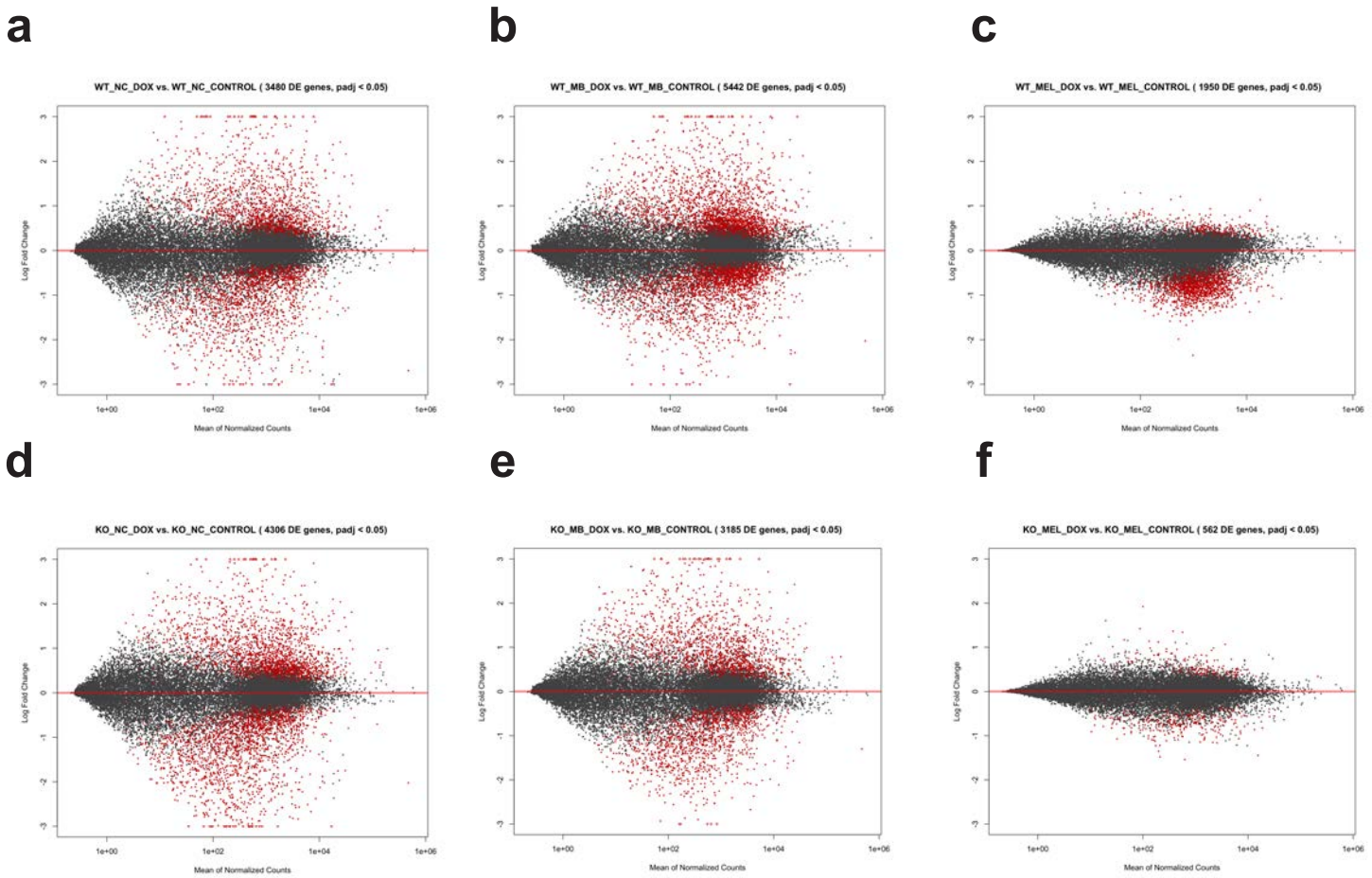

Figure 3.19 The transcriptional impact of mutant BRAF is context dependent.

The impact of mutant BRAF on transcription is plotted for WT (a-c) or TKO (d-f) cells in NC (a,d), MB (b,e) or MEL (c,f) cells. The mean of normalized counts of each gene is plotted against the log fold change following $BRAF^{V600E}$ within that condition. Adjusted p-value cut-off of 0.05 was used for significantly differentially expressed genes (red points). (RNA-seq analysis was performed in collaboration with the Dr. Tuan Trieu from the Khurana lab at Weill Cornell)

The relative transcriptional state of NC, MB, and MEL, as well as the global changes upon mutant BRAF activation can be visualized together using a principal component analysis (PCA). PCA uses an orthogonal transformation to convert global RNA-seq expression values into a set of principal components of diminishing importance. As a result the differences between transcriptional states can be roughly visualized in two-dimensions. The NC, MB, and MEL in the absence of DOX are segregated into three nearly distinct populations in PC1 vs. PC2 space (Figure 3.20). The TKO and WT cells for each differentiation state are mostly overlapping. Upon the introduction of DOX, the NC and MB cells dramatically move past the melanocytes in PCA space indicating a very large transcriptional change. Interestingly, upon the introduction of BRAF the melanocytes barely move in PCA space. They do move in the same direction as the NC and MB cells, but only a fraction as far. This visualizes the relatively small change in transcription of melanocytes upon the introduction of $BRAF^{V600E}$ in agreement with the plots in Figure 3.19. Finally, the TKO;NC + DOX and TKO;MB + DOX cluster together and separately from the WT;NC+DOX and WT;MB+DOX implying that the loss of tumor suppressors does change the final transcriptional state of the cells following $BRAF^{V600E}$ expression.

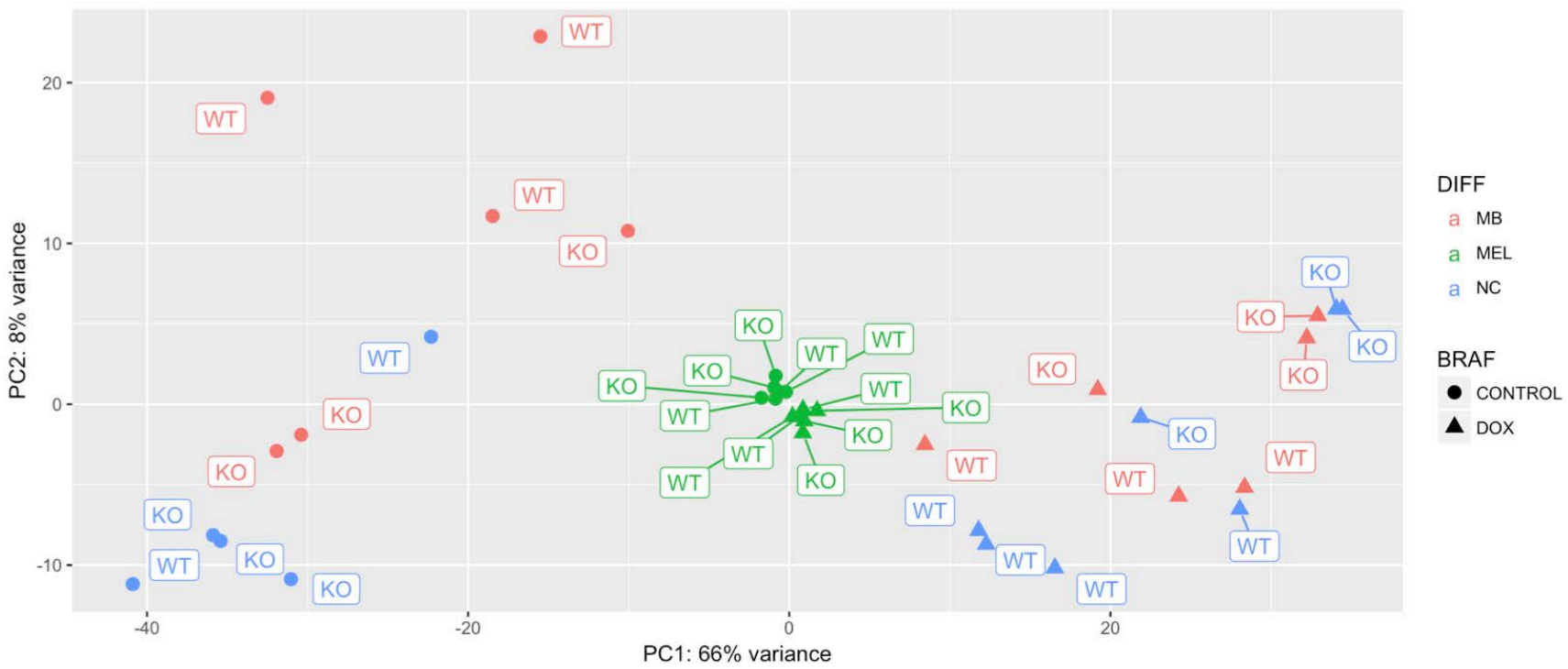

Figure 3.20 PCA analysis of the impact of mutant BRAF.

Principal component analysis of the RNA-seq data generated from all the samples. Samples exposed to DOX for two weeks are triangles and samples withheld from DOX are circles. NC = blue, MB = red, MEL = green. TKO =KO and WT = WT. (RNA-seq analysis was performed in collaboration with the Dr. Tuan Trieu from the Khurana lab at Weill Cornell)

The previous two figures clearly demonstrate that the extent of transcriptional change induced by $BRAF^{V600E}$ is very context dependent. To assess the overlap in transcriptional targets between conditions we created a six-part Venn Diagram (Figure 3.21). To simplify the presentation, the overlaps were collapsed onto two UpSeTR plots (one for genes that have increased expression in response to BRAF and one for decreased expression) [363]. UpSetR plots visualize the intersections of sets as a matrix in which the rows across the base represent the complete set and the columns represent the intersections. The total size of each set is shown in a bar chart to the left of the matrix. Connecting the sets with a darkened line shows the intersection of sets and the size of the intersection are shown in a bar chart in the Y-axis. For Figure 3.20, the x-axis is the six pairwise comparisons encompassing the total number of genes changed upon BRAF expression for each condition (2 genetic backgrounds and 3 differentiation states). The number of genes in common that are altered between conditions are illustrated through the bar graph. Interestingly, there is little overlap in transcriptional response to mutant BRAF expression. Figure 3.21a illustrates that the intersection of commonly up-regulated genes in response to $BRAF^{V600E}$ that are shared in all six conditions is only four genes (MMP1, LAMC2, ACTN1, and CDCP1). Furthermore, there aren't any down-regulated genes in common between all six conditions (Figure 3.21a). Together, these plots demonstrate that not only is the extent of transcriptional change to $BRAF^{V600E}$ context dependent but the transcriptional targets are context dependent as well.

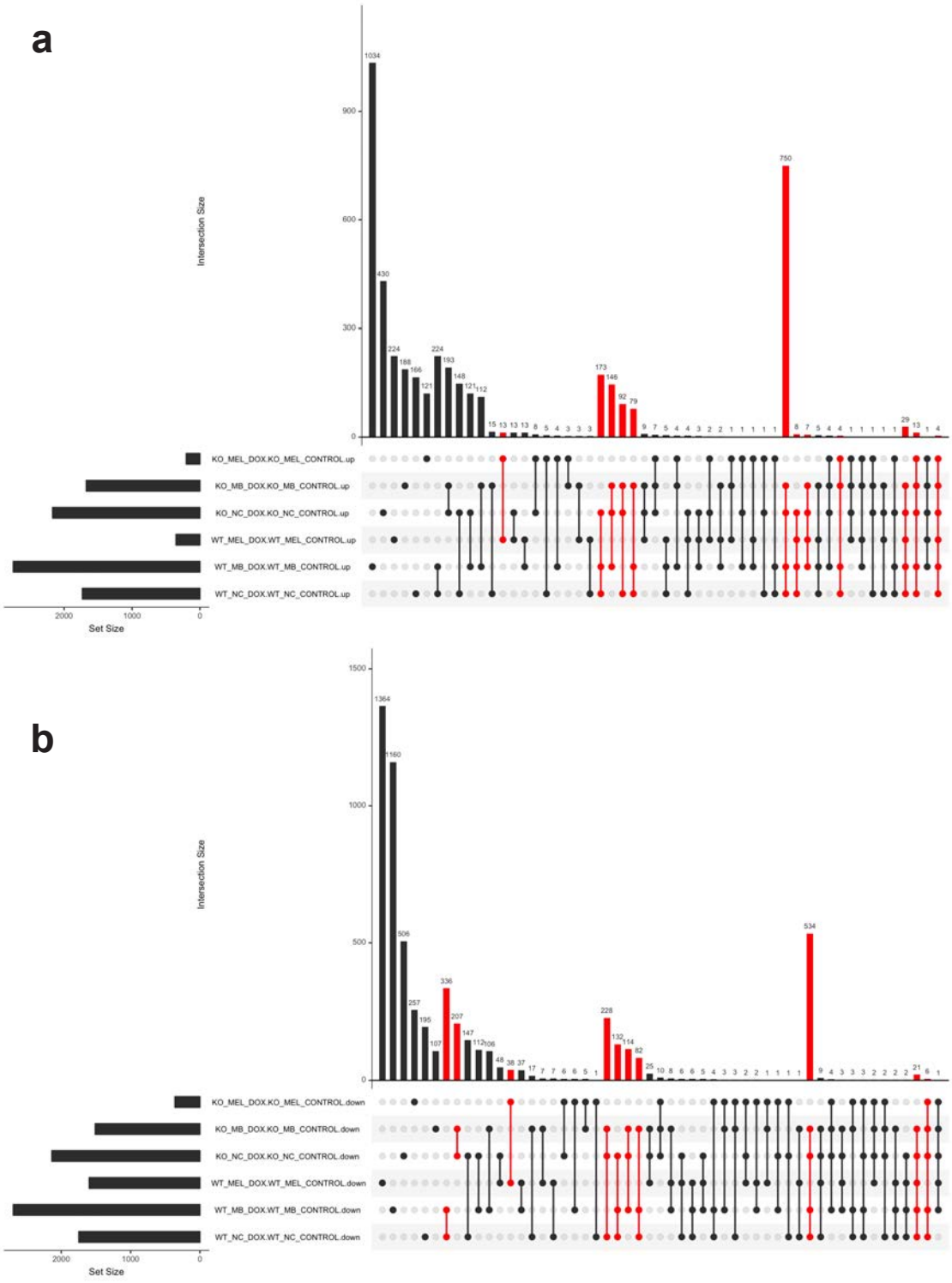

Figure 3.21 The transcriptional targets of BRAF^{V600E} are context dependent.
UpSetR plot for the (a) up-regulated genes (fold change>0) or (b) down-regulated genes (fold change<0) upon BRAF^{V600E} expression for the NC, MB, or MEL stage in WT or TKO cells. P-values < 0.05 are shown in red. (RNA-seq analysis performed in collaboration with the Dr. Tuan Trieu from the Khurana lab at Weill Cornell)

3.3 Discussion

Our study has established a readily scalable, defined protocol that generates pure populations of mature melanocyte with great efficiency using completely chemically defined media. Furthermore, our study has developed a DOX-inducible hESC for the temporally controlled expression of $BRAF^{V600E}$, enabling cancer and signaling modeling. Finally, our study has developed a series of hESC with every permutation loss of TP53, CDKN2A, RB1, and PTEN. The combinations of tumor suppressor losses will enable the careful systematic testing of each tumor suppressor as well as each combination. The various mutations will also aid us in understanding if the order of tumor suppressor loss or oncogene expression is important for tumor formation.

There is a very clear delineation of phenotypes depending on the genetic background and differentiation state of the cell of origin driving $BRAF^{V600E}$ transgene expression. Melanocytes are resistant to transcriptional control by $BRAF^{V600E}$ expression, independent of tumor suppressors. The loss of tumor suppressors does limit the number of down-regulated genes following $BRAF^{V600E}$ but does not rescue the global effects seen at the NC and MB stages. Similarly, melanocytes are resistant to transformation as quantified *in vitro* (EdU staining) or *in vivo* (xenograft assay). Conversely, $BRAF^{V600E}$ expression greatly distorts the transcriptional program of NC and MB in both WT and TKO genetic backgrounds. The transcriptional effect is mirrored in the *in vivo* transformation

assay where both NC and to a greater extent MB tumors grew in the TKO background.

The simplistic four-gene BRAF-induced transcriptional signature that is repeatedly up regulated in all conditions has seemingly diverse and random functions and does not seem to relate to a specific cellular role. The lack of a distinct functional uniform $BRAF^{V600E}$ signal across the different conditions is very intriguing and adds further evidence that the cell of origin will be indicative of eventual tumor formation. Future studies are being undertaken to understand the mechanism for transcriptional specificity between the cell phenotypes. Specific focus is being paid to genes that are commonly regulated in NC and MB but not in MEL. The most compelling hypothesis to data is that the BRAF signal is modulated by the different epigenetic states.

Tumor growth in the xenograft assay remains the gold standard transformation assay. The long latencies displayed by our hES-derived tumors are perplexing. We speculated that the latency is due to either the necessity for (1) additional genetic mutations to accumulate, (2), outgrowth of a tiny subpopulation (3) improper growth conditions, or (4) epigenetic changes. We have performed IMPACT DNA-sequencing on the outlier MEL tumor and a representative MB tumor pre- and post-injection of the mouse xenograft studies. The MB tumor did not accrue any additional mutations *in vivo*, suggesting that the sudden tumor growth following a long latency cannot be explained by additional mutations. The

MEL outlier tumor did accrue a mutation in DNMT3B while *in vivo*. DNMT3B is an established oncogene in melanoma and the mutation may explain why only a single MEL tumor grew out [364]. However, this is still preliminary and will require functional studies to test if the mutation is activating or inhibiting and the impact downstream. To test whether the latency results from the outgrowth of a subpopulation, dilution xenograft studies should be performed. To test for the necessity of re-shaping a poor microenvironment, the tumor could be re-transplanted. If the required changes were cell autonomous the secondary tumors should grow rapidly. If the required changes were related to the microenvironment the secondary tumors will retain long latency periods. Finally, to test if the long latencies result from an epigenetic change the epigenetic state and transcriptome of the cells should be assayed pre- and post- transplant. Additionally, the epigenetic state can be exogenously modified with drugs or over-expression studies.

CHAPTER FOUR: COMPARING MODELS SYSTEMS AND PATIENT DATA

4.1 Introduction

Genomic classifications of cutaneous melanomas are employed to guide clinical decisions. We hypothesize that cell of origin will impact the molecular identify of the resultant tumor, and that subgroups of melanoma patient samples will independently cluster with model tumors. To address this question at the transcriptional level we have collected gene expression data (RNA-sequencing) for tumors derived from each stage of differentiation in both model systems. For the hPSC-derived tumor models we have analyzed RNA-sequencing data from *in vitro* transformed cells (n=36; triplicate of 2 genotypes at 3 stages with or without DOX). For the zebrafish tumors, we have dissected whole tumors for RNA-seq analysis (n=12 for the neural crest or n=6 for melanoblast derived tumors). When analyzed independently, both hPSC-derived and zebrafish tumors segregate according to cell of origin using unsupervised clustering and principal component analysis.

4.2 Results

Comparison between transgenic fish tumors and hES-derived tumors

The zebrafish and human embryonic stem cell models performed similarly when challenged with oncogenic insults at the NC, MB, and MEL stage. In both scenarios MEL are resistant to transformation while the earlier stages formed tumors. MB-derived tumors most resemble melanoma at the morphological and

histological level in both models. NC-derived tumors resemble very poorly differentiated heterogeneous tumors with aspects of poorly differentiated melanoma. To compare the fish to human models, we used Gene set enrichment analysis (GSEA) to compare the transcriptome of the transgenic zebrafish tumors and the hES-derived cells. We first generated an ordered list of the differentially expressed genes between the *sox10*:BRAF tumors and the *mitfa*:BRAF zebrafish tumors. The differentially expressed genes were then used to query which hES-derived expression dataset most closely resembles the mitfa or sox10 derived tumors using GSEA. GSEA takes the ordered list of differentially expressed genes of the fish tumors and any pair of hES samples and queries which ordered dataset is the most similar. Of all the patient samples, the zebrafish *sox10*-derived tumors most strongly resemble the hES-derived NC cells, and the zebrafish *mitfa*-derived tumors most strongly resemble the hES-derived MB cells (Figure 4.1). This suggests that there is a core transcriptional commonality between the two model systems. The zebrafish *mitfa*-derived tumors resemble the WT hES-derived MB cells (NES = 1.71 and FDR q-value=0.0) even more than the WT hES-derived MEL cells (NES = N/A and FDR q-value=1.0). The zebrafish MB tumor is largely absent of pigmentation, which explains why transcriptionally clusters closer to hES MB rather than hES MEL.

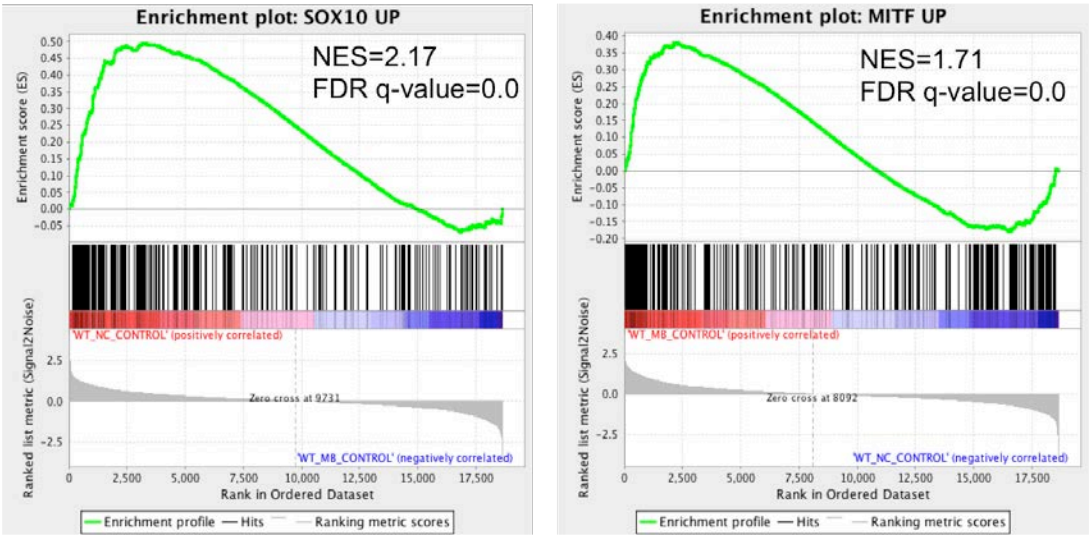

Figure 4.1 Zebrafish and hES model are transcriptionally similar.
Gene set enrichment analysis (GSEA) shows that sox10-derived zebrafish tumors most closely resemble WT hES-derived neural crest cells (left) and mitfa-derived zebrafish tumors most closely resemble WT hES-derived melanoblasts (right).

Comparison of human data to TCGA patients

To address the clinical relevance of our models we also compared our transcriptional data to the 331 primary and/or metastatic melanomas sequenced for the TCGA melanoma publication [141]. The TCGA samples consisted of 67 (20%) primary cutaneous melanomas (all originating from non-glabrous skin) and 266 (80%) metastases. The TCGA dataset is a very complete profiling with solution-based hybrid-capture whole-exome sequencing, DNA copy-number profiling by Affymetrix SNP 6.0 arrays, mRNA sequencing, microRNA sequencing, DNA methylation profiling, and reverse-phase protein array (RPPA) expression profiling. Based on the most prevalently mutated genes, the patients were clustered into one of four groups: mutant BRAF, mutant RAS, mutant NF1, and Triple-WT (wild-type).

A principal component analysis integrating whole transcriptome data from both our hES-derived cells and the TCGA patients clearly illustrates that the hES-derived cells resemble melanoma patients (Figure 4.2). Interestingly, the hES-derived models divide into two clusters that bookend the melanoma patients in PCA space. The MEL samples (largely encompassed within the red circle) represent one extreme of patients and the NC/MB samples (largely encompassed within the blue circle) represent the opposite extreme. The outlier TKO hES-derived MEL samples fall within the patch of patient samples. Whether these patients in the TCGA represent more or less differentiated tumors awaits further analysis.

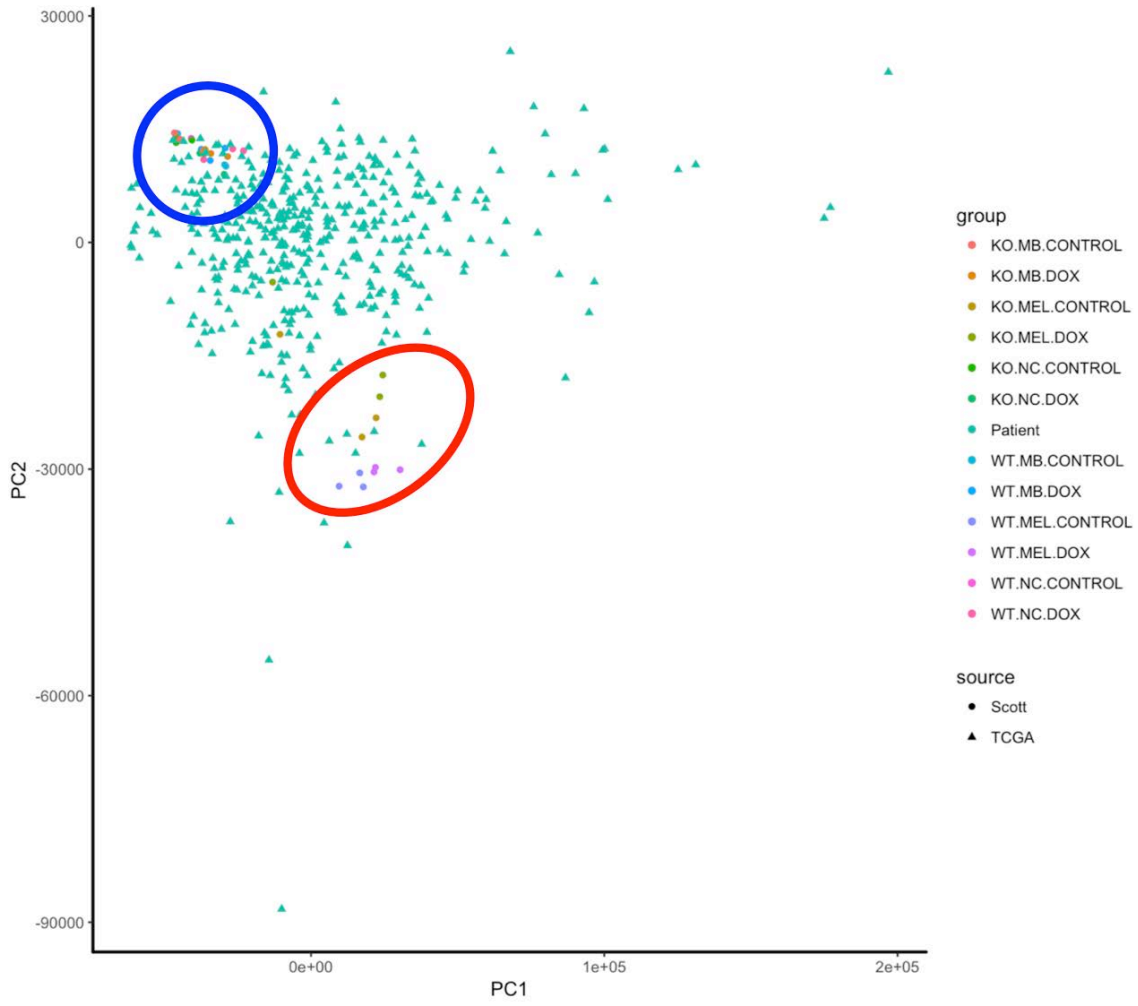

Figure 4.2 The hES-derived model clusters with TCGA melanoma patients.
Principal component analysis of whole transcriptome sequencing including the hES-derived cells and the TCGA patient data (RNA-seq analysis was performed in collaboration with the Dr. Tuan Trieu from the Khurana lab at Weill Cornell)

4.3 Discussion/Future Directions

The diversity between melanoma patients has been a long-appreciated but relatively poorly understood phenomenon. In the current study we present the first study hoping to model the differentiation status of melanoma based on the cell of origin using both hES-derived cells and transgenic zebrafish. In each

model system, we looked to drive oncogenesis in NC, MB or MEL cells and study the resulting tumor.

The two independent model systems behaved similarly when queried for the importance of cell of origin in melanoma formation. In both models, the melanocytes proved relatively resistant to transformation. Similarly, both models yielded tumors when NC and MB were transformed. Both tumors expressed $BRAF^{V600E}$, phosphorylated ERK, and SOX10 at very high levels. Interestingly the models diverged when comparing the relative levels of HuC/HuD and NCAM. The Melanoblast tumors more closely resemble typical melanoma, whereas the Neural Crest tumors resemble either a poorly differentiated melanoma or neuroblastoma.

To gain a deeper understanding of the similarities between models we compared the tumors transcriptionally. The comparison is not ideal as the hES-derived cells were profiled prior to transplantation and tumor outgrowth while the zebrafish transgenic cells were excised and profiled after large tumor outgrowth. Nonetheless, GSEA confirms a significant enrichment between the zebrafish NC and MB tumors and the hES-derived NC and MB respectively.

We utilized transcriptional profiling to inform the applicability of our model systems for modeling the broad spectrum of melanoma patients. To represent the diversity of melanoma patients we utilized the RNA-sequencing data from the

TCGA project. The PCA plot strongly supports the paradigm that melanoma patients represent a spectrum of differentiation states between NC/MB and MEL. Interestingly, the hES-derived cells represent the extremes of transcriptional states in PCA space amongst the broad range of melanoma patients. The hES-derived cells bookend the patient profiles. This plot powerfully endorses the importance of differentiation in defining diversity between patients and validates the hES and zebrafish melanoma models described in this thesis for representing the equivalent human disease.

CHAPTER FIVE: TRANSGENE ELECTROPORATION IN ADULT ZEBRAFISH (TEAZ)

5.1 Introduction

This Chapter describes work that was published in Disease Mechanisms and Modeling on the 27th of Septermber 2018 [365]. doi: 10.1242/dmm.034561.

The zebrafish has become an increasingly applied model in cancer biology at the interface of basic discovery and preclinical animal experimentation. The high fecundity and relatively simple husbandry enable large experimental series *in vivo*. Early cancer models in zebrafish were largely developed using mutagens such as MNNG or DMBA, which were later supplanted by transgenic technologies[366-368]. The initial transgenic cancer models were developed by injecting 1-cell zebrafish embryos with DNA constructs containing a promoter and oncogene. For example, T-cell ALL was modeled by transgene driven expression of the *MYC* oncogene using the *rag2* promoter, and melanomas generated by expressing $BRAF^{V600E}$ under the *mitfa* promoter in a $tp53^{-/-}$ germline mutant background [279, 337, 369].

Despite the documented power of transgenic tumor models for mechanism discovery and drug testing, current models have several significant drawbacks: i) the majority of established models do not exhibit spatio-temporal control, such that the timing and anatomical location of tumor onset remains variable [53, 60, 279], ii) they generally do not enable the introduction of serial somatic oncogenic

events for modeling second and third hit mutations after onset[281, 282]; and iii) discerning multifocal primary tumors versus true metastatic spread of a single tumor is challenging [60]. These issues all impose significant limitations for investigating tumor progression and metastasis.

Transplantation-based methods address some of these issues: tumors can be dissected off from a transgenic tumor-bearing animal or from patient-derived xenografts (PDXs), and then serially transplanted into recipient animals such as the *casper* recipient strain to allow detailed *in vivo* imaging [267, 268, 283-286]. Alternatively, stable cell lines can be generated from a transgenic animal, such as the ZMEL1 melanoma line, which can be similarly used for transplantation studies [268]. While these transplantation approaches allow for precise spatiotemporal control and are amenable to imaging of metastasis, these experiments often require immunosuppression of the recipients either through irradiation or genetic manipulation of immune cells [285], in addition to the initial generation of the suitable cell line. Recent work from the Langenau lab has shown that syngeneic fish can be used as transplant recipients, but these require that the tumors be developed in that particular genetic background, somewhat limiting their broad use across cancer [287]. Furthermore, transplantation cancer models implant foreign tumors into inherently artificial microenvironments.

A variety of Cre/Lox based approaches have been used in the zebrafish to control the cells that undergo initiation, including T-cell leukemia that can be

controlled by mRNA injection [369]. A further modification uses CreERT2 drivers, such that both the cell type and timing of gene expression can be controlled [370], and inducible expression has also been achieved with heat shock Cre constructs [371]. Despite these advances, there is still a paucity of verified Cre/Lox-based approaches to cancer in the zebrafish, as the transgenic animals have proven time-consuming to create, and require complex breeding schemes to generate the final required genotypes.

Based on this, we wished to develop an approach that would enable introduction of oncogenic elements directly into adult somatic tissue in a spatio-temporally controlled manner. In this manuscript, we report oncogenesis via Transgene Electroporation into Adult Zebrafish (TEAZ), which models how tumors natively form in somatic tissues in a fully immunocompetent adult zebrafish. Electroporation applies electrical pulses to generate pores within the cell membrane, enabling extracellular biomolecules (including DNA) to enter the cell [288, 289]. Electroporation is widely used for stable introduction of DNA elements into cells in tissue culture and into chick and mouse embryos. Electroporation has occasionally been utilized in adult zebrafish but these studies have been limited to cell tracking and transient morpholino knockdowns and have never been applied to cancer modeling [290-293, 372]. Several studies in mice have harnessed electroporation to introduce transgenes into select adult tissues, including retina, muscle, brain, and prostate [294-296] and has been used to model tumors such as pancreatic cancer [294, 298, 299]. However, these

approaches require surgery of the mice and can only be limited to a small number of animals at a time, limiting the number of subjects that can be reasonably studied in each experiment. Based on these prior observations and the very large cohorts we can generate, we reasoned that direct electroporation of oncogenic transgenic constructs into the zebrafish would be a straightforward, highly scalable approach to model tumor formation in cells of interest. Because electrodes and DNA solutions can be placed at defined locations, TEAZ allows for delivery of multiple transgenes specifically to the anatomical locations of interest. We find that TEAZ allows for the development of complex, aggressive melanomas driven by expression of oncogenic $BRAF^{V600E}$ in concert with loss of the tumor suppressors *p53* and *rb1*. These tumors are highly invasive and eventually metastasize to distant locations, unlike previous transgenic zebrafish melanoma models, which do not generally metastasize [279]. Given the wealth of functionally uncharted genetic lesions discovered from sequencing human tumors, TEAZ allows for testing of candidate mutations in a rapid, scalable *in vivo* system. More broadly, TEAZ can also be used to study somatic alteration of gene function in any adult tissue, which will have applications for diseases outside of cancer as well.

5.2 Results

Introduction of genetic elements into adult zebrafish via electroporation

The TEAZ method is designed to introduce genetic elements into specific locations within the adult zebrafish (Figure 5.1). The method has been optimized

for the use of plasmids generated in *E. coli* and purified using standard plasmid purification protocols (midi preps). To test this protocol, we anesthetized adult zebrafish, and then injected 1.0 µl purified plasmid DNA (1000ng/µl) directly under the dorsal fin. The injected zebrafish was then quickly placed into an agarose mold to position the animal upright. Using paddle-shaped electrodes, we directed electrical pulses across the injected region (electroporator set to LV mode, 45V, 5 pulses, 60ms pulse length, 1s pulse interval). To maximize expression in the skin as opposed to deeper tissues, the cathode paddle can be placed just above the surface where the DNA was injected as this will pull the negatively charged DNA towards the surface adjacent to the injection site. After electroporation, we placed the anesthetized zebrafish into fresh water for recovery and maintenance through standard husbandry. Including anesthetization, DNA injection, and electroporation, the entire protocol takes approximately 45-60 seconds per animal.

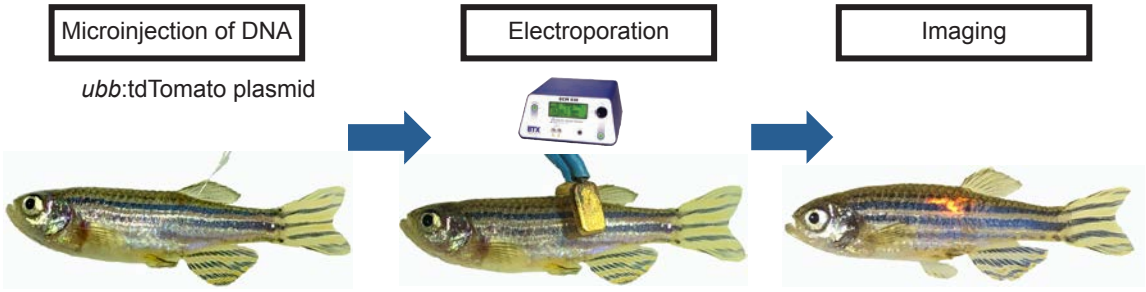

Figure 5.1 Transgene Electroporation into Adult Zebrafish (TEAZ).
Schematic representation of the method, applied for the introduction of ubb:tdTomato directly under the dorsal fin of adult zebrafish. The purified plasmid DNA (1µl of a 1000 ng/µl solution of ubb:dTomato) was injected into anesthetized zebrafish using a pulled glass micropipette. Electrical pulses are directed across the injected region (settings = LV mode, 45V, 5 pulses, 60ms pulse length, and 1s pulse interval). Reporter expression can be visualized by fluorescent microscopy (n=2/2).

To establish TEAZ, we injected wild-type zebrafish (*AB* strain) with a plasmid in which the zebrafish *ubiquitinB* promoter (*ubb*) [373] drives tdTomato expression (*ubb*:tdTomato). This vector was created using the Tol2 transposon system that is commonly deployed in the zebrafish [335, 336, 374-376]. In our studies, we did not use transposase mRNA because in preliminary tests we were unable to drive fluorescence from mRNA (either GFP or tdTomato) following electroporation (data not shown). After TEAZ, we imaged the electroporated zebrafish starting at 1 day post electroporation (1 dpe) and over the course of several months. Figure 5.2 shows an example animal, in which stable expression of tdTomato (under the *CMV* promoter) was detectable for up to 8 months (see Figure 5.2). Similarly, the stable expression of *ubb*:GFP-p2a-tdTomato was also detectable after 8 months post electroporation (n = 4/4).

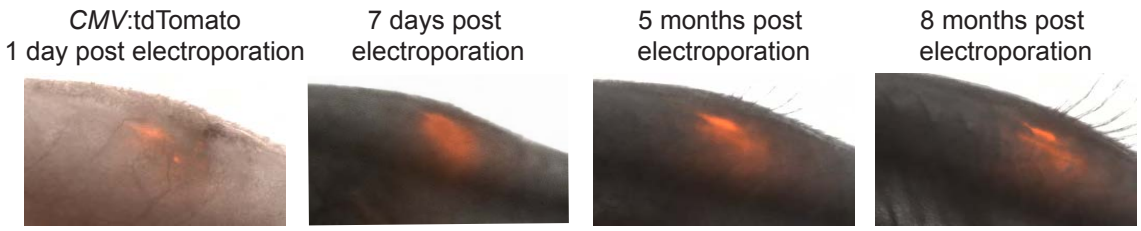

Figure 5.2 TEAZ signal is maintained long term.
(Electroporation of a CMV:tdTomato plasmid was performed and the animal followed for a period of 8 months (n=2/2). The fluorescent signal can be visualized as early as 1 day post-electroporation (dpe), with intensity peaking around one week and maintaining for at least 8 months.

We also tested whether the same *ubb* promoter and TEAZ would express in other parts of the animal by injecting it directly into the head. We observed robust expression of *ubb*:GFP in the head in 4 of the 5 animals electroporated (Figure 5.3). indicating TEAZ-mediated transgene activity is not restricted to a particular

location on the adult zebrafish body. At the site of electroporation there is initially a small area of tissue damage, that is rapidly healed within a week. We have never seen ectopic expression of the transgene away from the site of electroporation, nor have we observed any systemic toxicity or obvious procedure-caused death in several hundred similarly electroporated animals. In addition, to ensure lack of germline transmission, we electroporated several different constructs (Table 5.1), waited for adult expression, and then bred those animals to WT adults. We then screened the resultant embryos at both 1dpf and 4dpf and saw no animals with fluorescence (n=947 embryos). This indicates that the TEAZ method allows for highly focal, somatic transgenesis at the site of electroporation.

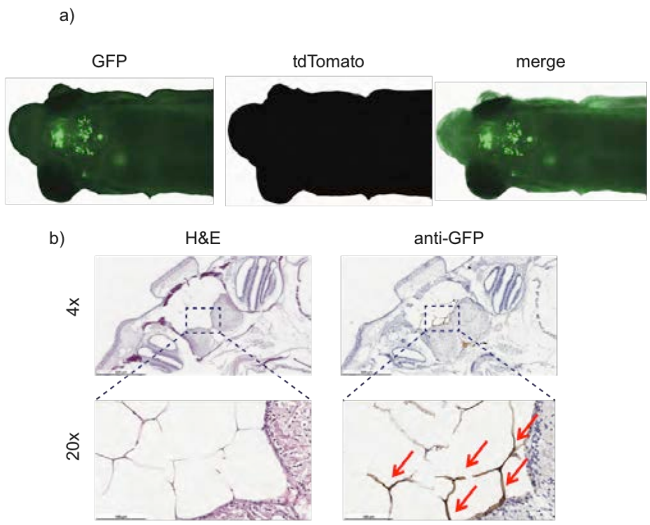

Figure 5.3 TEAZ can be used to introduce transgenes in the adult brain.
TEAZ can be used to introduce transgenes in the adult brain. (a) Purified plasmid encoding ubb:GFP (1µl of a 1000 ng/µl solution) was injected through the skull of an anesthetized casper zebrafish directly into the brain cavity using a pulled glass micropipette. The injected zebrafish is then electroporated across the dorsal-ventral axis of the head with the cathode positioned below the jaw and imaged for GFP fluorescence (n=4/5). (b) Pathology of the same electroporated casper zebrafish with hematoxylin and eosin or immunochemistry against GFP to demonstrate reporter expression. GFP expression highlighted with red arrows. Images are visualized at 4x and 20x where scale bars represent 500 µm and 100 µm respectively.

Absence of Germline Transmission with TEAZ

DNA Construct	Site of TEAZ	Days post TEAZ	Embryos 1DPF (fluorescent/total)	Embryos 4DPF (fluorescent/total)
p.mitf-TdTomato-sv40	Heart	70	0/18	0/18
p.ubi-TdTomato-sv40	Flank	140	0/521	0/521
p.ubi-GFP-sv40	Brain	182	0/195	0/195
p.sox10-GFP-sv40	Brain	189	0/213	0/213

Table 5.1 TEAZ does not transmit via the germline.
To ensure the absence of germline transmission following TEAZ, we electroporated several different constructs, waited for adult expression, and then bred those animals to WT adults. We screened the resultant embryos at both 1dpf and 4dpf and we did not see any fluorescent offspring (n=947 embryos).

TEAZ allows for simultaneous expression of multiple plasmids

Electroporation of multiple plasmids into cultured cells *in vitro* generally leads to joint uptake of the plasmids by cells and subsequent co-expression of the transgenes. To test this in the zebrafish, we performed TEAZ with two plasmids in a single injection. We co-injected the *ubb*:tdTomato plasmid along with a *ubb*:GFP plasmid (each at 0.5 µl of 1000ng/µl plasmid stock) and then monitored fluorescence. High magnification views demonstrated that 100% of the transgene expressing cells were double positive for both GFP and tdTomato (n=3/3 fish) (Figure 5.4). Consequently, TEAZ can be expanded to express and combine multiple transgenes in the adult zebrafish skin.

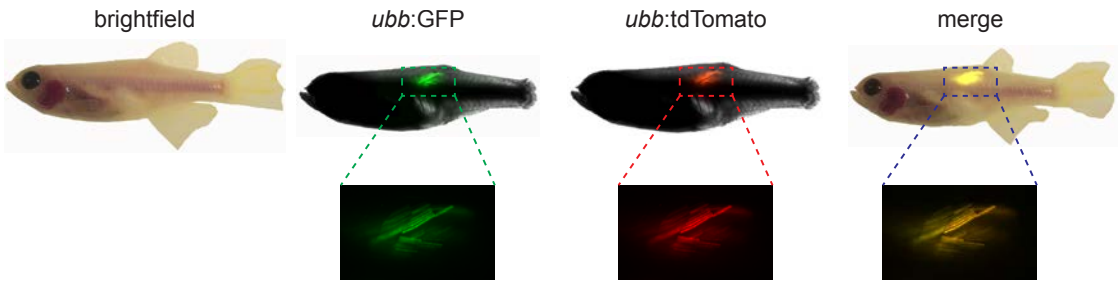

Figure 5.4 Multiple plasmids co-integrate using TEAZ.
Multiple plasmids will co-integrate in TEAZ. casper zebrafish were electroporated with a total volume of 1.0 µl (0.5 µl of 1000ng/µl ubb:GFP and 0.5 µl of 1000 ng/µl ubb:tdTomato) and imaged using BF, GFP, and tdTomato (n=3/3), revealing co-expression of the plasmids.

Maintenance of promoter specificity following electroporation

We next sought to determine whether TEAZ enables cell type-specific transgene expression. We co-electroporated *mitfa:tdTomato* [76] (which drives in melanocytes) and *ubb*:GFP (which drives ubiquitously) plasmids and then imaged the zebrafish using both tdTomato and GFP channels. A representative animal is shown in Figure 1d (n=9/9). As anticipated, we detected broad and strong expression of GFP from the *ubb* promoter [373]. In contrast, we found highly limited expression of the *mitfa*:tdTomato plasmid. High resolution imaging of the tdTomato-positive cells revealed a dendritic appearance that is consistent with the appearance of mature melanocytes (Figure 5.5).

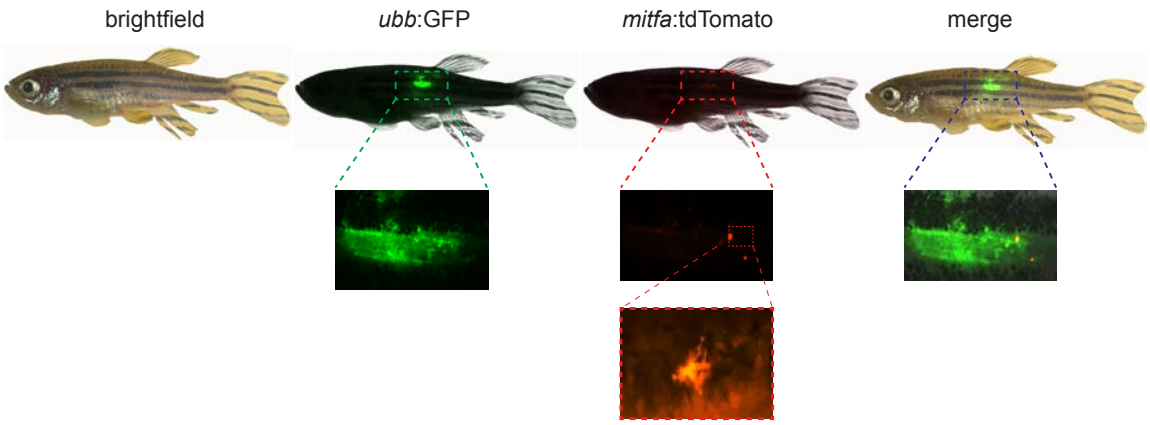

Figure 5.5 Promoter specificity is maintained using TEAZ.
Promoter specificity is maintained following TEAZ. AB fish were electroporated with 1.0 µl total volume (0.5 µl of 1000 ng/µl ubb:GFP and 0.5µl of 1000 ng/µl mitfa:tdTomato) and displayed highly restricted expression of the mitfa reporter plasmid, but widespread expression of the ubb plasmid (n=9/9). High-resolution imaging of the tdTomato-positive cells reveals a dendritic phenotype consistent with the melanocytic lineage.

We next tested expression in the heart using the cardiomyocyte-specific *myl7* promoter driving GFP (*myl7:GFP,* formerly referred to as *cmlc*:GFP) [377]. We injected and electroporated *myl7:GFP* plasmid directly into the beating heart muscle of an anesthetized adult zebrafish. We found strong and specific expression of GFP in the beating heart (n = 2/4) (Figure 5.6). Importantly, when *myl7*:GFP was electroporated below the dorsal fin (n=5) and *mitfa*:tdTomato was electroporated into the heart (n=5) fluorescence was not detected showing that expression is highly cell type specific and driven by promoter specificity. We conclude that TEAZ-mediated vector delivery maintains promoter specificity following electroporation, enabling us to target specific somatic cell types within specified regions of adult zebrafish.

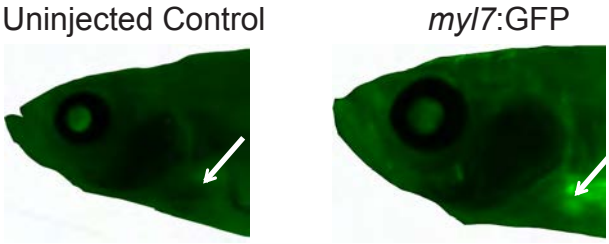

Figure 5.6 TEAZ can be used to introduce transgenes in the adult heart.
TEAZ can be extended to expression within the heart of adult zebrafish. Casper fish were injected into the heart through the gills with 1 µl of 1000ng/µl of a plasmid carrying the myl7:GFP transgene (along with a ubb:Cre cassette that is unrelated for the purposes of this study) (n=2/4). Heart is highlighted with white arrow.

Melanoma initiation requires multiple transgenes

We next sought to apply TEAZ to directly model melanoma formation in adult zebrafish, circumventing embryonic manipulations. We and others have previously used a traditional germline melanoma transgenic in which the *mitfa* promoter drives oncogenic $BRAF^{V600E}$ [279, 282]. In a $p53^{-/-}$ deficient background, these transgenic animals develop a 100% penetrant melanoma at 4-12 months of age without any additional transgenes [53, 279]. This original transgenic was further extended using the *MiniCoopR* system [154], in which the *mitfa* gene itself is knocked out, creating a strain with the genotype *mitfa*:$BRAF^{V600E}$;$p53^{-/-}$;$mitfa^{-/-}$ (heretofore referred to as the "*triple*" strain). When this *triple* strain is injected at the 1-cell embryo stage with a "rescue" plasmid containing an *mitfa:mitfa* and *mitfa*:GFP cassette *in cis*, the resultant animals have rescued GFP+ melanocytes that all go on to develop GFP+ melanomas as adults [154].

To test whether TEAZ is adaptable to this approach and could enable circumvention of initiating transgene expression at embryonic stages, we electroporated the *MiniCoopR:GFP* rescue cassette under the dorsal fin of *triple* strain adult zebrafish (Figure 5.7). We found that 8/10 injected animals developed GFP fluorescence at the site of injection, and remarkably, 1 of the animals developed rescued melanocytes. This indicates that it is possible to "rescue" melanophore development in a germline genetic defect (i.e. *mitfa*$^{-/-}$) by directly electroporating a minigene cassette into adult somatic tissues. However, none of these animals went on to develop melanoma over a period of 4 months, a duration that leads to melanoma in embryo injection-based experiments. This observation suggests that in TEAZ, additional genetic hits are necessary above and beyond BRAF and *p53*$^{-/-}$.

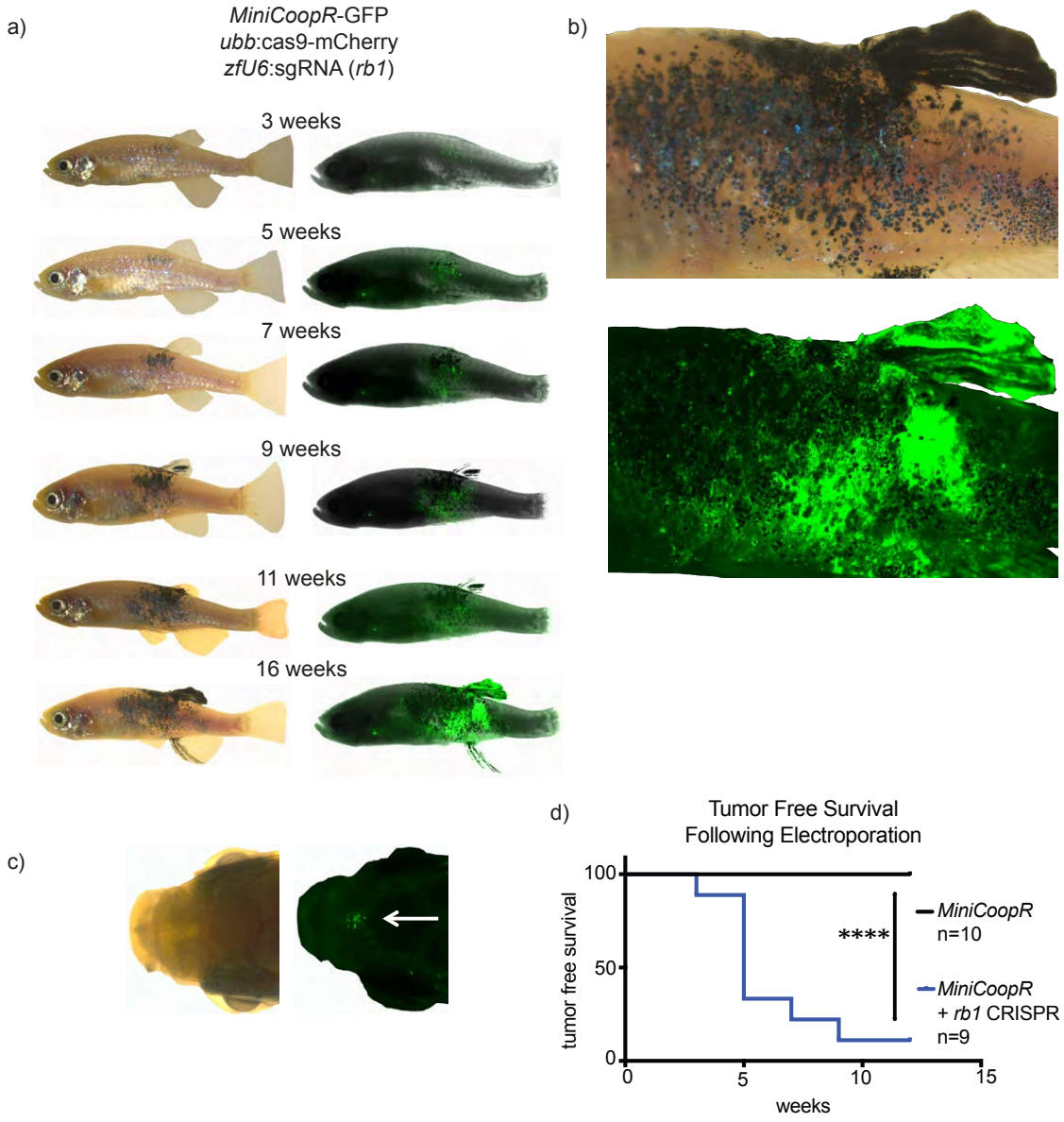

Figure 5.7 Generation of a novel melanoma model with TEAZ.

(a) mitfa:BRAFV600E;p53-/-;mitfa-/- zebrafish (triple strain) were electroporated with the miniCoopR:GFP plasmid that both rescues melanocytes and expresses GFP under the mitfa promoter, with (n=10) or without (n=9) two additional plasmids to genetically knockout rb1 (ubb:Cas9 and zfU6:sgRNA against rb1). The electroporated zebrafish were then imaged over time by both fluorescence and brightfield to monitor tumor development. Overall, 17/20 electroporated zebrafish had GFP+ cells. Tumor development in a representative zebrafish from the melanoma model including rb1 knockout is shown. (b) Higher-magnification view of the tumor-bearing animal shown in (a) at 16 weeks post-electroporation. (c) At 9 weeks post-electroporation, 4/8 zebrafish had evidence of GFP+ distant micrometastases in the head. (d) The loss of rb1 is essential for tumor initiation as visualized by the Kaplan-Meier curve comparing zebrafish electroporated with miniCoopR:GFP +/- rb1 gRNA. Log-rank (Mantel-Cox) test $p < 0.0001$.

TEAZ-mediated CRISPR of Rb1 stimulates melanoma in adults

In the *mitfa*$^{-/-}$ mutant background, there are no mature melanocytes [67] since *mitfa* is required for expression of melanocytic genes such as *pmel* and *tyr*. We suspected that there might be melanocytic-precursor cells in the *mitfa*-BRAF^{V600E};*p53*$^{-/-}$;*mitfa*$^{-/-}$ background that are largely quiescent and not actively cycling. We therefore aimed to knock out the function of the tumor suppressor Rb1 using CRISPR-Cas9, since *p53* and *Rb1* mutations have a tendency to be concurrent in human melanoma patients as seen in the cBIO Portal (p=0.017) [145, 378-382]. Rb1 normally acts to keep cells arrested in G1, and we therefore reasoned that loss of its function might provoke the cells to proceed through the cell cycle and be more amenable to full malignant transformation [266]. To test this hypothesis, we employed the *triple* strain, and electroporated three plasmids: 1) *miniCoopR:GFP*, 2) *ubb:Cas9*, and 3) *zU6:sgRNA* against *rb1* (see Methods for details). We found that of the 9 electroporated animals, 8/9 developed rescued melanocytes and went on to establish aggressively growing GFP+ lesions with the phenotypic appearance of frank melanomas (see Fig. 5.7a-c). The tumors appeared within 3-7 weeks, in striking contrast to the 3-6 months typically required for standard embryo-injection transgenics (see Figure 5.7d). To confirm the effect was due to introduced *rb1* mutations, we dissected the dorsal fin (tumor) and tail fin (control normal tissue) from the same adult zebrafish for sequence analysis. Deep sequencing of the two fins and CrispRVariants-based allele analysis validated that the tumor contained two independent frameshift

mutations in *rb1* at the PAM site that are characteristic of CRISPR mutations and that were not present in the control tail fin (Figure 5.8) [383, 384]. Although the percent of mutant reads was low in this analysis it is likely because we sequenced surrounding normal tissue was well as tumor. We previously performed whole-genome and exome sequencing on a series (n=53) of embryonic-transgenic zebrafish tumors and did not see any Rb1 mutations [385, 386].

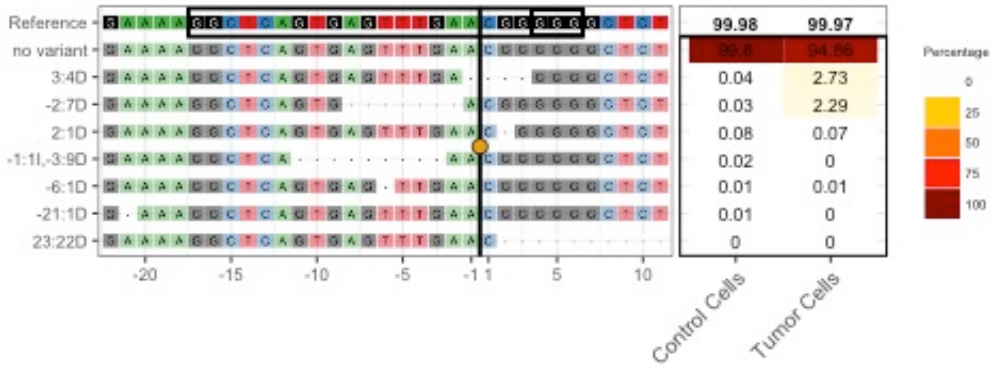

Figure 5.8 Genetic editing with TEAZ.

(a) *A melanoma was induced as described in Main Figure 2, using miniCoopR and sgRNA against rb1. At 10 weeks post-electroporation, the melanoma was excised (n=1), along with control tissue from the tailfin of the same fish that was not electroporated. The tissues were digested for genomic DNA and the rb1 locus was sequenced using multiplexed MiSEQ. In the tumor sample, we found a significant enrichment for two independent Cas9 induced mutations in rb1 close to the PAM site (3:4D and -2:7D) at an allele fraction over 2% each. A small number of these reads (0.04%) were found in the control tissue likely due to barcode contamination during sequencing multiplexing(Ballenghien et al., 2017). Yellow circle represents an inserted cytosine in -1:1I,-3:9D. (MiSEQ analysis performed in collaboration with the Dr. Helen Lindsay from the Mosimann lab at the University of Zurich)*

Consistent with the loss of Rb1 in TEAZ tumors, when we stained for phospho-Rb1 in both a TEAZ tumor and standard embryo injection F0 tumor (i.e. *mitfa*:BRAF injected into a p53-/- background without any cas9/gRNA) we found that most of the cells in the TEAZ tumor are phospho-Rb1 negative, whereas

most of the embryo injection tumor cells are rb1 positive (Figure 5.9). This IHC stains for phospho-Rb1 and not total Rb1 protein, as we do not have an antibody that effectively stains for this in our studies. These results reveal that TEAZ-mediated transformation of adult tissue can result in rapid melanoma onset using tumor-relevant genetic lesions.

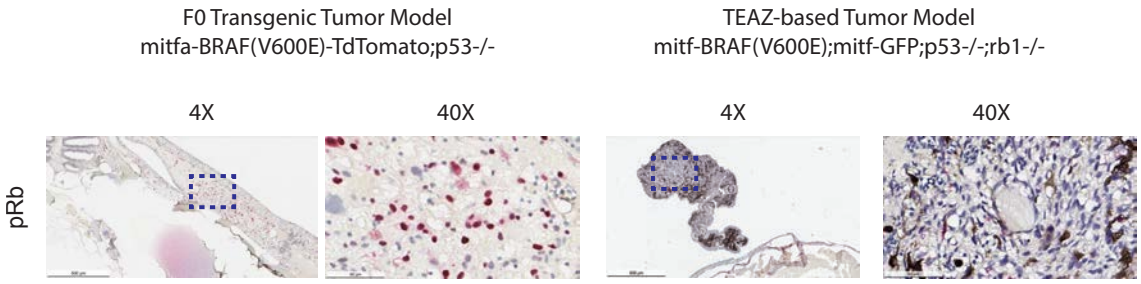

Figure 5.9 Genetic knockout of Rb1 using TEAZ.
Comparison of Rb1 expression in the F0 embryo injection melanoma (n=1) versus the TEAZ melanoma (n=1). On the left is a melanoma created by injection of an mitfa:BRAF-tdTomato(fusion) transgene into a p53-/- background. On the right is a TEAZ based melanoma created by electroporation of miniCoopR-GFP plus ubb:Cas9 plus zfU6:sgRNA against Rb1. Whereas most of the tumor in the traditional BRAF injected tumor is positive for Rb1 (red staining), the majority of the cells in the TEAZ tumor stain negatively.

To confirm that these lesions were truly tumorigenic, we followed a cohort of these TEAZ-treated zebrafish for a period of 4 months. By 5 weeks, primary melanomas could be visualized by both fluorescence and brightfield imaging. By 9 weeks, 4/8 remaining zebrafish had tumors that had rapidly progressed, and traversed the midline to the opposite side of the body. In 4/8 zebrafish, we noted evidence of GFP+ distant micrometastases in the head (Figure 5.7c).

To investigate further, we sacrificed 2 tumor-bearing animals along with 2 control animals and performed routine histology and anti-GFP staining. The first fish had a large protruding primary tumor with uniform GFP expression by fluorescence imaging. Histology of this tumor confirmed this with uniform anti-GFP staining, and H&E staining showed cells highly consistent with high-grade melanoma as determined by pathologist assessment (i.e. nuclear atypia and presence of melanin) (Figure 5.10a). We noted extensive invasion into the muscle (Figure 5.10b), which had not been previously seen in transgenic zebrafish melanoma modeling using $BRAF^{V600E}$ with $p53^{-/-}$. Along with this invasion phenotype, we identified micrometastases within the kidney (Figure 5.10c) and attached to blood vessels (Figure 5.10d).

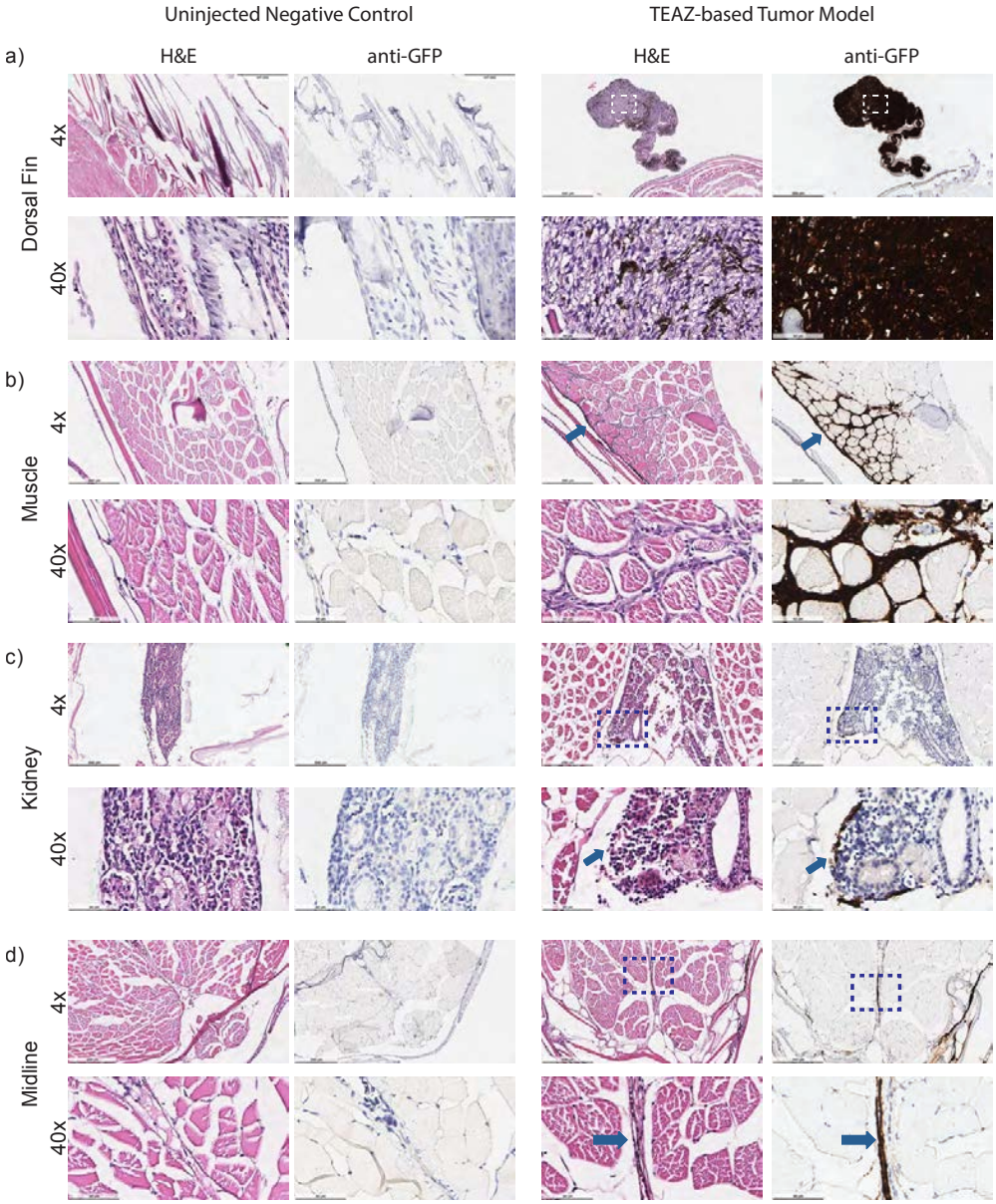

Figure 5.10 Melanoma model using TEAZ show evidence of rapid progression.

(a) Pathology of tumor-bearing zebrafish (n=1) (along with control zebrafish n=2) at 16 weeks post-electroporation stained with hematoxylin/eosin or anti-GFP immunohistochemistry demonstrates a large primary tumor that is uniformly GFP-positive. (b) Histology reveals evidence of extensive invasion into the muscle (see arrow) along with micrometastatic sites within the (c) kidney or along (d) blood vessels (see arrows). Images are visualized at 4x and 40x where scale bars represent 500 μm and 50 μm respectively. Boxes represent the area enlarged at 40x.

The second fish had an atypical tumor with variable GFP expression by fluorescence imaging, and histology showed a tumor of mixed histology in the vicinity of the injection needle: surface GFP-positive tumor cells consistent with a low grade melanoma, and a deeper tumor in the muscle that was GFP-negative consistent with a sarcoma (Figure 5.11a,b). This second non-melanoma tumor is likely due to inactivation of both *rb1* and *p53* in the muscle, as we used ubiquitous:Cas9 in our studies and this combination is commonly found in sarcomas [378, 381, 387-389]. We did not find any GFP staining or abnormal H&E in either of the control animals (Figure 5.10 and Figure 5.11). Taken together, our findings demonstrate that the TEAZ method can rapidly and robustly give rise to tumors in a highly defined spatiotemporal manner.

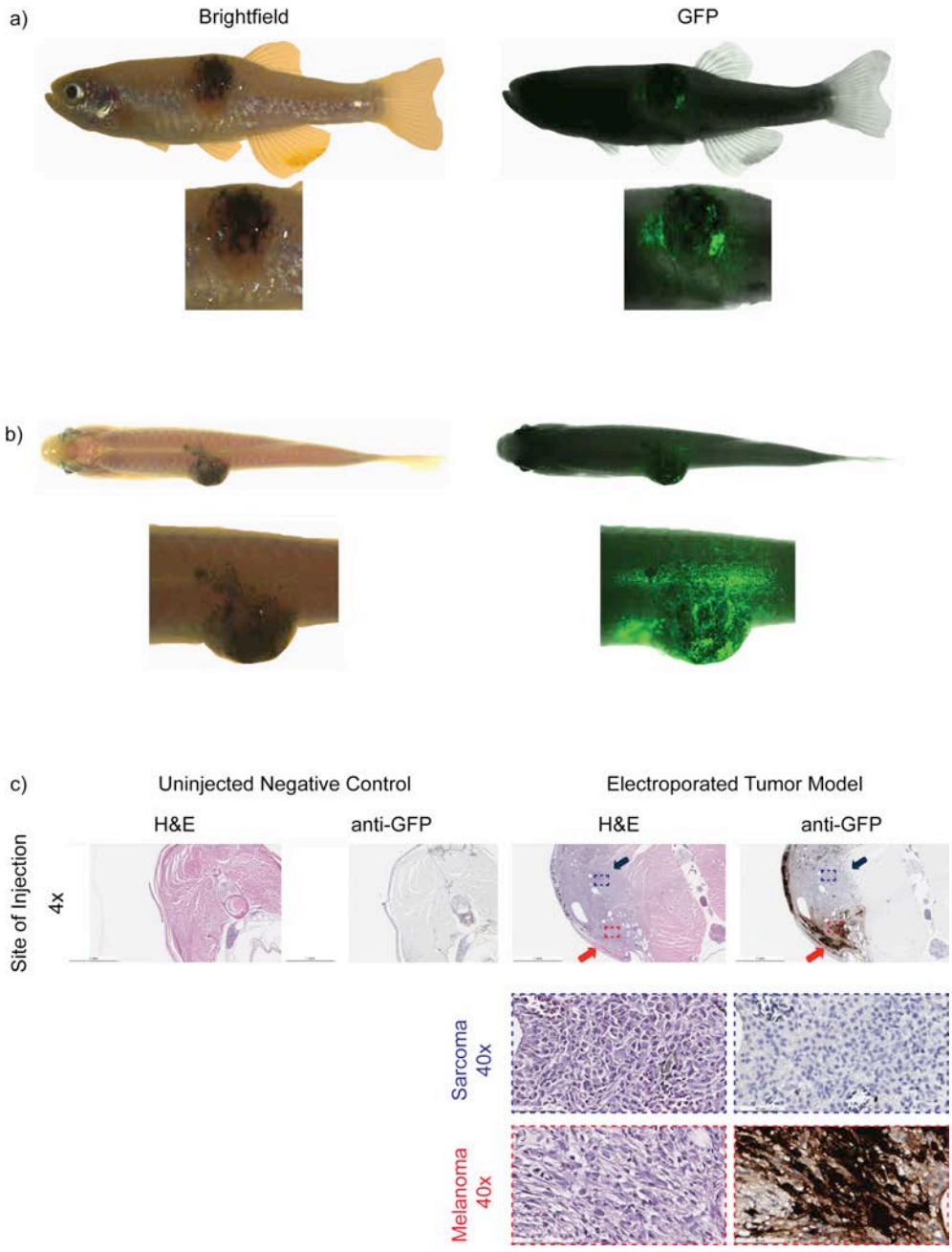

Figure 5.11 Evidence of tumor of mixed origin.

Cancer model using TEAZ shows evidence of one tumor of mixed origin (n=1). (a) Fluorescent and brightfield imaging demonstrated a large primary tumor at the site of electroporation at 12 weeks post-electroporation with patchy GFP expression. (b) Imaging the zebrafish dorsally illustrates the large raised tumor from the contour of the animal. (c) Pathology of the tumor by hematoxylin and eosin or immunochemistry against GFP revealed that part of the deep tumor was GFP-negative and did not resemble a melanoma, but instead appeared consistent with a sarcoma. Images are visualized at 4x and 40x where scale bars represent 1 mm and 50 μm respectively. The blue boxes represent the area of sarcoma enlarged at 40x and the red boxes represent the area of melanoma enlarged at 40x.

We previously showed that most melanomas, of both fish and human origin, overexpress a neural crest transcriptional program typified by crestin and sox10, making the latter gene particularly relevant for human melanoma. To compare our TEAZ based tumors to the more traditional embryo injection models, we performed immunohistochemistry of the melanomas using antibodies against SOX10, $BRAF^{V600E}$ and phospho-ERK (Figure 5.12). In agreement with previous models, we find that both the TEAZ melanomas and embryo injection transgenics have high levels of SOX10 protein expression. Additionally, both tumor types ubiquitously express both $BRAF^{V600E}$ and phospho-ERK, albeit to a lesser degree in the TEAZ tumor. This data suggests that the TEAZ melanomas are functionally similar to the embryo injection transgenics. One key difference is that we also document evidence of progression and distant metastasis using TEAZ.

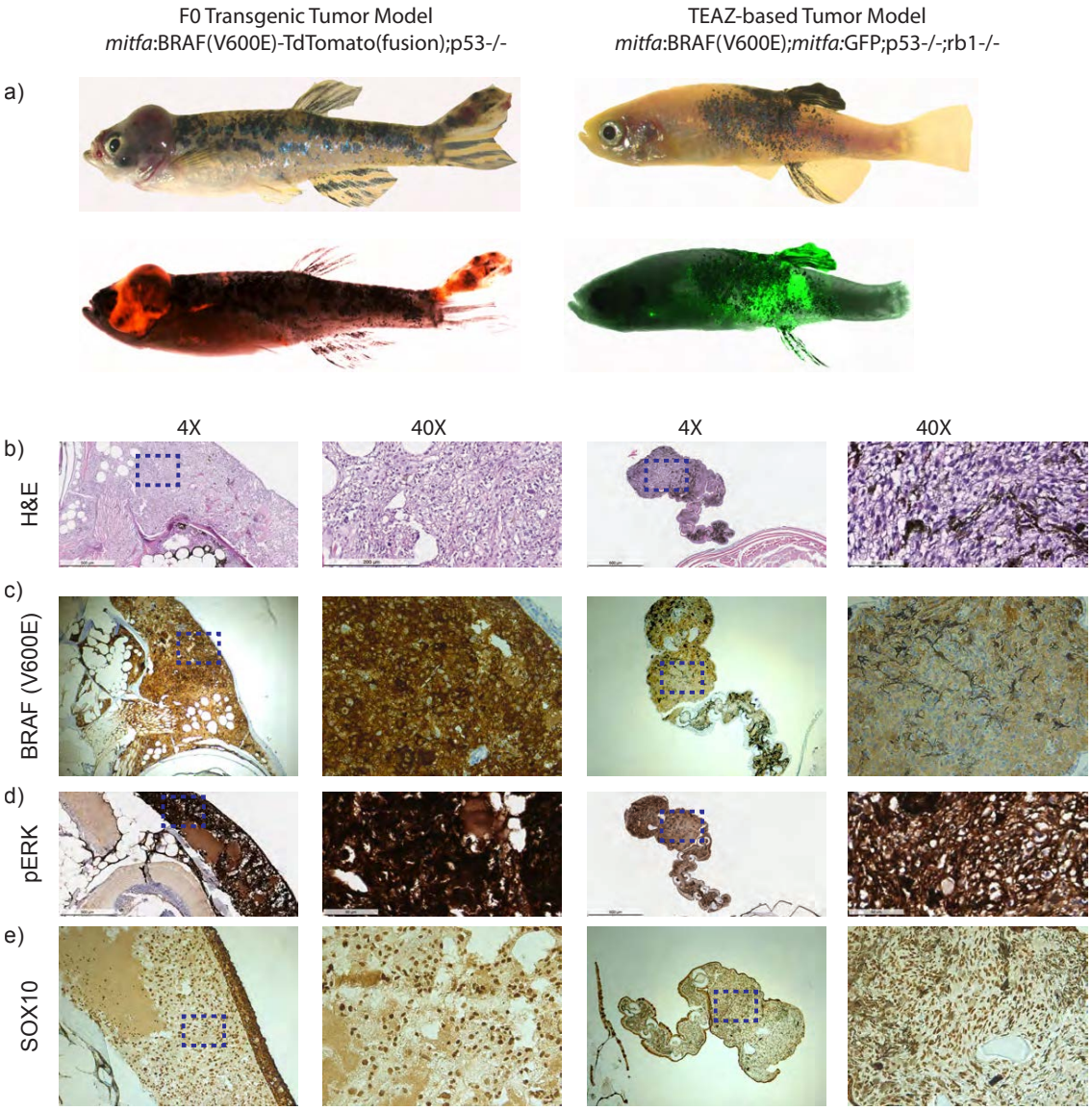

Figure 5.12 Histological comparison of transgenic melanoma to TEAZ melanoma.

(a) On the left is a melanoma created by injection of an mitfa:BRAF-tdTomato(fusion) transgene into a p53-/- background (n=1). On the right is a TEAZ based melanoma created by electroporation of miniCoopR-GFP plus ubb:Cas9 plus zfU6:sgRNA against Rb1 (n=1). (b) H&E staining of both tumors shows similar histology, although with increased melanin pigmentation in the TEAZ tumor. (c, d) Antibody staining against BRAFV600E shows that both tumors are widely positive, which correlates with high level of phospho-ERK staining. (e) Reflecting the neural crest origin of melanocytes, both tumors show strong nuclear expression of SOX10.

Somatic tumors are amenable to sequential transgenic manipulation

One of the major limitations of available genetic models is the inability to modify genes in a sequential order, mimicking *in vivo* tumor progression from malignant clones [390]. This limitation precludes the investigation into whether certain oncogenic events are driving initiation (which occur early) versus metastasis (when they may occur later). We therefore sought to determine if we could sequentially perform TEAZ to introduce new DNA elements into an already existing tumor. We selected a TEAZ-melanoma from the cohort above (4 months post-initial electroporation), and electroporated an *mitfa*:tdTomato plasmid directly into the tumor (Figure 5.13). Within 1 week after this second electroporation, we identified tdTomato-positive cells within the TEAZ-treated tumor (n=2/2). The tdTomato-cells have a dendritic appearance typical of a melanocytic cell.

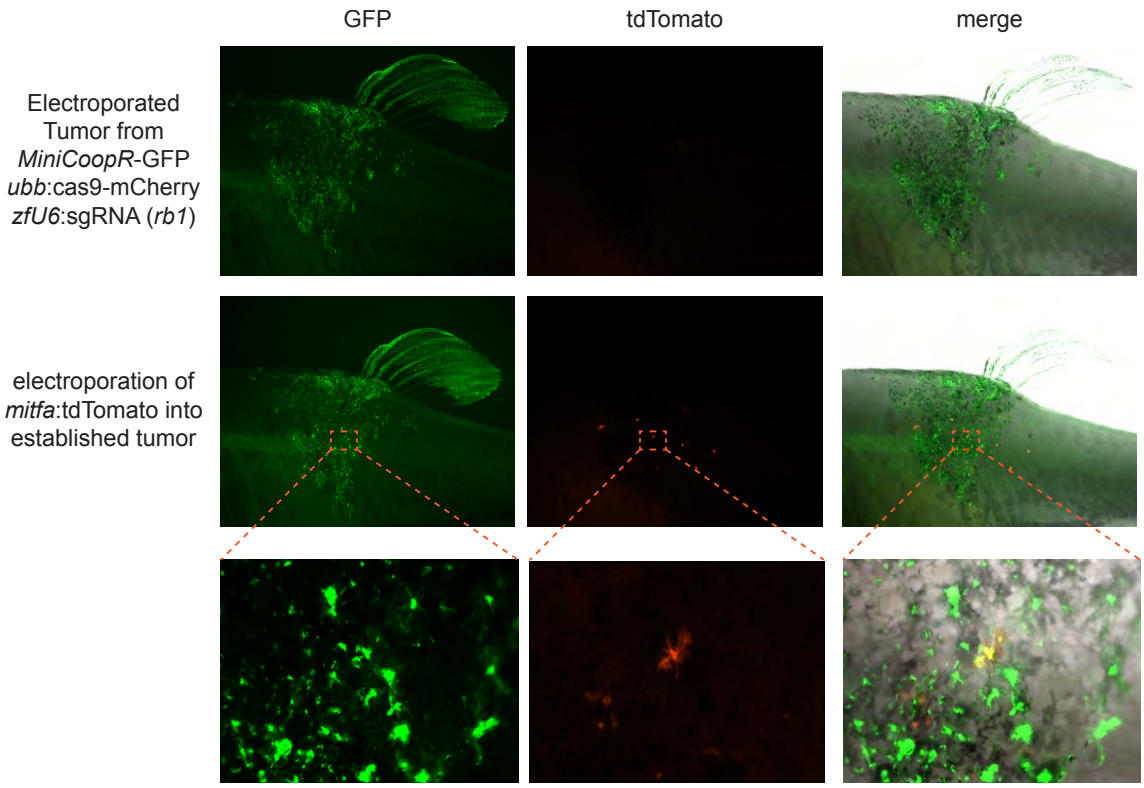

Figure 5.13 Cancer modeling with TEAZ enables sequential electroporation of transgenes.

A tumor bearing fish (created with rb1 sgRNA as in Figure 2) was imaged using GFP and tdTomato. As expected, only GFP+ tumor cells were seen with no expression in the tdTomato channel. This tumor was then electroporated with an mitfa:tdTomato plasmid and re-imaged 5 days later, showing areas that are now both GFP-positive and tdTomato-positive (n=2).

We also tested whether this sequential transgene electroporation into an existing tumor was of different efficiency that de novo electroporation into unperturbed tissue. To do this, we compared electroporation of mitf-tdTomato into an existing TEAZ tumor versus electroporation of *mitfa*:tdTomato plus *ubb*:GFP into an AB fish (the GFP was added here to control for the fact that TEAZ tumors are GFP positive). We then counted the number of tdTomato positive cells in both situations, and noted a greater number of positive cells when electroporating into the AB fish compared to the established tumor (Figure 5.14). However, while it

does appear that sequential electroporation into tumors may be slightly less efficient than de novo electroporation, it is still efficient enough for routine use in existing tumors and will allow for sequential modeling of genetic lesions.

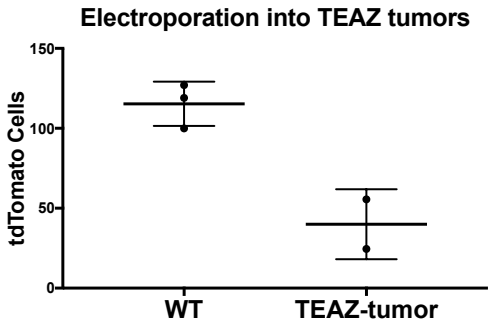

Figure 5.14 Efficiency of sequential TEAZ.

Evaluation of electroporation efficiency of mitfa:TdTomato into TEAZ tumors for sequential transgene electroporation vs. de novo electroporation into unperturbed tissue. We compared the number of red cells 4 days post electroporation of either mitfa:tdTomato into an existing TEAZ tumor (n=2) or electroporation of mitfa:tdTomato plus ubb:GFP into an AB fish (n=3) (the GFP was added here to control for the fact that TEAZ tumors are GFP positive)..

5.3 Discussion

We have developed TEAZ, an electroporation-based approach for expressing transgenes and creating mutations in somatic cell types of interest within a region of interest in the adult zebrafish. We successfully applied TEAZ to the generation of malignant melanoma, and our results show TEAZ can be used for sequential electroporation, which could be used to make increasingly complex tumor models. This model is amenable to initiating a tumor at a defined time and place, and will allow for a detailed analysis of tumor progression and metastasis in a fully immunocompetent zebrafish.

One major limitation of current transgenic cancer modeling in the zebrafish is the challenge of controlling both the timing and location of tumor initiation. Although both transplantation and Cre/Lox approaches can address some of these issues, neither fully solves the problem. Transplantation generally requires immune modulation of the recipient, and introduces relatively high cell burdens into tissue contexts that would not occur during natural tumor formation. Cre/Lox is extremely powerful but require multiple genetic crosses, and there are very few verified lines that exist for cancer modeling in the fish. In contrast, TEAZ rapidly allows for introduction of the required genetic elements in a multiplexed, complex manner.

Electroporation has been used as a mechanism for tumor initiation in mouse models of cancer. Both glioblastoma and oligoastrocytomas [391] have been induced into the developing fetus using *in utero* electroporation and the *piggyBAC* transposon system. In these studies, the transposase was included on the plasmid as a helper, although in our study we did not find Tol2 transposase to be necessary for highly stable transgene expression. Recent work [294, 298, 299] showed that plasmid delivery and electroporation could be used to initiate KRAS-driven pancreatic cancer in the adult mouse, and similar to our findings, can be complemented with CRISPR-Cas9-mediated genome editing. One exciting area that we believe TEAZ will open up is the possibility of new epithelial cancer models in the zebrafish, since that has not been developed on a very large scale.

One of the major advantages of our TEAZ system is the high efficiency we have observed. Once trained, we find that the rate of success of transgene expression approaches 100% of injected animals with 100% survival when done in the dorsal skin. Injections into other adult tissues such as the heart or head are more technically challenging and require more practice, and also results in higher death as expected (75% survival for heart, 62.5% survival for head). In our study of the melanomas, we found that overall, 88% of the fish developed GFP+ cells by 3 weeks, and all of those fish subsequently went on to develop tumors by 7 weeks. This timing is an advance over the previous standard transgenic melanoma models, even with the more rapid *MiniCoopR* mosaic approaches that speed up tumors with the addition of oncogenes such as *SETDB1* [154]. In addition, embryo injection remains a relatively laborious process, whereas we find that the adult electroporation is simple and fast and can be easily taught to inexperienced users.

One possibility that our TEAZ system opens up in the future is the ability to initiate adult-stage tumors in virtually any genetic background (i.e. the *casper* strain) or other existing transgenic line. In our studies using the miniCoopR background, we needed at least 3 genes to get efficient tumors: $BRAF^{V600E}$, $p53^{-/-}$ and $rb1^{-/-}$. This may or may not be related to the specifics of the miniCoopR system as the melanocyte progenitors likely have to re-enter the cell cycle. We also noted that our tumors formed faster than typical miniCoopR tumors, even

with the addition of genes such as SETDB1. This could relate to the specifics of the TEAZ approach or could simply be due to the accelerating effect of rb1 loss. It was surprising that the allelic fraction of rb1 mutations was low in our MiSeq analysis, but this may be because in isolating genomic DNA for sequencing we included large margins of surrounding normal tissue along with the tumor. Our staining for phospho-RB1 is suggestive that the majority of the tumor cells are deficient for this tumor suppressor. The extent of rb1 loss required for TEAZ tumors will need further analysis.

Metastasis and tumor progression have remained challenging to study using the zebrafish model; our results presented here suggest that TEAZ-mediated tumor modeling is amenable to studying metastasis in a high-throughput, immunocompetent model. Although transplantation-based approaches are powerful, they require immune system manipulation, such as irradiation or transplantation in genetically immuno-compromised zebrafish to counteract rejection [267, 268, 282, 285]. In contrast, TEAZ allows for tumor formation in fully immunocompetent animals. These features render the TEAZ model well-positioned to: (1) screen metastatic modulators to test rate, propensity, and latency; (2) selectively alter genes within specific cell types within the tumor microenvironment; (3) image the interplay between tumor cells and specific microenvironmental cell-types using widely available transgenic lines, and (4) introduce serial mutations to study order of progression or induce competition studies within a tumor.

CHAPTER SIX: CONCLUSIONS/FUTURE DIRECTIONS

Melanoma is a very heterogeneous disease genetically, transcriptionally, and clinically. Recent sequencing studies have identified mutational patterns leading to insights into the biological heterogeneity of melanoma with the hopes of enlightening better prognosis and therapy. However, genetic mutations alone are insufficient to explain the diverse spectrum of melanoma tumors in the clinic.

The purpose of this dissertation was to discern if the cell-of-origin of melanoma could partially explain the clinical and phenotypic diversity observed. The work was completed using zebrafish and human embryonic stem cell-derived melanocytes. Our initial, perhaps overly simple hypothesis, was not entirely correct. In both the fish and human models assayed, the melanoblast is uniquely capable of giving rise to bona fide melanoma. Initiating cancer in neural crest cells gave rise to very undifferentiated tumors that have elements of melanoma but are equal parts neuroblastoma or “neural crestoma”. Mature melanocytes proved resistant to cancer under the same conditions suggesting that the barrier for originating melanoma is higher in differentiated melanocytes. Taken together, these studies suggest that the differentiation state of the cell of origin is not responsible for the diversity observed in the clinic. Rather, the differentiation state capable of giving rise to melanoma under the experimental conditions is very narrow.

Perhaps one of the most surprising findings in our study came from the transcriptional profiling before or after $BRAF^{V600E}$ at the NC, MB or MEL stage in WT cells or in the absence of tumor suppressors (TP53, CDKN2A, and RB1). The transcriptional effect of $BRAF^{V600E}$ is very dependent on the stage of differentiation. Surprisingly, oncogenic BRAF has a very limited impact at the melanocyte stage when compared to isogenic cells at the NC or MB stage. Consistent with this, melanocytes were resistant to transformation when exposed to the identical genetic insults that transformed both NC and MB cells.

To assay the importance of the differentiation stage of the cell of origin in melanoma *in vivo* we studied transgenic zebrafish. Researchers had previously established that mutant BRAF induction at the MB stage in a p53 null fish is sufficient to drive melanoma with one hundred percent penetrance. Similarly to the findings *in vitro*, mutant BRAF induction at the NC stage drove tumorigenesis at a very high penetrance but the resultant tumors more closely resembled neuroblastoma or neural crestoma. Additionally, oncogenic BRAF induction at the MEL stage did not yield any tumors. Thus, the three stages of differentiation yielded the same phenotypes both *in vitro* and *in vivo*.

The small window of differentiation most apt to lead to melanoma formation suggests that melanoma is less likely to originate in fully differentiated melanocytes. As cells that are transcriptionally and phenotypically similar to either MB or NCC reside within the adult epidermis, where melanoma initiates,

these precursors are a potential source of melanoma. This is not meant to imply that melanoma cannot in any circumstance initiate in fully differentiated melanocytes as likely any cell in the body is capable of forming a tumor if insulted with enough genetic mutations. However, our body of work does suggest that melanocytes require more genetic mutations or changes in epigenetic state to transform than the precursor MB or NC cells.

6.1 Driving melanoma from melanocytes

The refractory nature of melanocytes offers a novel platform for studying transformation in cells that are primed but resistant to melanoma. The same genetic mutations that drive melanoma in melanoblasts are insufficient to drive tumor formation when introduced into differentiated melanocytes. Uncovering the proteins/pathways responsible for halting melanoma formation in melanocytes might offer a therapeutic strategy for halting tumorigenesis in established melanoma.

What is required for transformation of a melanocyte? In ongoing work, the White and Studer labs are now screening for factors that allow these melanocytes to become fully transformed, as this will tell us the minimal requirements that separate the melanoblasts from the melanocytes during oncogenesis. This can be done using either a candidate gene approach or unbiased approach.

Candidate gene approach: epigenetic modifiers

Studying the baseline transcriptional differences between melanoblasts and melanocytes offers one approach to pinpointing the mechanism(s) enabling a BRAF response in MB and not in MEL. A GSEA analysis comparing WT melanoblasts and WT melanocytes revealed that chromatin modifiers are amongst the most differentially expressed genes between these two cell types (Figure 6.1a). Employing the RNA-seq data, we find that the general class of chromatin modifying enzymes is vastly overexpressed in melanoblasts compared to melanocytes (Figure 6.1b). Furthermore, the chromatin modifiers that are most highly expressed in MB vs. MEL are similarly over-expressed or amplified in a high percentage of melanoma patients (Figure 6.1c). The impact of epigenetic regulators in melanoma has been previously shown to be important in oncogenesis [153, 155, 392, 393]. We hypothesize that the enriched expression of chromatin modifiers in melanoblasts makes the cell more transcriptionally plastic and responsive to mutant BRAF expression. A candidate-based approach is underway to over-express several key chromatin modifiers (CHD7, EZH2, CHD1l, ATAD2, BPTF, TNRC18) in an effort to transform TKO;iBRAF melanocytes. The candidates are being evaluated for their impact on proliferation and migration. Additionally, a qPCR panel has been assembled of representative genes that are dramatically dysregulated by mutant BRAF in MB/NC and not in MEL. Finally, the most important read out will be *in vivo* xenograft growth.

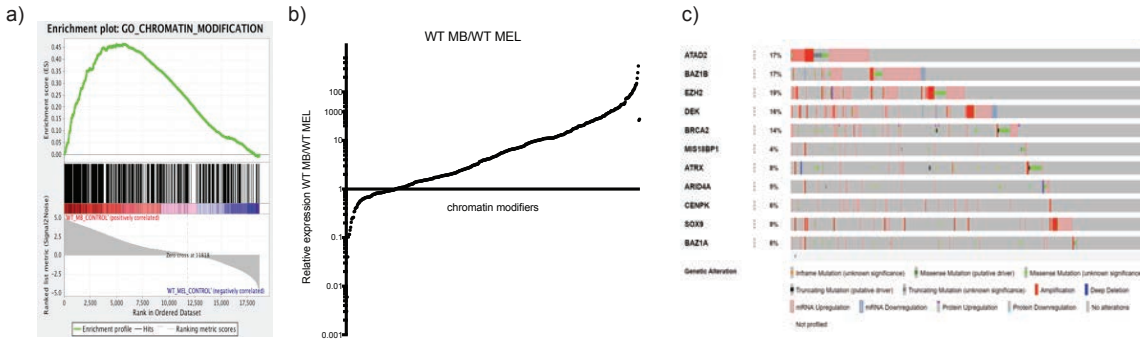

Figure 6.1 Melanoblasts are enriched in chromatin modifiers.

(a) Gene set enrichment analysis comparing WT melanoblast to WT melanocytes identified chromatin modifiers as the pathway most enriched in MB. (b) Epigenetic regulators are globally over-expressed in WT MB relative to WT MEL. The gene names (across the x-axis are intentionally not included as they would illegibly small. (c) The chromatin modifiers over represented in MB are similarly over-expressed in melanoma patients (adapted from cbioportal.com) [381].

Unbiased screen approach: cDNA/CRISPR pools

An unbiased screening approach can be enlisted to identify the proteins/pathways capable of transforming the TKO;iBRAF melanocytes after doxycycline induction. The melanocytes can be exposed to either cDNA or CRISPR libraries and screened for proliferative advantage either *in vitro* or *in vivo* xenograft growth. Towards that end, we are currently utilizing the Elledge lab cDNA whole-genome pool [394] to identify which genes, when overexpressed, can now allow for transformation of the melanocytes. A similar approach could be used via a pooled CRISPR/Cas9 library.

Further studies using transgenic zebrafish

Concomitant with the hES work, candidate genes are being tested to drive melanoma in *tyrp1*:BRAF^{V600E};p53$^{-/-}$ fish. The ease of transgenic zebrafish offers

a high throughput vertebrate model for testing candidate genes with large sample sizes. The cell-of-origin zebrafish future directions are focused on partial de-differentiation in pigmented melanocytes to release the brake on tumorigenesis. For example, $p53^{-/-}$ fish are being tracked with co-injections of *tyrp1*:$BRAF^{V600E}$ with *tryp1*:*sox10* and/or *tryp1*:*mitfa*.

Additionally, we are interested if the NC and MB driven tumors driven in Chapter 2 can be inter-converted by the overexpression of key transcription factors in the melanocyte pathway. Previous studies have demonstrated that over-expression of *sox10* in the melanocytes of *mitfa*:$BRAF^{V600E}$;$p53^{-/-}$ transgenic fish accelerates melanoma onset as compared with controls [60]. Would over-expression of *mitfa* in the neural crest progenitors of *sox10*:$BRAF^{V600E}$;$p53^{-/-}$ transgenic fish convert the tumors into melanomas? Would over expression of *sox10* in the differentiated melanocytes of *tryp1*:$BRAF^{V600E}$;$p53^{-/-}$ transgenic fish convert the nevi into melanoma? The zebrafish offers a high-throughput vertebrate model for testing the importance of candidate genes in determining the state of the resultant tumor.

6.2 Clinical Implications

Differentiation status is correlated with melanoma prognosis and is an active area of research. Generally, more differentiated tumors with higher levels of MITF are more proliferative. Conversely, undifferentiated tumors with a neural crest gene expression signature are more invasive and metastatic. Given that metastatic

melanoma is harder to treat and more lethal than proliferative melanoma, extensive clinical efforts were put into “differentiation therapy”. Differentiation therapy posited that by inducing differentiation in tumors the cancer cells would become less metastatic and ideally terminally differentiate and exit the cell cycle. Unfortunately, differentiation therapy was unsuccessful possibly due to the unintended consequence of creating partially differentiated cells that are both proliferative and migratory [324, 395-398]. Furthermore, changing the differentiation state of the tumor also impacts sensitivity to targeted therapy [246, 399, 400]. Surprisingly, the cell of origin does dictate the tumor type, but the cell of origin does not dictate the differentiation status within and between melanoma patients.

The melanocytes that do not form melanoma represent a poised pre-tumorigenic state. Further studies are being undertaken to appreciate why the MB are transformed and the MEL are not. Perhaps the implicated mechanisms will inform researchers how to treat MB-derived melanomas to act more like the non-cycling MEL cells. Alternatively those same pathways can be identified as avenues to clinically prevent poised-MEL from transforming akin to the MB.

6.3 Future Directions of TEAZ

TEAZ is a novel approach for introducing somatic mutations (rather than germline mutations) into select cells within the adult zebrafish. We have utilized TEAZ to generate a novel melanoma model. We have performed proof of

principle studies demonstrating that TEAZ can be used to introduce transgenes into the head, heart or pancreas. TEAZ is a rapid and easily transferrable approach for modeling normal development or diseases from cancer to cardiovascular diseases or neuronal defects.

Metastasis

Early detection and surgical resection of early-stage primary cutaneous melanoma is often curative, but the prognosis plunges precipitously for patients with metastases. Metastasis and tumor progression have remained challenging to study using the zebrafish model. TEAZ-mediated tumor modeling is amenable to studying metastasis in a high-throughput, immunocompetent model that is amenable to high-quality *in vivo* imaging. In contrast to transgenic fish, the local introduction of transgenes allows researchers to easily discern tumor spreading/metastasis from independent tumorigenesis. These features render the TEAZ model well positioned to screen metastatic modulators of metastasis rate, propensity, and latency.

The lab is pursuing a series of experiments with TEAZ at two adjascent sites within the same fish with distinct colors and genetics to test candidate genetics within the same organism. Electroporating two sites will allow for the perfect internal control as well as visualization of the interplay between cell types (Figure 6.2).

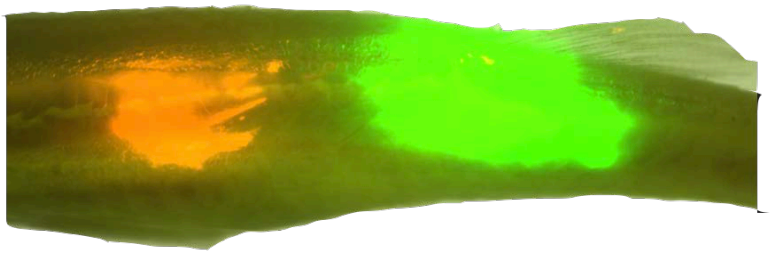

Figure 6.2 Two color TEAZ.
Proof of principle of electroporation of two distinct genetics with colors in different sites enables researchers to study candidate genes with the perfect internal control. This image is TEAZ of 500ng of ubb:GFP or ubb:TdTomato imaged 3-4 days post electroporation. (TEAZ and image produced by Dr. Thomas Beckham from the White Lab at MSKCC).

Serial mutations with TEAZ

TEAZ allows for the introduction of serial mutations within a tumor *in vivo* to introduce second, third, or even fourth transgenes/mutations for the first time. We have previously shown a proof of concept with the introduction of TdTomato into a select population of cells within an established melanoma (Figure 5.13). In the future, the second color expression can be tied to a transgene overexpression or gRNA driven mutation and comparative growth tracked over time. Serial mutations with TEAZ will be used to model the order of mutagenic events in melanoma progression. Alternatively, serial mutations are an alternative approach for inducing competition studies within a tumor.

Alter the tumor microenvironment using TEAZ

Significant attention has been paid to studying the “microenvironment” surrounding the tumor cells. However, the majority of work has been unable to dissect the impact of the local microenvironment from the greater systemic

macro-environment. By swapping the promoter driving transgene expression, TEAZ can be applied to alter genes within specific cell types within the immediate tumor microenvironment. Previous studies in the lab have demonstrated that the transgenic zebrafish melanoma model relies on external signaling produced in adipocytes or keratinocytes [62, 401]. However, these studies have been unable to distinguish if the signaling is derived from the immediate microenvironment or a largely systemic source. The signal source may direct the therapeutic implications of such discoveries.

Coupling TEAZ with established transgenic lines

Previously, creating transgenic tumors in a zebrafish strain of interest required time-consuming breeding and genotyping to obtain the final genotype of interest. In contrast, with TEAZ, one can electroporate a combination of oncogenes and gRNAs against tumor suppressors into any given genetic background directly, saving months of breeding and unused animals. To ensure specificity of the tumor types, it will be important to use tissue specific promoters to drive Cas9, to avoid mixed-histology tumors induced by ubiquitous Cas9 expression. The existing lines will allow for enhanced imaging of the interplay between tumor cells and specific microenvironmental cell-types such as T-cells [402], macrophages [403] or endothelial cells [404].

CHAPTER SEVEN: MATERIALS AND METHODS

7.1 Experimental models

Pluripotent Stem Cell Culture

Undifferentiated hESCs (H9/WA-09) and the derived Sox10:GFP, iBRAF, TKO;iBRAF stem cell lines were cultured in Essential 8^{TM} ES cell media on Vitronectin coated tissue culture treated dishes. Cell culture was performed at 37°C in a humidified atmosphere containing 5% CO2.

Passaging hES cells

Cells were maintained as previously described [300]. To passage hESC for maintenance cells were lightly dissociated in EDTA for 2.5 minutes before removing EDTA buffer. hESC clusters were lightly dissociated using E8 PBS. hESC were pelleted in the centrifuge (200 x g for 5 min). hESCs were washed gently with PBS and lightly triturated before pelleting again. hESCs were then passaged at 1:7. Cells were passaged for differentiation as previously described [300]. Before passaging hES cells for culture maintenance or differentiation, the hESC culture should be 70%–80% confluent. Cells were detached with EDTA dissociation buffer (5 min at RT). The EDTA was removed and the cells were vigorously dissociated in PBS to obtain single cells. The cells were passed through a 45-micron cell strainer and pelleted in the centrifuge (200 x g for 5 min). hESCs were washed gently with PBS and pelleted again. hESCs were then

plated at 200,000 cells per cm^2 in E8 medium with 10mM ROCKi and then incubated overnight in the 37°C incubator.

Neural Crest and Melanoblast Differentiation

Neural induction using the dual SMAD inhibition protocol was performed as previously described (Chambers et al., 2009; Chambers et al., 2011; Lee et al., 2010). Prior to differentiation hPSCs should be appear as a high density monolayer. The starting density depends on the genetic background as hES with tumor suppressors knocked out grow substantially faster and should be plated at a lower density. Wash cells with PBS or E6 media before starting the differentiation.

Day 0-2: Change media every day with E6 media containing 1ng/ml BMP4 + 10mM SB + 600nM CHIR.

Day 2-4: Change media with E6 media containing 10mM SB + 1.5mM CHIR.

Day 4-6: Change media with E6 media containing 1.5mM CHIR.

Day 6-11: Change media every day with E6 media containing 1.5mM CHIR + 5ng/ml BMP4 100nM EDN3 to cells

To prepare for FACS sort at day11, the cells were treated with Accutase and washed vigorously with PBS to get single cells. Cells were incubated with the cKIT antibody for >45 min on ice prior to filtering cells and sorting based on proper fluorescent negative controls.

NC cells: SOX10+cKIT- MB cells: SOX10+ cKIT+

Neural Crest and melanoblast maintenance

Cell suspension is maintained in ultra low attachment plates for suspension culture to form NC spheres.

Neural Crest/Melanoblast Maintenance media:

Neurobasal media supplemented with L-glutamine, non-essential amino acids, N2 supplement, B27 supplement, 10ng/ml FGF2 and 3mM CHIR99021.

Melanocyte differentiation

Follow the first 11 days of differentiation of hESC to NC/MB the follow the melanocyte specification previously described [8, 304]. There is no need to FACS sort for the melanocyte differentiation as the melanocyte media is selective. Wash day 11 cells with PBS and detach using Accutase. Suspend cells in Neurobasal media by manually pipetting up and down. Pellet the cells with a centrifuge for 5 min at 200 x g. Suspend the cells at 2,000,000 cells per ml in Melanocyte medium. Plate 10 µl droplets onto the dried PO/Lam/FN. Slowly add Melanocyte medium without disturbing the droplets. Continue feeding with Melanocyte medium every 2 to 3 days. Passage cells once a week at a ratio of ~1:6

Melanocyte media:

Neurobasal media + SCF 50ng/ml + cAMP 500 µM + Ascorbic Acid 100µM + FGF2 10ng/ml + CHIR 3 µM + B27 supplement + N2 supplement + BMP4 25ng/ml + EDN3 100nM.

hES AAVS1 Knock-In Strategy

Knock in strategy is derived from Zhu et al.[342, 343] In 100uL of cold nucleofection solution add TALEN plasmids and Donor plasmids and mix well.

TALEN-L: 1 µg (2.28uL of 437ng/uL)

TALEN-R: 1 µg (2.02uL of 494ng/uL)

Puro-Donor: 5 µg (24.2uL of 207ng/uL)

Neo-M2rtTA: 5 µg (9.24uL of 541ng/uL)

Treat cells with 0.05% Trypsin for ~ **1 min**. Stop trypsin with 10%DMEM. Break cell colonies into single cell suspension. Spin down cells at 200g X 5min. Suspend 5 million cells in the nucleofector solution. Electroporate hES using LONGZA B16 Program in AMAXA machine. Gently plate cells at **1:2** ratio over MEFs with ROCKi. 3-4 days after electroporation, add puromycin (1:2000) only for 3-4 days. One day later add geneticin (1:1000) for 4 days

hES knock-out strategy

Design gRNA. Order gBLOCK including a U6 promoter, gRNA target and gRNA scaffold. Clone the synthesized gBlock into an empty backbone vector such as pCR-Blunt II-TOPO. Electroporate hESC with cas9-gfp fusion protein and gRNA DNA. Sort for GFP one day post and then grow up colonies. Select for KO by sequencing

Zebrafish

Zebrafish Husbandry

Zebrafish were bred and maintained in the Zuckerman fish facility, in temperature (28°C), pH (7.4), and salinity-controlled conditions. All fish were maintained on a 14 hr on/10 hr off light cycle. The animal protocols described in this manuscript are approved from The MSKCC Institutional Animal Care and Use Committee (12-05-008).

Transgenic Lines

Transgenic lines used in these studies included wild-type (*AB*), *casper* [267, 405], and the *triple* line [154] (*mitfa*:BRAF^{V600E};*p53*$^{-/-}$;*mitfa*$^{-/-}$) (provided by the Houvras lab at Weill Cornell). TEAZ was equally successful in both male and female zebrafish. TEAZ was performed on zebrafish ranging from 4-12 months post fertilization.

Generating F0 Transgenic Lines

One-cell-stage p53$^{-/-}$ embryos were injected with the construct Tg(*promoter*:BRAF^{V600E}-TdTomato fusion;cmlc2:eGFP) at 25 ng/µl with Tol2 mRNA at 20 ng/µl. Embryos were screened at 48 hpf for the presence of GFP in the heart as well as TdTomato in the rest of the body. Flourescent-positive

embryos were grown to adulthood and studied as F0 transgenics or outcrossed to identify founders that gave germline transmission of the transgene.

Electroporation of adult Zebrafish

At the time of electroporation, recipient adult zebrafish were anesthetized in 0.2% Tricaine. The plasmid of interest was resuspended at 1000ng/µl in ddH2O, and 1.0 µl was injected into the dorsal skin, head or heart (using a pulled glass micropipette). No transposase mRNA was used in these studies. We have successfully tested a range of concentrations from 400-2000 ng/µl and from 0.5-2.0µl. Following injection, the zebrafish were immediately placed upright in an agarose mold for ease of handling and electrodes were placed on either side of the fish surrounding the injection site. The cathode paddle was generally placed on the same side as the injection to promote the DNA entering cells closer to the surface of the fish but the cathode and anode can be swapped to promote integration into cells deeper within the animal. We used the ECM 830 Electro Square Porator from BTX Harvard Apparatus and the Genepaddles, 3 x 5 mm. For all experiments described, the LV mode was used with a voltage of 45V, 5 pulses, 60ms pulse length, and 1s pulse interval. The electroporated zebrafish were immediately returned to flowing fresh water after electroporation. Electroporated zebrafish were imaged within 4 dpe to ensure successful TEAZ, and then serially imaged for up to 8 months using brightfield and fluorescence imaging. For electroporation of deeper tissues such as heart or brain, the same glass electrode was used to inject the DNA but penetrated more deeply directly

into those tissues. The electroporation paddles were positioned around those organs, but still kept on the surface of the animal with the same electrical settings.

Zebrafish imaging and image processing

Adult zebrafish were imaged using an upright Zeiss Discovery V16 equipped with a motorized stage, brightfield, and GFP and tdTomato filter sets. To acquire images, zebrafish were lightly anaesthetized with 0.2% Tricaine. Images were acquired with the Zeiss Zen software v1, and the post image processing was done using Fiji [406].

Tumorigenesis assay

Transgenic zebrafish were generated via injection into melanoma-prone ($p53^{-/-}$) one-cell embryos, and stable lines were selected for using fluorescence. Fish were checked weekly for tumors from 4 weeks post fertilization (wpf) to 50 wpf. Fish with tumors were removed from the study. A Kaplan-Meier survival curve was generated using GraphPad Prism 7.

Mouse

Xenograft studies were performed by injecting 500,000 cells subcutaneously into the flanks of non-obese diabetic-severe combined immune-deficiency (NOD-SCID) mice (3 mice or 6 injections per a group).

7.2 Molecular Biology

Purified plasmids were generated using the Gateway system and isolated from *E.coli* using the Qiagen HiSpeed Plasmid Maxi Kit. The *MiniCoopR* vector was provided by the Houvras lab. The zebrafish *U6* promoter was cloned out of genomic DNA as previously described [268]. The sgRNA against *rb1* was designed using the CHOPCHOP software and has the 20 basepair sequence: GGCTCAGTGAGTTTGAACGG [407, 408]. The *ubb* promoter was as described previously [373], and the Cas9-mCherry fusion plasmid was subcloned from Addgene number *78313* [383]. All final plasmids were constructed using Gateway technology and the Tol2kit as previously described [335, 336].
List of all plasmids used: *ubb*:GFP *[373] and ubb*:tdTomato (both in Tol2kit plasmid backbone *#394*), *zfU6*:Rb1gRNA [268], *mitfa*:tdTomato [67], *myl7*:GFP [377], *MiniCoopR* [154], *ubb*:Cas9-mCherry fusion [383] (all in Tol2kit plasmid backbone *#395*). For the Rb1 miniCoopR experiments, the following concentrations of plasmids were used: MiniCoopRgfp (370ng), *ubb*:Cas9 (205ng), *zfU6*:sgRNA against rb1 (285ng)

7.3 Methods

Total RNA extraction, cDNA isolation, and qRT-PCR analysis

Lyse cells in 1ml Trizol. Use Phase Lock Gel-Heavy tubes and chloroform to extract the RNA. Elute out the RNA with isopropanol. Wash with 75% EtOH. Pellet the RNA. Dissolve pellet in water. cDNA was generated using the BioRad iScript cDNA Synthesis Kit. Primers for real-time quantitative PCR (qRT-PCR) were obtained from Applied Biosystems with BioRad SsoFast Evagreen Supermix.

Western blot analysis

Wash and trypsinize cells as usual. Add lysis buffer (RIPA buffer + HALT Protease) to cells. Sonicate for 3x1min with 5 minutes on ice between pulses. Pellet cell waste and proceed with cell lysate supernatant. Quantify supernatant by Precision Red (BioRad). Prepare lysates with Laemmli buffer. Load NuPAGE 4-12% Bis-TRIS Invitrogen gels with MES SDS Running Buffer. Run at 100-120V for 2 hours. Proteins were transferred onto nitrocellulose membranes and immunoblotted using ECL Prime for a developing reagent.

Immunofluorescence

Adherent cells were fixed with 4% paraformaldehyde for 15 minutes, washed with PBS and permeabilized using 0.3% Triton X in PBS for 5 minutes before blocking with 5% fetal bovine serum in PBS. Primary antibodies used for microscopy

included GFP (Abcam), Sox10 (Santa Cruz), HMB45 (Dako), MITF (Abcam), TYRP1 (Santa Cruz).

Flow cytometry

For flow cytometry, cells were dissociated with accutase and blocked with 2% FBS in PBS before staining. EdU and c-kit (eBioscience) was the only antibody used for flow cytometry.

EdU Analysis

The cells were pulsed with 10 μM EdU for 30 minutes at 37°C. EdU detection was performed following manufacturer's instructions (Click-iTTM Plus EdU Flow Cytometry Assay Kits, Cat. no. C10634). Briefly, the cells were fixed for 15 min at RT using 100ul of Click-iT fixative per pellet and then washed with 3 mL of 1% BSA in PBS. The cells were then incubated for 30 minutes at RT in the dark. For 500ul of total reaction volume, we used 438 μl D-PBS, 10 μl Copper protectant, 2.5 μl Alexa Fluor 647 picolyl azide and 50 μl Reaction Buffer Additive. The cells were then washed with 3ml of 1x Click-iT saponin-based permeabilization and wash reagent, stained for DNA content (Hoechst) and analyzed by flow cytometer.

Histology

Selected zebrafish were fixed in 4% PFA for 48 hours at 4°C and then paraffin embedded. Fish were sectioned at 5 uM and placed on Apex Adhesive slides, baked at 60C, and then stained with H&E or antibodies against GFP (Abcam, ab183734. 1:100), $BRAF^{V600E}$ (Abcam, ab228461, 1:400), phospho-RB1 (Cell Signalling, 8516s. 1:400), phospho-ERK (Cell Signalling, 4370,1:100), or SOX10 (Cell Marque, 383A-76, 1:50). All histology was performed by Histowiz (http://www.histowiz.com) and the staining was performed by either Histowiz or the Hollmann Laboratory and reviewed by a pathologist (T.H.).

Quantification and statistical analysis

All animals were tracked for tumor free survival and measured using the Kaplan–Meier method. The differences between groups were analyzed using the log-rank statistics. Where indicated levels of significance were marked by asterisk as follows (*) $p \leq 0.05$; (**) $p \leq 0.01$; (***) $p \leq 0.001$. Throughout this study, averages across independent experiments were reported as means +/- standard error of the mean unless otherwise indicated. For all two-way comparisons, unpaired t-tests were considered statistically significant if $p \leq 0.05$.

RNA-sequencing

RNA-seq was done by Genewiz. RNA library preparation with polyA selection. Illumina HiSeq, 2x150bp configuration. Data analysis was conducted using the Limma package, the DESeq2 package UpSETR.

MiSEQ analysis

Reads were mapped to the zebrafish genome version *GRCHz10* using bwa version 0.7.13-r1126. Mutation quantification was performed using CrispRVariants version 1.7.4 [384]. MiSEQ reads can be accessed through the NIH Sequence Read Archive (SRA) (accession code SRP147816).

1. Lin JY, Fisher DE. Melanocyte biology and skin pigmentation. Nature. 2007;445(7130):843-50. doi: 10.1038/nature05660. PubMed PMID: 17314970.
2. Greco G, Panzella L, Verotta L, d'Ischia M, Napolitano A. Uncovering the structure of human red hair pheomelanin: benzothiazolylthiazinodihydroisoquinolines as key building blocks. J Nat Prod. 2011;74(4):675-82. doi: 10.1021/np100740n. PubMed PMID: 21341762.
3. Sajjad Ali Shah AS, Muhammad Irshad, Masroor Ellahi Babar, Tanveer Hussain, Abdul Wajid, Nazakat H Memon and Muhammad Idrees. Oculocutaneous Albinism in Pakistan: A Review. Journal of Cancer Science & Therapy. 2018;10(9). Epub sep 07, 2018. doi: 10.4172/1948-5956.1000552.
4. Wasmeier C, Hume AN, Bolasco G, Seabra MC. Melanosomes at a glance. Journal of cell science. 2008;121(Pt 24):3995-9. doi: 10.1242/jcs.040667. PubMed PMID: 19056669.
5. Chen KG, Valencia JC, Lai B, Zhang G, Paterson JK, Rouzaud F, et al. Melanosomal sequestration of cytotoxic drugs contributes to the intractability of malignant melanomas. Proc Natl Acad Sci U S A. 2006;103(26):9903-7. doi: 10.1073/pnas.0600213103. PubMed PMID: 16777967; PubMed Central PMCID: PMCPMC1502551.
6. Chen KG, Leapman RD, Zhang G, Lai B, Valencia JC, Cardarelli CO, et al. Influence of melanosome dynamics on melanoma drug sensitivity. J Natl Cancer Inst. 2009;101(18):1259-71. doi: 10.1093/jnci/djp259. PubMed PMID: 19704071; PubMed Central PMCID: PMCPMC2744727.
7. Borovansky J, Mirejovsky P, Riley PA. Possible relationship between abnormal melanosome structure and cytotoxic phenomena in malignant melanoma. Neoplasma. 1991;38(4):393-400. PubMed PMID: 1922572.
8. Mica Y, Lee G, Chambers SM, Tomishima MJ, Studer L. Modeling neural crest induction, melanocyte specification, and disease-related pigmentation defects in hESCs and patient-specific iPSCs. Cell reports. 2013;3(4):1140-52. doi: 10.1016/j.celrep.2013.03.025. PubMed PMID: 23583175; PubMed Central PMCID: PMCPMC3681528.
9. Raposo G, Marks MS. The dark side of lysosome-related organelles: specialization of the endocytic pathway for melanosome biogenesis. Traffic. 2002;3(4):237-48. PubMed PMID: 11929605.
10. Hearing VJ. Biogenesis of pigment granules: a sensitive way to regulate melanocyte function. J Dermatol Sci. 2005;37(1):3-14. doi: 10.1016/j.jdermsci.2004.08.014. PubMed PMID: 15619429.
11. Harper DC, Theos AC, Herman KE, Tenza D, Raposo G, Marks MS. Premelanosome amyloid-like fibrils are composed of only golgi-processed forms of Pmel17 that have been proteolytically processed in endosomes. J Biol Chem. 2008;283(4):2307-22. doi: 10.1074/jbc.M708007200. PubMed PMID: 17991747; PubMed Central PMCID: PMCPMC2430631.

12. Raposo G, Marks MS. Melanosomes--dark organelles enlighten endosomal membrane transport. Nat Rev Mol Cell Biol. 2007;8(10):786-97. doi: 10.1038/nrm2258. PubMed PMID: 17878918; PubMed Central PMCID: PMCPMC2786984.
13. Hearing VJ. Biochemical control of melanogenesis and melanosomal organization. J Investig Dermatol Symp Proc. 1999;4(1):24-8. PubMed PMID: 10537003.
14. Cichorek M, Wachulska M, Stasiewicz A, Tyminska A. Skin melanocytes: biology and development. Postepy Dermatol Alergol. 2013;30(1):30-41. doi: 10.5114/pdia.2013.33376. PubMed PMID: 24278043; PubMed Central PMCID: PMCPMC3834696.
15. Ghanem G, Fabrice J. Tyrosinase related protein 1 (TYRP1/gp75) in human cutaneous melanoma. Mol Oncol. 2011;5(2):150-5. doi: 10.1016/j.molonc.2011.01.006. PubMed PMID: 21324755; PubMed Central PMCID: PMCPMC5528278.
16. Jackson IJ. A cDNA encoding tyrosinase-related protein maps to the brown locus in mouse. Proc Natl Acad Sci U S A. 1988;85(12):4392-6. PubMed PMID: 3132713; PubMed Central PMCID: PMCPMC280435.
17. Hoek KS, Schlegel NC, Eichhoff OM, Widmer DS, Praetorius C, Einarsson SO, et al. Novel MITF targets identified using a two-step DNA microarray strategy. Pigment cell & melanoma research. 2008;21(6):665-76. doi: 10.1111/j.1755-148X.2008.00505.x. PubMed PMID: 19067971.
18. Kobayashi T, Urabe K, Orlow SJ, Higashi K, Imokawa G, Kwon BS, et al. The Pmel 17/silver locus protein. Characterization and investigation of its melanogenic function. J Biol Chem. 1994;269(46):29198-205. PubMed PMID: 7961886.
19. Tachibana M. Sound needs sound melanocytes to be heard. Pigment cell research / sponsored by the European Society for Pigment Cell Research and the International Pigment Cell Society. 1999;12(6):344-54. PubMed PMID: 10614574.
20. Goldgeier MH, Klein LE, Klein-Angerer S, Moellmann G, Nordlund JJ. The distribution of melanocytes in the leptomeninges of the human brain. The Journal of investigative dermatology. 1984;82(3):235-8. PubMed PMID: 6699426.
21. Double KL, Ben-Shachar D, Youdim MB, Zecca L, Riederer P, Gerlach M. Influence of neuromelanin on oxidative pathways within the human substantia nigra. Neurotoxicol Teratol. 2002;24(5):621-8. PubMed PMID: 12200193.
22. Zecca L, Tampellini D, Gatti A, Crippa R, Eisner M, Sulzer D, et al. The neuromelanin of human substantia nigra and its interaction with metals. J Neural Transm (Vienna). 2002;109(5-6):663-72. doi: 10.1007/s007020200055. PubMed PMID: 12111458.
23. Brito FC, Kos L. Timeline and distribution of melanocyte precursors in the mouse heart. Pigment cell & melanoma research. 2008;21(4):464-70. doi: 10.1111/j.1755-148X.2008.00459.x. PubMed PMID: 18444965.
24. Yajima I, Larue L. The location of heart melanocytes is specified and the level of pigmentation in the heart may correlate with coat color. Pigment cell & melanoma research. 2008;21(4):471-6. doi: 10.1111/j.1755-148X.2008.00483.x. PubMed PMID: 18627529.

25. Randhawa M, Huff T, Valencia JC, Younossi Z, Chandhoke V, Hearing VJ, et al. Evidence for the ectopic synthesis of melanin in human adipose tissue. FASEB J. 2009;23(3):835-43. doi: 10.1096/fj.08-116327. PubMed PMID: 18971261; PubMed Central PMCID: PMCPMC2653983.
26. Hu DN, Savage HE, Roberts JE. Uveal melanocytes, ocular pigment epithelium, and Muller cells in culture: in vitro toxicology. Int J Toxicol. 2002;21(6):465-72. doi: 10.1080/10915810290169891. PubMed PMID: 12537643.
27. Thingnes J, Lavelle TJ, Hovig E, Omholt SW. Understanding the melanocyte distribution in human epidermis: an agent-based computational model approach. PloS one. 2012;7(7):e40377. doi: 10.1371/journal.pone.0040377. PubMed PMID: 22792296; PubMed Central PMCID: PMCPMC3392240.
28. Pritchard LE, Turnbull AV, White A. Pro-opiomelanocortin processing in the hypothalamus: impact on melanocortin signalling and obesity. J Endocrinol. 2002;172(3):411-21. PubMed PMID: 11874690.
29. Cui R, Widlund HR, Feige E, Lin JY, Wilensky DL, Igras VE, et al. Central role of p53 in the suntan response and pathologic hyperpigmentation. Cell. 2007;128(5):853-64. doi: 10.1016/j.cell.2006.12.045. PubMed PMID: 17350573.
30. Goldman L, Schafer AI. Goldman-Cecil medicine. 25th edition. ed. Philadelphia, PA: Elsevier/Saunders; 2016. 2 volumes (xl, 2722, I108 pages) p.
31. Lo JA, Fisher DE. The melanoma revolution: from UV carcinogenesis to a new era in therapeutics. Science. 2014;346(6212):945-9. doi: 10.1126/science.1253735. PubMed PMID: 25414302; PubMed Central PMCID: PMCPMC4701046.
32. Wolf Horrell EM, Boulanger MC, D'Orazio JA. Melanocortin 1 Receptor: Structure, Function, and Regulation. Front Genet. 2016;7:95. doi: 10.3389/fgene.2016.00095. PubMed PMID: 27303435; PubMed Central PMCID: PMCPMC4885833.
33. Searle AG. An extension series in the mouse. J Hered. 1968;59(6):341-2. PubMed PMID: 5713934.
34. Levy C, Khaled M, Fisher DE. MITF: master regulator of melanocyte development and melanoma oncogene. Trends in molecular medicine. 2006;12(9):406-14. doi: 10.1016/j.molmed.2006.07.008. PubMed PMID: 16899407.
35. Slominski A, Paus R. Melanogenesis is coupled to murine anagen: toward new concepts for the role of melanocytes and the regulation of melanogenesis in hair growth. The Journal of investigative dermatology. 1993;101(1 Suppl):90S-7S. PubMed PMID: 8326158.
36. Nishimura EK, Jordan SA, Oshima H, Yoshida H, Osawa M, Moriyama M, et al. Dominant role of the niche in melanocyte stem-cell fate determination. Nature. 2002;416(6883):854-60. doi: 10.1038/416854a. PubMed PMID: 11976685.
37. Steingrimsson E, Copeland NG, Jenkins NA. Melanocyte stem cell maintenance and hair graying. Cell. 2005;121(1):9-12. doi: 10.1016/j.cell.2005.03.021. PubMed PMID: 15820674.
38. Alonso L, Fuchs E. The hair cycle. Journal of cell science. 2006;119(Pt 3):391-3. doi: 10.1242/jcs02793. PubMed PMID: 16443746.
39. Thibaut S, de Becker E, Bernard BA, Huart M, Fiat F, Baghdadli N, et al. Chronological ageing of human hair keratin fibres. Int J Cosmet Sci. 2010;32(6):422-34. doi: 10.1111/j.1468-2494.2009.00570.x. PubMed PMID: 20384898.

40. Stenn KS, Paus R. Controls of hair follicle cycling. Physiol Rev. 2001;81(1):449-94. doi: 10.1152/physrev.2001.81.1.449. PubMed PMID: 11152763.
41. Hearing VJ, Leong SPL. From melanocytes to melanoma : the progression to malignancy. Totowa, N.J.: Humana Press; 2006. xvii, 678 p. p.
42. Yamaguchi Y, Brenner M, Hearing VJ. The regulation of skin pigmentation. J Biol Chem. 2007;282(38):27557-61. doi: 10.1074/jbc.R700026200. PubMed PMID: 17635904.
43. Glover JD, Knolle S, Wells KL, Liu D, Jackson IJ, Mort RL, et al. Maintenance of distinct melanocyte populations in the interfollicular epidermis. Pigment cell & melanoma research. 2015;28(4):476-80. doi: 10.1111/pcmr.12375. PubMed PMID: 25847135; PubMed Central PMCID: PMCPMC4973853.
44. Tobin DJ. The cell biology of human hair follicle pigmentation. Pigment cell & melanoma research. 2011;24(1):75-88. doi: 10.1111/j.1755-148X.2010.00803.x. PubMed PMID: 21070612.
45. Slominski A, Wortsman J, Plonka PM, Schallreuter KU, Paus R, Tobin DJ. Hair follicle pigmentation. The Journal of investigative dermatology. 2005;124(1):13-21. doi: 10.1111/j.0022-202X.2004.23528.x. PubMed PMID: 15654948; PubMed Central PMCID: PMCPMC1201498.
46. White RM, Zon LI. Melanocytes in development, regeneration, and cancer. Cell Stem Cell. 2008;3(3):242-52. doi: 10.1016/j.stem.2008.08.005. PubMed PMID: 18786412.
47. Huang X, Saint-Jeannet JP. Induction of the neural crest and the opportunities of life on the edge. Dev Biol. 2004;275(1):1-11. doi: 10.1016/j.ydbio.2004.07.033. PubMed PMID: 15464568.
48. Morrison SJ, White PM, Zock C, Anderson DJ. Prospective identification, isolation by flow cytometry, and in vivo self-renewal of multipotent mammalian neural crest stem cells. Cell. 1999;96(5):737-49. doi: 10.1016/S0092-8674(00)80583-8. PubMed PMID: 10089888.
49. Elworthy S, Pinto JP, Pettifer A, Cancela ML, Kelsh RN. Phox2b function in the enteric nervous system is conserved in zebrafish and is sox10-dependent. Mechanisms of development. 2005;122(5):659-69. doi: 10.1016/j.mod.2004.12.008. PubMed PMID: 15817223.
50. Harris ML, Baxter LL, Loftus SK, Pavan WJ. Sox proteins in melanocyte development and melanoma. Pigment cell & melanoma research. 2010;23(4):496-513. doi: 10.1111/j.1755-148X.2010.00711.x. PubMed PMID: 20444197; PubMed Central PMCID: PMC2906668.
51. Herbarth B, Pingault V, Bondurand N, Kuhlbrodt K, Hermans-Borgmeyer I, Puliti A, et al. Mutation of the Sry-related Sox10 gene in Dominant megacolon, a mouse model for human Hirschsprung disease. Proc Natl Acad Sci U S A. 1998;95(9):5161-5. PubMed PMID: 9560246; PubMed Central PMCID: PMC20231.
52. Southard-Smith EM, Kos L, Pavan WJ. Sox10 mutation disrupts neural crest development in Dom Hirschsprung mouse model. Nature genetics. 1998;18(1):60-4. doi: 10.1038/ng0198-60. PubMed PMID: 9425902.
53. White RM, Cech J, Ratanasirintrawoot S, Lin CY, Rahl PB, Burke CJ, et al. DHODH modulates transcriptional elongation in the neural crest and melanoma.

Nature. 2011;471(7339):518-22. Epub 2011/03/25. doi: 10.1038/nature09882. PubMed PMID: 21430780; PubMed Central PMCID: PMC3759979.
54. Baggiolini A, Varum S, Mateos JM, Bettosini D, John N, Bonalli M, et al. Premigratory and migratory neural crest cells are multipotent in vivo. Cell Stem Cell. 2015;16(3):314-22. doi: 10.1016/j.stem.2015.02.017. PubMed PMID: 25748934.
55. Shyamala K, Yanduri S, Girish HC, Murgod S. Neural crest: The fourth germ layer. J Oral Maxillofac Pathol. 2015;19(2):221-9. doi: 10.4103/0973-029X.164536. PubMed PMID: 26604500; PubMed Central PMCID: PMCPMC4611932.
56. Dutton KA, Pauliny A, Lopes SS, Elworthy S, Carney TJ, Rauch J, et al. Zebrafish colourless encodes sox10 and specifies non-ectomesenchymal neural crest fates. Development. 2001;128(21):4113-25. PubMed PMID: 11684650.
57. Kim J, Lo L, Dormand E, Anderson DJ. SOX10 maintains multipotency and inhibits neuronal differentiation of neural crest stem cells. Neuron. 2003;38(1):17-31. PubMed PMID: 12691661.
58. Hou L, Arnheiter H, Pavan WJ. Interspecies difference in the regulation of melanocyte development by SOX10 and MITF. Proc Natl Acad Sci U S A. 2006;103(24):9081-5. doi: 10.1073/pnas.0603114103. PubMed PMID: 16757562; PubMed Central PMCID: PMC1482569.
59. Luo R, An M, Arduini BL, Henion PD. Specific pan-neural crest expression of zebrafish Crestin throughout embryonic development. Developmental dynamics : an official publication of the American Association of Anatomists. 2001;220(2):169-74. doi: 10.1002/1097-0177(2000)9999:9999<::AID-DVDY1097>3.0.CO;2-1. PubMed PMID: 11169850.
60. Kaufman CK, Mosimann C, Fan ZP, Yang S, Thomas AJ, Ablain J, et al. A zebrafish melanoma model reveals emergence of neural crest identity during melanoma initiation. Science. 2016;351(6272):aad2197. doi: 10.1126/science.aad2197. PubMed PMID: 26823433; PubMed Central PMCID: PMCPMC4868069.
61. Fattahi F, Steinbeck JA, Kriks S, Tchieu J, Zimmer B, Kishinevsky S, et al. Deriving human ENS lineages for cell therapy and drug discovery in Hirschsprung disease. Nature. 2016;531(7592):105-9. doi: 10.1038/nature16951. PubMed PMID: 26863197; PubMed Central PMCID: PMCPMC4846424.
62. Kim IS, Heilmann S, Kansler ER, Zhang Y, Zimmer M, Ratnakumar K, et al. Microenvironment-derived factors driving metastatic plasticity in melanoma. Nat Commun. 2017;8:14343. doi: 10.1038/ncomms14343. PubMed PMID: 28181494; PubMed Central PMCID: PMCPMC5309794.
63. Jo A, Denduluri S, Zhang B, Wang Z, Yin L, Yan Z, et al. The versatile functions of Sox9 in development, stem cells, and human diseases. Genes Dis. 2014;1(2):149-61. doi: 10.1016/j.gendis.2014.09.004. PubMed PMID: 25685828; PubMed Central PMCID: PMCPMC4326072.
64. Passeron T, Valencia JC, Bertolotto C, Hoashi T, Le Pape E, Takahashi K, et al. SOX9 is a key player in ultraviolet B-induced melanocyte differentiation and pigmentation. Proc Natl Acad Sci U S A. 2007;104(35):13984-9. doi: 10.1073/pnas.0705117104. PubMed PMID: 17702866; PubMed Central PMCID: PMCPMC1955778.

65. Dupin E, Glavieux C, Vaigot P, Le Douarin NM. Endothelin 3 induces the reversion of melanocytes to glia through a neural crest-derived glial-melanocytic progenitor. Proc Natl Acad Sci U S A. 2000;97(14):7882-7. PubMed PMID: 10884419; PubMed Central PMCID: PMC16639.
66. Gleason BC, Crum CP, Murphy GF. Expression patterns of MITF during human cutaneous embryogenesis: evidence for bulge epithelial expression and persistence of dermal melanoblasts. J Cutan Pathol. 2008;35(7):615-22. doi: 10.1111/j.1600-0560.2007.00881.x. PubMed PMID: 18312434; PubMed Central PMCID: PMCPMC2935278.
67. Lister JA, Robertson CP, Lepage T, Johnson SL, Raible DW. nacre encodes a zebrafish microphthalmia-related protein that regulates neural-crest-derived pigment cell fate. Development. 1999;126(17):3757-67. PubMed PMID: 10433906.
68. Hou L, Panthier JJ, Arnheiter H. Signaling and transcriptional regulation in the neural crest-derived melanocyte lineage: interactions between KIT and MITF. Development. 2000;127(24):5379-89. PubMed PMID: 11076759.
69. Phung B, Sun J, Schepsky A, Steingrimsson E, Ronnstrand L. C-KIT signaling depends on microphthalmia-associated transcription factor for effects on cell proliferation. PloS one. 2011;6(8):e24064. doi: 10.1371/journal.pone.0024064. PubMed PMID: 21887372; PubMed Central PMCID: PMC3161112.
70. Opdecamp K, Nakayama A, Nguyen MT, Hodgkinson CA, Pavan WJ, Arnheiter H. Melanocyte development in vivo and in neural crest cell cultures: crucial dependence on the Mitf basic-helix-loop-helix-zipper transcription factor. Development. 1997;124(12):2377-86. PubMed PMID: 9199364.
71. Planque N, Raposo G, Leconte L, Anezo O, Martin P, Saule S. Microphthalmia transcription factor induces both retinal pigmented epithelium and neural crest melanocytes from neuroretina cells. J Biol Chem. 2004;279(40):41911-7. doi: 10.1074/jbc.M404964200. PubMed PMID: 15277526.
72. Tachibana M, Takeda K, Nobukuni Y, Urabe K, Long JE, Meyers KA, et al. Ectopic expression of MITF, a gene for Waardenburg syndrome type 2, converts fibroblasts to cells with melanocyte characteristics. Nature genetics. 1996;14(1):50-4. doi: 10.1038/ng0996-50. PubMed PMID: 8782819.
73. Elworthy S, Lister JA, Carney TJ, Raible DW, Kelsh RN. Transcriptional regulation of mitfa accounts for the sox10 requirement in zebrafish melanophore development. Development. 2003;130(12):2809-18. PubMed PMID: 12736222.
74. Cooper CD, Linbo TH, Raible DW. Kit and foxd3 genetically interact to regulate melanophore survival in zebrafish. Developmental dynamics : an official publication of the American Association of Anatomists. 2009;238(4):875-86. doi: 10.1002/dvdy.21910. PubMed PMID: 19301400; PubMed Central PMCID: PMCPMC2730777.
75. Steingrimsson E, Copeland NG, Jenkins NA. Melanocytes and the microphthalmia transcription factor network. Annu Rev Genet. 2004;38:365-411. doi: 10.1146/annurev.genet.38.072902.092717. PubMed PMID: 15568981.
76. Lister JA, Close J, Raible DW. Duplicate mitf genes in zebrafish: complementary expression and conservation of melanogenic potential. Dev Biol. 2001;237(2):333-44. doi: 10.1006/dbio.2001.0379. PubMed PMID: 11543618.

77. Curran K, Raible DW, Lister JA. Foxd3 controls melanophore specification in the zebrafish neural crest by regulation of Mitf. Dev Biol. 2009;332(2):408-17. doi: 10.1016/j.ydbio.2009.06.010. PubMed PMID: 19527705; PubMed Central PMCID: PMCPMC2716409.
78. Hocker TL, Singh MK, Tsao H. Melanoma genetics and therapeutic approaches in the 21st century: moving from the benchside to the bedside. The Journal of investigative dermatology. 2008;128(11):2575-95. doi: 10.1038/jid.2008.226. PubMed PMID: 18927540.
79. Guyonneau L, Murisier F, Rossier A, Moulin A, Beermann F. Melanocytes and pigmentation are affected in dopachrome tautomerase knockout mice. Mol Cell Biol. 2004;24(8):3396-403. PubMed PMID: 15060160; PubMed Central PMCID: PMCPMC381679.
80. Iemura A, Tsai M, Ando A, Wershil BK, Galli SJ. The c-kit ligand, stem cell factor, promotes mast cell survival by suppressing apoptosis. The American journal of pathology. 1994;144(2):321-8. PubMed PMID: 7508684; PubMed Central PMCID: PMCPMC1887147.
81. Williams DE, de Vries P, Namen AE, Widmer MB, Lyman SD. The Steel factor. Dev Biol. 1992;151(2):368-76. PubMed PMID: 1376287.
82. Yoshida H, Kunisada T, Grimm T, Nishimura EK, Nishioka E, Nishikawa SI. Review: melanocyte migration and survival controlled by SCF/c-kit expression. J Investig Dermatol Symp Proc. 2001;6(1):1-5. doi: 10.1046/j.0022-202x.2001.00006.x. PubMed PMID: 11764276.
83. Yoshida H, Kunisada T, Kusakabe M, Nishikawa S, Nishikawa SI. Distinct stages of melanocyte differentiation revealed by anlaysis of nonuniform pigmentation patterns. Development. 1996;122(4):1207-14. PubMed PMID: 8620847.
84. Chiasson BJ, Tropepe V, Morshead CM, van der Kooy D. Adult mammalian forebrain ependymal and subependymal cells demonstrate proliferative potential, but only subependymal cells have neural stem cell characteristics. J Neurosci. 1999;19(11):4462-71. PubMed PMID: 10341247.
85. Lois C, Alvarez-Buylla A. Proliferating subventricular zone cells in the adult mammalian forebrain can differentiate into neurons and glia. Proc Natl Acad Sci U S A. 1993;90(5):2074-7. PubMed PMID: 8446631; PubMed Central PMCID: PMCPMC46023.
86. Altman J, Das GD. Autoradiographic and histological evidence of postnatal hippocampal neurogenesis in rats. J Comp Neurol. 1965;124(3):319-35. PubMed PMID: 5861717.
87. Kuhn HG, Dickinson-Anson H, Gage FH. Neurogenesis in the dentate gyrus of the adult rat: age-related decrease of neuronal progenitor proliferation. J Neurosci. 1996;16(6):2027-33. PubMed PMID: 8604047.
88. Altman J. Autoradiographic and histological studies of postnatal neurogenesis. IV. Cell proliferation and migration in the anterior forebrain, with special reference to persisting neurogenesis in the olfactory bulb. J Comp Neurol. 1969;137(4):433-57. doi: 10.1002/cne.901370404. PubMed PMID: 5361244.

89. Barker N, Bartfeld S, Clevers H. Tissue-resident adult stem cell populations of rapidly self-renewing organs. Cell Stem Cell. 2010;7(6):656-70. doi: 10.1016/j.stem.2010.11.016. PubMed PMID: 21112561.
90. Wagers AJ, Weissman IL. Plasticity of adult stem cells. Cell. 2004;116(5):639-48. PubMed PMID: 15006347.
91. Spangrude GJ, Heimfeld S, Weissman IL. Purification and characterization of mouse hematopoietic stem cells. Science. 1988;241(4861):58-62. PubMed PMID: 2898810.
92. Mauro A. Satellite cell of skeletal muscle fibers. J Biophys Biochem Cytol. 1961;9:493-5. PubMed PMID: 13768451; PubMed Central PMCID: PMCPMC2225012.
93. Kobielak K, Pasolli HA, Alonso L, Polak L, Fuchs E. Defining BMP functions in the hair follicle by conditional ablation of BMP receptor IA. J Cell Biol. 2003;163(3):609-23. doi: 10.1083/jcb.200309042. PubMed PMID: 14610062; PubMed Central PMCID: PMCPMC2173651.
94. Alonso L, Fuchs E. Stem cells of the skin epithelium. Proc Natl Acad Sci U S A. 2003;100 Suppl 1:11830-5. doi: 10.1073/pnas.1734203100. PubMed PMID: 12913119; PubMed Central PMCID: PMCPMC304094.
95. Bjerknes M, Cheng H. Clonal analysis of mouse intestinal epithelial progenitors. Gastroenterology. 1999;116(1):7-14. PubMed PMID: 9869596.
96. Forbes S, Vig P, Poulsom R, Thomas H, Alison M. Hepatic stem cells. J Pathol. 2002;197(4):510-8. doi: 10.1002/path.1163. PubMed PMID: 12115866.
97. Toma JG, Akhavan M, Fernandes KJ, Barnabe-Heider F, Sadikot A, Kaplan DR, et al. Isolation of multipotent adult stem cells from the dermis of mammalian skin. Nature cell biology. 2001;3(9):778-84. doi: 10.1038/ncb0901-778. PubMed PMID: 11533656.
98. Jiang Y, Jahagirdar BN, Reinhardt RL, Schwartz RE, Keene CD, Ortiz-Gonzalez XR, et al. Pluripotency of mesenchymal stem cells derived from adult marrow. Nature. 2002;418(6893):41-9. doi: 10.1038/nature00870. PubMed PMID: 12077603.
99. Pittenger MF, Mackay AM, Beck SC, Jaiswal RK, Douglas R, Mosca JD, et al. Multilineage potential of adult human mesenchymal stem cells. Science. 1999;284(5411):143-7. PubMed PMID: 10102814.
100. Mimeault M, Batra SK. Recent progress on tissue-resident adult stem cell biology and their therapeutic implications. Stem Cell Rev. 2008;4(1):27-49. doi: 10.1007/s12015-008-9008-2. PubMed PMID: 18288619; PubMed Central PMCID: PMCPMC3828649.
101. Neves J, Sousa-Victor P, Jasper H. Rejuvenating Strategies for Stem Cell-Based Therapies in Aging. Cell Stem Cell. 2017;20(2):161-75. doi: 10.1016/j.stem.2017.01.008. PubMed PMID: 28157498; PubMed Central PMCID: PMCPMC5681350.
102. Nishimura EK, Granter SR, Fisher DE. Mechanisms of hair graying: incomplete melanocyte stem cell maintenance in the niche. Science. 2005;307(5710):720-4. doi: 10.1126/science.1099593. PubMed PMID: 15618488.

103. Conboy IM, Rando TA. Aging, stem cells and tissue regeneration: lessons from muscle. Cell Cycle. 2005;4(3):407-10. doi: 10.4161/cc.4.3.1518. PubMed PMID: 15725724.
104. Raveh-Amit H, Berzsenyi S, Vas V, Ye D, Dinnyes A. Tissue resident stem cells: till death do us part. Biogerontology. 2013;14(6):573-90. doi: 10.1007/s10522-013-9469-9. PubMed PMID: 24085521; PubMed Central PMCID: PMCPMC3879821.
105. Schultz MB, Sinclair DA. When stem cells grow old: phenotypes and mechanisms of stem cell aging. Development. 2016;143(1):3-14. doi: 10.1242/dev.130633. PubMed PMID: 26732838; PubMed Central PMCID: PMCPMC4725211.
106. Kowalczyk MS, Tirosh I, Heckl D, Rao TN, Dixit A, Haas BJ, et al. Single-cell RNA-seq reveals changes in cell cycle and differentiation programs upon aging of hematopoietic stem cells. Genome research. 2015;25(12):1860-72. doi: 10.1101/gr.192237.115. PubMed PMID: 26430063; PubMed Central PMCID: PMCPMC4665007.
107. Oh J, Lee YD, Wagers AJ. Stem cell aging: mechanisms, regulators and therapeutic opportunities. Nature medicine. 2014;20(8):870-80. doi: 10.1038/nm.3651. PubMed PMID: 25100532; PubMed Central PMCID: PMCPMC4160113.
108. Rossi DJ, Bryder D, Zahn JM, Ahlenius H, Sonu R, Wagers AJ, et al. Cell intrinsic alterations underlie hematopoietic stem cell aging. Proc Natl Acad Sci U S A. 2005;102(26):9194-9. doi: 10.1073/pnas.0503280102. PubMed PMID: 15967997; PubMed Central PMCID: PMCPMC1153718.
109. Alt EU, Senst C, Murthy SN, Slakey DP, Dupin CL, Chaffin AE, et al. Aging alters tissue resident mesenchymal stem cell properties. Stem Cell Res. 2012;8(2):215-25. doi: 10.1016/j.scr.2011.11.002. PubMed PMID: 22265741.
110. Silver AF, Chase HB, Potten CS. Melanocyte precursor cells in the hair follicle germ during the dormat stage (telogen). Experientia. 1969;25(3):299-301. PubMed PMID: 5781547.
111. Cock AG, Cohen J. The melanoblast reservoir available to a feather papilla. J Embryol Exp Morphol. 1958;6(4):530-45. PubMed PMID: 13611133.
112. Amoh Y, Hoffman RM. Isolation and culture of hair follicle pluripotent stem (hfPS) cells and their use for nerve and spinal cord regeneration. Methods in molecular biology. 2010;585:401-20. doi: 10.1007/978-1-60761-380-0_28. PubMed PMID: 19908019.
113. Hauser S, Widera D, Qunneis F, Muller J, Zander C, Greiner J, et al. Isolation of novel multipotent neural crest-derived stem cells from adult human inferior turbinate. Stem cells and development. 2012;21(5):742-56. doi: 10.1089/scd.2011.0419. PubMed PMID: 22128806; PubMed Central PMCID: PMC3296122.
114. Kanno H, Kubo A, Yoshizumi T, Mikami T, Maegawa J. Isolation of Multipotent Nestin-Expressing Stem Cells Derived from the Epidermis of Elderly Humans and TAT-VHL Peptide-Mediated Neuronal Differentiation of These Cells. International journal of molecular sciences. 2013;14(5):9604-17. doi: 10.3390/ijms14059604. PubMed PMID: 23644888; PubMed Central PMCID: PMC3676801.

115. Nagel S, Rohr F, Weber C, Kier J, Siemers F, Kruse C, et al. Multipotent nestin-positive stem cells reside in the stroma of human eccrine and apocrine sweat glands and can be propagated robustly in vitro. PloS one. 2013;8(10):e78365. doi: 10.1371/journal.pone.0078365. PubMed PMID: 24205211; PubMed Central PMCID: PMC3813437.
116. Sieber-Blum M, Grim M. The adult hair follicle: cradle for pluripotent neural crest stem cells. Birth defects research Part C, Embryo today : reviews. 2004;72(2):162-72. doi: 10.1002/bdrc.20008. PubMed PMID: 15269890.
117. Yang R, Xu X. Isolation and culture of neural crest stem cells from human hair follicles. Journal of visualized experiments : JoVE. 2013;(74). doi: 10.3791/3194. PubMed PMID: 23608752.
118. Osawa M, Egawa G, Mak SS, Moriyama M, Freter R, Yonetani S, et al. Molecular characterization of melanocyte stem cells in their niche. Development. 2005;132(24):5589-99. doi: 10.1242/dev.02161. PubMed PMID: 16314490.
119. Grichnik JM, Ali WN, Burch JA, Byers JD, Garcia CA, Clark RE, et al. KIT expression reveals a population of precursor melanocytes in human skin. The Journal of investigative dermatology. 1996;106(5):967-71. doi: 10.1111/1523-1747.ep12338471. PubMed PMID: 8618059.
120. Fernandes KJ, McKenzie IA, Mill P, Smith KM, Akhavan M, Barnabe-Heider F, et al. A dermal niche for multipotent adult skin-derived precursor cells. Nature cell biology. 2004;6(11):1082-93. doi: 10.1038/ncb1181. PubMed PMID: 15517002.
121. Biernaskie J, Paris M, Morozova O, Fagan BM, Marra M, Pevny L, et al. SKPs derive from hair follicle precursors and exhibit properties of adult dermal stem cells. Cell Stem Cell. 2009;5(6):610-23. doi: 10.1016/j.stem.2009.10.019. PubMed PMID: 19951689; PubMed Central PMCID: PMCPMC2828150.
122. Jinno H, Morozova O, Jones KL, Biernaskie JA, Paris M, Hosokawa R, et al. Convergent genesis of an adult neural crest-like dermal stem cell from distinct developmental origins. Stem cells. 2010;28(11):2027-40. doi: 10.1002/stem.525. PubMed PMID: 20848654; PubMed Central PMCID: PMCPMC3087810.
123. Johnston AP, Naska S, Jones K, Jinno H, Kaplan DR, Miller FD. Sox2-mediated regulation of adult neural crest precursors and skin repair. Stem Cell Reports. 2013;1(1):38-45. doi: 10.1016/j.stemcr.2013.04.004. PubMed PMID: 24052940; PubMed Central PMCID: PMCPMC3757738.
124. McKenzie IA, Biernaskie J, Toma JG, Midha R, Miller FD. Skin-derived precursors generate myelinating Schwann cells for the injured and dysmyelinated nervous system. J Neurosci. 2006;26(24):6651-60. doi: 10.1523/JNEUROSCI.1007-06.2006. PubMed PMID: 16775154.
125. Toma JG, McKenzie IA, Bagli D, Miller FD. Isolation and characterization of multipotent skin-derived precursors from human skin. Stem cells. 2005;23(6):727-37. doi: 10.1634/stemcells.2004-0134. PubMed PMID: 15917469.
126. Wong CE, Paratore C, Dours-Zimmermann MT, Rochat A, Pietri T, Suter U, et al. Neural crest-derived cells with stem cell features can be traced back to multiple lineages in the adult skin. J Cell Biol. 2006;175(6):1005-15. doi: 10.1083/jcb.200606062. PubMed PMID: 17158956; PubMed Central PMCID: PMCPMC2064709.

127. Li L, Fukunaga-Kalabis M, Yu H, Xu X, Kong J, Lee JT, et al. Human dermal stem cells differentiate into functional epidermal melanocytes. Journal of cell science. 2010;123(Pt 6):853-60. doi: 10.1242/jcs.061598. PubMed PMID: 20159965; PubMed Central PMCID: PMC2831759.
128. Sieber-Blum M, Grim M, Hu YF, Szeder V. Pluripotent neural crest stem cells in the adult hair follicle. Developmental dynamics : an official publication of the American Association of Anatomists. 2004;231(2):258-69. doi: 10.1002/dvdy.20129. PubMed PMID: 15366003.
129. Hu YF, Zhang ZJ, Sieber-Blum M. An epidermal neural crest stem cell (EPI-NCSC) molecular signature. Stem cells. 2006;24(12):2692-702. doi: 10.1634/stemcells.2006-0233. PubMed PMID: 16931771.
130. Clewes O, Narytnyk A, Gillinder KR, Loughney AD, Murdoch AP, Sieber-Blum M. Human epidermal neural crest stem cells (hEPI-NCSC)--characterization and directed differentiation into osteocytes and melanocytes. Stem Cell Rev. 2011;7(4):799-814. doi: 10.1007/s12015-011-9255-5. PubMed PMID: 21455606; PubMed Central PMCID: PMCPMC3252033.
131. Adameyko I, Lallemend F, Aquino JB, Pereira JA, Topilko P, Muller T, et al. Schwann cell precursors from nerve innervation are a cellular origin of melanocytes in skin. Cell. 2009;139(2):366-79. doi: 10.1016/j.cell.2009.07.049. PubMed PMID: 19837037.
132. Furlan A, Adameyko I. Schwann cell precursor: a neural crest cell in disguise? Dev Biol. 2018. doi: 10.1016/j.ydbio.2018.02.008. PubMed PMID: 29454705.
133. Furlan A, Dyachuk V, Kastriti ME, Calvo-Enrique L, Abdo H, Hadjab S, et al. Multipotent peripheral glial cells generate neuroendocrine cells of the adrenal medulla. Science. 2017;357(6346). doi: 10.1126/science.aal3753. PubMed PMID: 28684471; PubMed Central PMCID: PMCPMC6013038.
134. Shakhova O, Sommer L. Neural crest-derived stem cells. StemBook. Cambridge (MA)2008.
135. AmericanCancerSociety. Melanoma Skin Cancer 2018. Available from: http://www.cancer.org/cancer/skincancer-melanoma/detailedguide/melanoma-skin-cancer-key-statistics.
136. Oliveria SA, Saraiya M, Geller AC, Heneghan MK, Jorgensen C. Sun exposure and risk of melanoma. Arch Dis Child. 2006;91(2):131-8. doi: 10.1136/adc.2005.086918. PubMed PMID: 16326797; PubMed Central PMCID: PMCPMC2082713.
137. Friedman RJ, Rigel DS, Kopf AW. Early detection of malignant melanoma: the role of physician examination and self-examination of the skin. CA Cancer J Clin. 1985;35(3):130-51. PubMed PMID: 3921200.
138. . Available from: http://www.jurmo.ch/work_model.php.
139. Gaggioli C, Sahai E. Melanoma invasion - current knowledge and future directions. Pigment cell research / sponsored by the European Society for Pigment Cell Research and the International Pigment Cell Society. 2007;20(3):161-72. doi: 10.1111/j.1600-0749.2007.00378.x. PubMed PMID: 17516924.
140. Kvam E, Tyrrell RM. Induction of oxidative DNA base damage in human skin cells by UV and near visible radiation. Carcinogenesis. 1997;18(12):2379-84. PubMed PMID: 9450485.

141. Cancer Genome Atlas N. Genomic Classification of Cutaneous Melanoma. Cell. 2015;161(7):1681-96. doi: 10.1016/j.cell.2015.05.044. PubMed PMID: 26091043; PubMed Central PMCID: PMCPMC4580370.
142. Brash DE. UV signature mutations. Photochem Photobiol. 2015;91(1):15-26. doi: 10.1111/php.12377. PubMed PMID: 25354245; PubMed Central PMCID: PMCPMC4294947.
143. Howard BD, Tessman I. Identification of the Altered Bases in Mutated Single-Stranded DNA. 3. Mutagenesis by Ultraviolet Light. J Mol Biol. 1964;9:372-5. PubMed PMID: 14202273.
144. Mead MN. Benefits of sunlight: a bright spot for human health. Environmental health perspectives. 2008;116(4):A160-7. doi: 10.1289/ehp.116-a160. PubMed PMID: 18414615; PubMed Central PMCID: PMCPMC2290997.
145. Hodis E, Watson IR, Kryukov GV, Arold ST, Imielinski M, Theurillat JP, et al. A landscape of driver mutations in melanoma. Cell. 2012;150(2):251-63. doi: 10.1016/j.cell.2012.06.024. PubMed PMID: 22817889; PubMed Central PMCID: PMCPMC3600117.
146. Martincorena I, Campbell PJ. Somatic mutation in cancer and normal cells. Science. 2015;349(6255):1483-9. doi: 10.1126/science.aab4082. PubMed PMID: 26404825.
147. Martincorena I, Roshan A, Gerstung M, Ellis P, Van Loo P, McLaren S, et al. Tumor evolution. High burden and pervasive positive selection of somatic mutations in normal human skin. Science. 2015;348(6237):880-6. doi: 10.1126/science.aaa6806. PubMed PMID: 25999502; PubMed Central PMCID: PMCPMC4471149.
148. Vogelstein B, Papadopoulos N, Velculescu VE, Zhou S, Diaz LA, Jr., Kinzler KW. Cancer genome landscapes. Science. 2013;339(6127):1546-58. doi: 10.1126/science.1235122. PubMed PMID: 23539594; PubMed Central PMCID: PMCPMC3749880.
149. Baca SC, Prandi D, Lawrence MS, Mosquera JM, Romanel A, Drier Y, et al. Punctuated evolution of prostate cancer genomes. Cell. 2013;153(3):666-77. doi: 10.1016/j.cell.2013.03.021. PubMed PMID: 23622249; PubMed Central PMCID: PMCPMC3690918.
150. Poynter JN, Elder JT, Fullen DR, Nair RP, Soengas MS, Johnson TM, et al. BRAF and NRAS mutations in melanoma and melanocytic nevi. Melanoma research. 2006;16(4):267-73. doi: 10.1097/01.cmr.0000222600.73179.f3. PubMed PMID: 16845322.
151. Tschandl P, Berghoff AS, Preusser M, Burgstaller-Muehlbacher S, Pehamberger H, Okamoto I, et al. NRAS and BRAF mutations in melanoma-associated nevi and uninvolved nevi. PloS one. 2013;8(7):e69639. doi: 10.1371/journal.pone.0069639. PubMed PMID: 23861977; PubMed Central PMCID: PMCPMC3704624.
152. Kumar R, Angelini S, Snellman E, Hemminki K. BRAF mutations are common somatic events in melanocytic nevi. The Journal of investigative dermatology. 2004;122(2):342-8. doi: 10.1046/j.0022-202X.2004.22225.x. PubMed PMID: 15009715.

153. Zingg D, Debbache J, Schaefer SM, Tuncer E, Frommel SC, Cheng P, et al. The epigenetic modifier EZH2 controls melanoma growth and metastasis through silencing of distinct tumour suppressors. Nat Commun. 2015;6:6051. doi: 10.1038/ncomms7051. PubMed PMID: 25609585.
154. Ceol CJ, Houvras Y, Jane-Valbuena J, Bilodeau S, Orlando DA, Battisti V, et al. The histone methyltransferase SETDB1 is recurrently amplified in melanoma and accelerates its onset. Nature. 2011;471(7339):513-7. Epub 2011/03/25. doi: 10.1038/nature09806. PubMed PMID: 21430779; PubMed Central PMCID: PMC3348545.
155. Lian CG, Xu Y, Ceol C, Wu F, Larson A, Dresser K, et al. Loss of 5-hydroxymethylcytosine is an epigenetic hallmark of melanoma. Cell. 2012;150(6):1135-46. doi: 10.1016/j.cell.2012.07.033. PubMed PMID: 22980977; PubMed Central PMCID: PMCPMC3770275.
156. Huang FW, Hodis E, Xu MJ, Kryukov GV, Chin L, Garraway LA. Highly recurrent TERT promoter mutations in human melanoma. Science. 2013;339(6122):957-9. doi: 10.1126/science.1229259. PubMed PMID: 23348506.
157. Horn S, Figl A, Rachakonda PS, Fischer C, Sucker A, Gast A, et al. TERT promoter mutations in familial and sporadic melanoma. Science. 2013;339(6122):959-61. doi: 10.1126/science.1230062. PubMed PMID: 23348503.
158. Zhang XY, Zhang PY. Genetics and epigenetics of melanoma. Oncol Lett. 2016;12(5):3041-4. doi: 10.3892/ol.2016.5093. PubMed PMID: 27899960; PubMed Central PMCID: PMCPMC5103895.
159. Moran B, Silva R, Perry AS, Gallagher WM. Epigenetics of malignant melanoma. Semin Cancer Biol. 2018;51:80-8. doi: 10.1016/j.semcancer.2017.10.006. PubMed PMID: 29074395.
160. Straume O, Smeds J, Kumar R, Hemminki K, Akslen LA. Significant impact of promoter hypermethylation and the 540 C>T polymorphism of CDKN2A in cutaneous melanoma of the vertical growth phase. The American journal of pathology. 2002;161(1):229-37. doi: 10.1016/S0002-9440(10)64174-0. PubMed PMID: 12107107; PubMed Central PMCID: PMCPMC1850679.
161. Spugnardi M, Tommasi S, Dammann R, Pfeifer GP, Hoon DS. Epigenetic inactivation of RAS association domain family protein 1 (RASSF1A) in malignant cutaneous melanoma. Cancer research. 2003;63(7):1639-43. PubMed PMID: 12670917.
162. Mirmohammadsadegh A, Marini A, Nambiar S, Hassan M, Tannapfel A, Ruzicka T, et al. Epigenetic silencing of the PTEN gene in melanoma. Cancer research. 2006;66(13):6546-52. doi: 10.1158/0008-5472.CAN-06-0384. PubMed PMID: 16818626.
163. Fiziev P, Akdemir KC, Miller JP, Keung EZ, Samant NS, Sharma S, et al. Systematic Epigenomic Analysis Reveals Chromatin States Associated with Melanoma Progression. Cell reports. 2017;19(4):875-89. doi: 10.1016/j.celrep.2017.03.078. PubMed PMID: 28445736; PubMed Central PMCID: PMCPMC5473172.
164. Lander ES, Linton LM, Birren B, Nusbaum C, Zody MC, Baldwin J, et al. Initial sequencing and analysis of the human genome. Nature. 2001;409(6822):860-921. doi: 10.1038/35057062. PubMed PMID: 11237011.

165. Djebali S, Davis CA, Merkel A, Dobin A, Lassmann T, Mortazavi A, et al. Landscape of transcription in human cells. Nature. 2012;489(7414):101-8. doi: 10.1038/nature11233. PubMed PMID: 22955620; PubMed Central PMCID: PMCPMC3684276.
166. Leucci E, Vendramin R, Spinazzi M, Laurette P, Fiers M, Wouters J, et al. Melanoma addiction to the long non-coding RNA SAMMSON. Nature. 2016;531(7595):518-22. doi: 10.1038/nature17161. PubMed PMID: 27008969.
167. Wang S, Fan W, Wan B, Tu M, Jin F, Liu F, et al. Characterization of long noncoding RNA and messenger RNA signatures in melanoma tumorigenesis and metastasis. PloS one. 2017;12(2):e0172498. doi: 10.1371/journal.pone.0172498. PubMed PMID: 28225791; PubMed Central PMCID: PMCPMC5321451.
168. Hulstaert E, Brochez L, Volders PJ, Vandesompele J, Mestdagh P. Long non-coding RNAs in cutaneous melanoma: clinical perspectives. Oncotarget. 2017;8(26):43470-80. doi: 10.18632/oncotarget.16478. PubMed PMID: 28415644; PubMed Central PMCID: PMCPMC5522162.
169. Lemmon MA, Schlessinger J. Cell signaling by receptor tyrosine kinases. Cell. 2010;141(7):1117-34. doi: 10.1016/j.cell.2010.06.011. PubMed PMID: 20602996; PubMed Central PMCID: PMCPMC2914105.
170. Avruch J, Khokhlatchev A, Kyriakis JM, Luo Z, Tzivion G, Vavvas D, et al. Ras activation of the Raf kinase: tyrosine kinase recruitment of the MAP kinase cascade. Recent Prog Horm Res. 2001;56:127-55. PubMed PMID: 11237210.
171. Northwood IC, Gonzalez FA, Wartmann M, Raden DL, Davis RJ. Isolation and characterization of two growth factor-stimulated protein kinases that phosphorylate the epidermal growth factor receptor at threonine 669. J Biol Chem. 1991;266(23):15266-76. PubMed PMID: 1651322.
172. Zakrzewska M, Haugsten EM, Nadratowska-Wesolowska B, Oppelt A, Hausott B, Jin Y, et al. ERK-mediated phosphorylation of fibroblast growth factor receptor 1 on Ser777 inhibits signaling. Sci Signal. 2013;6(262):ra11. doi: 10.1126/scisignal.2003087. PubMed PMID: 23405013.
173. Ueki K, Matsuda S, Tobe K, Gotoh Y, Tamemoto H, Yachi M, et al. Feedback regulation of mitogen-activated protein kinase kinase kinase activity of c-Raf-1 by insulin and phorbol ester stimulation. J Biol Chem. 1994;269(22):15756-61. PubMed PMID: 8195229.
174. Brummer T, Naegele H, Reth M, Misawa Y. Identification of novel ERK-mediated feedback phosphorylation sites at the C-terminus of B-Raf. Oncogene. 2003;22(55):8823-34. doi: 10.1038/sj.onc.1207185. PubMed PMID: 14654779.
175. Brunet A, Pages G, Pouyssegur J. Growth factor-stimulated MAP kinase induces rapid retrophosphorylation and inhibition of MAP kinase kinase (MEK1). FEBS Lett. 1994;346(2-3):299-303. PubMed PMID: 8013650.
176. Hanafusa H, Torii S, Yasunaga T, Nishida E. Sprouty1 and Sprouty2 provide a control mechanism for the Ras/MAPK signalling pathway. Nature cell biology. 2002;4(11):850-8. doi: 10.1038/ncb867. PubMed PMID: 12402043.
177. Owens DM, Keyse SM. Differential regulation of MAP kinase signalling by dual-specificity protein phosphatases. Oncogene. 2007;26(22):3203-13. doi: 10.1038/sj.onc.1210412. PubMed PMID: 17496916.

178. Lake D, Correa SA, Muller J. Negative feedback regulation of the ERK1/2 MAPK pathway. Cell Mol Life Sci. 2016;73(23):4397-413. doi: 10.1007/s00018-016-2297-8. PubMed PMID: 27342992; PubMed Central PMCID: PMCPMC5075022.
179. Poulikakos PI, Persaud Y, Janakiraman M, Kong X, Ng C, Moriceau G, et al. RAF inhibitor resistance is mediated by dimerization of aberrantly spliced BRAF(V600E). Nature. 2011;480(7377):387-90. doi: 10.1038/nature10662. PubMed PMID: 22113612; PubMed Central PMCID: PMC3266695.
180. Davies H, Bignell GR, Cox C, Stephens P, Edkins S, Clegg S, et al. Mutations of the BRAF gene in human cancer. Nature. 2002;417(6892):949-54. doi: 10.1038/nature00766. PubMed PMID: 12068308.
181. Chapman PB, Hauschild A, Robert C, Haanen JB, Ascierto P, Larkin J, et al. Improved survival with vemurafenib in melanoma with BRAF V600E mutation. The New England journal of medicine. 2011;364(26):2507-16. doi: 10.1056/NEJMoa1103782. PubMed PMID: 21639808; PubMed Central PMCID: PMC3549296.
182. Sharma P, Wagner K, Wolchok JD, Allison JP. Novel cancer immunotherapy agents with survival benefit: recent successes and next steps. Nature reviews Cancer. 2011;11(11):805-12. doi: 10.1038/nrc3153. PubMed PMID: 22020206; PubMed Central PMCID: PMC3426440.
183. Solit DB, Rosen N. Towards a Unified Model of RAF Inhibitor Resistance. Cancer discovery. 2014;4(1):27-30. doi: 10.1158/2159-8290.CD-13-0961. PubMed PMID: 24402945.
184. Fisher R, Larkin J. Vemurafenib: a new treatment for BRAF-V600 mutated advanced melanoma. Cancer management and research. 2012;4:243-52. doi: 10.2147/CMAR.S25284. PubMed PMID: 22904646; PubMed Central PMCID: PMC3421463.
185. Wagle N, Emery C, Berger MF, Davis MJ, Sawyer A, Pochanard P, et al. Dissecting therapeutic resistance to RAF inhibition in melanoma by tumor genomic profiling. Journal of clinical oncology : official journal of the American Society of Clinical Oncology. 2011;29(22):3085-96. doi: 10.1200/JCO.2010.33.2312. PubMed PMID: 21383288; PubMed Central PMCID: PMC3157968.
186. Flaherty KT, Robert C, Hersey P, Nathan P, Garbe C, Milhem M, et al. Improved survival with MEK inhibition in BRAF-mutated melanoma. The New England journal of medicine. 2012;367(2):107-14. doi: 10.1056/NEJMoa1203421. PubMed PMID: 22663011.
187. Flaherty KT, Infante JR, Daud A, Gonzalez R, Kefford RF, Sosman J, et al. Combined BRAF and MEK inhibition in melanoma with BRAF V600 mutations. The New England journal of medicine. 2012;367(18):1694-703. doi: 10.1056/NEJMoa1210093. PubMed PMID: 23020132; PubMed Central PMCID: PMCPMC3549295.
188. Long GV, Stroyakovskiy D, Gogas H, Levchenko E, de Braud F, Larkin J, et al. Combined BRAF and MEK inhibition versus BRAF inhibition alone in melanoma. The New England journal of medicine. 2014;371(20):1877-88. doi: 10.1056/NEJMoa1406037. PubMed PMID: 25265492.
189. Wagle N, Van Allen EM, Treacy DJ, Frederick DT, Cooper ZA, Taylor-Weiner A, et al. MAP kinase pathway alterations in BRAF-mutant melanoma patients with

acquired resistance to combined RAF/MEK inhibition. Cancer discovery. 2014;4(1):61-8. doi: 10.1158/2159-8290.CD-13-0631. PubMed PMID: 24265154; PubMed Central PMCID: PMCPMC3947296.
190. Page DB, Postow MA, Callahan MK, Allison JP, Wolchok JD. Immune modulation in cancer with antibodies. Annual review of medicine. 2014;65:185-202. doi: 10.1146/annurev-med-092012-112807. PubMed PMID: 24188664.
191. Ribas A, Wolchok JD. Cancer immunotherapy using checkpoint blockade. Science. 2018;359(6382):1350-5. doi: 10.1126/science.aar4060. PubMed PMID: 29567705.
192. Sharma P, Hu-Lieskovan S, Wargo JA, Ribas A. Primary, Adaptive, and Acquired Resistance to Cancer Immunotherapy. Cell. 2017;168(4):707-23. doi: 10.1016/j.cell.2017.01.017. PubMed PMID: 28187290; PubMed Central PMCID: PMCPMC5391692.
193. Ribas A. Releasing the Brakes on Cancer Immunotherapy. The New England journal of medicine. 2015;373(16):1490-2. doi: 10.1056/NEJMp1510079. PubMed PMID: 26348216.
194. Wolchok JD, Chiarion-Sileni V, Gonzalez R, Rutkowski P, Grob JJ, Cowey CL, et al. Overall Survival with Combined Nivolumab and Ipilimumab in Advanced Melanoma. The New England journal of medicine. 2017;377(14):1345-56. doi: 10.1056/NEJMoa1709684. PubMed PMID: 28889792; PubMed Central PMCID: PMCPMC5706778.
195. Prieto PA, Yang JC, Sherry RM, Hughes MS, Kammula US, White DE, et al. CTLA-4 blockade with ipilimumab: long-term follow-up of 177 patients with metastatic melanoma. Clinical cancer research : an official journal of the American Association for Cancer Research. 2012;18(7):2039-47. doi: 10.1158/1078-0432.CCR-11-1823. PubMed PMID: 22271879; PubMed Central PMCID: PMCPMC3319861.
196. Zaretsky JM, Garcia-Diaz A, Shin DS, Escuin-Ordinas H, Hugo W, Hu-Lieskovan S, et al. Mutations Associated with Acquired Resistance to PD-1 Blockade in Melanoma. The New England journal of medicine. 2016;375(9):819-29. doi: 10.1056/NEJMoa1604958. PubMed PMID: 27433843; PubMed Central PMCID: PMCPMC5007206.
197. Yee C, Thompson JA, Byrd D, Riddell SR, Roche P, Celis E, et al. Adoptive T cell therapy using antigen-specific CD8+ T cell clones for the treatment of patients with metastatic melanoma: in vivo persistence, migration, and antitumor effect of transferred T cells. Proc Natl Acad Sci U S A. 2002;99(25):16168-73. doi: 10.1073/pnas.242600099. PubMed PMID: 12427970; PubMed Central PMCID: PMCPMC138583.
198. Rosenberg SA, Dudley ME. Adoptive cell therapy for the treatment of patients with metastatic melanoma. Curr Opin Immunol. 2009;21(2):233-40. doi: 10.1016/j.coi.2009.03.002. PubMed PMID: 19304471; PubMed Central PMCID: PMCPMC3459355.
199. Quail DF, Joyce JA. Microenvironmental regulation of tumor progression and metastasis. Nature medicine. 2013;19(11):1423-37. doi: 10.1038/nm.3394. PubMed PMID: 24202395.

200. Khalil DN, Smith EL, Brentjens RJ, Wolchok JD. The future of cancer treatment: immunomodulation, CARs and combination immunotherapy. Nat Rev Clin Oncol. 2016;13(6):394. doi: 10.1038/nrclinonc.2016.65. PubMed PMID: 27118494; PubMed Central PMCID: PMCPMC5558237.
201. Kudchadkar RR, Gonzalez R, Lewis K. New targeted therapies in melanoma. Cancer control : journal of the Moffitt Cancer Center. 2013;20(4):282-8. PubMed PMID: 24077404.
202. Laga AC, Murphy GF. Cellular heterogeneity in vertical growth phase melanoma. Arch Pathol Lab Med. 2010;134(12):1750-7. doi: 10.1043/2009-0394-RAR.1. PubMed PMID: 21128771.
203. Wang JX, Fukunaga-Kalabis M, Herlyn M. Crosstalk in skin: melanocytes, keratinocytes, stem cells, and melanoma. J Cell Commun Signal. 2016;10(3):191-6. doi: 10.1007/s12079-016-0349-3. PubMed PMID: 27553358; PubMed Central PMCID: PMCPMC5055506.
204. Hay ED. An overview of epithelio-mesenchymal transformation. Acta Anat (Basel). 1995;154(1):8-20. PubMed PMID: 8714286.
205. Brabletz T, Kalluri R, Nieto MA, Weinberg RA. EMT in cancer. Nature reviews Cancer. 2018;18(2):128-34. doi: 10.1038/nrc.2017.118. PubMed PMID: 29326430.
206. Kalluri R, Weinberg RA. The basics of epithelial-mesenchymal transition. J Clin Invest. 2009;119(6):1420-8. doi: 10.1172/JCI39104. PubMed PMID: 19487818; PubMed Central PMCID: PMCPMC2689101.
207. Jolly MK, Boareto M, Huang B, Jia D, Lu M, Ben-Jacob E, et al. Implications of the Hybrid Epithelial/Mesenchymal Phenotype in Metastasis. Front Oncol. 2015;5:155. doi: 10.3389/fonc.2015.00155. PubMed PMID: 26258068; PubMed Central PMCID: PMCPMC4507461.
208. Beerling E, Seinstra D, de Wit E, Kester L, van der Velden D, Maynard C, et al. Plasticity between Epithelial and Mesenchymal States Unlinks EMT from Metastasis-Enhancing Stem Cell Capacity. Cell reports. 2016;14(10):2281-8. doi: 10.1016/j.celrep.2016.02.034. PubMed PMID: 26947068; PubMed Central PMCID: PMCPMC4802222.
209. Barrallo-Gimeno A, Nieto MA. The Snail genes as inducers of cell movement and survival: implications in development and cancer. Development. 2005;132(14):3151-61. doi: 10.1242/dev.01907. PubMed PMID: 15983400.
210. Yang J, Mani SA, Donaher JL, Ramaswamy S, Itzykson RA, Come C, et al. Twist, a master regulator of morphogenesis, plays an essential role in tumor metastasis. Cell. 2004;117(7):927-39. doi: 10.1016/j.cell.2004.06.006. PubMed PMID: 15210113.
211. Korpal M, Lee ES, Hu G, Kang Y. The miR-200 family inhibits epithelial-mesenchymal transition and cancer cell migration by direct targeting of E-cadherin transcriptional repressors ZEB1 and ZEB2. J Biol Chem. 2008;283(22):14910-4. doi: 10.1074/jbc.C800074200. PubMed PMID: 18411277; PubMed Central PMCID: PMCPMC3258899.
212. Micalizzi DS, Farabaugh SM, Ford HL. Epithelial-mesenchymal transition in cancer: parallels between normal development and tumor progression. J Mammary Gland Biol Neoplasia. 2010;15(2):117-34. doi: 10.1007/s10911-010-9178-9. PubMed PMID: 20490631; PubMed Central PMCID: PMCPMC2886089.

213. Wang J, Wei Q, Wang X, Tang S, Liu H, Zhang F, et al. Transition to resistance: An unexpected role of the EMT in cancer chemoresistance. Genes Dis. 2016;3(1):3-6. doi: 10.1016/j.gendis.2016.01.002. PubMed PMID: 28491932; PubMed Central PMCID: PMCPMC5421998.
214. Fischer KR, Durrans A, Lee S, Sheng J, Li F, Wong ST, et al. Epithelial-to-mesenchymal transition is not required for lung metastasis but contributes to chemoresistance. Nature. 2015;527(7579):472-6. doi: 10.1038/nature15748. PubMed PMID: 26560033; PubMed Central PMCID: PMCPMC4662610.
215. Zheng X, Carstens JL, Kim J, Scheible M, Kaye J, Sugimoto H, et al. Epithelial-to-mesenchymal transition is dispensable for metastasis but induces chemoresistance in pancreatic cancer. Nature. 2015;527(7579):525-30. doi: 10.1038/nature16064. PubMed PMID: 26560028; PubMed Central PMCID: PMCPMC4849281.
216. Krebs AM, Mitschke J, Lasierra Losada M, Schmalhofer O, Boerries M, Busch H, et al. The EMT-activator Zeb1 is a key factor for cell plasticity and promotes metastasis in pancreatic cancer. Nature cell biology. 2017;19(5):518-29. doi: 10.1038/ncb3513. PubMed PMID: 28414315.
217. Tran HD, Luitel K, Kim M, Zhang K, Longmore GD, Tran DD. Transient SNAIL1 expression is necessary for metastatic competence in breast cancer. Cancer research. 2014;74(21):6330-40. doi: 10.1158/0008-5472.CAN-14-0923. PubMed PMID: 25164016; PubMed Central PMCID: PMCPMC4925010.
218. Lapidot T, Sirard C, Vormoor J, Murdoch B, Hoang T, Caceres-Cortes J, et al. A cell initiating human acute myeloid leukaemia after transplantation into SCID mice. Nature. 1994;367(6464):645-8. doi: 10.1038/367645a0. PubMed PMID: 7509044.
219. Pardal R, Clarke MF, Morrison SJ. Applying the principles of stem-cell biology to cancer. Nature reviews Cancer. 2003;3(12):895-902. doi: 10.1038/nrc1232. PubMed PMID: 14737120.
220. Clevers H. The cancer stem cell: premises, promises and challenges. Nature medicine. 2011;17(3):313-9. doi: 10.1038/nm.2304. PubMed PMID: 21386835.
221. Fang D, Nguyen TK, Leishear K, Finko R, Kulp AN, Hotz S, et al. A tumorigenic subpopulation with stem cell properties in melanomas. Cancer research. 2005;65(20):9328-37. doi: 10.1158/0008-5472.CAN-05-1343. PubMed PMID: 16230395.
222. Schatton T, Murphy GF, Frank NY, Yamaura K, Waaga-Gasser AM, Gasser M, et al. Identification of cells initiating human melanomas. Nature. 2008;451(7176):345-9. doi: 10.1038/nature06489. PubMed PMID: 18202660; PubMed Central PMCID: PMCPMC3660705.
223. Schatton T, Frank MH. Cancer stem cells and human malignant melanoma. Pigment cell & melanoma research. 2008;21(1):39-55. doi: 10.1111/j.1755-148X.2007.00427.x. PubMed PMID: 18353142; PubMed Central PMCID: PMCPMC2885609.
224. Zabierowski SE, Herlyn M. Melanoma stem cells: the dark seed of melanoma. Journal of clinical oncology : official journal of the American Society of Clinical Oncology. 2008;26(17):2890-4. doi: 10.1200/JCO.2007.15.5465. PubMed PMID: 18539969.

225. Frank NY, Pendse SS, Lapchak PH, Margaryan A, Shlain D, Doeing C, et al. Regulation of progenitor cell fusion by ABCB5 P-glycoprotein, a novel human ATP-binding cassette transporter. J Biol Chem. 2003;278(47):47156-65. doi: 10.1074/jbc.M308700200. PubMed PMID: 12960149.
226. Boiko AD, Razorenova OV, van de Rijn M, Swetter SM, Johnson DL, Ly DP, et al. Human melanoma-initiating cells express neural crest nerve growth factor receptor CD271. Nature. 2010;466(7302):133-7. doi: 10.1038/nature09161. PubMed PMID: 20596026; PubMed Central PMCID: PMCPMC2898751.
227. Quintana E, Shackleton M, Sabel MS, Fullen DR, Johnson TM, Morrison SJ. Efficient tumour formation by single human melanoma cells. Nature. 2008;456(7222):593-8. doi: 10.1038/nature07567. PubMed PMID: 19052619; PubMed Central PMCID: PMC2597380.
228. Quintana E, Shackleton M, Foster HR, Fullen DR, Sabel MS, Johnson TM, et al. Phenotypic heterogeneity among tumorigenic melanoma cells from patients that is reversible and not hierarchically organized. Cancer cell. 2010;18(5):510-23. doi: 10.1016/j.ccr.2010.10.012. PubMed PMID: 21075313; PubMed Central PMCID: PMC3031091.
229. Giese A, Bjerkvig R, Berens ME, Westphal M. Cost of migration: invasion of malignant gliomas and implications for treatment. Journal of clinical oncology : official journal of the American Society of Clinical Oncology. 2003;21(8):1624-36. doi: 10.1200/JCO.2003.05.063. PubMed PMID: 12697889.
230. Baylin SB, Ohm JE. Epigenetic gene silencing in cancer - a mechanism for early oncogenic pathway addiction? Nature reviews Cancer. 2006;6(2):107-16. doi: 10.1038/nrc1799. PubMed PMID: 16491070.
231. Weeraratna AT, Jiang Y, Hostetter G, Rosenblatt K, Duray P, Bittner M, et al. Wnt5a signaling directly affects cell motility and invasion of metastatic melanoma. Cancer cell. 2002;1(3):279-88. PubMed PMID: 12086864.
232. Sadeghi RS, Kulej K, Kathayat RS, Garcia BA, Dickinson BC, Brady DC, et al. Wnt5a signaling induced phosphorylation increases APT1 activity and promotes melanoma metastatic behavior. Elife. 2018;7. doi: 10.7554/eLife.34362. PubMed PMID: 29648538; PubMed Central PMCID: PMCPMC5919757.
233. Anastas JN, Kulikauskas RM, Tamir T, Rizos H, Long GV, von Euw EM, et al. WNT5A enhances resistance of melanoma cells to targeted BRAF inhibitors. J Clin Invest. 2014;124(7):2877-90. doi: 10.1172/JCI70156. PubMed PMID: 24865425; PubMed Central PMCID: PMCPMC4071371.
234. Seftor EA, Brown KM, Chin L, Kirschmann DA, Wheaton WW, Protopopov A, et al. Epigenetic transdifferentiation of normal melanocytes by a metastatic melanoma microenvironment. Cancer research. 2005;65(22):10164-9. doi: 10.1158/0008-5472.CAN-05-2497. PubMed PMID: 16288000.
235. Carreira S, Goodall J, Aksan I, La Rocca SA, Galibert MD, Denat L, et al. Mitf cooperates with Rb1 and activates p21Cip1 expression to regulate cell cycle progression. Nature. 2005;433(7027):764-9. doi: 10.1038/nature03269. PubMed PMID: 15716956.
236. Loercher AE, Tank EM, Delston RB, Harbour JW. MITF links differentiation with cell cycle arrest in melanocytes by transcriptional activation of INK4A. J Cell

Biol. 2005;168(1):35-40. doi: 10.1083/jcb.200410115. PubMed PMID: 15623583; PubMed Central PMCID: PMCPMC2171666.
237. Carreira S, Goodall J, Denat L, Rodriguez M, Nuciforo P, Hoek KS, et al. Mitf regulation of Dia1 controls melanoma proliferation and invasiveness. Genes & development. 2006;20(24):3426-39. doi: 10.1101/gad.406406. PubMed PMID: 17182868; PubMed Central PMCID: PMCPMC1698449.
238. Wellbrock C, Marais R. Elevated expression of MITF counteracts B-RAF-stimulated melanocyte and melanoma cell proliferation. J Cell Biol. 2005;170(5):703-8. doi: 10.1083/jcb.200505059. PubMed PMID: 16129781; PubMed Central PMCID: PMCPMC2171350.
239. Garraway LA, Widlund HR, Rubin MA, Getz G, Berger AJ, Ramaswamy S, et al. Integrative genomic analyses identify MITF as a lineage survival oncogene amplified in malignant melanoma. Nature. 2005;436(7047):117-22. doi: 10.1038/nature03664. PubMed PMID: 16001072.
240. McGill GG, Horstmann M, Widlund HR, Du J, Motyckova G, Nishimura EK, et al. Bcl2 regulation by the melanocyte master regulator Mitf modulates lineage survival and melanoma cell viability. Cell. 2002;109(6):707-18. PubMed PMID: 12086670.
241. Widlund HR, Horstmann MA, Price ER, Cui J, Lessnick SL, Wu M, et al. Beta-catenin-induced melanoma growth requires the downstream target Microphthalmia-associated transcription factor. J Cell Biol. 2002;158(6):1079-87. doi: 10.1083/jcb.200202049. PubMed PMID: 12235125; PubMed Central PMCID: PMCPMC2173224.
242. Du J, Widlund HR, Horstmann MA, Ramaswamy S, Ross K, Huber WE, et al. Critical role of CDK2 for melanoma growth linked to its melanocyte-specific transcriptional regulation by MITF. Cancer cell. 2004;6(6):565-76. doi: 10.1016/j.ccr.2004.10.014. PubMed PMID: 15607961.
243. Muller J, Krijgsman O, Tsoi J, Robert L, Hugo W, Song C, et al. Low MITF/AXL ratio predicts early resistance to multiple targeted drugs in melanoma. Nat Commun. 2014;5:5712. doi: 10.1038/ncomms6712. PubMed PMID: 25502142; PubMed Central PMCID: PMCPMC4428333.
244. Fane ME, Chhabra Y, Smith AG, Sturm RA. BRN2, a POUerful driver of melanoma phenotype switching and metastasis. Pigment cell & melanoma research. 2018. doi: 10.1111/pcmr.12710. PubMed PMID: 29781575.
245. Hoek KS, Schlegel NC, Brafford P, Sucker A, Ugurel S, Kumar R, et al. Metastatic potential of melanomas defined by specific gene expression profiles with no BRAF signature. Pigment cell research / sponsored by the European Society for Pigment Cell Research and the International Pigment Cell Society. 2006;19(4):290-302. doi: 10.1111/j.1600-0749.2006.00322.x. PubMed PMID: 16827748.
246. Tap WD, Gong KW, Dering J, Tseng Y, Ginther C, Pauletti G, et al. Pharmacodynamic characterization of the efficacy signals due to selective BRAF inhibition with PLX4032 in malignant melanoma. Neoplasia. 2010;12(8):637-49. PubMed PMID: 20689758; PubMed Central PMCID: PMC2915408.
247. Eichhoff OM, Zipser MC, Xu M, Weeraratna AT, Mihic D, Dummer R, et al. The immunohistochemistry of invasive and proliferative phenotype switching in melanoma: a case report. Melanoma research. 2010;20(4):349-55. doi:

10.1097/CMR.0b013e32833bd89e. PubMed PMID: 20526217; PubMed Central PMCID: PMC2901773.
248. Hoek KS, Eichhoff OM, Schlegel NC, Dobbeling U, Kobert N, Schaerer L, et al. In vivo switching of human melanoma cells between proliferative and invasive states. Cancer research. 2008;68(3):650-6. doi: 10.1158/0008-5472.CAN-07-2491. PubMed PMID: 18245463.
249. Falletta P, Sanchez-Del-Campo L, Chauhan J, Effern M, Kenyon A, Kershaw CJ, et al. Translation reprogramming is an evolutionarily conserved driver of phenotypic plasticity and therapeutic resistance in melanoma. Genes & development. 2017;31(1):18-33. doi: 10.1101/gad.290940.116. PubMed PMID: 28096186; PubMed Central PMCID: PMCPMC5287109.
250. Pinner S, Jordan P, Sharrock K, Bazley L, Collinson L, Marais R, et al. Intravital imaging reveals transient changes in pigment production and Brn2 expression during metastatic melanoma dissemination. Cancer research. 2009;69(20):7969-77. doi: 10.1158/0008-5472.CAN-09-0781. PubMed PMID: 19826052; PubMed Central PMCID: PMC2763120.
251. Webster MR, Kugel CH, 3rd, Weeraratna AT. The Wnts of change: How Wnts regulate phenotype switching in melanoma. Biochim Biophys Acta. 2015;1856(2):244-51. doi: 10.1016/j.bbcan.2015.10.002. PubMed PMID: 26546268; PubMed Central PMCID: PMCPMC4668201.
252. Roesch A, Paschen A, Landsberg J, Helfrich I, Becker JC, Schadendorf D. Phenotypic tumour cell plasticity as a resistance mechanism and therapeutic target in melanoma. Eur J Cancer. 2016;59:109-12. doi: 10.1016/j.ejca.2016.02.023. PubMed PMID: 27023049.
253. Slaughter DP, Southwick HW, Smejkal W. Field cancerization in oral stratified squamous epithelium; clinical implications of multicentric origin. Cancer. 1953;6(5):963-8. PubMed PMID: 13094644.
254. Schwitalla S, Fingerle AA, Cammareri P, Nebelsiek T, Goktuna SI, Ziegler PK, et al. Intestinal tumorigenesis initiated by dedifferentiation and acquisition of stem-cell-like properties. Cell. 2013;152(1-2):25-38. doi: 10.1016/j.cell.2012.12.012. PubMed PMID: 23273993.
255. Liao D, Corle C, Seagroves TN, Johnson RS. Hypoxia-inducible factor-1alpha is a key regulator of metastasis in a transgenic model of cancer initiation and progression. Cancer research. 2007;67(2):563-72. doi: 10.1158/0008-5472.CAN-06-2701. PubMed PMID: 17234764.
256. Sell S. Cellular origin of cancer: dedifferentiation or stem cell maturation arrest? Environmental health perspectives. 1993;101 Suppl 5:15-26. doi: 10.1289/ehp.93101s515. PubMed PMID: 7516873; PubMed Central PMCID: PMCPMC1519468.
257. Rygaard J, Povlsen CO. Heterotransplantation of a human malignant tumour to "Nude" mice. Acta Pathol Microbiol Scand. 1969;77(4):758-60. PubMed PMID: 5383844.
258. Hidalgo M, Amant F, Biankin AV, Budinska E, Byrne AT, Caldas C, et al. Patient-derived xenograft models: an emerging platform for translational cancer research. Cancer discovery. 2014;4(9):998-1013. doi: 10.1158/2159-8290.CD-14-0001. PubMed PMID: 25185190; PubMed Central PMCID: PMCPMC4167608.

259. Einarsdottir BO, Bagge RO, Bhadury J, Jespersen H, Mattsson J, Nilsson LM, et al. Melanoma patient-derived xenografts accurately model the disease and develop fast enough to guide treatment decisions. Oncotarget. 2014;5(20):9609-18. doi: 10.18632/oncotarget.2445. PubMed PMID: 25228592; PubMed Central PMCID: PMCPMC4259423.
260. Krepler C, Xiao M, Sproesser K, Brafford PA, Shannan B, Beqiri M, et al. Personalized Preclinical Trials in BRAF Inhibitor-Resistant Patient-Derived Xenograft Models Identify Second-Line Combination Therapies. Clinical cancer research : an official journal of the American Association for Cancer Research. 2016;22(7):1592-602. doi: 10.1158/1078-0432.CCR-15-1762. PubMed PMID: 26673799; PubMed Central PMCID: PMCPMC4818716.
261. Garman B, Anastopoulos IN, Krepler C, Brafford P, Sproesser K, Jiang Y, et al. Genetic and Genomic Characterization of 462 Melanoma Patient-Derived Xenografts, Tumor Biopsies, and Cell Lines. Cell reports. 2017;21(7):1936-52. doi: 10.1016/j.celrep.2017.10.052. PubMed PMID: 29141224; PubMed Central PMCID: PMCPMC5709812.
262. Krepler C, Sproesser K, Brafford P, Beqiri M, Garman B, Xiao M, et al. A Comprehensive Patient-Derived Xenograft Collection Representing the Heterogeneity of Melanoma. Cell reports. 2017;21(7):1953-67. doi: 10.1016/j.celrep.2017.10.021. PubMed PMID: 29141225; PubMed Central PMCID: PMCPMC5726788.
263. Gupta PB, Kuperwasser C, Brunet JP, Ramaswamy S, Kuo WL, Gray JW, et al. The melanocyte differentiation program predisposes to metastasis after neoplastic transformation. Nature genetics. 2005;37(10):1047-54. Epub 2005/09/06. doi: 10.1038/ng1634. PubMed PMID: 16142232; PubMed Central PMCID: PMC1694635.
264. Chudnovsky Y, Adams AE, Robbins PB, Lin Q, Khavari PA. Use of human tissue to assess the oncogenic activity of melanoma-associated mutations. Nature genetics. 2005;37(7):745-9. Epub 2005/06/14. doi: 10.1038/ng1586. PubMed PMID: 15951821; PubMed Central PMCID: PMC3063773.
265. Michaloglou C, Vredeveld LC, Soengas MS, Denoyelle C, Kuilman T, van der Horst CM, et al. BRAFE600-associated senescence-like cell cycle arrest of human naevi. Nature. 2005;436(7051):720-4. doi: 10.1038/nature03890. PubMed PMID: 16079850.
266. Yu H, McDaid R, Lee J, Possik P, Li L, Kumar SM, et al. The role of BRAF mutation and p53 inactivation during transformation of a subpopulation of primary human melanocytes. The American journal of pathology. 2009;174(6):2367-77. doi: 10.2353/ajpath.2009.081057. PubMed PMID: 19389934; PubMed Central PMCID: PMC2684200.
267. White RM, Sessa A, Burke C, Bowman T, LeBlanc J, Ceol C, et al. Transparent adult zebrafish as a tool for in vivo transplantation analysis. Cell Stem Cell. 2008;2(2):183-9. doi: 10.1016/j.stem.2007.11.002. PubMed PMID: 18371439; PubMed Central PMCID: PMCPMC2292119.
268. Heilmann S, Ratnakumar K, Langdon E, Kansler E, Kim I, Campbell NR, et al. A Quantitative System for Studying Metastasis Using Transparent Zebrafish. Cancer research. 2015;75(20):4272-82. doi: 10.1158/0008-5472.CAN-14-3319. PubMed PMID: 26282170; PubMed Central PMCID: PMCPMC4609292.

269. Ley RD. Animal models of ultraviolet radiation (UVR)-induced cutaneous melanoma. Front Biosci. 2002;7:d1531-4. PubMed PMID: 12045011.
270. Zeng Z, Richardson J, Verduzco D, Mitchell DL, Patton EE. Zebrafish have a competent p53-dependent nucleotide excision repair pathway to resolve ultraviolet B-induced DNA damage in the skin. Zebrafish. 2009;6(4):405-15. doi: 10.1089/zeb.2009.0611. PubMed PMID: 20047468; PubMed Central PMCID: PMCPMC2804931.
271. Bardeesy N, Wong KK, DePinho RA, Chin L. Animal models of melanoma: recent advances and future prospects. Advances in cancer research. 2000;79:123-56. PubMed PMID: 10818679.
272. Klein-Szanto AJ, Silvers WK, Mintz B. Ultraviolet radiation-induced malignant skin melanoma in melanoma-susceptible transgenic mice. Cancer research. 1994;54(17):4569-72. PubMed PMID: 8062242.
273. Broome Powell M, Gause PR, Hyman P, Gregus J, Lluria-Prevatt M, Nagle R, et al. Induction of melanoma in TPras transgenic mice. Carcinogenesis. 1999;20(9):1747-53. PubMed PMID: 10469620.
274. Husain Z, Pathak MA, Flotte T, Wick MM. Role of ultraviolet radiation in the induction of melanocytic tumors in hairless mice following 7,12-dimethylbenz(a)anthracene application and ultraviolet irradiation. Cancer research. 1991;51(18):4964-70. PubMed PMID: 1909931.
275. Wajapeyee N, Serra RW, Zhu X, Mahalingam M, Green MR. Oncogenic BRAF induces senescence and apoptosis through pathways mediated by the secreted protein IGFBP7. Cell. 2008;132(3):363-74. doi: 10.1016/j.cell.2007.12.032. PubMed PMID: 18267069; PubMed Central PMCID: PMC2266096.
276. Dankort D, Curley DP, Cartlidge RA, Nelson B, Karnezis AN, Damsky WE, Jr., et al. Braf(V600E) cooperates with Pten loss to induce metastatic melanoma. Nature genetics. 2009;41(5):544-52. doi: 10.1038/ng.356. PubMed PMID: 19282848; PubMed Central PMCID: PMC2705918.
277. Dhomen N, Reis-Filho JS, da Rocha Dias S, Hayward R, Savage K, Delmas V, et al. Oncogenic Braf induces melanocyte senescence and melanoma in mice. Cancer cell. 2009;15(4):294-303. doi: 10.1016/j.ccr.2009.02.022. PubMed PMID: 19345328.
278. Bardeesy N, Bastian BC, Hezel A, Pinkel D, DePinho RA, Chin L. Dual inactivation of RB and p53 pathways in RAS-induced melanomas. Mol Cell Biol. 2001;21(6):2144-53. doi: 10.1128/MCB.21.6.2144-2153.2001. PubMed PMID: 11238948; PubMed Central PMCID: PMCPMC86838.
279. Patton EE, Widlund HR, Kutok JL, Kopani KR, Amatruda JF, Murphey RD, et al. BRAF mutations are sufficient to promote nevi formation and cooperate with p53 in the genesis of melanoma. Curr Biol. 2005;15(3):249-54. doi: 10.1016/j.cub.2005.01.031. PubMed PMID: 15694309.
280. Marumoto T, Tashiro A, Friedmann-Morvinski D, Scadeng M, Soda Y, Gage FH, et al. Development of a novel mouse glioma model using lentiviral vectors. Nature medicine. 2009;15(1):110-6. doi: 10.1038/nm.1863. PubMed PMID: 19122659; PubMed Central PMCID: PMCPMC2671237.

281. Mione MC, Trede NS. The zebrafish as a model for cancer. Dis Model Mech. 2010;3(9-10):517-23. doi: 10.1242/dmm.004747. PubMed PMID: 20354112; PubMed Central PMCID: PMCPMC2931530.
282. White R, Rose K, Zon L. Zebrafish cancer: the state of the art and the path forward. Nature reviews Cancer. 2013;13(9):624-36. Epub 2013/08/24. doi: 10.1038/nrc3589. PubMed PMID: 23969693.
283. Fior R, Povoa V, Mendes RV, Carvalho T, Gomes A, Figueiredo N, et al. Single-cell functional and chemosensitive profiling of combinatorial colorectal therapy in zebrafish xenografts. Proc Natl Acad Sci U S A. 2017;114(39):E8234-E43. doi: 10.1073/pnas.1618389114. PubMed PMID: 28835536; PubMed Central PMCID: PMCPMC5625889.
284. Siolas D, Hannon GJ. Patient-derived tumor xenografts: transforming clinical samples into mouse models. Cancer research. 2013;73(17):5315-9. doi: 10.1158/0008-5472.CAN-13-1069. PubMed PMID: 23733750; PubMed Central PMCID: PMCPMC3766500.
285. Tang Q, Moore JC, Ignatius MS, Tenente IM, Hayes MN, Garcia EG, et al. Imaging tumour cell heterogeneity following cell transplantation into optically clear immune-deficient zebrafish. Nat Commun. 2016;7:10358. doi: 10.1038/ncomms10358. PubMed PMID: 26790525; PubMed Central PMCID: PMCPMC4735845.
286. Zeng A, Ye T, Cao D, Huang X, Yang Y, Chen X, et al. Identify a Blood-Brain Barrier Penetrating Drug-TNB using Zebrafish Orthotopic Glioblastoma Xenograft Model. Scientific reports. 2017;7(1):14372. doi: 10.1038/s41598-017-14766-2. PubMed PMID: 29085081; PubMed Central PMCID: PMCPMC5662771.
287. Blackburn JS, Liu S, Langenau DM. Quantifying the frequency of tumor-propagating cells using limiting dilution cell transplantation in syngeneic zebrafish. Journal of visualized experiments : JoVE. 2011;(53):e2790. doi: 10.3791/2790. PubMed PMID: 21775966; PubMed Central PMCID: PMCPMC3196193.
288. Wong TK, Neumann E. Electric field mediated gene transfer. Biochemical and biophysical research communications. 1982;107(2):584-7. PubMed PMID: 7126230.
289. Neumann E, Schaefer-Ridder M, Wang Y, Hofschneider PH. Gene transfer into mouse lyoma cells by electroporation in high electric fields. The EMBO journal. 1982;1(7):841-5. PubMed PMID: 6329708; PubMed Central PMCID: PMCPMC553119.
290. Hoegler KJ, Distel M, Koster RW, Horne JH. Targeting olfactory bulb neurons using combined in vivo electroporation and Gal4-based enhancer trap zebrafish lines. Journal of visualized experiments : JoVE. 2011;(54). doi: 10.3791/2964. PubMed PMID: 21860381; PubMed Central PMCID: PMCPMC3217634.
291. Munch J, Gonzalez-Rajal A, de la Pompa JL. Notch regulates blastema proliferation and prevents differentiation during adult zebrafish fin regeneration. Development. 2013;140(7):1402-11. doi: 10.1242/dev.087346. PubMed PMID: 23344707.
292. Rambabu KM, Rao SH, Rao NM. Efficient expression of transgenes in adult zebrafish by electroporation. BMC biotechnology. 2005;5:29. doi: 10.1186/1472-6750-5-29. PubMed PMID: 16221312; PubMed Central PMCID: PMCPMC1266056.

293. Thummel R, Bailey TJ, Hyde DR. In vivo electroporation of morpholinos into the adult zebrafish retina. Journal of visualized experiments : JoVE. 2011;(58):e3603. doi: 10.3791/3603. PubMed PMID: 22231802; PubMed Central PMCID: PMCPMC3369653.
294. Maresch R, Mueller S, Veltkamp C, Ollinger R, Friedrich M, Heid I, et al. Multiplexed pancreatic genome engineering and cancer induction by transfection-based CRISPR/Cas9 delivery in mice. Nat Commun. 2016;7:10770. doi: 10.1038/ncomms10770. PubMed PMID: 26916719; PubMed Central PMCID: PMCPMC4773438.
295. Nomura T, Nishimura Y, Gotoh H, Ono K. Rapid and efficient gene delivery into the adult mouse brain via focal electroporation. Scientific reports. 2016;6:29817. doi: 10.1038/srep29817. PubMed PMID: 27430903; PubMed Central PMCID: PMCPMC4949460.
296. Swartz M, Eberhart J, Mastick GS, Krull CE. Sparking new frontiers: using in vivo electroporation for genetic manipulations. Dev Biol. 2001;233(1):13-21. doi: 10.1006/dbio.2001.0181. PubMed PMID: 11319854.
297. Yarmush ML, Golberg A, Sersa G, Kotnik T, Miklavcic D. Electroporation-based technologies for medicine: principles, applications, and challenges. Annual review of biomedical engineering. 2014;16:295-320. doi: 10.1146/annurev-bioeng-071813-104622. PubMed PMID: 24905876.
298. Jung S, Choi HJ, Park HK, Jo W, Jang S, Ryu JE, et al. Electroporation markedly improves Sleeping Beauty transposon-induced tumorigenesis in mice. Cancer Gene Ther. 2014;21(8):333-9. doi: 10.1038/cgt.2014.33. PubMed PMID: 24992966.
299. Park JS, Lim KM, Park SG, Jung SY, Choi HJ, Lee DH, et al. Pancreatic cancer induced by in vivo electroporation-enhanced sleeping beauty transposon gene delivery system in mouse. Pancreas. 2014;43(4):614-8. doi: 10.1097/MPA.0000000000000102. PubMed PMID: 24713671.
300. Tchieu J, Zimmer B, Fattahi F, Amin S, Zeltner N, Chen S, et al. A Modular Platform for Differentiation of Human PSCs into All Major Ectodermal Lineages. Cell Stem Cell. 2017;21(3):399-410 e7. doi: 10.1016/j.stem.2017.08.015. PubMed PMID: 28886367; PubMed Central PMCID: PMCPMC5737635.
301. Chambers SM, Qi Y, Mica Y, Lee G, Zhang XJ, Niu L, et al. Combined small-molecule inhibition accelerates developmental timing and converts human pluripotent stem cells into nociceptors. Nature biotechnology. 2012;30(7):715-20. doi: 10.1038/nbt.2249. PubMed PMID: 22750882; PubMed Central PMCID: PMCPMC3516136.
302. Lee G, Kim H, Elkabetz Y, Al Shamy G, Panagiotakos G, Barberi T, et al. Isolation and directed differentiation of neural crest stem cells derived from human embryonic stem cells. Nature biotechnology. 2007;25(12):1468-75. doi: 10.1038/nbt1365. PubMed PMID: 18037878.
303. Gaspard N, Vanderhaeghen P. Mechanisms of neural specification from embryonic stem cells. Curr Opin Neurobiol. 2010;20(1):37-43. doi: 10.1016/j.conb.2009.12.001. PubMed PMID: 20080043.
304. Callahan SJ, Mica Y, Studer L. Feeder-free Derivation of Melanocytes from Human Pluripotent Stem Cells. Journal of visualized experiments : JoVE.

2016;(109):e53806. doi: 10.3791/53806. PubMed PMID: 26967464; PubMed Central PMCID: PMCPMC4828213.
305. Kriks S, Shim JW, Piao J, Ganat YM, Wakeman DR, Xie Z, et al. Dopamine neurons derived from human ES cells efficiently engraft in animal models of Parkinson's disease. Nature. 2011;480(7378):547-51. doi: 10.1038/nature10648. PubMed PMID: 22056989; PubMed Central PMCID: PMCPMC3245796.
306. Steinbeck JA, Choi SJ, Mrejeru A, Ganat Y, Deisseroth K, Sulzer D, et al. Optogenetics enables functional analysis of human embryonic stem cell-derived grafts in a Parkinson's disease model. Nature biotechnology. 2015;33(2):204-9. doi: 10.1038/nbt.3124. PubMed PMID: 25580598; PubMed Central PMCID: PMCPMC5117952.
307. Barker RA, Parmar M, Studer L, Takahashi J. Human Trials of Stem Cell-Derived Dopamine Neurons for Parkinson's Disease: Dawn of a New Era. Cell Stem Cell. 2017;21(5):569-73. doi: 10.1016/j.stem.2017.09.014. PubMed PMID: 29100010.
308. Barker RA, Studer L, Cattaneo E, Takahashi J, consortium GFP. G-Force PD: a global initiative in coordinating stem cell-based dopamine treatments for Parkinson's disease. NPJ Parkinsons Dis. 2015;1:15017. doi: 10.1038/npjparkd.2015.17. PubMed PMID: 28725685; PubMed Central PMCID: PMCPMC5516551.
309. Takahashi K, Yamanaka S. Induction of pluripotent stem cells from mouse embryonic and adult fibroblast cultures by defined factors. Cell. 2006;126(4):663-76. doi: 10.1016/j.cell.2006.07.024. PubMed PMID: 16904174.
310. Takahashi K, Tanabe K, Ohnuki M, Narita M, Ichisaka T, Tomoda K, et al. Induction of pluripotent stem cells from adult human fibroblasts by defined factors. Cell. 2007;131(5):861-72. doi: 10.1016/j.cell.2007.11.019. PubMed PMID: 18035408.
311. Crespo M, Vilar E, Tsai SY, Chang K, Amin S, Srinivasan T, et al. Colonic organoids derived from human induced pluripotent stem cells for modeling colorectal cancer and drug testing. Nature medicine. 2017;23(7):878-84. doi: 10.1038/nm.4355. PubMed PMID: 28628110; PubMed Central PMCID: PMCPMC6055224.
312. Gingold J, Zhou R, Lemischka IR, Lee DF. Modeling Cancer with Pluripotent Stem Cells. Trends Cancer. 2016;2(9):485-94. doi: 10.1016/j.trecan.2016.07.007. PubMed PMID: 27722205; PubMed Central PMCID: PMCPMC5050918.
313. Huang L, Holtzinger A, Jagan I, BeGora M, Lohse I, Ngai N, et al. Ductal pancreatic cancer modeling and drug screening using human pluripotent stem cell- and patient-derived tumor organoids. Nature medicine. 2015;21(11):1364-71. doi: 10.1038/nm.3973. PubMed PMID: 26501191; PubMed Central PMCID: PMCPMC4753163.
314. Kim H, Schaniel C. Modeling Hematological Diseases and Cancer With Patient-Specific Induced Pluripotent Stem Cells. Front Immunol. 2018;9:2243. doi: 10.3389/fimmu.2018.02243. PubMed PMID: 30323816; PubMed Central PMCID: PMCPMC6172418.
315. Lee DF, Su J, Kim HS, Chang B, Papatsenko D, Zhao R, et al. Modeling familial cancer with induced pluripotent stem cells. Cell. 2015;161(2):240-54. doi:

10.1016/j.cell.2015.02.045. PubMed PMID: 25860607; PubMed Central PMCID: PMCPMC4397979.
316. Marin Navarro A, Susanto E, Falk A, Wilhelm M. Modeling cancer using patient-derived induced pluripotent stem cells to understand development of childhood malignancies. Cell Death Discov. 2018;4:7. doi: 10.1038/s41420-017-0009-2. PubMed PMID: 29531804; PubMed Central PMCID: PMCPMC5841293.
317. Zhu D, Kong CSL, Gingold JA, Zhao R, Lee DF. Induced Pluripotent Stem Cells and Induced Pluripotent Cancer Cells in Cancer Disease Modeling. Adv Exp Med Biol. 2018. doi: 10.1007/5584_2018_257. PubMed PMID: 30069853.
318. Duan S, Yuan G, Liu X, Ren R, Li J, Zhang W, et al. PTEN deficiency reprogrammes human neural stem cells towards a glioblastoma stem cell-like phenotype. Nat Commun. 2015;6:10068. doi: 10.1038/ncomms10068. PubMed PMID: 26632666; PubMed Central PMCID: PMCPMC4686761.
319. Mulero-Navarro S, Sevilla A, Roman AC, Lee DF, D'Souza SL, Pardo S, et al. Myeloid Dysregulation in a Human Induced Pluripotent Stem Cell Model of PTPN11-Associated Juvenile Myelomonocytic Leukemia. Cell reports. 2015;13(3):504-15. doi: 10.1016/j.celrep.2015.09.019. PubMed PMID: 26456833; PubMed Central PMCID: PMCPMC4618050.
320. Funato K, Major T, Lewis PW, Allis CD, Tabar V. Use of human embryonic stem cells to model pediatric gliomas with H3.3K27M histone mutation. Science. 2014;346(6216):1529-33. doi: 10.1126/science.1253799. PubMed PMID: 25525250; PubMed Central PMCID: PMCPMC4995593.
321. Nakhleh RE WM, Rocamora A, Swanson PE, Dehner LP. Morphologic diversity in malignant melanomas. Am J Clin Pathol. 1990;93(6):731-40.
322. Egger ME, Callender GG, McMasters KM, Ross MI, Martin RC, 2nd, Edwards MJ, et al. Diversity of stage III melanoma in the era of sentinel lymph node biopsy. Annals of surgical oncology. 2013;20(3):956-63. doi: 10.1245/s10434-012-2701-z. PubMed PMID: 23064795.
323. Albino AP, Lloyd KO, Houghton AN, Oettgen HF, Old LJ. Heterogeneity in surface antigen and glycoprotein expression of cell lines derived from different melanoma metastases of the same patient. Implications for the study of tumor antigens. The Journal of experimental medicine. 1981;154(6):1764-78. PubMed PMID: 6976407; PubMed Central PMCID: PMC2186539.
324. Houghton AN, Real FX, Davis LJ, Cordon-Cardo C, Old LJ. Phenotypic heterogeneity of melanoma. Relation to the differentiation program of melanoma cells. The Journal of experimental medicine. 1987;165(3):812-29. PubMed PMID: 3102678; PubMed Central PMCID: PMC2188299.
325. Thomson TM, Real FX, Murakami S, Cordon-Cardo C, Old LJ, Houghton AN. Differentiation antigens of melanocytes and melanoma: analysis of melanosome and cell surface markers of human pigmented cells with monoclonal antibodies. The Journal of investigative dermatology. 1988;90(4):459-66. Epub 1988/04/01. PubMed PMID: 3280698.
326. Chien AJ, Moore EC, Lonsdorf AS, Kulikauskas RM, Rothberg BG, Berger AJ, et al. Activated Wnt/beta-catenin signaling in melanoma is associated with decreased proliferation in patient tumors and a murine melanoma model. Proc Natl Acad Sci U

S A. 2009;106(4):1193-8. doi: 10.1073/pnas.0811902106. PubMed PMID: 19144919; PubMed Central PMCID: PMC2626610.
327. Chien PKaAJ. The Role of Cellular Differentiation and Cell Fate in Malignant Melanoma. In: Murph M, editor. Research on Melanoma: A Glimpse into Current Directions and Future Trends. http://www.intechopen.com/books/research-on-melanoma-a-glimpse-into-current-directions-and-future-trends/the-role-of-cellular-differentiation-and-cell-fate-in-malignant-melanoma: InTech; 2011. p. 287-308.
328. Friedmann-Morvinski D, Verma IM. Dedifferentiation and reprogramming: origins of cancer stem cells. EMBO Rep. 2014;15(3):244-53. doi: 10.1002/embr.201338254. PubMed PMID: 24531722; PubMed Central PMCID: PMCPMC3989690.
329. Gidekel Friedlander SY, Chu GC, Snyder EL, Girnius N, Dibelius G, Crowley D, et al. Context-dependent transformation of adult pancreatic cells by oncogenic K-Ras. Cancer cell. 2009;16(5):379-89. doi: 10.1016/j.ccr.2009.09.027. PubMed PMID: 19878870; PubMed Central PMCID: PMCPMC3048064.
330. Storer NY, White RM, Uong A, Price E, Nielsen GP, Langenau DM, et al. Zebrafish rhabdomyosarcoma reflects the developmental stage of oncogene expression during myogenesis. Development. 2013;140(14):3040-50. doi: 10.1242/dev.087858. PubMed PMID: 23821038; PubMed Central PMCID: PMC3699286.
331. Straessler KM, Jones KB, Hu H, Jin H, van de Rijn M, Capecchi MR. Modeling clear cell sarcomagenesis in the mouse: cell of origin differentiation state impacts tumor characteristics. Cancer cell. 2013;23(2):215-27. doi: 10.1016/j.ccr.2012.12.019. PubMed PMID: 23410975; PubMed Central PMCID: PMCPMC3640275.
332. Grichnik JM, Burch JA, Schulteis RD, Shan S, Liu J, Darrow TL, et al. Melanoma, a tumor based on a mutant stem cell? The Journal of investigative dermatology. 2006;126(1):142-53. doi: 10.1038/sj.jid.5700017. PubMed PMID: 16417230.
333. Hoerter JD, Bradley P, Casillas A, Chambers D, Weiswasser B, Clements L, et al. Does melanoma begin in a melanocyte stem cell? Journal of skin cancer. 2012;2012:571087. doi: 10.1155/2012/571087. PubMed PMID: 23316368; PubMed Central PMCID: PMC3536063.
334. Collas P, Alestrom P. Nuclear localization signals enhance germline transmission of a transgene in zebrafish. Transgenic Res. 1998;7(4):303-9. PubMed PMID: 9859218.
335. Kawakami K, Shima A, Kawakami N. Identification of a functional transposase of the Tol2 element, an Ac-like element from the Japanese medaka fish, and its transposition in the zebrafish germ lineage. Proc Natl Acad Sci U S A. 2000;97(21):11403-8. doi: 10.1073/pnas.97.21.11403. PubMed PMID: 11027340; PubMed Central PMCID: PMCPMC17212.
336. Kwan KM, Fujimoto E, Grabher C, Mangum BD, Hardy ME, Campbell DS, et al. The Tol2kit: a multisite gateway-based construction kit for Tol2 transposon transgenesis constructs. Developmental dynamics : an official publication of the American Association of Anatomists. 2007;236(11):3088-99. doi: 10.1002/dvdy.21343. PubMed PMID: 17937395.

337. Berghmans S, Murphey RD, Wienholds E, Neuberg D, Kutok JL, Fletcher CD, et al. tp53 mutant zebrafish develop malignant peripheral nerve sheath tumors. Proc Natl Acad Sci U S A. 2005;102(2):407-12. doi: 10.1073/pnas.0406252102. PubMed PMID: 15630097; PubMed Central PMCID: PMCPMC544293.
338. Carney TJ, Dutton KA, Greenhill E, Delfino-Machin M, Dufourcq P, Blader P, et al. A direct role for Sox10 in specification of neural crest-derived sensory neurons. Development. 2006;133(23):4619-30. doi: 10.1242/dev.02668. PubMed PMID: 17065232.
339. Zou J, Beermann F, Wang J, Kawakami K, Wei X. The Fugu tyrp1 promoter directs specific GFP expression in zebrafish: tools to study the RPE and the neural crest-derived melanophores. Pigment cell research / sponsored by the European Society for Pigment Cell Research and the International Pigment Cell Society. 2006;19(6):615-27. doi: 10.1111/j.1600-0749.2006.00349.x. PubMed PMID: 17083488; PubMed Central PMCID: PMCPMC2920493.
340. Ceol CJ, Houvras Y, White RM, Zon LI. Melanoma biology and the promise of zebrafish. Zebrafish. 2008;5(4):247-55. Epub 2009/01/13. doi: 10.1089/zeb.2008.0544. PubMed PMID: 19133823; PubMed Central PMCID: PMC2784934.
341. Asgharzadeh S, Pique-Regi R, Sposto R, Wang H, Yang Y, Shimada H, et al. Prognostic significance of gene expression profiles of metastatic neuroblastomas lacking MYCN gene amplification. J Natl Cancer Inst. 2006;98(17):1193-203. doi: 10.1093/jnci/djj330. PubMed PMID: 16954472.
342. Gonzalez F, Zhu Z, Shi ZD, Lelli K, Verma N, Li QV, et al. An iCRISPR platform for rapid, multiplexable, and inducible genome editing in human pluripotent stem cells. Cell Stem Cell. 2014;15(2):215-26. doi: 10.1016/j.stem.2014.05.018. PubMed PMID: 24931489; PubMed Central PMCID: PMCPMC4127112.
343. Zhu Z, Gonzalez F, Huangfu D. The iCRISPR platform for rapid genome editing in human pluripotent stem cells. Methods Enzymol. 2014;546:215-50. doi: 10.1016/B978-0-12-801185-0.00011-8. PubMed PMID: 25398343; PubMed Central PMCID: PMCPMC4418970.
344. Smith JR, Maguire S, Davis LA, Alexander M, Yang F, Chandran S, et al. Robust, persistent transgene expression in human embryonic stem cells is achieved with AAVS1-targeted integration. Stem cells. 2008;26(2):496-504. doi: 10.1634/stemcells.2007-0039. PubMed PMID: 18024421.
345. Xia J, Jia P, Hutchinson KE, Dahlman KB, Johnson D, Sosman J, et al. A meta-analysis of somatic mutations from next generation sequencing of 241 melanomas: a road map for the study of genes with potential clinical relevance. Mol Cancer Ther. 2014;13(7):1918-28. doi: 10.1158/1535-7163.MCT-13-0804. PubMed PMID: 24755198; PubMed Central PMCID: PMCPMC4090262.
346. Greenman C, Stephens P, Smith R, Dalgliesh GL, Hunter C, Bignell G, et al. Patterns of somatic mutation in human cancer genomes. Nature. 2007;446(7132):153-8. doi: 10.1038/nature05610. PubMed PMID: 17344846; PubMed Central PMCID: PMCPMC2712719.
347. Cong L, Ran FA, Cox D, Lin S, Barretto R, Habib N, et al. Multiplex genome engineering using CRISPR/Cas systems. Science. 2013;339(6121):819-23. doi:

10.1126/science.1231143. PubMed PMID: 23287718; PubMed Central PMCID: PMCPMC3795411.
348. Qi LS, Larson MH, Gilbert LA, Doudna JA, Weissman JS, Arkin AP, et al. Repurposing CRISPR as an RNA-guided platform for sequence-specific control of gene expression. Cell. 2013;152(5):1173-83. doi: 10.1016/j.cell.2013.02.022. PubMed PMID: 23452860; PubMed Central PMCID: PMCPMC3664290.
349. Mali P, Yang L, Esvelt KM, Aach J, Guell M, DiCarlo JE, et al. RNA-guided human genome engineering via Cas9. Science. 2013;339(6121):823-6. doi: 10.1126/science.1232033. PubMed PMID: 23287722; PubMed Central PMCID: PMCPMC3712628.
350. Musunuru K. Available from: https://www.addgene.org/44719/.
351. Chen G, Gulbranson DR, Hou Z, Bolin JM, Ruotti V, Probasco MD, et al. Chemically defined conditions for human iPSC derivation and culture. Nature methods. 2011;8(5):424-9. doi: 10.1038/nmeth.1593. PubMed PMID: 21478862; PubMed Central PMCID: PMCPMC3084903.
352. Compton LA, Murphy GF, Lian CG. Diagnostic Immunohistochemistry in Cutaneous Neoplasia: An Update. Dermatopathology (Basel). 2015;2(1):15-42. doi: 10.1159/000377698. PubMed PMID: 27047932; PubMed Central PMCID: PMCPMC4816435.
353. Aisner DL, Maker A, Rosenberg SA, Berman DM. Loss of S100 antigenicity in metastatic melanoma. Hum Pathol. 2005;36(9):1016-9. doi: 10.1016/j.humpath.2005.07.010. PubMed PMID: 16153466; PubMed Central PMCID: PMCPMC2656365.
354. Mohamed A, Gonzalez RS, Lawson D, Wang J, Cohen C. SOX10 expression in malignant melanoma, carcinoma, and normal tissues. Appl Immunohistochem Mol Morphol. 2013;21(6):506-10. doi: 10.1097/PAI.0b013e318279bc0a. PubMed PMID: 23197006.
355. Miettinen M, Fernandez M, Franssila K, Gatalica Z, Lasota J, Sarlomo-Rikala M. Microphthalmia transcription factor in the immunohistochemical diagnosis of metastatic melanoma: comparison with four other melanoma markers. Am J Surg Pathol. 2001;25(2):205-11. PubMed PMID: 11176069.
356. Pilloni L, Bianco P, Difelice E, Cabras S, Castellanos ME, Atzori L, et al. The usefulness of c-Kit in the immunohistochemical assessment of melanocytic lesions. Eur J Histochem. 2011;55(2):e20. doi: 10.4081/ejh.2011.e20. PubMed PMID: 22193299; PubMed Central PMCID: PMCPMC3284155.
357. Bonnelykke-Behrndtz ML, Steiniche T, Damsgaard TE, Georgsen JB, Danielsen A, Bastholt L, et al. MelanA-negative spindle-cell associated melanoma, a distinct inflammatory phenotype correlated with dense infiltration of CD163 macrophages and loss of E-cadherin. Melanoma research. 2015;25(2):113-8. doi: 10.1097/CMR.0000000000000138. PubMed PMID: 25602697.
358. Katerji H, Childs JM, Bratton LE, Peyre CG, Huber AR. Primary Esophageal Melanoma with Aberrant CD56 Expression: A Potential Diagnostic Pitfall. Case Rep Pathol. 2017;2017:9052637. doi: 10.1155/2017/9052637. PubMed PMID: 29230340; PubMed Central PMCID: PMCPMC5694584.
359. Winter C, Pawel B, Seiser E, Zhao H, Raabe E, Wang Q, et al. Neural cell adhesion molecule (NCAM) isoform expression is associated with neuroblastoma

differentiation status. Pediatr Blood Cancer. 2008;51(1):10-6. doi: 10.1002/pbc.21475. PubMed PMID: 18213713.
360. Shi Y, Liu R, Zhang S, Xia YY, Yang HJ, Guo K, et al. Neural cell adhesion molecule potentiates invasion and metastasis of melanoma cells through CAMP-dependent protein kinase and phosphatidylinositol 3-kinase pathways. Int J Biochem Cell Biol. 2011;43(4):682-90. doi: 10.1016/j.biocel.2011.01.016. PubMed PMID: 21277992.
361. Carpentier AF, Rosenfeld MR, Delattre JY, Whalen RG, Posner JB, Dalmau J. DNA vaccination with HuD inhibits growth of a neuroblastoma in mice. Clinical cancer research : an official journal of the American Association for Cancer Research. 1998;4(11):2819-24. PubMed PMID: 9829748.
362. Kawaguchi J, Nichols J, Gierl MS, Faial T, Smith A. Isolation and propagation of enteric neural crest progenitor cells from mouse embryonic stem cells and embryos. Development. 2010;137(5):693-704. doi: 10.1242/dev.046896. PubMed PMID: 20147374; PubMed Central PMCID: PMCPMC2827682.
363. Conway JR, Lex A, Gehlenborg N. UpSetR: an R package for the visualization of intersecting sets and their properties. Bioinformatics. 2017;33(18):2938-40. doi: 10.1093/bioinformatics/btx364. PubMed PMID: 28645171; PubMed Central PMCID: PMCPMC5870712.
364. Micevic G, Muthusamy V, Damsky W, Theodosakis N, Liu X, Meeth K, et al. DNMT3b Modulates Melanoma Growth by Controlling Levels of mTORC2 Component RICTOR. Cell reports. 2016;14(9):2180-92. doi: 10.1016/j.celrep.2016.02.010. PubMed PMID: 26923591; PubMed Central PMCID: PMCPMC4785087.
365. Callahan SJ, Tepan S, Zhang YM, Lindsay H, Burger A, Campbell NR, et al. Cancer modeling by Transgene Electroporation in Adult Zebrafish (TEAZ). Dis Model Mech. 2018;11(9). doi: 10.1242/dmm.034561. PubMed PMID: 30061297; PubMed Central PMCID: PMCPMC6177007.
366. Beckwith LG, Moore JL, Tsao-Wu GS, Harshbarger JC, Cheng KC. Ethylnitrosourea induces neoplasia in zebrafish (Danio rerio). Lab Invest. 2000;80(3):379-85. PubMed PMID: 10744073.
367. Spitsbergen JM, Tsai HW, Reddy A, Miller T, Arbogast D, Hendricks JD, et al. Neoplasia in zebrafish (Danio rerio) treated with 7,12-dimethylbenz[a]anthracene by two exposure routes at different developmental stages. Toxicol Pathol. 2000;28(5):705-15. doi: 10.1177/019262330002800511. PubMed PMID: 11026607.
368. Pliss GB, Zabezhinski MA, Petrov AS, Khudoley VV. Peculiarities of N-nitramines carcinogenic action. Arch Geschwulstforsch. 1982;52(8):629-34. PubMed PMID: 6984817.
369. Langenau DM, Traver D, Ferrando AA, Kutok JL, Aster JC, Kanki JP, et al. Myc-induced T cell leukemia in transgenic zebrafish. Science. 2003;299(5608):887-90. doi: 10.1126/science.1080280. PubMed PMID: 12574629.
370. Hans S, Kaslin J, Freudenreich D, Brand M. Temporally-controlled site-specific recombination in zebrafish. PloS one. 2009;4(2):e4640. doi: 10.1371/journal.pone.0004640. PubMed PMID: 19247481; PubMed Central PMCID: PMCPMC2645673.

371. Hans S, Freudenreich D, Geffarth M, Kaslin J, Machate A, Brand M. Generation of a non-leaky heat shock-inducible Cre line for conditional Cre/lox strategies in zebrafish. Developmental dynamics : an official publication of the American Association of Anatomists. 2011;240(1):108-15. doi: 10.1002/dvdy.22497. PubMed PMID: 21117149.
372. Rao NM, Rambabu KM, Rao SH. Electroporation of adult zebrafish. Methods in molecular biology. 2008;423:289-98. doi: 10.1007/978-1-59745-194-9_21. PubMed PMID: 18370207.
373. Mosimann C, Kaufman CK, Li P, Pugach EK, Tamplin OJ, Zon LI. Ubiquitous transgene expression and Cre-based recombination driven by the ubiquitin promoter in zebrafish. Development. 2011;138(1):169-77. doi: 10.1242/dev.059345. PubMed PMID: 21138979; PubMed Central PMCID: PMCPMC2998170.
374. Villefranc JA, Amigo J, Lawson ND. Gateway compatible vectors for analysis of gene function in the zebrafish. Developmental dynamics : an official publication of the American Association of Anatomists. 2007;236(11):3077-87. doi: 10.1002/dvdy.21354. PubMed PMID: 17948311; PubMed Central PMCID: PMCPMC4518551.
375. Balciunas D, Wangensteen KJ, Wilber A, Bell J, Geurts A, Sivasubbu S, et al. Harnessing a high cargo-capacity transposon for genetic applications in vertebrates. PLoS Genet. 2006;2(11):e169. doi: 10.1371/journal.pgen.0020169. PubMed PMID: 17096595; PubMed Central PMCID: PMCPMC1635535 and SCE are all founders of a gene therapy company called Discovery Genomics, Incorporated.
376. Kawakami K. Tol2: a versatile gene transfer vector in vertebrates. Genome Biol. 2007;8 Suppl 1:S7. doi: 10.1186/gb-2007-8-s1-s7. PubMed PMID: 18047699; PubMed Central PMCID: PMCPMC2106836.
377. Huang CJ, Tu CT, Hsiao CD, Hsieh FJ, Tsai HJ. Germ-line transmission of a myocardium-specific GFP transgene reveals critical regulatory elements in the cardiac myosin light chain 2 promoter of zebrafish. Developmental dynamics : an official publication of the American Association of Anatomists. 2003;228(1):30-40. doi: 10.1002/dvdy.10356. PubMed PMID: 12950077.
378. Cerami E, Gao J, Dogrusoz U, Gross BE, Sumer SO, Aksoy BA, et al. The cBio cancer genomics portal: an open platform for exploring multidimensional cancer genomics data. Cancer discovery. 2012;2(5):401-4. doi: 10.1158/2159-8290.CD-12-0095. PubMed PMID: 22588877.
379. Krauthammer M, Kong Y, Ha BH, Evans P, Bacchiocchi A, McCusker JP, et al. Exome sequencing identifies recurrent somatic RAC1 mutations in melanoma. Nature genetics. 2012;44(9):1006-14. doi: 10.1038/ng.2359. PubMed PMID: 22842228; PubMed Central PMCID: PMCPMC3432702.
380. Berger MF, Hodis E, Heffernan TP, Deribe YL, Lawrence MS, Protopopov A, et al. Melanoma genome sequencing reveals frequent PREX2 mutations. Nature. 2012;485(7399):502-6. doi: 10.1038/nature11071. PubMed PMID: 22622578; PubMed Central PMCID: PMCPMC3367798.
381. Gao J, Aksoy BA, Dogrusoz U, Dresdner G, Gross B, Sumer SO, et al. Integrative analysis of complex cancer genomics and clinical profiles using the cBioPortal. Sci

Signal. 2013;6(269):pl1. doi: 10.1126/scisignal.2004088. PubMed PMID: 23550210; PubMed Central PMCID: PMCPMC4160307.
382. Hugo W, Zaretsky JM, Sun L, Song C, Moreno BH, Hu-Lieskovan S, et al. Genomic and Transcriptomic Features of Response to Anti-PD-1 Therapy in Metastatic Melanoma. Cell. 2016;165(1):35-44. doi: 10.1016/j.cell.2016.02.065. PubMed PMID: 26997480; PubMed Central PMCID: PMCPMC4808437.
383. Burger A, Lindsay H, Felker A, Hess C, Anders C, Chiavacci E, et al. Maximizing mutagenesis with solubilized CRISPR-Cas9 ribonucleoprotein complexes. Development. 2016;143(11):2025-37. doi: 10.1242/dev.134809. PubMed PMID: 27130213.
384. Lindsay H, Burger A, Biyong B, Felker A, Hess C, Zaugg J, et al. CrispRVariants charts the mutation spectrum of genome engineering experiments. Nature biotechnology. 2016;34(7):701-2. doi: 10.1038/nbt.3628. PubMed PMID: 27404876.
385. Yen J, White RM, Wedge DC, Van Loo P, de Ridder J, Capper A, et al. The genetic heterogeneity and mutational burden of engineered melanomas in zebrafish models. Genome Biol. 2013;14(10):R113. doi: 10.1186/gb-2013-14-10-r113. PubMed PMID: 24148783; PubMed Central PMCID: PMCPMC3983654.
386. Kansler ER, Verma A, Langdon EM, Simon-Vermot T, Yin A, Lee W, et al. Melanoma genome evolution across species. BMC Genomics. 2017;18(1):136. doi: 10.1186/s12864-017-3518-8. PubMed PMID: 28173755; PubMed Central PMCID: PMCPMC5297047.
387. Gonin-Laurent N, Hadj-Hamou NS, Vogt N, Houdayer C, Gauthiers-Villars M, Dehainault C, et al. RB1 and TP53 pathways in radiation-induced sarcomas. Oncogene. 2007;26(41):6106-12. doi: 10.1038/sj.onc.1210404. PubMed PMID: 17369843.
388. Perot G, Chibon F, Montero A, Lagarde P, de The H, Terrier P, et al. Constant p53 pathway inactivation in a large series of soft tissue sarcomas with complex genetics. The American journal of pathology. 2010;177(4):2080-90. doi: 10.2353/ajpath.2010.100104. PubMed PMID: 20884963; PubMed Central PMCID: PMCPMC2947301.
389. Stratton MR, Moss S, Warren W, Patterson H, Clark J, Fisher C, et al. Mutation of the p53 gene in human soft tissue sarcomas: association with abnormalities of the RB1 gene. Oncogene. 1990;5(9):1297-301. PubMed PMID: 2216456.
390. McGranahan N, Swanton C. Clonal Heterogeneity and Tumor Evolution: Past, Present, and the Future. Cell. 2017;168(4):613-28. doi: 10.1016/j.cell.2017.01.018. PubMed PMID: 28187284.
391. Chen F, Becker A, LoTurco J. Overview of Transgenic Glioblastoma and Oligoastrocytoma CNS Models and Their Utility in Drug Discovery. Curr Protoc Pharmacol. 2016;72:14 37 1-12. doi: 10.1002/0471141755.ph1437s72. PubMed PMID: 26995546; PubMed Central PMCID: PMCPMC5043528.
392. Scahill CM, Digby Z, Sealy IM, Wojciechowska S, White RJ, Collins JE, et al. Loss of the chromatin modifier Kdm2aa causes BrafV600E-independent spontaneous melanoma in zebrafish. PLoS Genet. 2017;13(8):e1006959. doi: 10.1371/journal.pgen.1006959. PubMed PMID: 28806732; PubMed Central PMCID: PMCPMC5570503.

393. Darp R, Ceol C. Chromatin modification: A novel insight into BRAF-independent spontaneous melanoma. Pigment cell & melanoma research. 2018;31(1):9-10. doi: 10.1111/pcmr.12648. PubMed PMID: 28971591.
394. Sack LM, Davoli T, Li MZ, Li Y, Xu Q, Naxerova K, et al. Profound Tissue Specificity in Proliferation Control Underlies Cancer Drivers and Aneuploidy Patterns. Cell. 2018;173(2):499-514 e23. doi: 10.1016/j.cell.2018.02.037. PubMed PMID: 29576454.
395. Abdi EA, Tan YH, McPherson TA. Natural human interferon-beta in metastatic malignant melanoma. A phase II study. Acta Oncol. 1988;27(6b):815-7. PubMed PMID: 3233168.
396. Villares GJ, Zigler M, Wang H, Melnikova VO, Wu H, Friedman R, et al. Targeting melanoma growth and metastasis with systemic delivery of liposome-incorporated protease-activated receptor-1 small interfering RNA. Cancer research. 2008;68(21):9078-86. doi: 10.1158/0008-5472.CAN-08-2397. PubMed PMID: 18974154; PubMed Central PMCID: PMCPMC2597081.
397. Kee D, McArthur G. Targeted therapies for cutaneous melanoma. Hematol Oncol Clin North Am. 2014;28(3):491-505. doi: 10.1016/j.hoc.2014.02.003. PubMed PMID: 24880943.
398. Ravandi F, Estrov Z, Kurzrock R, Breitmeyer JB, Maschek BJ, Talpaz M. A phase I study of recombinant interferon-beta in patients with advanced malignant disease. Clinical cancer research : an official journal of the American Association for Cancer Research. 1999;5(12):3990-8. PubMed PMID: 10632330.
399. Konieczkowski DJ, Johannessen CM, Abudayyeh O, Kim JW, Cooper ZA, Piris A, et al. A melanoma cell state distinction influences sensitivity to MAPK pathway inhibitors. Cancer discovery. 2014;4(7):816-27. doi: 10.1158/2159-8290.CD-13-0424. PubMed PMID: 24771846; PubMed Central PMCID: PMCPMC4154497.
400. Saez-Ayala M, Montenegro MF, Sanchez-Del-Campo L, Fernandez-Perez MP, Chazarra S, Freter R, et al. Directed phenotype switching as an effective antimelanoma strategy. Cancer cell. 2013;24(1):105-19. doi: 10.1016/j.ccr.2013.05.009. PubMed PMID: 23792190.
401. Zhang M, Di Martino JS, Bowman RL, Campbell NR, Baksh SC, Simon-Vermot T, et al. Adipocyte-Derived Lipids Mediate Melanoma Progression via FATP Proteins. Cancer discovery. 2018;8(8):1006-25. doi: 10.1158/2159-8290.CD-17-1371. PubMed PMID: 29903879; PubMed Central PMCID: PMCPMC6192670.
402. Dee CT, Nagaraju RT, Athanasiadis EI, Gray C, Fernandez Del Ama L, Johnston SA, et al. CD4-Transgenic Zebrafish Reveal Tissue-Resident Th2- and Regulatory T Cell-like Populations and Diverse Mononuclear Phagocytes. J Immunol. 2016;197(9):3520-30. doi: 10.4049/jimmunol.1600959. PubMed PMID: 27694495; PubMed Central PMCID: PMCPMC5073357.
403. Ellett F, Pase L, Hayman JW, Andrianopoulos A, Lieschke GJ. mpeg1 promoter transgenes direct macrophage-lineage expression in zebrafish. Blood. 2011;117(4):e49-56. doi: 10.1182/blood-2010-10-314120. PubMed PMID: 21084707; PubMed Central PMCID: PMCPMC3056479.
404. Lawson ND, Weinstein BM. In vivo imaging of embryonic vascular development using transgenic zebrafish. Dev Biol. 2002;248(2):307-18. PubMed PMID: 12167406.

405. D'Agati G, Beltre R, Sessa A, Burger A, Zhou Y, Mosimann C, et al. A defect in the mitochondrial protein Mpv17 underlies the transparent casper zebrafish. Dev Biol. 2017;430(1):11-7. doi: 10.1016/j.ydbio.2017.07.017. PubMed PMID: 28760346; PubMed Central PMCID: PMCPMC5617342.
406. Schindelin J, Arganda-Carreras I, Frise E, Kaynig V, Longair M, Pietzsch T, et al. Fiji: an open-source platform for biological-image analysis. Nature methods. 2012;9(7):676-82. doi: 10.1038/nmeth.2019. PubMed PMID: 22743772; PubMed Central PMCID: PMCPMC3855844.
407. Montague TG, Cruz JM, Gagnon JA, Church GM, Valen E. CHOPCHOP: a CRISPR/Cas9 and TALEN web tool for genome editing. Nucleic Acids Res. 2014;42(Web Server issue):W401-7. doi: 10.1093/nar/gku410. PubMed PMID: 24861617; PubMed Central PMCID: PMCPMC4086086.
408. Labun K, Montague TG, Gagnon JA, Thyme SB, Valen E. CHOPCHOP v2: a web tool for the next generation of CRISPR genome engineering. Nucleic Acids Res. 2016;44(W1):W272-6. doi: 10.1093/nar/gkw398. PubMed PMID: 27185894; PubMed Central PMCID: PMCPMC4987937.